

New molecular sequences for two genera of marine planarians facilitate determination of their position in the phylogenetic tree, with new records for two species (*Platyhelminthes*, *Tricladida*, *Maricola*)

Hee-Min Yang¹, Ronald Sluys², Masaharu Kawakatsu³, Gi-Sik Min¹

1 Department of Biological Sciences, Inha University, Incheon, Republic of Korea **2** Naturalis Biodiversity Center, P.O. Box 9517, 2300 RA Leiden, The Netherlands **3** 9-jo 9-chome 1-8, Shinkotoni, Kita-ku, Sapporo, Hokkaido, Japan

Corresponding author: *Ronald Sluys* (Ronald.Sluys@naturalis.nl)

Academic editor: *D. Gibson* | Received 1 May 2018 | Accepted 19 June 2018 | Published 9 August 2018

<http://zoobank.org/CDA06D24-FD1D-4C04-80F3-4C3E093388C0>

Citation: Yang H-M, Sluys R, Kawakatsu M, Min G-S (2018) New molecular sequences for two genera of marine planarians facilitate determination of their position in the phylogenetic tree, with new records for two species (*Platyhelminthes*, *Tricladida*, *Maricola*). *ZooKeys* 781: 1–17. <https://doi.org/10.3897/zookeys.781.26324>

Abstract

For the first time, molecular sequences of the 18S ribosomal DNA were generated for representatives of the genera *Obrimoposthia* Sluys & Ball, 1989 and *Paucumara* Sluys, 1989 of the suborder of the marine triclad, or *Maricola*, by analyzing the species *Obrimoposthia wandeli* (Hallez, 1906) and *Paucumara trigonocephala* (Ijima & Kaburaki, 1916). On the basis of this molecular data the phylogenetic position of these two genera in the phylogenetic tree of the *Maricola* was determined and compared with their position in the phylogeny based on the analysis of anatomical features. New records for these two species are documented and their taxonomic status is determined on the basis of histological studies.

Keywords

Antarctica, molecular phylogeny, new records, *Obrimoposthia*, *Paucumara*, South Korea

Introduction

Although the marine planarians or Maricola Hallez, 1892 form only a small suborder of triclad flatworms, comprising approximately 80 species, they exhibit a rather great anatomical diversity, which at times makes it difficult to recognize homological character states and thus to analyse their phylogenetic relationships. The first comprehensive study of the phylogenetic relationships among the marine triclads was undertaken by Sluys (1989) and was based on anatomical and morphological features. As morphological support for a monophyletic Maricola was postulated the autapomorphic presence of adhesive papillae arranged in the ventral annular zone, the latter constituting an autapomorphy for the entire group of triclads (Sluys 1989). More recently, Ax (2008) correctly argued that this marginal band with adhesive papillae is a plesiomorphic feature and therefore cannot support the presumed monophyly of the Maricola. Nevertheless, recent phylogenetic studies on the triclads consistently recover the Maricola as a monophyletic taxon (see Charbagi-Barbierou et al. 2011, Sluys et al. 2014, Harrath et al. 2016). The same molecular studies reveal relationships within the Maricola that differ from those hypothesized by Sluys (1989), thus suggesting that eventually major changes in the current taxonomy of the group may be necessary.

Unfortunately, the number of species incorporated in molecular phylogenetic studies of marine planarians is rather small, as for only a handful of species gene sequences are publicly available. Therefore, it is as yet not possible to draw firm conclusions about the phylogeny, and thus the taxonomy, of maricolans based on such molecular studies. In this paper we contribute to the solution of this problem by making available gene sequences of two other species of marine planarian, *Paucumara trigonocephala* (Ijima & Kaburaki, 1916) and *Obrimoposthia wandeli* (Hallez, 1906), which previously have not been examined. On the basis of this molecular data we analyze the phylogenetic position of the respective genera in the phylogenetic tree of the Maricola and compare this result with their position in the phylogeny based on the analysis of anatomical features. In addition, we document new records for these two species as well as their taxonomic status, as deduced from histological studies.

Materials and methods

Collected worms were transferred live to the laboratory, where specimens of *Paucumara trigonocephala* and *Obrimoposthia wandeli* were incubated under dark conditions at temperatures of 18 °C and 4 °C, respectively. For morphological study specimens were killed in 10% glacial acetic acid and, subsequently, fixed for 24 hours in Bouin's fluid, and stored in 70% ethanol. For histological processing specimens were first dehydrated in a graded ethanol series, cleared in clove oil and then embedded in synthetic wax. Serial sections were made at intervals of 5 µm and 8 µm, mounted on albumen-coated slides, stained with Mallory-Heidenhain/Cason (see Winsor and Sluys 2018), and, subsequently, cover glasses were mounted with DPX. Reconstructions of the copulatory complex were ob-

Table 1. List of species taxa of which 18S rDNA gene data was used for constructing the phylogenetic trees, with accession numbers for gene sequences available from GenBank.

Classification	Species	GenBank number
Suborder Maricola Hallez, 1892		
Family Cercyridae Böhmig, 1906	<i>Cercyra hastata</i>	KM200902
	<i>Sabussowia dioica</i>	JN009785
	<i>Sabussowia ronaldi</i>	KM200923
Family Uteriporidae Böhmig, 1906	<i>Ectoplana limuli</i>	D85088
	<i>Obrimoposthia wandeli</i>	MH108586
	<i>Paucumara trigonocephala</i>	MH108587
	<i>Sluysia triapertura</i>	MF383119
	<i>Uteriporus</i> sp.	AF013148
Family Bdellouridae Diesing, 1862	<i>Bdelloura candida</i>	Z99947
	<i>Palombiella stephensoni</i>	DQ666008
	<i>Pentacoelum kazukolinda</i>	KM200905
Family Procerodidae Diesing, 1862	<i>Procerodes dohrni</i>	JN009783
	<i>Procerodes littoralis</i>	Z99950
	<i>Procerodes plebeius</i>	DQ665997
Incertae sedis	<i>Maricola</i> sp.	KC869825
Suborder Cavernicola Sluys, 1990		
	<i>Cavernicola</i> sp.	KC869823
	<i>Novomitchellia bursaelongata</i>	KU096054
Suborder Continenticola Carranza, Littlewood, Clough, Ruiz-Trillo, Bagnù & Riutort, 1998		
Family Dugesiidae Ball, 1974	<i>Dugesia gonocephala</i>	DQ666002
	<i>Dugesia japonica</i>	D83382
	<i>Dugesia ryukyuensis</i>	AF050433
	<i>Dugesia subtentaculata</i>	AF013155
Family Planariidae Stimpson, 1857	<i>Crenobia alpina</i>	M58345
	<i>Phagocata vitta</i>	DQ665998
	<i>Polycelis felina</i>	DQ665996
Order Fecampiida Rohde, Luton & Johnson, 1994		
	<i>Kronborgia isopodicola</i>	AJ012513
	<i>Piscinquilinus</i> sp.	AJ012512
	<i>Urastoma cyprinae</i>	AF167422

tained by using a camera lucida attached to a compound microscope. The material is deposited in the National Institute of Biological Resources (NIBR), Seoul, Republic of Korea and Naturalis Biodiversity Center, Leiden, The Netherlands (ZMA collection code).

Before performing the molecular analysis, specimens of *P. trigonocephala* and *O. wandeli* were first starved for more than seven days. Genomic DNA was extracted, using LaboPass^M Tissue Mini Kit (Cosmogenetech, Seoul, South Korea), from either starved live worms or from 100% ethanol fixed specimens that before fixation had been starved also for seven days. We obtained two 18S ribosomal DNA sequences from both species. To infer their position in the phylogenetic tree of the triclads we constructed Bayesian Inference (BI) and Maximum-likelihood (ML) trees, using 24 planarians as ingroup and three fecampioid species as outgroup taxa (Table 1).

The 18S ribosomal DNA gene was amplified using Polymerase Chain Reaction (PCR) with four primers: 1F, 4F, 7R, 9R (see Carranza et al. 1996). The PCR amplifications were conducted in a final volume of 35 μ L under the following conditions: 2 min at 94 °C, 40 cycles of 20 s at 95 °C, 30 s at 45 °C, and 1 min at 72 °C, and 5 min at 72 °C as a final extension. After purifying PCR products, using LaboPass^M PCR Purification Kit (Cosmogenetech, Seoul, Republic of Korea), 18S gene sequences were determined from both strands by Macrogen Inc. (Seoul, Republic of Korea) by using the 3730xl DNA analyser with the same primers that were used in the PCR. For constructing the 18S rDNA phylogenetic tree, we used genomic data of 27 species, including three outgroup taxa (Table 1). The sequences were aligned using MAFFT version 7 (Kato et al. 2017) (using the G-INS-i iterative refinement method and with the other options set as default) and checked using BioEdit 7.2.6.1 (Hall 1999). Regions that could not be clearly aligned were excluded using Gblocks version 0.91b (Castresana and Talavera 2007) (with the option of half allowed gap positions and minimum length of a block being 6). The final length of the alignment was 1,398bp. To find the best-fit evolutionary model, we used Jmodeltest2 (Darriba et al. 2012). GTR+I+G model was selected by applying the Akaike information criterion. We used Mr Bayes v 3.2 (Ronquist et al. 2012) and RaxML 8.2.10 (Stamatakis 2014) to infer phylogenies with the Bayesian Inference (BI) and Maximum-likelihood (ML) method, respectively. For BI method, two runs for 5 million generations and 25% burn-in was used under the GTR+I+G model. For the ML analysis, we performed 10,000 replicates with the same model. BI and ML trees were visualized using Figtree v1.4.3 and edited by using Adobe^R Photoshop^R CS5.

Abbreviations used in the figures

bc	bursal canal;	od	oviduct;
br	brain;	pb	penis bulb;
ca	common atrium;	pg	penis gland;
cb	copulatory bursa;	ph	pharynx;
cod	common oviduct;	pp	penis papilla;
cvd	common vas deferens;	sg	shell gland;
ed	ejaculatory duct;	spt	septum;
el	eye lens;	ug	unicellular gland;
go	gonopore;	vd	vas deferens;
in	intestine;	vi	vitellaria
mo	mouth opening;		

Results

Phylogeny

The BI and ML phylogenetic trees showed the same topology (Figure 1). The suborders Cavernicola Sluys, 1990, Continenticola Carranza et al., 1998, and several of their

1

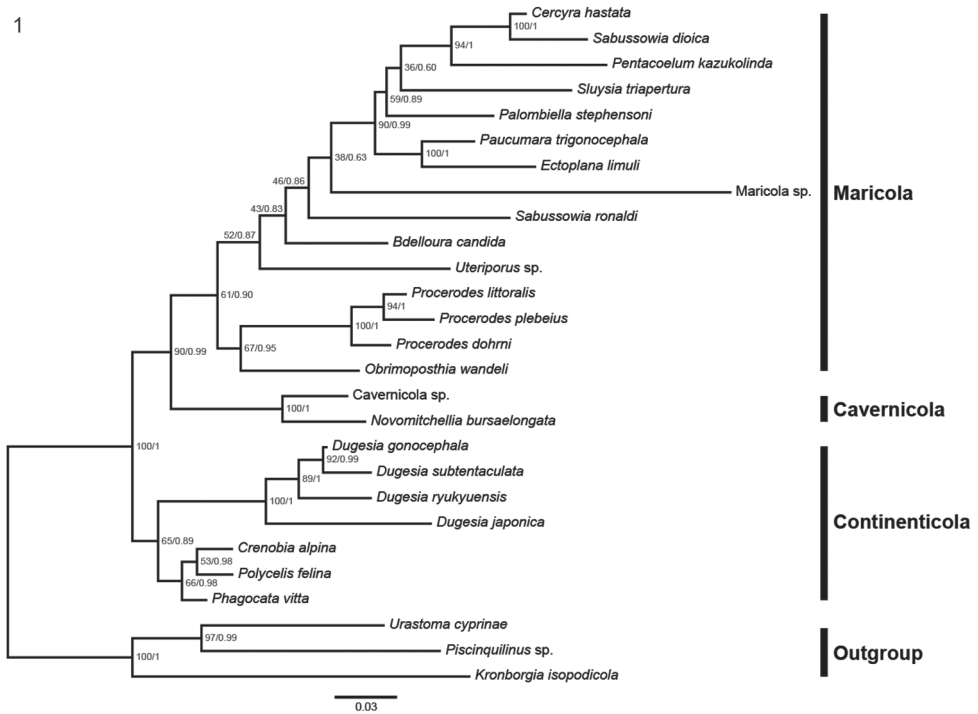


Figure 1. Maximum-likelihood tree based on 18S ribosomal DNA sequences. Numbers on nodes represent support values for Maximum-Likelihood (bootstrap –BO) and Bayesian Inference (posterior probability – PP): BO/PP. Scale bar indicates number of nucleotide substitutions per site.

inclusive lower taxa, form monophyletic groups. The *Maricola* Hallez, 1892 is also a monophyletic group, although the relationships within this group do not always reflect current taxonomy. For example, only the family Procerodidae Diesing, 1862 forms a monophylum, while current families Bdellouridae Diesing, 1862, Uteriporidae Böhmig, 1906 and Cercyridae Böhmig, 1906 form polyphyletic groups in our tree.

In the phylogenetic tree, the inferred positions of species belonging to the current families Bdellouridae, Uteriporidae and Cercyridae are supported only by BI, as the bootstrap supports for ML are < 75. The species *Cercyra hastata* Schmidt, 1861, *Sabussowia dioica* (Claparède, 1863), *Pentacoelum kazukolinda* (Kawakatsu & Mitchell, 1984), *Paucumara trigonocephala* and *Ectoplana limuli* (Ijima & Kaburaki, 1916) form an exception, in that their positions in our tree are supported by both ML and BI.

Paucumara trigonocephala and *Obrimoposthia wandeli* are currently classified as belonging to the Uteriporidae. In our phylogenetic tree *P. trigonocephala* forms a highly supported clade with *Ectoplana limuli*, currently also classified as an Uteriporidae species. The position of *O. wandeli* is also inferred with high posterior probability value in the BI tree and this species forms a clade with the family Procerodidae, here represented by three species included in our analysis. However, in the ML tree (not shown but with the same topology as the BI tree), the clade formed by the

three species of *Procerodes* and *Obrimoposthia* (Figure 1) had only a bootstrap support value of 67.

The unidentified species *Maricola* sp. shows a very long branch that differs strongly from the branch lengths of other maricolans. Together with the low support values (bootstrap: 38; posterior probability: 0.63) this suggests that the molecular sequence of *Maricola* sp. may be corrupted.

Systematic and integrative account

Order TRICLADIDA Lang, 1884

Suborder MARICOLA Hallez, 1892

Family UTERIPORIDAE Böhmig, 1906

Genus *Paucumara* Sluys, 1989

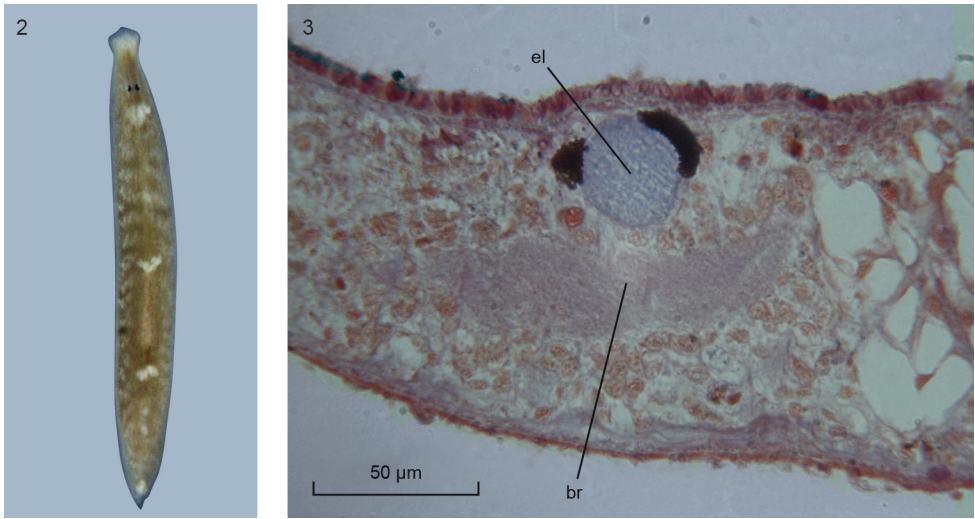
***Paucumara trigonocephala* (Ijima & Kaburaki, 1916)**

Material examined. NIBRIV0000821277, Sacheon-si, Gyeongsangnam-do, Republic of Korea (35°05'05"N 128°03'14"E), 7 June 2017, coll. H-M. Yang, sagittal sections on 2 slide; ZMA V.Pl. 7279.1, *ibid.*, sagittal sections on 3 slides; V.Pl. 7279.2, *ibid.*, horizontal sections on 1 slide; V.Pl. 7279.3, *ibid.*, transverse sections on 6 slides.

ZMA V.Pl. 6807, shore of Lake Hi-numa, near the Park, Ibaraki-machi, Higashi-Ibaraki-gun, Ibaraki Prefecture, Kantô Region, Honshû, Japan, 13 August 2007, coll. S. Chinone, preserved specimens. ZMA V.Pl. 6810, *ibid.*, 31 August 2007, coll. S. Chinone, preserved specimens.

Comparative description and discussion. The external features and anatomy of the specimens from South Korea correspond in all essential details to the descriptions of this species published earlier (see Sluys 1989, Sluys and Ball 1990, Sluys and Kawakatsu 2000). Preserved specimens measured up to approx. 3 mm in length and 1 mm in width. In particular, the shape of the body and the position of the eyes in living specimens (Figure 2) are very similar to the situation in Australian specimens, as documented in Sluys (1989) and Sluys and Kawakatsu (2000). The two eyes are set close to the mid-line of the body and positioned at a considerable distance posterior to the anterior body margin.

The shape of the front end of the body is very characteristic: anterior to the eyes the body first narrows to give rise to a kind of “neck” and then widens to form a triangular, obtusely pointed head with broadly rounded auricles (Figure 2). At the level of the auricles there is a broad, creamy-white patch that extends across the body. A similar kind of patch is located immediately behind the eyes, albeit that it does not extend from one lateral body margin to the other but is confined to mid-dorsum. Additional creamy-white spots may be located directly in front of and behind the pharyngeal pocket and at the very tip of the tail. In point of fact, each of the pharyngeal patches may actually consist of two spots situated close together. These pharyngeal spots as well as the one at



Figures 2–3. *Paucumara trigonocephala*. **2** Dorsal view of live specimen from South Korea. Scale bar not available **3** ZMA V.Pl. 7279.1, microphotograph of eye lens; anterior to the left.

the tip of the tail were not present in every specimen examined and neither were they reported earlier in the available literature.

In the specimens from South Korea the entire dorsal surface is provided with a brownish pigmentation. The pigment granules are more or less evenly distributed, but accumulations occur in front of the eyes, where there is a broad, transverse band, and in the form of a brown stripe on either side of the pharyngeal pocket and a band of brown pigment running between the eyes. A brownish colouration, on both dorsal and ventral body surface, was described also for specimens from northern Australia (Sluys and Kawakatsu 2000).

With respect to their anatomy, the South Korean animals exhibit a distinct lens in each of their eyes (Figure 3) and a copulatory apparatus (Figs 4, 5) similar to that documented for animals from other parts of the range of the species (see Sluys and Ball 1990, Sluys and Kawakatsu 2000, and references therein). The penis papilla is a stubby cone. Immediately after having penetrated the penis bulb, the vasa deferentia unite to form a common vas deferens, which communicates with a much broader ejaculatory duct. At its distal, ventral section the latter receives the openings of erythrophilic penis glands. The sac-shaped copulatory bursa fills the entire dorso-ventral space; it is connected with the common atrium by means of a bursal canal that is lined with an infranucleated epithelium. The major portion of the bursal canal is rather wide and irregularly shaped, but the part near its opening into the common atrium is narrow. This lower, proximal portion of the bursal canal receives the separate openings of the oviducts. Unfortunately, in specimens NIBRIV0000821277, ZMA V.Pl. 7279.1, and ZMA V.Pl. 7279.2 we were unable to trace the oviducts and only in the transversally sectioned specimen ZMA V.Pl. 7279.3 did we observe the oviducts separately opening

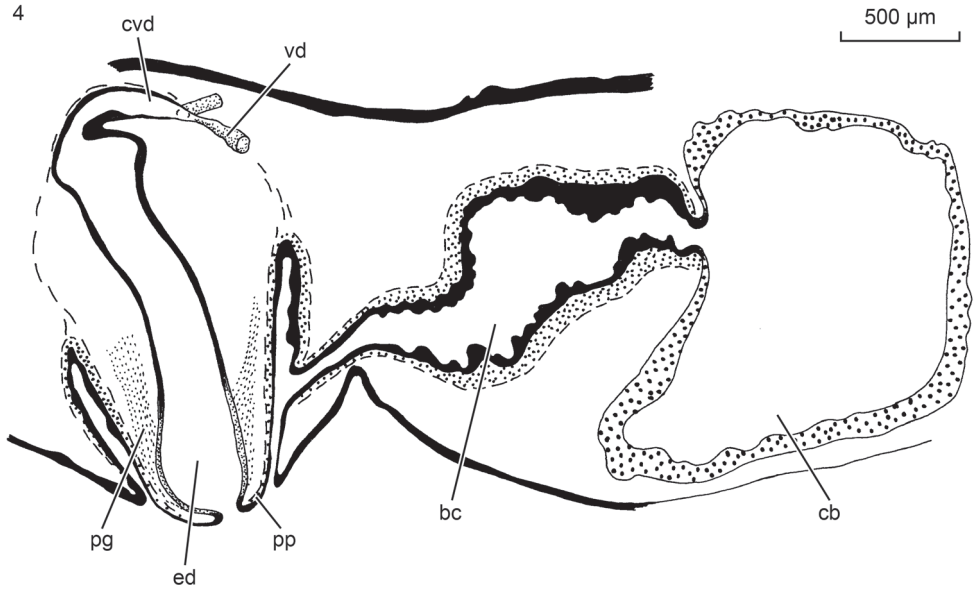
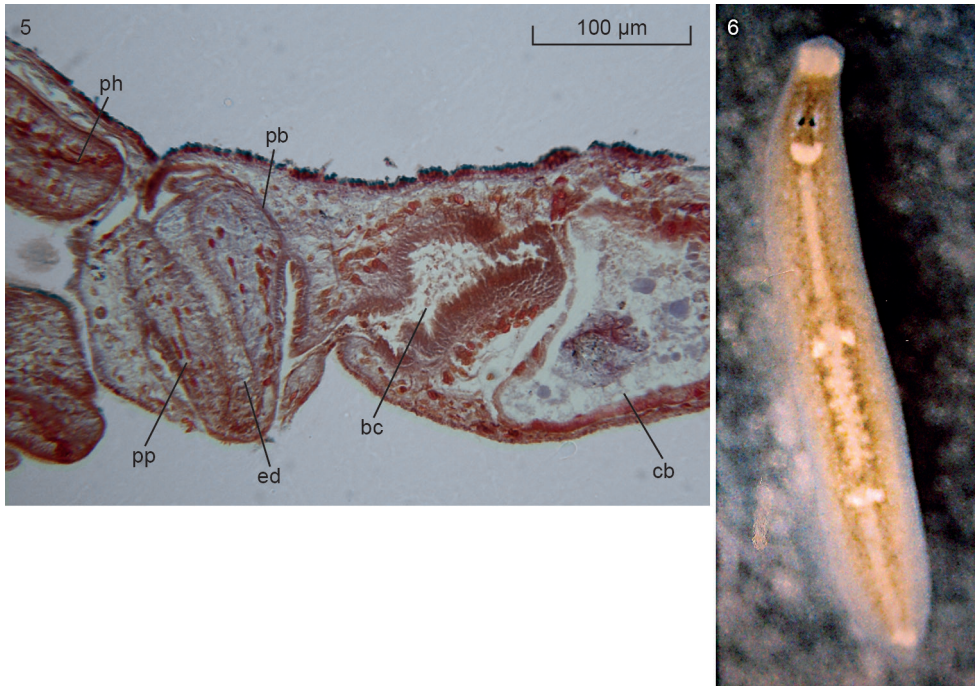


Figure 4. *Paucumara trigonocephala*. ZMA V.Pl. 7279.1, sagittal reconstruction of the copulatory apparatus; anterior to left.

into the bursal canal. The entire bursal canal is covered with a well-developed, subepithelial layer of circular muscle, followed by a thin layer of longitudinal muscle.

According to Sluys (1989), Sluys and Ball (1990), and Sluys and Kawakatsu (2000), the bursal canal receives along its entire length numerous openings of erythrophilic glands, the cell bodies of which are located ectally to the surrounding coat of muscle. These glands are different from the shell glands, which open into the bursal canal ectally to the oviducal openings. In the present material we observed that indeed at places a granular, erythrophilic secretion is discharged into the lumen of the bursal canal. However, this secretion is not easy to detect and apparently in our specimens this situation is much less developed than as described in the literature for other specimens of *Paucumara trigonocephala*. We were unable to detect shell glands in our animals from South Korea.

Previous records of *Paucumara trigonocephala* from Japan, Australia, the Bismarck Archipelago and probably Hong Kong were summarized in Sluys and Ball (1988), Sluys (1989), and Sluys and Kawakatsu (2000). We do here document a new locality for Japan, viz., Lake Hi-numa; this is a lake that is connected with the sea and, thus, has a low level of salinity. Histological sections have not been prepared of the preserved specimens available from this locality (see Material examined) but a picture of a live specimen (Figure 6) leaves little doubt about its specific identity. It is noteworthy that this animal also exhibits the whitish patches in the pharyngeal region and at the tip of the tail (see above).



Figures 5–6. *Paucumara trigonocephala*. **5** ZMA V.Pl. 7279.1, microphotograph of sagittal section of the copulatory apparatus; anterior to the left **6** Dorsal view of live specimen from Lake Hi-numa, Japan. Scale bar not available.

Although the species was probably observed in Hongkong as early as 1857 (see Sluys 1989) our present animals from South Korea represent the first substantiated record of *P. trigonocephala* from continental Asia. Here, the animals were collected from brackish water with a low salinity level, the bottom consisting of mud with small stones and being devoid of any aquatic vegetation. This habitat is in agreement with the fact that all over its range the animals show the same characteristic ecology, in that they live in low-salinity biotopes, which during ebb tide even may be entirely fresh (Kaburaki 1922, Sluys and Kawakatsu 2000).

In the molecular phylogenetic trees generated by Souza et al. (2018) their new genus and species *Shuysia triapertura* Leal-Zanchet & Souza, 2018 is the sister-group of the ectocommensal species *Ectoplana limuli* (Ijima & Kaburaki, 1916), albeit that this relationship only has low support in their trees. In our tree (Figure 1) the topology has changed slightly in that *P. trigonocephala* has become the sister-species of *E. limuli*, while *S. triapertura* forms part of a group of five species that constitutes the sister-taxon of *E. limuli* plus *P. trigonocephala*. That *E. limuli* and *P. trigonocephala* share a sister-group relationship conforms with the current taxonomy of the Maricola, in which both species are classified amongst members of the subfamily Ectoplaninae Bresslau, 1933 (Sluys 1989).

Genus *Obrimoposthia* Sluys & Ball, 1989***Obrimoposthia wandeli* (Hallez, 1906)**

synonym: *Procerodes sanderi* [Hauser, 1987]

Material examined. NIBRIV0000813547, King George Island, South Shetland Islands, 62°12'31"S – 58°47'42"W, 2 February 2017, coll. Hee-Min Yang, sagittal sections on 11 slides; ZMA V.Pl. 7280.1, *ibid.*, sagittal sections on 14 slides. The animals were collected from a pebble beach; temperature of the sea surface water was 0–1°C; at a depth of 10m water temperature was 1–0°C. Many worms were observed to be attached to the seaweed Kelp.

ZMA V.Pl. 951.1, King George Island, South Shetland Islands, 1983, sagittal sections on 15 slides; V.Pl. 951.2, *ibid.*, whole mount on 1 slide; V.Pl. 951.3, *ibid.*, sagittal sections on 13 slides; V.Pl. 951.4, *ibid.*, sagittal sections on 13 slides; V.Pl. 951.5, *ibid.*, transverse sections on 19 slides; V.Pl. 951.6, *ibid.*, horizontal sections on 8 slides.

Holotype *Procerodes sanderi*: MZU PL. 00290, sagittal sections on 48 slides (nos. A-140/A-188).

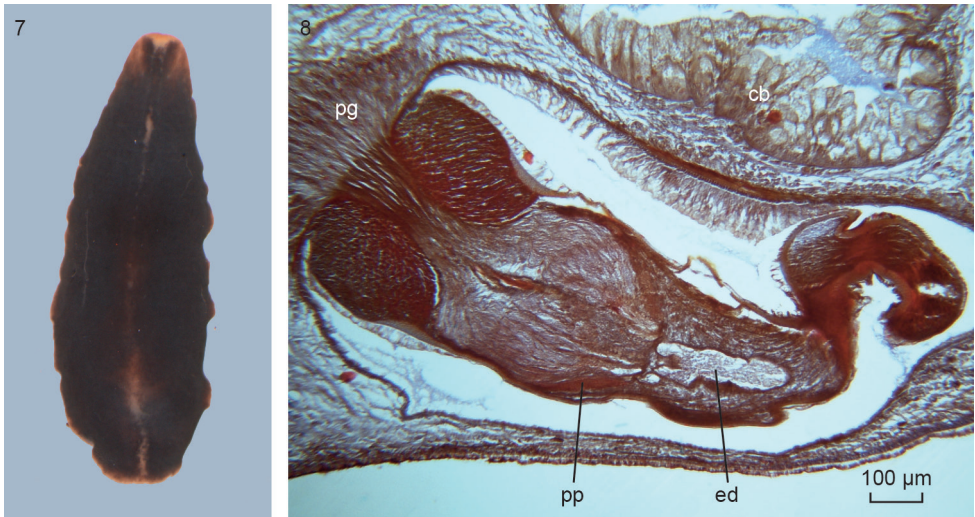
MZU PL. 00291, sagittal sections on 30 slides (nos. A788-821) of presumed specimen of *Procerodes sanderi* from the original collection of J. Hauser.

Comparative description. Preserved specimens, collected in 2017, up to approx. 11 × 3.5 mm, thus being somewhat larger than reported for preserved animals of *Obrimoposthia wandeli* (Hallez, 1906), which measured 4–8 mm in length and 2.5–4 mm in width (Sluys 1989). However, much of this variation in size may be due to different fixatives used in the field, resulting in different states of contraction of the animals. Nevertheless, preserved specimens of the sample ZMA V.Pl. 951 also were quite large, measuring 8–10 × 3–5 mm.

Dorsal surface of our animals from 2017 mottled blackish or dark brown, with a pale mid-dorsal stripe, which is only weakly developed on the middle portion of the body (Figure 7). At the front end of the body the dark pigmentation gives way to a broad, pale patch on either side of the body, extending from the eyes towards the antero-lateral body margins; further there is a pale patch on the mid-frontal body margin. In this way the dark pigmentation on the head forms a kind of V-shaped pattern; the same pattern was described for other specimens of *O. wandeli* (Sluys 1989). The external appearance and colouration of our 2017 specimens fully agree with that of specimens of *P. sanderi* as originally described in 1987 (see figure in Anonymous 1987).

In the specimens from the 2017 sample the small, rounded testes are situated ventrally and extend from immediately behind the ovaries to somewhat posteriorly to the copulatory apparatus, as may be the case also in other specimens of *O. wandeli* (Sluys 1989). The anatomy of the penis papilla of these specimens from the 2017 sample is precisely the same as that documented for *O. wandeli* (see Sluys and Ball 1988, Sluys and De Vries 1988, Sluys 1989) (Figure 8).

The several specimens available from the population of King George Island revealed the presence of intraspecific variability in the female reproductive system. Generally,



Figures 7–8. *Obrimoposthia wandeli*. **7** Dorsal view of preserved specimen from King George Island. Scale bar not available **8** NIBRIV0000813547, microphotograph of sagittal section of penis papilla; anterior to the left.

O. wandeli has been described as having a bursal canal that shows a distinct T-junction, with the posterior branch of the T forming a kind of diverticulum that receives the opening of the common oviduct (see Sluys 1989, fig. 141). In some animals from King George Island such a T-junction is indeed present (ZMA V.Pl. 951.1, V.Pl. 951.4, V.Pl. 951.6). However, in others, the situation is different in that in these animals the common oviduct opens, via a constriction, into the bursal canal, which from there on runs antero-dorsad and then gently curves rather abruptly ventrad to open into the common atrium (Figs 9, 10). This portion of the bursal canal shows a clear, lateral bend during its course towards the common atrium (Figure 11), as reported earlier for *O. wandeli* (Sluys 1989). From the side of this obliquely, antero-dorsally running part of the bursal canal arises a branch that runs more or less straight forward to communicate with the copulatory bursa (Figure 9). Precisely the same situation is present in the holotype of *P. sanderi* (Figure 12). In some presumed specimens of *P. sanderi* the branch that runs to the bursa may even originate very close to the point where the common oviduct communicates with the bursal canal (Figure 13).

The entire bursal canal, including its side branch, is lined with an infranucleated epithelium and is surrounded by a thick, subepithelial layer of circular muscle, bounded by a much thinner layer of longitudinal muscle. Oviducts and common oviduct are lined with a nucleated epithelium and are surrounded by a thin layer of circular muscles. The entire bursal canal is surrounded by a broad zone of unicellular glands, which discharge their erythrophilic secretion into the canal. Erythrophilic shell glands discharge their secretion into the ventral portion of the bursal canal, near its communication with the common atrium.

Discussion. In an anonymous article in a bulletin, the late Josef Hauser described the presumed new species *Procerodes sanderi* [Hauser, 1987] (Anonymous 1987). That

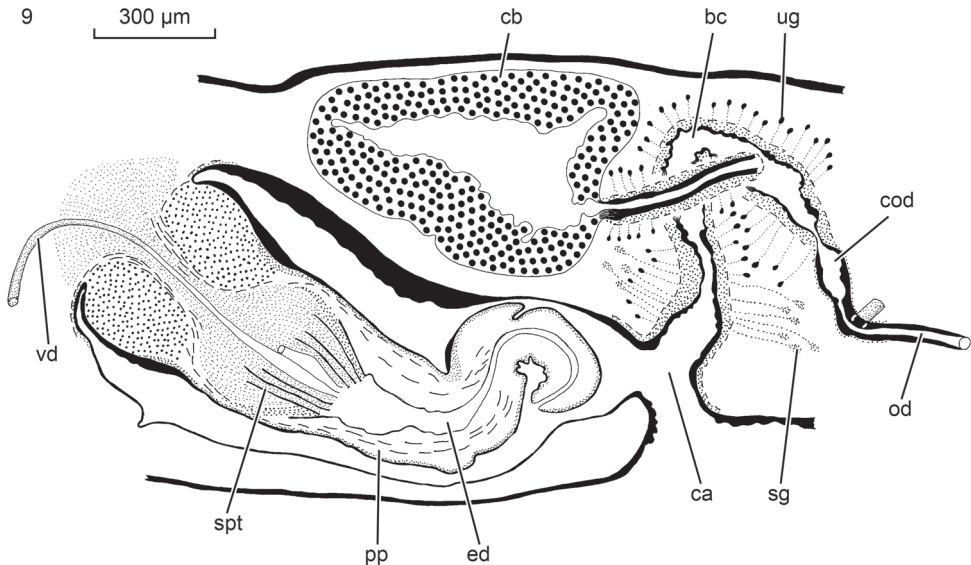
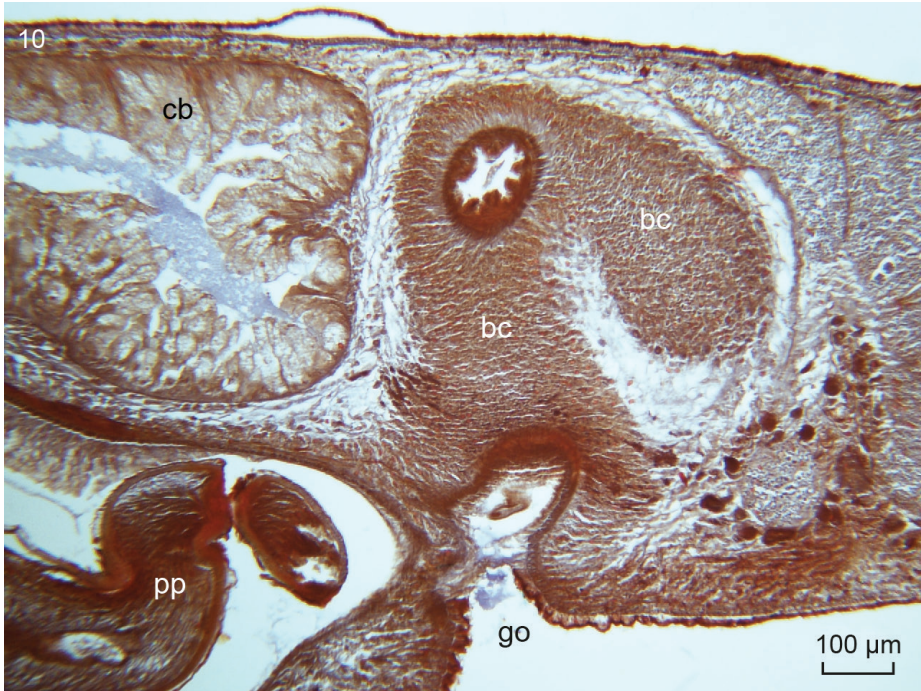


Figure 9. *Obrimoposthia wandeli*. NIBRIV0000813547, sagittal reconstruction of the copulatory apparatus; anterior to the left.

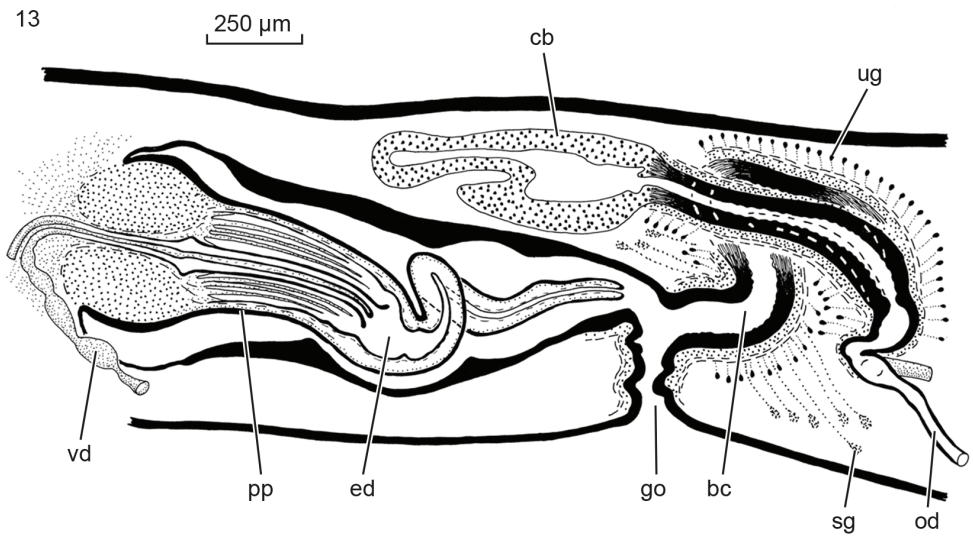
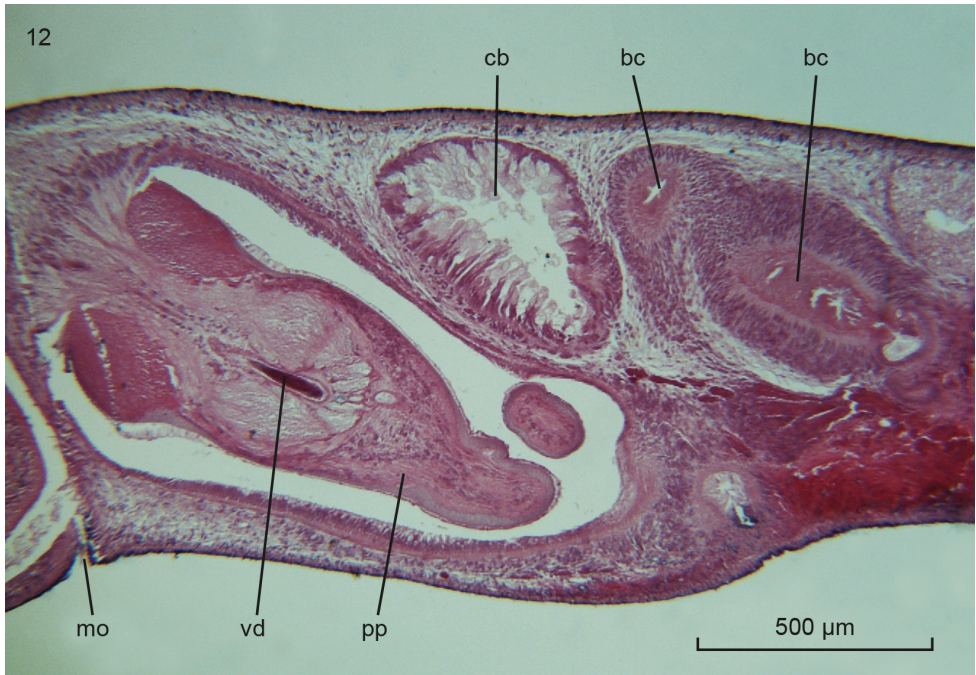
Hauser was indeed the author of this article was apparent, for example, from the fact that in 1988 and 1989 he corresponded on this subject with both Masaharu Kawakatsu and Ronald Sluys and that he forwarded to these workers photocopies of the article. Furthermore, in the article the new species is attributed to Hauser. In his article Hauser claimed that the anatomy of *P. sanderi* was different from congeneric species, including species currently assigned to the genus *Obrimoposthia*. Unfortunately, the article did not provide a reconstruction drawing of the copulatory apparatus, while the short description of the reproductive apparatus in the Portuguese language neither did make clear the anatomical differences between the new species and its congeners. Furthermore, the material that Hauser made available to both Sluys and Kawakatsu, consisting of printed photographs, histological slides, and reconstruction drawings, at the time did not convince these two workers that indeed the specimens represented a new species. As a result, in his monograph Sluys (1989) synonymized *Procerodes sanderi* with *Obrimoposthia wandeli*. In their joint publication, Sluys and Kawakatsu (2005) reiterated their conclusion, as expressed also in correspondence with Hauser, that the species *P. sanderi* is synonymous with *O. wandeli*.

Nevertheless, examination of our new material collected in 2017, as well as re-examination of specimens from King George Island that were collected in 1983 and were part of Hauser's samples, including a specimen that he had designated as the holotype specimen of *P. sanderi*, revealed that at least within this population there is clear intraspecific variation in the construction of the female copulatory apparatus.

In earlier studies (e.g., Sluys and Kawakatsu 2005) the deviant course of the bursal canal in some specimens of *O. wandeli* from King George Island, i.e. absence of the



Figures 10–11. *Obrimoposthia wandeli*. **10** NIBRIV0000813547, microphotograph of sagittal section of the copulatory apparatus; anterior to the left **11** ZMA V.Pl. 951.5, microphotograph of transverse section through the bursal canal and gonopore.



Figures 12–13. *Obrimoposthia wandeli*. **12** MZUPL 00290-A163, microphotograph of sagittal section of copulatory apparatus of holotype of *Procerothes sanderi*; anterior to the left **13** MZU PL. 00291(nos. A788-821), sagittal reconstruction of the copulatory apparatus of presumed specimen of *Procerothes sanderi*.

T-junction and origination of a duct from the side of the bursal canal, was not clearly observed as no reconstruction drawings were made of the various specimens. The present series of material that is available undeniably shows that the intraspecific variability of this population is exhibited by animals collected both in 1983 and 2017. Therefore, we do here consider this variability in the course of the bursal canal, as described above, to be a constant, stable feature of at least the population from King George Island and probably for other populations of *O. wandeli* as well.

One might contemplate an alternative explanation for the deviant course of the bursal canal. As the specimens from King George Island were somewhat larger than generally reported for *O. wandeli* (see above), one may view their copulatory apparatus as having reached the final stage of maturation. However, although we can envision structures becoming larger during maturation, we believe it to be unlikely for anatomical organs to become structurally different. In other words, we consider it unlikely that upon maturation a T-junction in the bursal canal will re-assemble in such a way that it develops into a duct with a distinct loop from which originates a side-branch that runs to the copulatory bursa. Therefore, we consider these different expressions of the course of the bursal canal and its connection with the copulatory bursa to be the result of intraspecific variation, independent of the stage of maturation.

In our phylogenetic tree (Figure 1) *O. wandeli* is the sister-group of the genus *Procerodes* Girard, 1850. This reflects the taxonomic history of the current members of the genus *Obrimoposthia*, most of which were formerly assigned to the genus *Procerodes*. However, it became increasingly clear that in the past the genus *Procerodes* constituted an unnatural assemblage of species that belonged to different natural groups (Sluys 1986), one such group being formed by the present members of the genus *Obrimoposthia* (Sluys and Ball 1988, Sluys 1989). This has resulted in the situation that in the most recent taxonomy of the Maricola the genera *Procerodes* and *Obrimoposthia* are even classified in different families, viz. Procerodidae Diesing, 1862 and Uteriporidae Böhmig, 1906, respectively (Sluys 1989, Sluys et al. 2009). In the phylogenetic tree of the Uteriporidae based on morphological characters, the genus *Obrimoposthia* is closely related to *Paucumara* Sluys, 1989 and *Ectoplana* Kaburaki, 1917 (Sluys 1989, fig. 302), both belonging to the subfamily Ectoplaninae Bresslau, 1933. It is clear that in our present tree (Figure 1) *Obrimoposthia* is rather far removed from *Ectoplana* and *Paucumara*.

Acknowledgements

We are grateful to Dr. S. Chinone for making available preserved animals and a photo of a live specimen of *Paucumara trigonocephala* from Japan. Dr. A. Leal-Zanchet (UNISINOS, São Leopoldo, Brazil) is thanked for making available the type specimen of *Procerodes sanderi*. M. Hermsen (Naturalis Biodiversity Center) is thanked for the digital rendering of the figures. The study was supported by a grant from the National Institute of Biological Resources (NIBR), funded by the Ministry of Environment (MOE) of the Republic of Korea (NIBR201801202, NIBR201722202).

References

- Anonymous (1987) Uma nova planária na Antártica. Comissão Interministerial para Recursos do Mar/Informativo 2(3): 3.
- Ax P (2008) Plathelminthes aus Brackgewässern der Nordhalbkugel. Akademie der Wissenschaften und der Literatur, Mainz, Abhandlungen der Mathematisch-naturwissenschaftlichen Klasse, Jhrg. 2008, 1: 1–696.
- Carranza S, Giribet G, Ribera C, Baguña J, Riutort M (1996) Evidence that two types of 18S rDNA coexist in the genome of *Dugesia (Schmidtea) mediterranea* (Platyhelminthes, Turbellaria, Tricladida). *Molecular Biology and Evolution* 13(6): 824–832. <https://doi.org/10.1093/oxfordjournals.molbev.a025643>
- Castreseana J, Talavera G (2007) Improvement of phylogenies after removing divergent and ambiguously aligned blocks from protein sequence alignments. *Systematic Biology* 56(4): 564–577. <https://doi.org/10.1080/10635150701472164>
- Charbagi-Barbirou K, Álvarez-Presas M, Vila-Farré M, Gammoudi M, Tekaya S, Riutort M (2011) Marine triclads (Platyhelminthes, Tricladida, Maricola), a preliminary molecular approach to their phylogeny. *Cahiers de Biologie Marine* 52: 303–311.
- Darriba D, Taboada GL, Doallo R, Posada D (2012) jModelTest2: more models, new heuristics and parallel computing. *Nature Methods* 9(8): 772. <https://doi.org/10.1038/nmeth.2109>
- Guindon S, Gascuel O (2003) A simple, fast and accurate method to estimate large phylogenies by maximum-likelihood. *Systematic Biology* 52(5): 696–704. <https://doi.org/10.1080/10635150390235520>
- Hall TA (1999) BioEdit: a user-friendly biological sequence alignment editor and analysis program for Windows 95/98/NT. *Nucleic Acids Symposium Series* 41: 95–98.
- Harrath AH, Mansour L, Lagnika M, Sluys R, Boutin C, Alwasel S, Poch A, Riutort M (2016) A molecular analysis of the phylogenetic position of the suborder Cavernicola within the Tricladida (Platyhelminthes), with the description of a new species of stygobiont flatworm from Benin. *Zoological Journal of the Linnean Society* 178: 482–491. <https://doi.org/10.1111/zoj.12430>
- Kaburaki T (1922) On some Japanese Tricladida Maricola, with a note on the classification of the group. *Journal of the College of Science, Imperial University of Tokyo* 44: 1–54. [1 pl.]
- Katoh K, Standley DM (2013) MAFFT multiple sequence alignment software version 7: improvements in performance and usability. *Molecular Biology and Evolution* 30(4): 772–780. <http://doi.org/10.1093/molbev/mst010>
- Ronquist F, Teslenko M, Van Der Mark P, Ayres DL, Darling A, Höhna S, Larget B, Liu L, Suchard MA, Huelsenbeck JP (2012) MrBayes 3.2: efficient Bayesian phylogenetic inference and model choice across a large model. *Systematic Biology* 61(3): 539–542. <https://doi.org/10.1093/sysbio/sys029>
- Sluys R (1986) Taxonomic studies on marine triclads (Turbellaria, Tricladida, Maricola). *Hydrobiologia* 132: 257–262. <https://doi.org/10.1007/BF00046258>
- Sluys R (1989) A monograph of the marine triclads. A. A. Balkema, Rotterdam and Brookfield, 463 pp.

- Sluys R, Ball IR (1988) A synopsis of the marine triclads of Australia and New Zealand (Platyhelminthes: Tricladida: Maricola). *Invertebrate Taxonomy* 2: 915–959. <https://doi.org/10.1071/IT9880915>
- Sluys R, Ball IR (1990) The aquatic triclads (Platyhelminthes, Tricladida) of the Bismarck Archipelago. *Steenstrupia* 16: 13–20.
- Sluys R, Kawakatsu M (2000) New, southernmost record of *Paucumara trigonocephala* (Platyhelminthes, Tricladida, Maricola) from Queensland, with documentation of earlier records from Japan. *The Queensland Naturalist* 38: 24–30.
- Sluys R, Kawakatsu M (2005) Biodiversity of marine planarians revisited (Platyhelminthes, Tricladida, Maricola). *Journal of Natural History* 39: 445–467. <https://doi.org/10.1080/00222930410001671309>
- Sluys R, Kawakatsu M, Riutort M, Baguñà J (2009) A new higher classification of planarian flatworms (Platyhelminthes, Tricladida). *Journal of Natural History* 43: 1763–1777. <https://doi.org/10.1080/00222930902741669>
- Sluys R, Vila-Farré, M, Álvarez-Presas, M, Riutort, M, Kawakatsu, M, Tulp AS (2015) The diet and distribution of *Pentacoelum kazukolinda* (Kawakatsu & Mitchell, 1984), a maricolan planarian with a freshwater ecology. *Zoologica Scripta* 44: 72–91. <https://doi.org/10.1111/zsc.12084>
- Souza S, Riutort M, Ferreira RL, Leal-Zanchet A (2018) An integrative taxonomic approach reveals the first marine triclad (Platyhelminthes) trapped in a cave from a semiarid Neotropical environment. *Invertebrate Systematics* 32: 627–638. <https://doi.org/10.1071/IS17062>
- Stamatakis A (2014) RAxML version 8: a tool for phylogenetic analysis and post-analysis of large phylogenies. *Bioinformatics* 30(9): 1312–1313. <https://doi.org/10.1093/bioinformatics/btu033>
- Winsor L, Sluys R (2018) Basic histological techniques for planarians. In: Rink J (Ed.) *The planarian model system: Methods and Protocols*. Springer Science+Business Media, New York, 285–351. https://doi.org/10.1007/978-1-4939-7802-1_9

A revision of the subgenus *Dudaica* Strand of the genus *Drosophila* Fallén, with descriptions of six new species (Diptera, Drosophilidae)

Takehiro K. Katoh^{1,*}, Guang Zhang^{1,*}, Masanori J. Toda²,
Awit Suwito³, Jian-Jun Gao^{1,4}

1 State Key Laboratory for Conservation and Utilization of Bioresources in Yunnan, Yunnan University, 2 Cuihubeilu, Kunming, Yunnan 650091, China **2** Hokkaido University Museum, Hokkaido University, N10, W8, Kita-ku, Sapporo 060-0810, Japan **3** Zoology Division (Museum Zoologicum Bogoriense), Research Center for Biology-LIPI, Cibinong, Bogor 16911, Indonesia **4** Laboratory of Ecology and Evolutionary Biology, Yunnan University, 2 Cuihubeilu, Kunming, Yunnan 650091, China

Corresponding author: Jian-Jun Gao (gaojj@ynu.edu.cn)

Academic editor: R. Meier | Received 11 June 2018 | Accepted 17 July 2018 | Published 9 August 2018

<http://zoobank.org/8035F589-CED1-4CC3-AE43-B737FF782157>

Citation: Katoh TK, Zhang G, Toda MJ, Suwito A, Gao J-J (2018) A revision of the subgenus *Dudaica* Strand of the genus *Drosophila* Fallén, with descriptions of six new species (Diptera, Drosophilidae). ZooKeys 781: 19–50. <https://doi.org/10.3897/zookeys.781.27354>

Abstract

The subgenus *Dudaica* Strand of the genus *Drosophila* Fallén has been known to comprise only two species: *Drosophila (Dudaica) senilis* Duda, 1926 (recorded from Indonesia, Philippines, Vietnam, Bhutan, and India) and *D. malayana* (Takada, 1976) (recorded from Malaysia). In the present study, this subgenus is revised, with *D. malayana* redescribed and six new species discovered and described from China, Malaysia, and Indonesia: *gracilipalpis* Katoh & Gao, **sp. n.**, *puberula* Katoh & Gao, **sp. n.**, *albipalpis* Katoh, Toda & Gao, **sp. n.**, *qiongzhouensis* Katoh & Gao, **sp. n.**, *orthophallata* Katoh, Toda & Gao, **sp. n.**, and *dissimilis* Katoh & Gao, **sp. n.** Both morphological and molecular data (DNA barcodes) are used to distinguish the above species. A key to species of this subgenus is provided.

Keywords

China, DNA barcoding, Southeast Asia, taxonomy

* Authors contributed equally to this study.

Introduction

Duda (1926) established the monotypic subgenus *Macropalpus* Duda (type species: *Drosophila senilis* Duda, 1926 from Sumatra) in the genus *Drosophila* Fallén, and defined it by the following diagnostic characters: (1) palpus distinctly large, long and broad, lacking prominent setae, (2) scutellum large, apically broadly rounded, and (3) costal break turned inwards onto thickened end of R_1 . Later, Strand (1943) proposed *Dudaica* as a replacement name of the subgenus *Macropalpus*, since the name *Macropalpus* had been preoccupied. In a revision of the genus *Zygothrica* Wiedemann, Grimaldi (1990a) transferred *Z. malayana* Takada, 1976 from *Zygothrica* into *Drosophila* (*Dudaica*), referring to Takada's (1976) original description, and mentioned that an undetermined species of *Dudaica*, but distinct from *malayana*, was present in New Guinea. According to previous records, *D. senilis* is widely distributed in the Oriental region, from not only Sumatra (the type locality) but also the Philippines and Java (Wheeler 1981), India (Gupta and Sundaran 1990), Bhutan (De and Gupta 1996), and Vietnam (Sidorenko 1996).

The phylogenetic position of the subgenus *Dudaica* remains unresolved. Grimaldi (1990b) proposed a revised phylogenetic classification of the family Drosophilidae, based on a cladistic analysis for a set of 120 species (including *D. senilis*) representing genera and subgenera of the family. Grimaldi's final consensus cladogram placed *D. senilis* most close to *D. (Drosophila) monochaeta* Sturtevant, 1927, and both formed a cluster with *Idiomyia* s. lat. However, he was "not confident of the homologies for the two features suggesting this relationship [reduction in number of interfrontal setulae (ap. 67) and a reduced, simple spermatheca (ap. 217)]". Yassin (2013) revised the subgeneric classification of *Drosophila* in light of molecular and morphological data, and proposed diagnoses for the subgenera, including *Dudaica*. However, his proposal that *Dudaica* is closely related to the genera *Hirtodrosophila* Duda, *Paraliodrosophila* Duda and *Zygothrica* was elicited solely by a single morphological trait, i.e., the shape of the "gonopods", but not by molecular data.

In this paper, we revise the subgenus *Dudaica*, and add six new species discovered from China, Malaysia, and Indonesia to this subgenus, by identifying them with the aid of DNA sequences of the 658-bp barcoding region of the mitochondrial COI (cytochrome *c* oxidase subunit I) gene. We also redescribe the known species *D. malayana*, based on specimens newly collected from Malaysia and Indonesia. Finally, a key to all the eight species of *Dudaica* is given.

Materials and methods

All specimens employed in the present study were collected from China, Malaysia, and Indonesia (Table 1). They were mostly captured from herb layer in forest by net sweeping, and preserved immediately in either 70% or 100% ethanol for morphological observation and DNA sequencing, respectively.

Specimens were first identified as of the subgenus *Dudaica*, based on their overall resemblance to the two known species of this subgenus, *D. senilis* and *D. malayana*, especially in body color pattern, shape of palpus, and structures of male/female terminalia. The holotype specimen of *D. malayana* was examined for the reference. As for *D. senilis*, we referred to Duda's (1926) original description, Gupta and Sundaran's (1990) redescription of terminalia, and Grimaldi's (1990b) character states in his cladistic analysis. All specimens were then sorted into known or putatively new species in light of morphology. For this, external morphology was examined, numbers of morphometric characters were measured, and detailed structures in male/female terminalia, head and mouth parts were observed by the same methods as in Li et al. (2014).

The specimens were then subjected to DNA barcoding analysis (Hebert et al. 2003), with total DNA extracted from a right hind- or mid-leg, or small piece(s) of abdominal tissue picked from the abdominal dissection cut, using the TIANamp® Genomic DNA Kit. DNA sequences of the 658-bp barcoding region of the mitochondrial COI gene were then amplified with the Folmer et al.'s (1994) primer pair, following the procedures as in Li et al. (2014). The PCR products were purified and sequenced with ABI3730 sequencer. The obtained DNA sequences were edited and aligned in the SeqMan module of the DNASTar package (DNASTar Inc. 1996) and MEGA7 (Kumar et al. 2016), respectively. A molecular phylogenetic tree was constructed by using Bayesian Inference (BI) method in MrBayes v3.2.6 (Ronquist et al. 2012), with the sequence data partitioned into two subsets by codon position, i.e., 1st+2nd codon positions and 3rd codon position. In BI, two independent runs of MCMC with four chains each (three heated and one cold) were conducted simultaneously for 5,000,000 generations, and trees were sampled every 100 generations. The analysis was stopped after verifying convergence statistics using Tracer v1.6 (Rambaut et al. 2014), and the first 20% of the tree samples were discarded as burn-in. Nucleotide substitution model was determined for each data set using jModelTest 2.1.10 (Guindon and Gascuel 2003, Darriba et al. 2012) using the Bayesian Information Criterion (BIC; Schwarz 1978). In addition, we employed the Automatic Barcode Gap Discovery (ABGD; Puillandre et al. 2012) and the General Mixed Yule-coalescent (GMYC; Pons et al. 2006) analyses for the molecular species delimitation. The ABGD analysis was run on the web-interface (<http://www.wabi.snv.jussieu.fr/public/abgd/abgdweb.html>) with the default settings [$P_{\min} = 0.001$, $P_{\max} = 0.1$, Steps = 10, X (a proxy for minimum gap width) = 1.5, Nb bins (for distance distribution) = 20]. All three distances applicable in the web-interface, JC69 (Jukes and Cantor 1969), K2P (Kimura 1980), and simple distances (i.e., p-distances) were used for the analyses. The GMYC was performed using the package "splits" (<http://r-forge.r-project.org/projects/splits>) in R, with the single-threshold strategy and default scaling parameters. An ultrametric tree for the GMYC was generated by BEAST v2.4.5 (Bouckaert et al. 2014) using the Yule prior and the HKY (Hasegawa et al. 1985) with a proportion of invariable sites (+I) model, with 5,000,000 MCMC generations. In addition, the intra- and inter specific p-distances for the species in *Dudaica* were calculated with MEGA7 and summarized.

Table I. List of species and specimens examined in the present study.

Species	Sex	Voucher # ^a	Collection site	Elevation (m)	Collection date	GenBank accession #
<i>malayana</i> (Takada, 1976)	♂	#03903	Poring, Sabah, Malaysia	600	20.iii.2008	MH410612
	♂	#03904	Ditto	600	13.iii.2008	MH410613
	♀	n/a	Gunung Poteng, West Kalimantan, Indonesia	220	4.xii.1996	n/a
<i>gracilpalpis</i> sp. n.	♂	#00033	Xishuangbanna Tropical Botanical Garden, Mengla, Xishuangbanna, Yunnan, China	650	19.iii.2006	MH410614
	♂	#03423	Ditto	650	27–28. ix.2011	MH410620
	♂	#06001	Ditto	650	28.ix.2011	MH410624
	♂	#00484	Wangtianshu, Mengla, Xishuangbanna, Yunnan, China	670	22–25.iv.2007	MH410615
	♂	#00491	Ditto	670	30.ix.2011	MH410617
	♂	#03364	Ditto	670	30.ix.2011	MH410619
	♂	#03424	Ditto	670	30.ix.2011	MH410621
	♂	#03425	Ditto	670	30.ix.2011	MH410622
	♀	#00485	Ditto	670	22–25.iv.2007	MH410616
	♀	#00492	Ditto	670	30.ix.2011	MH410618
	♂	#03902	Bogor, West Java, Indonesia	260	14–15.xi.2009	MH410623
<i>puberula</i> sp. n.	♂	#03365	Xishuangbanna Tropical Botanical Garden, Mengla, Xishuangbanna, Yunnan, China	650	27–28. ix.2011	MH410626
	♀	#03426	Ditto	650	19.iii.2006	MH410631
	♂	#00480	Wangtianshu, Mengla, Xishuangbanna, Yunnan, China	670	22–25.iv.2007	MH410625
	♂	#03366	Ditto	670	30.ix.2011	MH410627
	♂	#03367	Ditto	670	30.ix.2011	MH410628
	♂	#03368	Ditto	670	30.ix.2011	MH410629
	♂	#03369	Ditto	670	30.ix.2011	MH410630
<i>albipalpis</i> sp. n.	♂	#03908	Cikaniki, Gunung Halimun, West Java, Indonesia	1050	4.xi.2009	MH410632
<i>qiongzhouensis</i> sp. n.	♂	#03310	Jianfengling National Nature Reserve, Ledong, Hainan, China	750	17–20.iv.2008	MH410633
	♂	#03311	Ditto	750	17–20.iv.2008	MH410634
	♂	#03312	Ditto	750	17–20.iv.2008	MH410635
	♂	#03418	Ditto	750	17–20.iv.2008	MH410639
	♂	#03419	Ditto	750	17–20.iv.2008	MH410640
	♂	#03420	Ditto	750	17–20.iv.2008	MH410641
	♀	#03313	Ditto	750	17–20.iv.2008	MH410636
	♀	#03314	Ditto	750	17–20.iv.2008	MH410637
	♀	#03315	Ditto	750	17–20.iv.2008	MH410638
	♀	#03422	Ditto	750	17–20.iv.2008	MH410642
<i>orthophallata</i> sp. n.	♂	#00177	Ulu Senagang, Crocker Range, Sabah, Malaysia	540	18.x.1999	n/a
	♀	#03905	Park Headquarters, Mt. Kinabalu, Sabah, Malaysia	1700	11.iii.2008	MH410644
	♀	#03906	Ditto	1700	11.iii.2008	MH410645
<i>dissimilis</i> sp. n.	♂	#00430	Hesong, Xiding, Menghai, Xishuangbanna, Yunnan, China	1900	7.iv.2011	MH410646

^a Numbers in bold indicate holotypes of new species.

For species illustration, the external morphology and detailed structures of male and female terminalia, and head and mouth parts were microphotographed using a Dino-Lite® Microscope Eyepiece Camera (ANMO Electronics Corporation). We followed McAlpine (1981) for morphological terminology, and Zhang and Toda (1992) for definitions of measurements and indices. The examined specimens are deposited in the following institutions:

- KIZ** Kunming Natural History Museum of Zoology, Kunming Institute of Zoology, Chinese Academy of Sciences, Kunming, China
KPSP Kinabalu Park, Sabah Parks, Sabah, Malaysia
ITBC Institute for Tropical Biology and Conservation, Universiti Malaysia Sabah, Kota Kinabalu, Sabah, Malaysia
MZB Museum Zoologicum Bogoriense, Bogor, Indonesia
SEHU Systematic Entomology, The Hokkaido University Museum, Hokkaido University, Sapporo, Japan

Results

A total of 34 COI sequences of 658-bp were determined in this study (Table 1). We failed to determine the COI sequence for the male specimen #00177 (of *D. orthophallata* sp. n. to be described here), probably due to poor quality of the total DNA extracted from this specimen, which was collected in 1999. Also, one female specimen of *D. malayana*, which was the oldest one examined here, was not used for DNA analysis. The HKY+I model was selected for both of the '1st+2nd codon positions' and '3rd codon position' partitions as the best nucleotide substitution model for BI analysis.

Figure 1 illustrates the unrooted BI tree built with the 34 COI sequences and the results for the molecular species delimitation. The ABGD and GMYC analyses resulted in the same hypothesis: the studied sequences were sorted into seven hypothetical species, except for at P (prior intraspecific divergence) = 0.001 in ABGD using JC69 and K2P distances where eight species including a paraphyletic one were proposed. These seven Molecular Operational Taxonomic Units (hypothetical species) were supported by morphological data as well. In addition, the highest intraspecific (i.e., within-lineage) p -distance was 0.0163, while the lowest interspecific (i.e., among-lineage) p -distance was 0.0796, indicating a broad barcoding gap (Table 2). Thus, in consequence of integrative species delineation based on molecular and morphological data, we recognized seven (one known and six new) species within our studied samples of the subgenus *Dudaica*: *D. malayana* (Takada, 1976), *D. gracilipalpis* sp. n., *D. puberula* sp. n., *D. albipalpis* sp. n., *D. qiongzhouensis* sp. n., *D. orthophallata* sp. n., and *D. dissimilis* sp. n.

Among them, *D. qiongzhouensis* sp. n. and *D. albipalpis* sp. n. are very similar in morphology to each other. The diagnoses for these species are supplemented with

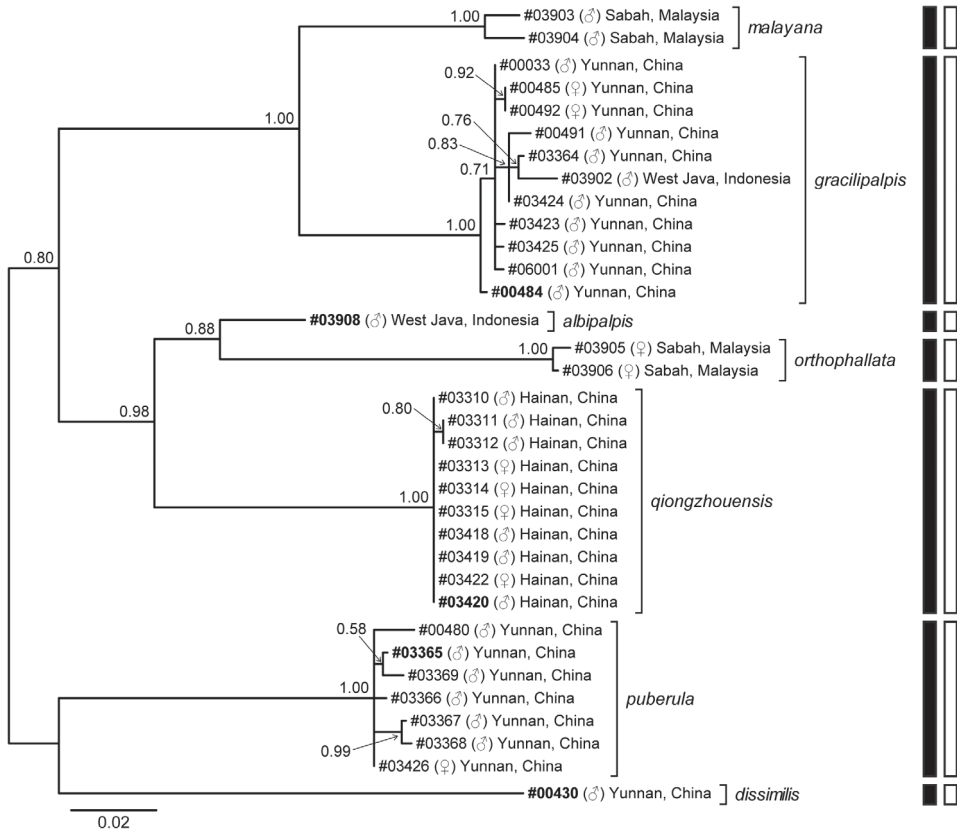


Figure 1. Bayesian tree of seven species of the subgenus *Dudaica* based on COI gene sequences, with indication of the results of molecular species delimitation by the ABGD (solid bars) and GMYC (open bars) analyses. Label of each operational taxonomic unit (OTU) is given in the format of “voucher number (gender) province of collection locality” (bold voucher numbers: holotype specimens). Numbers beside nodes are posterior probabilities.

“pure” molecular diagnostic characters, which are defined as sites with fixed status in the COI sequence alignments within the focal species but differing from the other species (Sarkar et al. 2002, DeSalle et al. 2005) (Table 3).

Taxonomy

Subgenus *Dudaica* Strand, 1943

Dudaica Strand, 1943: 212. New name for *Macropalpus* Duda.

Macropalpus Duda, 1926: 63. Type species: *Drosophila senilis* Duda, 1926. Preoccupied by *Macropalpus* Ratzeburg, 1844 (Braconidae). Proposed as a subgenus.

Table 2. Summary of intra- and interspecific p-distances.

Species	Intraspecific distance		Interspecific distance ^b						
	Mean (SE) ^a	Range	1	2	3	4	5	6	7
1. <i>malayana</i> (Takada)	0.0163 (n/a)	0.0163		0.0796-0.0906	0.1279-0.1378	0.1195-0.1248	0.1262-0.1356	0.1343-0.1392	0.1230-0.1244
2. <i>gracilipalpis</i> sp. n.	0.0057 (0.0014)	0.0000-0.0144	0.0832 (0.0106)		0.1260-0.1386	0.1125-0.1172	0.1225-0.1279	0.1431-0.1528	0.1293-0.1335
3. <i>puberula</i> sp. n.	0.0089 (0.0023)	0.0015-0.0152	0.1321 (0.0128)	0.1329 (0.0132)		0.0949-0.1004	0.1231-0.1262	0.1254-0.1336	0.1227-0.1277
4. <i>albipalpis</i> sp. n.	n/a	n/a	0.1221 (0.0129)	0.1143 (0.0129)	0.0964 (0.0114)		0.0844-0.0861	0.0870-0.0896	0.1215
5. <i>qiongzhouensis</i> sp. n.	0.0005 (0.0005)	0.0000-0.0015	0.1304 (0.0130)	0.1245 (0.0115)	0.1248 (0.0123)	0.0858 (0.0113)		0.1135-0.1184	0.1178
6. <i>orthophallata</i> sp. n.	0.0035 (n/a)	0.0035	0.1361 (0.0138)	0.1456 (0.0143)	0.1297 (0.0137)	0.0883 (0.0114)	0.1154 (0.0134)		0.1360-0.1385
7. <i>dissimilis</i> sp. n.	n/a	n/a	0.1237 (0.0133)	0.1313 (0.0127)	0.1260 (0.0126)	0.1215 (n/a)	0.1178 (0.0124)	0.1373 (0.0144)	

^a SE, standard error; ^b Values of mean p-distance (SE) below diagonal, value ranges of p-distance above diagonal.

Table 3. Selected diagnostic nucleotide sites (indicated in square brackets) for *D. albipalpis* sp. n. and *D. qiongzhouensis* sp. n. in the COI sequences. Sequences of the other five species in the subgenus *Dudaica* are shown for comparison.

Species	Sequence	Diagnostic nucleotide sites				
		92	226	391	589	
<i>albipalpis</i> sp. n.	#03908	T	T	[C]	[T]	
	#03310	[C]	[C]	T	C	
	#03311	[C]	[C]	T	C	
	#03312	[C]	[C]	T	C	
	#03313	[C]	[C]	T	C	
	<i>qiongzhouensis</i> sp. n.	#03314	[C]	[C]	T	C
		#03315	[C]	[C]	T	C
		#03418	[C]	[C]	T	C
		#03419	[C]	[C]	T	C
#03420		[C]	[C]	T	C	
#03422		[C]	[C]	T	C	
<i>malayana</i> (Takada)		#03903	T	T	T	C
	#03904	T	T	T	C	
<i>gracilipalpis</i> sp. n.	#00484	T	T	T	C	
	#00033	T	T	T	C	
	#00485	T	T	T	C	
	#00491	T	T	T	C	
	#00492	T	T	T	C	
	#03364	T	T	T	C	
	#03423	T	T	T	C	
	#03424	T	T	T	C	
	#03425	T	T	T	C	
	#03902	T	T	T	C	
	#06001	T	T	T	C	
<i>puberula</i> sp. n.	#00480	T	T	T	C	
	#03365	T	T	T	C	
	#03366	T	T	T	C	
	#03367	T	T	T	C	
	#03368	T	T	T	C	
	#03369	T	T	T	C	
<i>orthophallata</i> sp. n.	#03426	T	T	T	C	
	#03905	T	T	T	C	
<i>dissimilis</i> sp. n.	#03906	T	T	T	C	
	#00430	T	T	T	C	

Diagnosis. Head, scutum, and scutellum mostly milky white, contrasting with mostly dark brown thoracic pleura (Figures 2–4). Scutellum large, more or less rounded apically in dorsal view (Figures 2, 3). Wing fuscous, somewhat wavy (Figures 2, 3).

Common characters. *Head* (Figures 2–9): Eye red, with dense interfacetal setulae; longest axis of eye slightly oblique (nearly rectangular in *dissimilis* sp. n.) against body axis. Ocellar triangle convex; ocellar setae inserted outside triangle made by ocelli. Anterior reclinate orbital seta situated slightly before proclinate orbital seta or just lateral to it (between proclinate and posterior reclinate orbital setae in *dissimilis* sp. n.) (Figure 4). Pedicel dorsolaterally dark brown (Figure 4); first flagellomere pubescent; arista with 6–8 dorsal and 2–4 ventral branches in addition to terminal bifurcation; terminal bifur-

cation moderate. Facial carina high, broad. Gena anteriorly dark brown. Occiput ventrally dark brown. Postgena medially dark brown. Postocellar setae present (Figure 5). Supracervical setae tapered, thin, apically curved and slightly blunt (Figure 5). Cibarium not thickened on anterior margin in lateral view (slightly thickened in *dissimilis* sp. n.); anterior portion slightly dilated; anterolateral corners slightly protruded; dorsal wall pear-shaped, with posterior portion oval; anterior sensilla four, arranged in square; medial sensilla apically sharp, arranged in anteriorly slightly convergent rows; posterior sensilla apically blunt, arranged in anteriorly divergent rows (Figures 6, 7). Clypeus thick at median portion (except for *dissimilis* sp. n.) (Figures 6, 7). Palpus distinctly large, long and broad (Figures 4, 9) (except for *dissimilis* sp. n.), pubescent, setigerous, distally flat (except for *dissimilis* sp. n.) (Figures 9). Prementum dark brown, swollen at the distal end in lateral view (Figure 8). Labellum with five pseudotracheae per side.

Thorax (Figures 2, 3): Postpronotal lobe with 1–3 prominent (lowermost the longest) and 0–4 short setae. Scutum narrowly dark brown along antermost margin. Thoracic pleura mostly covered with broad, dark brown, more or less blurry, longitudinal stripes (except for *dissimilis* sp. n.). Basal scutellar setae divergent; apical scutellar setae cruciate. Acrostichal setulae in six, somewhat regular rows. Mid katepisternal seta much shorter than anterior and posterior ones, but distinct from setulae in row below it; caudoventral corner of katepisternum with one long, prominent seta.

Wing (Figures 2, 3) pale grayish yellow to grayish yellow, elliptic, rounded distally (not so elliptic in *dissimilis* sp. n.), wrinkled especially at basal portion of R_{4+5} ; longitudinal veins brown except for R_{2+3} (pale brown), basal section of M_1 (dark brown), and CuA_1 (dark brown) (except for *dissimilis* sp. n.); crossveins shaded at r-m and dm-cu; C_1 setae two, subequal; R_{2+3} distally slightly curved to costa; R_{4+5} basally diverged from M_1 , distally nearly parallel with M_1 ; M_1 more or less sinuate; A_1 well developed, as stout as other veins. Halter entirely grayish yellow to grayish brown.

Legs (Figures 2, 3, 10A, 11A) pale grayish yellow to grayish brown. Preapical dorsal setae present on tibiae of all legs; apical setae present on fore- and mid-leg tibiae. Fore-leg first tarsomere with one subproximal and one apical, short, black spines.

Abdomen (Figures 2, 3): Tergite 1 nearly entirely dark brown, 2 to 6 pale yellow, each with anterior and caudal dark brown bands; anterior bands medially sometimes interrupted; caudal bands medially and laterally extended anteriorad (except for *dissimilis* sp. n.). Female tergite 7 nearly entirely pale yellow. Sternites somewhat quadrate, grayish brown to dark brown.

Male terminalia (Figures 10B–K, 11B–L, 12A–K, 13, 14A–K, 15A–H, 16): Epandrium pale brown, pubescent except for anterior sub-dorsal to -ventral margin, ventrally narrowed, ventroapically rounded, with setae on caudodorsal and ventral portions; lobe-like apodeme present anterosubdorsally. Cercus dark brown, nearly entirely pubescent, separated from epandrium, caudoventrally with distinct process (except for *senilis* and *dissimilis* sp. n.). Surstylus more or less quadrangular; dorsoproximal portion broadly fused to epandrium, with sclerotized ridge connecting epandrium and surstylus (except for *dissimilis* sp. n.); outer surface not pubescent, anterosubmedially concaved; caudal margin with a slightly sinuate row of peg-like, apically more or less roundish prensisetae decreasing in size ventrally; ventral portion with apically pointed

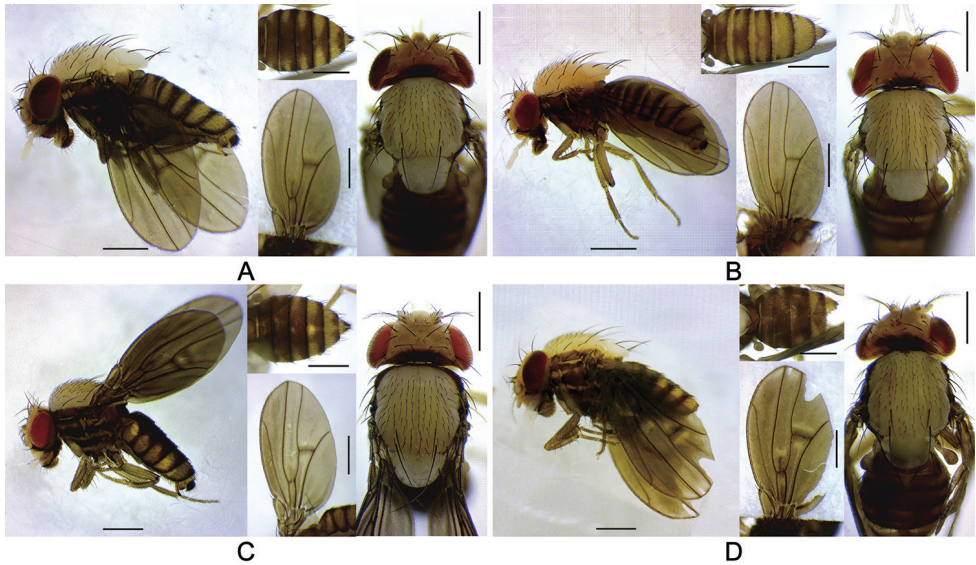


Figure 2. Left lateral habitus, thorax, wing, and abdomen of *Dudaica* species (part 1). **A** *malayana* (Takada) (#03904) **B** *gracilipalpis* sp. n. (paratype #03902) **C** *puberula* sp. n. (holotype #03365) **D** *albipalpis* (holotype #03908). Scale bars: 0.5 mm.

spines on either inner or outer surface: spines on inner, subventral surface longer, somewhat curved upwards. Tenth sternite pale brown, moderately sclerotized, antero-medially wrinkled (flat in *dissimilis* sp. n.). Hypandrium narrowly triangular (except for *orthophallata* sp. n. and *dissimilis* sp. n.), anteriorly with narrow, well developed apodeme, not pubescent (except for *malayana*, *gracilipalpis* sp. n., and *puberula* sp. n.), caudolaterally with a pair of somewhat expanded lobes; a pair of paramedian setae present on the portion fused to paramere. Paramere elongated, apically rounded in ventral view (except for *puberula* sp. n.), ventrosubapically with 1–2 sensilla (three in *dissimilis* sp. n.), basally fused to aedeagus, ventrally fused to hypandrium. Aedeagus rod-like, fused to aedeagal apodeme, pale brown to brown, apically darker, slightly curved dorsad (straight in *orthophallata* sp. n.); aedeagal guide and basal processes absent; apodeme anteriorly expanded in lateral view, shorter than aedeagus.

Female terminalia (Figures 10L–N, 11M–O, 12L–N, 14L–N, 15I, J): Tergite 8 pale brown, pubescent dorsally to caudolaterally. Epiproct dark brown, entirely pubescent. Hypoproct dark brown, laterally pubescent. Sternite 7 grayish brown, caudally darker, caudomedially deeply notched, nearly entirely pubescent; setae on caudal portion rather long. Oviscapt valve with stout lateral and marginal ovisensilla increasing in size posteriad; apical ovisensillum stout and the largest, bent outwards. Spermathecal capsule pale brown, spherical.

Included species. *senilis* Duda, *malayana* (Takada), *gracilipalpis* Katoh & Gao, sp. n., *puberula* Katoh & Gao, sp. n., *albipalpis* Katoh, Toda & Gao, sp. n., *qiongzhouensis* Katoh & Gao, sp. n., *orthophallata* Katoh, Toda & Gao, sp. n., and *dissimilis* Katoh & Gao, sp. n.

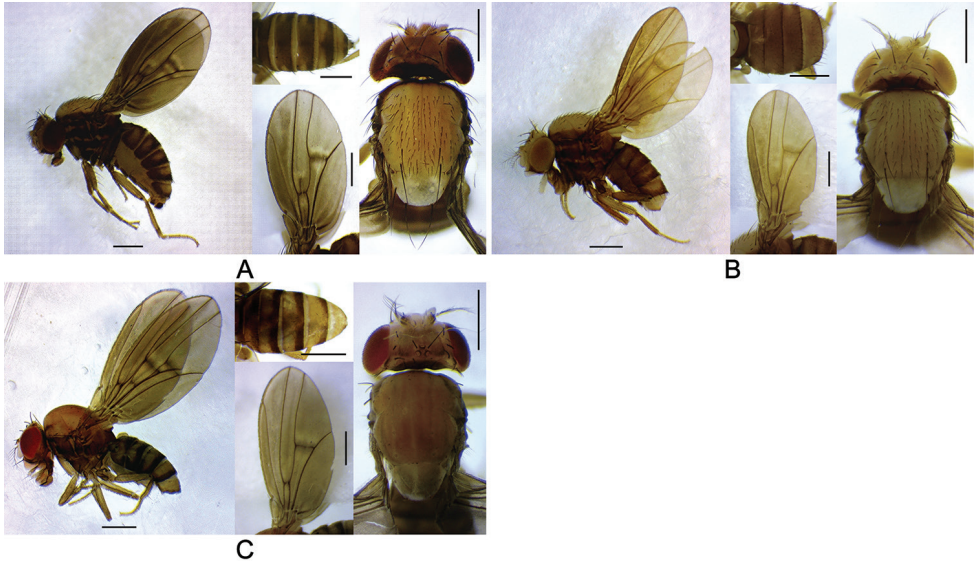


Figure 3. Left lateral habitus, thorax, wing, and abdomen of *Dudaica* species (part 2). **A** *qiongzhouensis* (holotype #03420) **B** *orthophallata* sp. n. (holotype #00177) **C** *dissimilis* (holotype #00430). Scale bars: 0.5 mm.

Key to the species

In this key, not only morphological characters but also the selected “pure” diagnostic nucleotide sites of COI are used to distinguish between *albipalpis* sp. n. and *qiongzhouensis* sp. n. (see also Table 2). The numbers of cited figures of Duda (1926) and Gupta and Sundaran (1990) are given as figure D26 and figure G&S90, respectively.

- 1 Palpus sinuate, with several stout setae only on basal portion (Figures 4A, B, 9A, B; figure D26–13) **2**
- Palpus nearly straight, with several stout setae scattered on entire length (Figures 11C–G, 16C–G) **4**
- 2 Cercus without distinct caudoventral process (figure G&S90–2E) *senilis* Duda, 1926
- Cercus with distinct caudoventral process (Figures 10F, 11F) **3**
- 3 Foreleg tibia with two apical setae (Figure 10A) *malayana* (Takada, 1976)
- Foreleg tibia with one apical seta (Figure 11A) *gracilipalpis* Katoh & Gao, sp. n.
- 4 Palpus medio- to baso-laterally dark grayish brown, with one apical, stout, prominent seta (Figure 9G); postpronotal lobe brownish white in upper half, dark brown in lower half (Figure 3C); notopleuron brownish white (Figure 3C); cercus without caudoventral process (Figure 16C, E) *dissimilis* Katoh & Gao, sp. n.
- Palpus entirely white, without apical, prominent seta (Figure 9C–F); postpronotal lobe entirely dark brown (Figures 2C, D, 3A, B); notopleuron dark

- brown (Figures 2C, D, 3A, B); cercus with distinct caudoventral process (Figures 12–14E, 7C) **5**
- 5 Palpus with 3–4 prominent, stout setae on outer, lateral surface (Figure 9C); hypandrium pubescent on the portion fused to paramere (Figure 12I, J); paramere apically sharp (Figure 12I–K); female abdominal tergite 8 caudodorsally lacking setae..... ***puberula* Katoh & Gao, sp. n.**
- Palpus with many setae varied in size on outer, lateral surface (Figure 9D–F); hypandrium not pubescent; paramere apically round in ventral view, round or truncate in lateral view (Figures 13J, K, 14J, K, 15G, H); female abdominal tergite 8 caudodorsally with 3–4 setae **6**
- 6 Aedeagus apically without small, acute claw, subapically swollen in lateral view (Figure 15G); oviscapt valve with 17–19 marginal ovisensilla (Figure 15I, J) ***orthophallata* Katoh, Toda & Gao, sp. n.**
- Aedeagus apically with small, acute claw, subapically not swollen in lateral view (Figures 13H, I, 14H, I); oviscapt valve with ca. 14 marginal ovisensilla (Figure 14L, M) **7**
- 7 Palpus broad, flat, not so rod-shaped in lateral view (Figure 9D); paramere apically truncated in lateral view (Figure 13K); nucleotide status in COI sequence = T (thymidine), T, C (cytosine), and T at sites 92, 226, 391, and 589, respectively (Table 3) ***albipalpis* Katoh, Toda & Gao, sp. n.**
- Palpus slender, not so flat, somewhat rod-shaped in lateral view (Figure 9E); paramere apically rounded in lateral view (Figure 14K); nucleotide status in COI sequence = C, C, T, and C at sites 92, 226, 391, and 589, respectively (Table 3) ***qiongzhouensis* Katoh & Gao, sp. n.**

***Drosophila (Dudaica) malayana* (Takada, 1976)**

Figures 2A, 4–6A, 8A, 9A, 10

Zygothrica malayana Takada, 1976: 68.

Drosophila (Dudaica) malayana: Grimaldi 1990a: 30.

Specimens examined. MALAYSIA: 2♂ (holotype and paratype of *Zygothrica malayana* Takada, 1976), near Kuala Lumpur, Peninsular Malaysia, 3.vii.1972, H Takada (SEHU); 2♂, Poring, Sabah, 16.iii.1999, MJ Toda (KPSP, SEHU); 1♂ (#03904), same except for 13.iii.2008 (KIZ); 1♂ (#03903), same except for 20.iii.2008 (SEHU). INDONESIA: 1♂, 1♀, Gunung Poteng, West Kalimantan, 4.xii.1996, MJ Toda (MZB, SEHU).

Diagnosis. Palpus long, sinuate, with several stout setae only on basal portion (Figure 9A). Foreleg tibia with two apical setae (Figure 10A). Cercus with distinct caudoventral process (Figure 10F). Hypandrium pubescent on caudolateral lobes (Figure 10J).

Supplementary and revised description. Adult ♂ and ♀. *Head* (Figures 2A, 4–6A, 8A, 9A): Arista with 7–8 dorsal and four ventral branches. Supracervical setae

25–30 per side; postocular setae 15–16 per side. Cibarium with ca. eight medial and ca. ten posterior sensilla per side. Prementum with five (one proximal, two lateral, and two distal) pairs of setae.

Thorax (Figure 2A): Postpronotal lobe milky white in upper half, dark brown in lower half, with 2–3 prominent but no short setae. Right and left dorsocentral setae nearly parallel. Notopleuron milky white. Thoracic pleura with three, sometimes rather indistinct stripes.

Legs (Figures 2A, 10A): Foreleg first tarsomere shorter than total length of four succeeding tarsomeres. Mid- and hind-leg first tarsomeres shorter than or as long as total length of four succeeding tarsomeres.

Abdomen (Figure 2A): Anterior bands on tergite 6 medially broadly interrupted.

Male terminalia (Figure 10B–K): Epandrium with ca. three and ca. 13 long setae per side on caudodorsal and ventral portions, respectively. Cercus with 23–24 setae. Surstylus with ca. nine prensisetae and 7–8 ventral spines. Paramere apically rounded in lateral view, with 1–2 sensilla. Aedeagus dorsoapically with a small, acute claw; apodeme slightly longer than 1/2 length of aedeagus.

Female terminalia (Figure 10L–N): Tergite 8 with two small setae on ventral portion but no on caudodorsal portion. Oviscapt valve yellowish brown, with three lateral, 13 marginal ovisensilla, and four (three dorsal, one ventral) subterminal, inner, trichoid ovisensilla. Spermathecal capsule slightly longer than broad; introvert ca. 1/5 height of capsule.

Measurements (in mm): BL (straight distance from anterior edge of pedicel to tip of abdomen) = 2.13–2.39/2.27 (range in 2♂/1♀ specimens), ThL (distance from anterior notal margin to apex of scutellum) = 0.98–1.08/1.01, WL (distance from humeral cross vein to wing apex) = 1.78–1.92/1.73, WW (maximum wing width) = 0.89–0.96/0.86.

Indices. FW/HW (frontal width/head width) = 0.56–0.60 (range in 2♂ and 1♀ specimens), ch/o (maximum width of gena/maximum diameter of eye) = 0.08–0.12, pror (proclinate orbital seta/posterior reclinate orbital seta in length) = 0.61–0.62, rcorb (anterior reclinate orbital seta/posterior reclinate orbital seta in length) = 0.29–0.32, vb (subvibrissa/vibrissa in length) = 0.41–0.59, orbito (distance between proclinate and posterior reclinate orbital setae/distance between inner vertical and posterior reclinate orbital setae) = 0.50–0.67, dcl (anterior dorsocentral seta/posterior dorsocentral seta in length) = 0.64–0.71, sctl (basal scutellar seta/apical scutellar seta in length) = 0.95–0.98, sterno (anterior katepisternal seta/posterior katepisternal seta in length) = 0.59–0.74, dcp (distance between ipsilateral dorsocentral setae/distance between anterior dorsocentral setae) = 0.39–0.44, sctlp (distance between ipsilateral scutellar setae/distance between apical scutellar setae) = 0.94–1.09, C (2nd costal section between subcostal break and R_{2+3} /3rd costal section between R_{2+3} and R_{4+5}) = 1.75–1.81, 4c (3rd costal section between R_{2+3} and R_{4+5} /M₁ between r-m and dm-cu) = 1.25–1.36, 4v (M₁ between dm-cu and wing margin/M₁ between r-m and dm-cu) = 1.75–1.95, 5x (CuA₁ between dm-cu and wing margin/dm-cu between M₁ and CuA₁) = 2.12–2.25, ac (3rd costal section between R_{2+3} and R_{4+5} /distance between distal ends of R_{4+5} and M₁) =

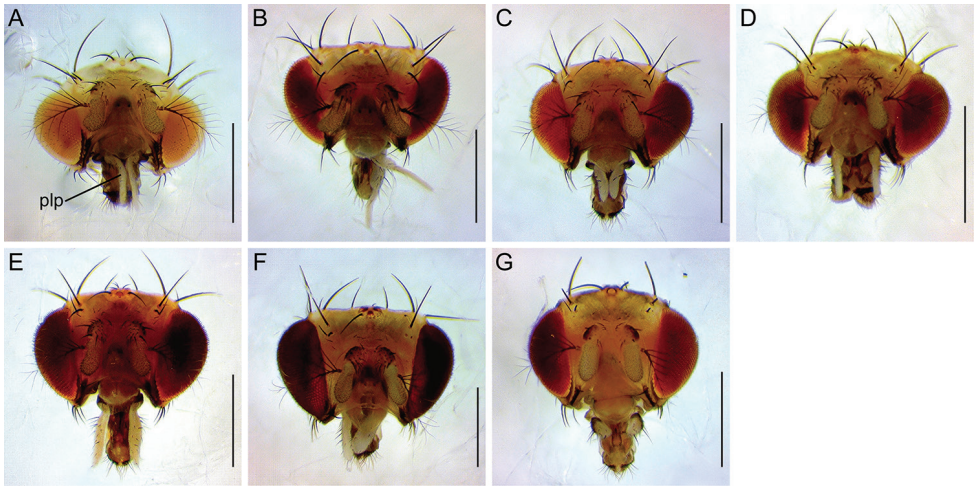


Figure 4. Head (anterior view). **A** *malayana* (Takada) (#03903) **B** *gracilipalpis* sp. n. (paratype #00492) **C** *puberula* sp. n. (paratype #03366) **D** *albipalpis* sp. n. (holotype #03908) **E** *qiongzhouensis* sp. n. (paratype #03313) **F** *orthophallata* sp. n. (paratype #03905) **G** *dissimilis* sp. n. (holotype #00430). Abbreviation: plp = palpus. Scale bars: 0.5 mm.

2.56–3.00, M (CuA_1 between dm-cu and wing margin/ M_1 between r-m and dm-cu) = 0.75–0.86, C3F (length of heavy setation in 3rd costal section/length of 3rd costal section) = 0.50–0.62.

Distribution. Malaysia (Peninsular Malaysia, Sabah*), Indonesia* (West Kalimantan). *New records.

Remarks. *Drosophila malayana* was originally described based only on male specimens collected from Peninsular Malaysia, with illustrations but only a very brief description of male terminalia (Takada 1976). We examined the type specimens of this species, and found that they share the following specific characters with the specimens collected from Borneo (Sabah and West Kalimantan): two strong setae present apically on foreleg tibia and distinctly pubescent caudolateral lobes of hypandrium. Based on these morphological characters, we identified the latter specimens as *D. malayana*, and described the female terminalia for the first time. However, our identification needs to be confirmed by DNA barcode data of additional specimens from the type locality in the future.

***Drosophila (Dudaica) gracilipalpis* Katoh & Gao, sp. n.**

<http://zoobank.org/A1FE2033-50A4-40D8-BAD0-0BA5B93B4890>

Figures 2B, 4–6B, 8B, 9B, 11

Type material. *Holotype* ♂ (#00484): CHINA: Wangtianshu, Mengla, Yunnan, ca. 670 m a.s.l., 22–25.iv.2007, JJ Gao (KIZ).

Paratypes. INDONESIA: 1♂ (#03902), Bogor, West Java, 14–15.xi.2009, MJ Toda (MZB). CHINA: 1♂ (#00033), Xishuangbanna Tropical Botanical Garden,

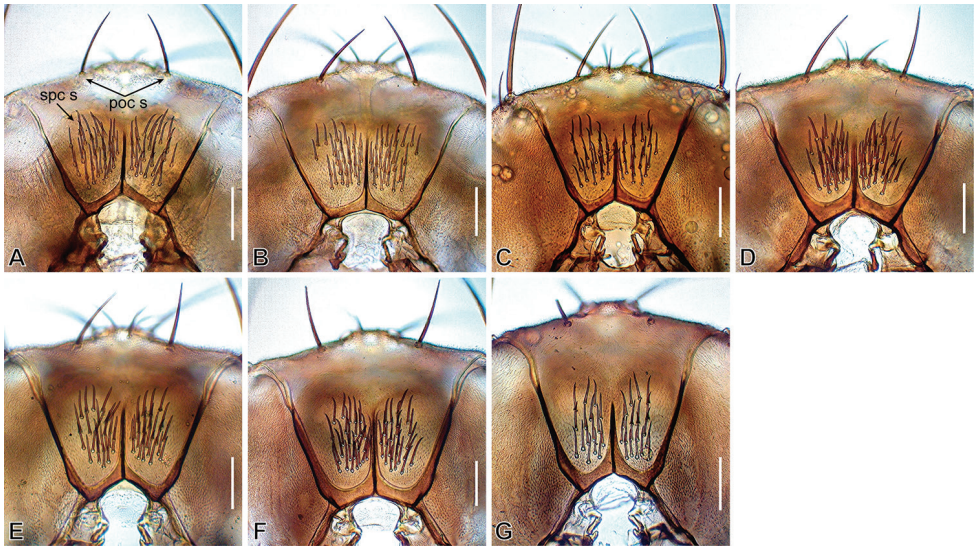


Figure 5. Postocciput (caudal view). **A** *malayana* (Takada) (#03903) **B** *gracilipalpis* sp. n. (paratype #00492) **C** *puberula* sp. n. (paratype #03366) **D** *albipalpis* sp. n. (holotype #03908) **E** *qiongzhouensis* sp. n. (paratype #03313) **F** *orthophallata* sp. n. (paratype #03905) **G** *dissimilis* sp. n. (holotype #00430). Abbreviations: poc s = postocellar setae, spc s = supracerical setae. Scale bars: 0.1 mm.

Mengla, Yunnan, ca. 650 m a.s.l., 19.iii.2006, MJ Toda & KT Takano (KIZ); 1♂ (#03423), same except for 27–28.ix.2011, JJ Gao (KIZ); 1♂ (#06001), same except for 28.ix.2011, JJ Gao (KIZ); 1♀ (#00485), same data as holotype (KIZ); 4♂, 1♀ (#00491, #00492, #03364, #03424, #03425), same except for 30.ix.2011 (KIZ).

Diagnosis. Palpus long, sinuate, with several stout setae only on basal portion (Figure 9B). Foreleg tibia with one apical seta (Figure 11A). Cercus with distinct caudoventral process (Figure 11F). Hypandrium pubescent, but very indistinctly, on caudolateral lobes (Figure 11J).

Description (characters in common with *D. malayana* not repeated). Adult ♂ and ♀. **Head** (Figures 2B, 4–6B, 8B, 9B): Arista with 7–8 dorsal and 3–4 ventral branches. Supracerical setae 26–27 per side; postocular setae 12–14 per side. Cibarium with ca. ten medial and ca. nine posterior sensilla per side. Prementum with six (one proximal, three lateral, and two distal) pairs of setae.

Thorax (Figure 2B): Postpronotal lobe with two prominent and rarely 1–2 short setae. Stripes on thoracic pleura mostly confluent with each other.

Abdomen (Figure 2B): Anterior bands on tergites 5 and/or 6 (and 7 in female) medially broadly interrupted.

Male terminalia (Figure 11B–L): Epandrium with ca. two and 10–12 long setae per side on caudodorsal and ventral portions, respectively. Cercus with 22–24 setae. Surstylus with 8–9 prenisetae and ca. seven ventral spines. Paramere ventrosubapically with one sensillum (longer in Indonesian specimen than in Chinese ones). Aedeagal apodeme ca. 1/2 length of aedeagus.

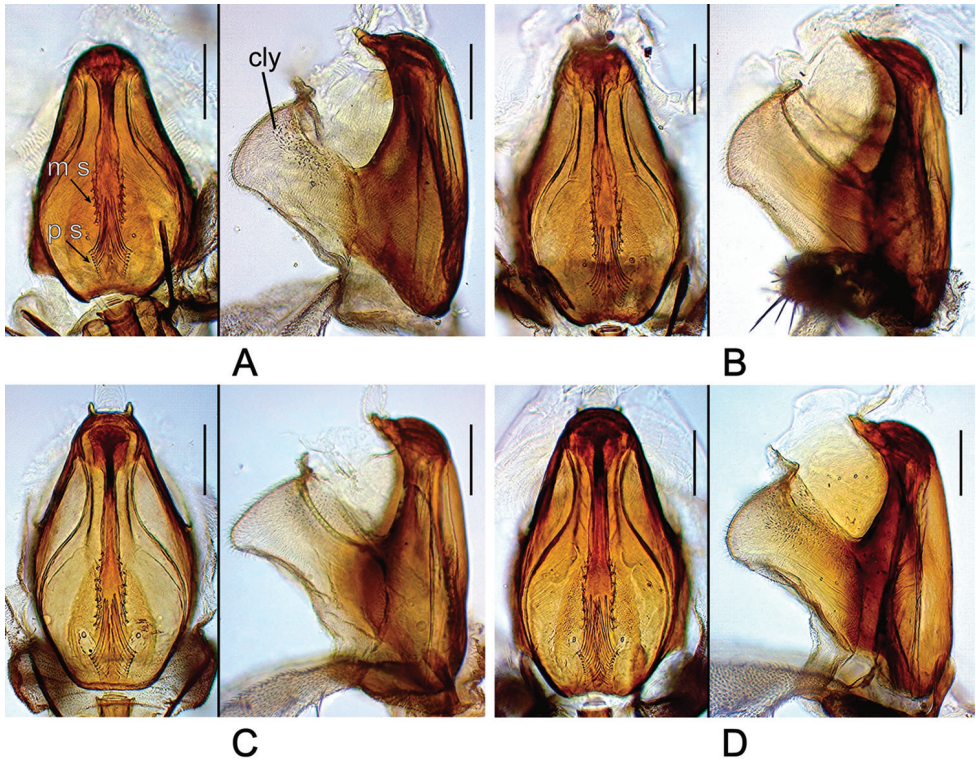


Figure 6. Cibarium of *Dudaica* species (part 1; dorsal and lateral views). **A** *malayana* (Takada) (#03903) **B** *gracilipalpis* sp. n. (paratype #00492) **C** *puberula* sp. n. (paratype #03366) **D** *albipalpis* sp. n. (holotype #03908). Abbreviations: cly = clypeus, m s = medial sensilla, p s = posterior sensilla. Scale bars: 0.1 mm.

Female terminalia (Figure 11M–O): Tergite 8 with 4–5 small setae on ventral portion but no on caudodorsal portion. Oviscapt valve with three lateral and 12–13 marginal ovisensilla. Spermathecal capsule apically slightly narrowed, slightly broader than long.

Measurements (in mm): BL = 2.20 in holotype (range in 8♂/2♀ paratypes: 1.63–2.50/2.03–2.63), ThL = 1.00 (0.88–1.06/0.98–1.06), WL = 1.84 (1.60–2.15/2.03–2.10), WW = 0.92 (0.83–1.04/1.02–1.06).

Indices. FW/HW = 0.59 (range in 8♂ and 2♀, or less if noted, paratypes: 0.58–0.63), ch/o = 0.12 (0.07–0.13), prorb = 0.65 (6♂, 2♀: 0.46–0.63), rcorb = 0.30 (7♂, 2♀: 0.20–0.37), vb = 0.45 (7♂, 2♀: 0.22–0.60), orbito = 0.63 (0.50–0.64), dcl = 0.72 (0.63–0.79), sctl = 1.26 (7♂, 1♀: 0.94–1.12), sterno = 0.56 (0.44–0.71), dcp = 0.38 (0.41–0.57), sctlp = 0.95 (0.91–1.00), C = 1.70 (1.56–2.00), 4c = 1.45 (1.32–1.58), 4v = 2.05 (1.83–2.26), 5x = 2.38 (1.80–2.43), ac = 2.90 (2.87–3.29), M = 0.90 (0.75–0.95), C3F = 0.56 (0.52–0.59).

Distribution. Indonesia (West Java), China (Yunnan).

Etymology. Referring to the long and thin palpus.

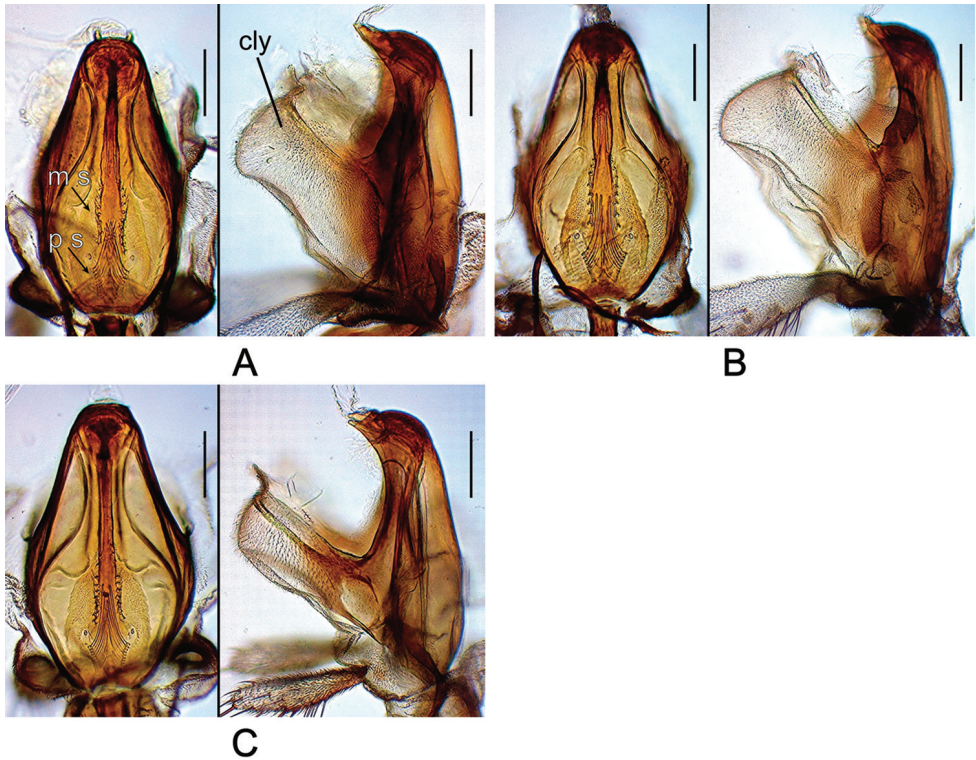


Figure 7. Cibarium of *Dudaica* species (part 2). **A** *qiongzhouensis* sp. n. (paratype #03313) **B** *orthophallata* sp. n. (paratype #03905) **C** *dissimilis* (holotype #00430). Scale bars: 0.1 mm.

Remarks. This species closely resembles the foregoing species, *D. malayana*, in having the long, sinuate palpus and pubescent caudolateral lobe of hypandrium, but can be distinguished from the latter by having only one apical seta on foreleg tibia.

***Drosophila (Dudaica) puberula* Katoh & Gao, sp. n.**

<http://zoobank.org/94250D73-99A0-4C92-958C-5C1BFA018C08>

Figures 2C, 4–6C, 8C, 9C, 12

Type material. *Holotype* ♂ (#03365): CHINA: Xishuangbanna Tropical Botanical Garden, Mengla, Yunnan, ca. 650 m a.s.l., 27–28.ix.2011, JJ Gao (KIZ).

Paratypes. CHINA: 1♀ (#03426), same except for 19.iii.2006, MJ Toda and K Takenaka (KIZ); 5♂, Wangtianshu, Mengla, Yunnan, ca. 670 m a.s.l., 22–25.iv.2007 (#00480) or 30.ix.2011 (#03366–69), JJ Gao (KIZ, SEHU).

Diagnosis. Palpus slightly shorter than arista, with 3–4 prominent, stout setae on outer lateral surface (Figure 9C). Hypandrium pubescent on portion fused to paramere (Figure 12I, J). Paramere apically sharp (Figure 12I–K).

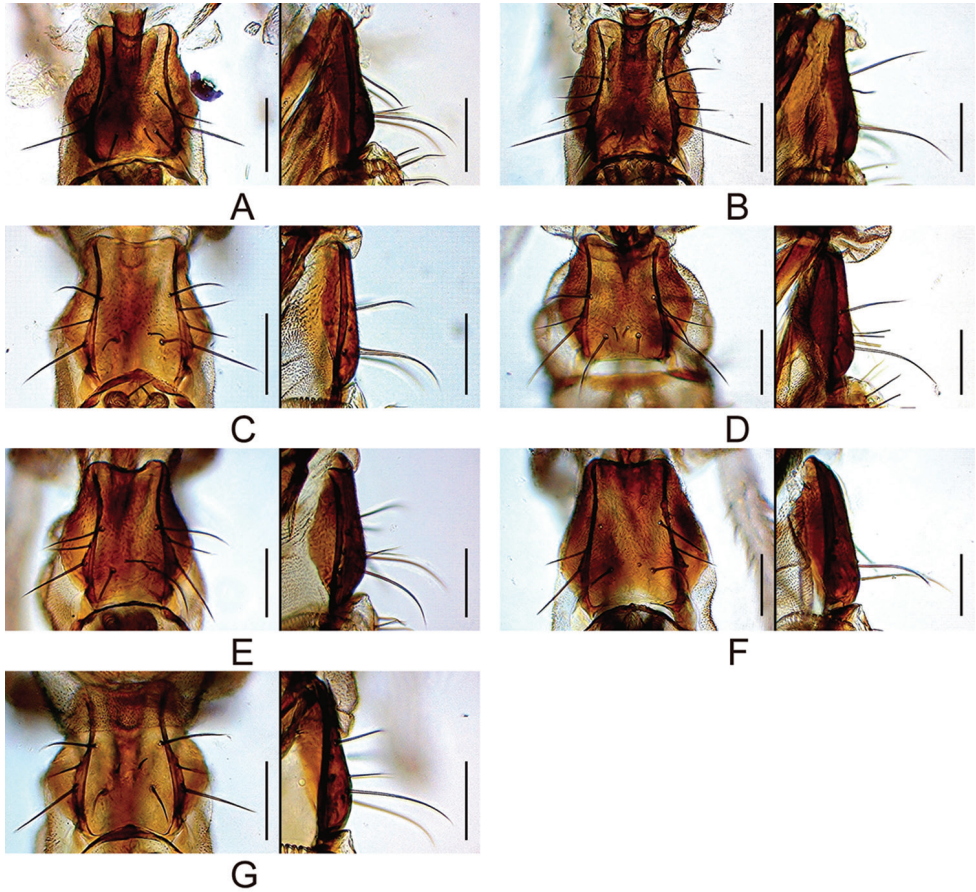


Figure 8. Prementum (ventral and lateral views). **A** *malayana* (Takada) (#03903) **B** *gracilipalpis* sp. n. (paratype #00492) **C** *puberula* sp. n. (paratype #03366) **D** *albipalpis* sp. n. (holotype #03908) **E** *qiongzhouensis* sp. n. (paratype #03313) **F** *orthophallata* sp. n. (paratype #03905) **G** *dissimilis* sp. n. (holotype #00430). Scale bars: 0.1 mm.

Description (characters in common with *D. gracilipalpis* sp. n. not repeated). Adult ♂ and ♀. *Head* (Figures 2C, 4–6C, 8C, 9C): Arista with 6–8 dorsal and 2–3 ventral branches. Supracervical setae 20–21 per side; postocular setae 15–18 per side. Cibarium with ca. nine medial and ca. eight posterior sensilla per side. Prementum with 5–6 (one proximal, 2–3 lateral, and two distal) pairs of setae.

Thorax (Figure 2C): Postpronotal lobe entirely dark brown, with 1–3 prominent and 2–4 short setae. Right and left dorsocentral setae slightly convergent. Notopleuron dark brown. Thoracic pleura with four stripes.

Legs (Figure 2C): First tarsomeres of all legs shorter than total length of four succeeding tarsomeres; mid-leg first tarsomere with one subproximal short, black spine.

Male terminalia (Figure 12A–K): Epandrium with ca. three and 10–13 long setae per side on caudodorsal and ventral portions, respectively. Cercus with 33–35 setae.

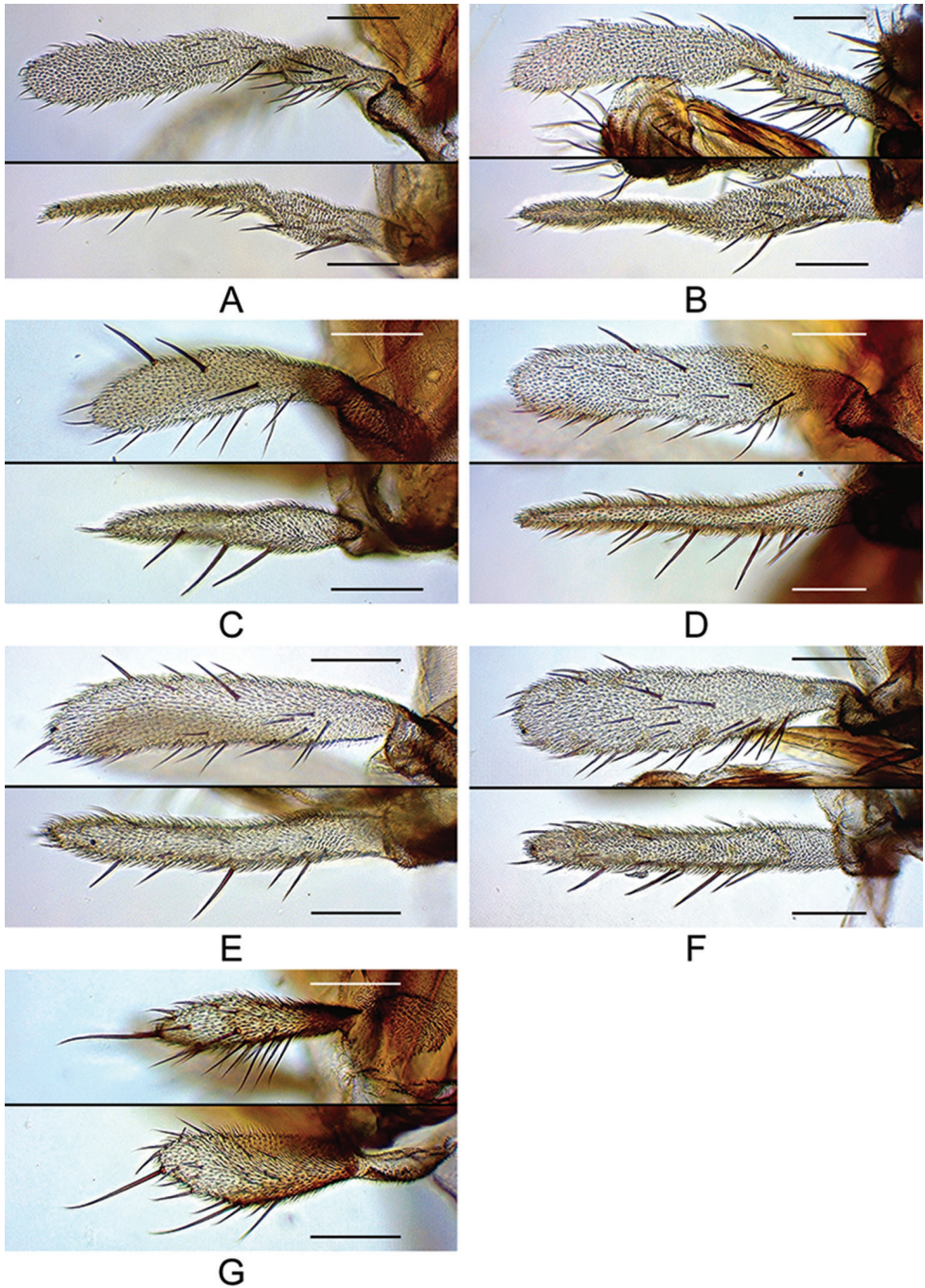


Figure 9. Palpus (lateral and dorsal views; only A is photographed at right side and flipped horizontally). **A** *malayana* (Takada) (#03903) **B** *gracilipalpis* sp. n. (paratype #00492) **C** *puberula* sp. n. (paratype #03366) **D** *albipalpis* sp. n. (holotype #03908) **E** *qiongzhouensis* sp. n. (paratype #03313) **F** *orthophallata* sp. n. (paratype #03905) **G** *dissimilis* sp. n. (holotype #00430). Scale bars: 0.1 mm.

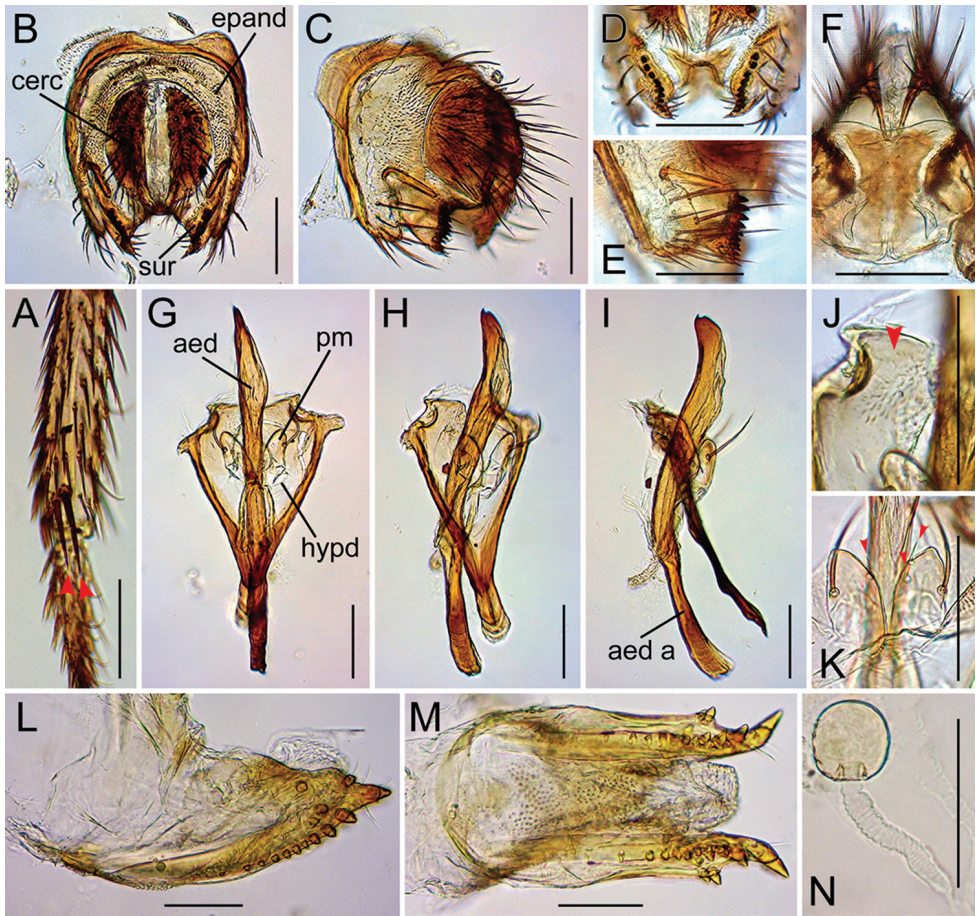


Figure 10. *Drosophila (Dudaica) malayana* (Takada) (**A, K** #03903 **B–J** #03904 **L–N** female specimen). **A** tibia of right foreleg (apical setae indicated with red arrowheads; ventral view) **B, C** periphallal organs (caudal and caudolateral view, respectively) **D** surstyli (caudoventral view) **E** surstylus and epandrial ventral lobe (caudolateral view) **F** tenth sternite and ventral protrusions of cerci (ventral view) **G–I** phallic organs (ventral, ventrolateral, and lateral view, respectively) **J** pubescence on caudolateral lobe of hypandrium (indicated with red arrowhead; caudoventral view) **K** sensilla (indicated with red arrowheads) and apical portion of parameres (ventral view) **L, M** oviscapt (lateral and ventral view, respectively) **N** spermatheca. Abbreviations: aed = aedeagus, aed a = aedeagal apodeme, cerc = cercus, epand = epandrium, hypd = hypandrium, pm = paramere, sur = surstylus. Scale bars: 0.1 mm.

Surstylus with ca. nine prensisetae and ca. eight ventral spines. Hypandrium not pubescent on caudolateral lobes. Paramere apically with one sensillum. Aedeagus apically darkened; apodeme laterally flat in muscle-attaching portion.

Female terminalia (Figure 12L–N): Tergite 8 with ca. four small setae on ventral portion but no on caudodorsal portion. Oviscapt valve with three lateral and 13–14 marginal ovisensilla. Spermathecal capsule apically round, not narrowed.

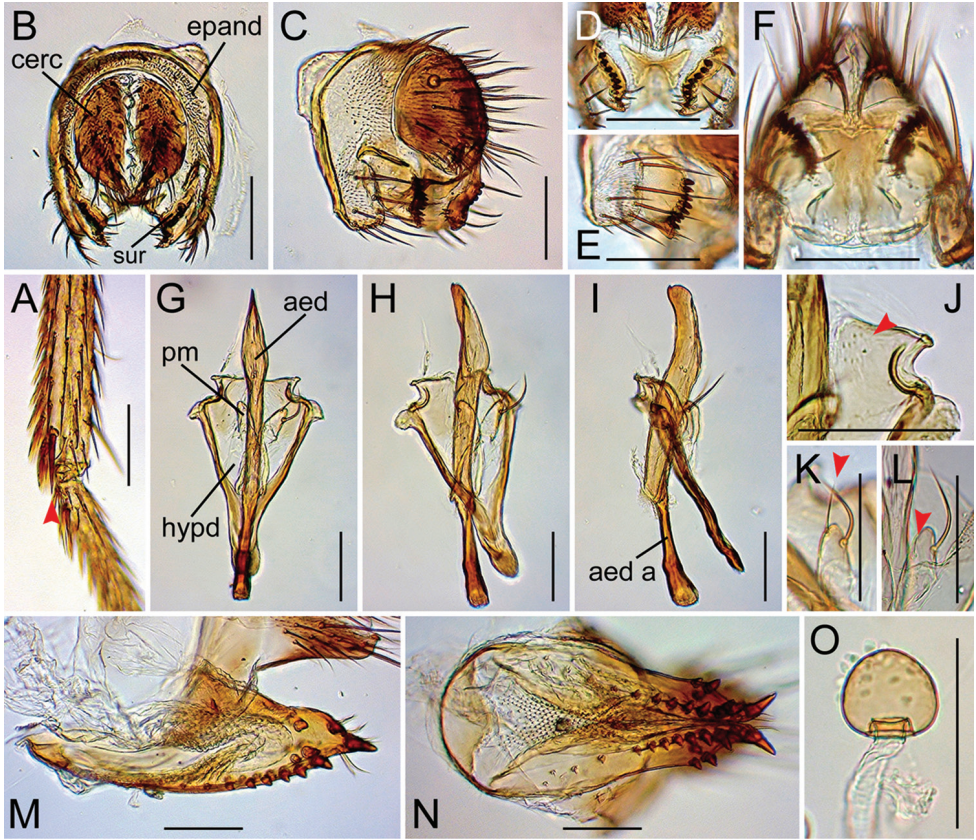


Figure 11. *Drosophila (Dudaica) gracilipalpis* sp. n. (A, M–O paratype #00492 B–K paratype #03902 L paratype #00491). A tibia of right foreleg (apical seta indicated with red arrowhead; ventral view) B, C peripheralhallic organs (caudal and caudolateral view, respectively) D surstyli (caudoventral view) E surstylus and epandrial ventral lobe (caudolateral view) F tenth sternite and ventral protrusions of cerci (ventral view) G–I phallic organs (ventral, ventrolateral, and lateral view, respectively) J pubescence on caudolateral lobe of hypandrium (indicated with red arrowhead; caudoventral view) K, L sensilla (indicated with red arrowheads) and apical portion of parameres (ventral view; Indonesian and Chinese specimen, respectively) M, N oviscapts (lateral and ventral view, respectively) O spermatheca. Scale bars: 0.1 mm.

Measurements (in mm): BL = 2.30 in holotype (range in 5♂/1♀ paratypes: 1.92–2.43/2.69), ThL = 0.88 (0.98–1.14/1.30), WL = 1.86 (1.82–2.10/2.35), WW = 0.98 (0.88–1.10/1.20).

Indices. FW/HW = 0.57 (range in 5♂ and 1♀, or less if noted, paratypes: 0.55–0.58), ch/o = 0.11 (0.07–0.18), prorrb = 0.61 (0.54–0.58), rcorrb = 0.30 (5♂: 0.27–0.38), vb = 0.34 (0.33–0.41), orbito = 0.63 (0.50–0.75), dcl = 0.65 (4♂, 1♀: 0.55–0.74), sctl = 1.05 (4♂, 1♀: 1.00–1.10), sterno = 0.67 (5♂: 0.42–0.67), dcp = 0.52 (0.42–0.55), sctlp = 1.05 (0.78–1.00), C = 1.67 (1.50–1.79), 4c = 1.43 (1.36–1.58),

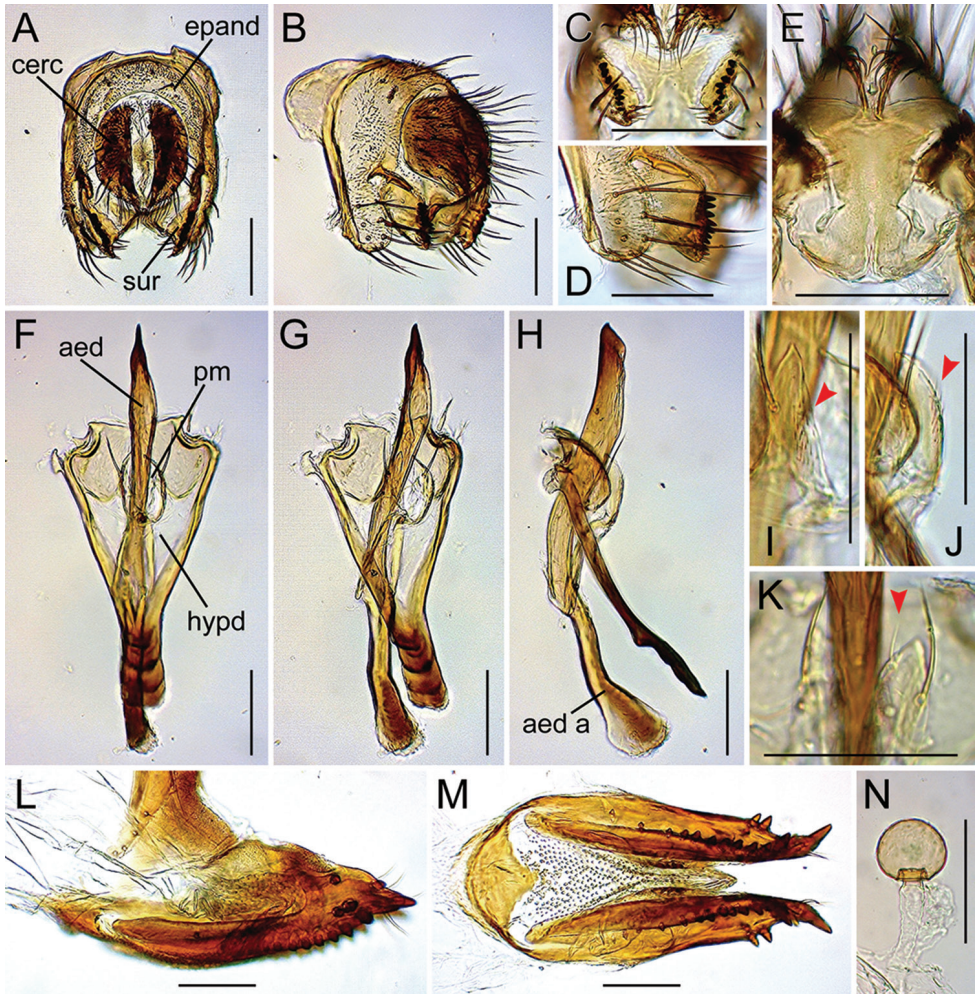


Figure 12. *Drosophila (Dudaica) puberula* sp. n. (A–J paratype #03366; K holotype #03365 L–M paratype #03426). A, B periphallal organs (caudal and caudolateral view, respectively) C surstyli (caudoventral view) D surstylus and epandrial ventral lobe (caudolateral view) E tenth sternite and ventral protrusions of cerci (ventral view) F–H phallic organs (ventral, ventrolateral, and lateral view, respectively) I, J pubescence (indicated with red arrowheads) and apical portion of parameres (ventrolateral and lateral view, respectively) K sensillum (indicated with red arrowhead) and apical portion of parameres (ventral view) L, M oviscapt (lateral and ventral view, respectively) N spermatheca. Scale bars: 0.1 mm.

$4v = 2.00$ (1.75–2.16), $5x = 1.70$ (1.79–2.11), $ac = 3.00$ (2.83–3.58), $M = 0.81$ (0.76–0.89), $C3F = 0.55$ (0.53–0.59).

Distribution. China (Yunnan).

Etymology. Referring to the pubescence of hypandrium on the portion fused to paramere in the new species.

***Drosophila (Dudaica) albipalpis* Katoh, Toda & Gao, sp. n.**

<http://zoobank.org/BC85BE2C-0720-4B19-BCF5-2BB361F96BC5>

Figures 2D, 4–6D, 8D, 9D, 13

Type material. *Holotype* ♂ (#03908): INDONESIA: Cikaniki, Gunung Halimun, West Java, 4.xi.2009, MJ Toda (MZB).

Diagnosis. Palpus broad, flat, with a few moderate setae on outer lateral surface (Figure 9D). Paramere apically truncated in lateral view (Figure 13K). Aedeagus apically finely serrated along ventrolateral margin (Figure 13I). Nucleotide status in COI sequence = C and T at sites 391 and 589, respectively (Table 3).

Description (characters in common with *D. puberula* sp. n. not repeated). Adult ♂. *Head* (Figures 2D, 4–6D, 8D, 9D): Arista with eight dorsal and three ventral branches. Supracervical setae 24–27 per side; postocular setae 14–17 per side. Cibarium with ca. nine medial and ca. 13 posterior sensilla per side. Prementum with five (one proximal, two lateral, and two distal) pairs of setae.

Thorax (Figure 2D): Postpronotal lobe with two prominent and three short setae. Anterior dorsocentral setae slightly convergent; posterior dorso-central setae nearly parallel. Thoracic pleura with four indistinct stripes.

Legs (Figures 2D): First tarsomeres of all legs slightly shorter than total length of four succeeding tarsomeres.

Male terminalia (Figure 13): Cercus with 29–32 setae, including ca. ten ventral, small ones. Surstylus with ca. ten prenisetae and ca. eleven ventral spines. Hypandrium not pubescent. Paramere apically rounded in ventral view, with 1–2 sensilla. Aedeagus apically not darkened.

Measurements (in mm): BL = 2.50 in holotype, ThL = 1.08, WL = 2.10, WW = n/a.

Indices. FW/HW = 0.59, ch/o = 0.09, prorb = 0.63, rcorb = 0.24, vb = n/a, orbito = 0.50, dcl = 0.67, sclt = 1.02, sterno = 0.70, dcp = 0.50, scltp = 0.91, C = 1.71, 4c = 1.31, 4v = 1.65, 5x = 1.38, ac = 2.83, M = 0.69, C3F = 0.49.

Distribution. Indonesia (West Java).

Etymology. Referring to the white palpus in the new species.

***Drosophila (Dudaica) qiongzhouensis* Katoh & Gao, sp. n.**

<http://zoobank.org/EBC67347-3CC4-4598-A9AC-248A04D7571F>

Figures 3A, 4E, 5E, 7A, 8E, 9E, 14

Type material. *Holotype* ♂ (#03420): CHINA: Jianfengling National Nature Reserve, Ledong, Hainan, ca. 750 m a.s.l., 17–20.iv.2008, JJ Gao (KIZ).

Paratypes. CHINA: 5♂, 4♀ (#03310–15, #03418, #03419, #03422), same data as holotype (KIZ, SEHU).

Diagnosis. Palpus slender, not so flat, somewhat rod-shaped in lateral view, with a few moderate setae on outer lateral surface (Figure 9E). Paramere apically rounded

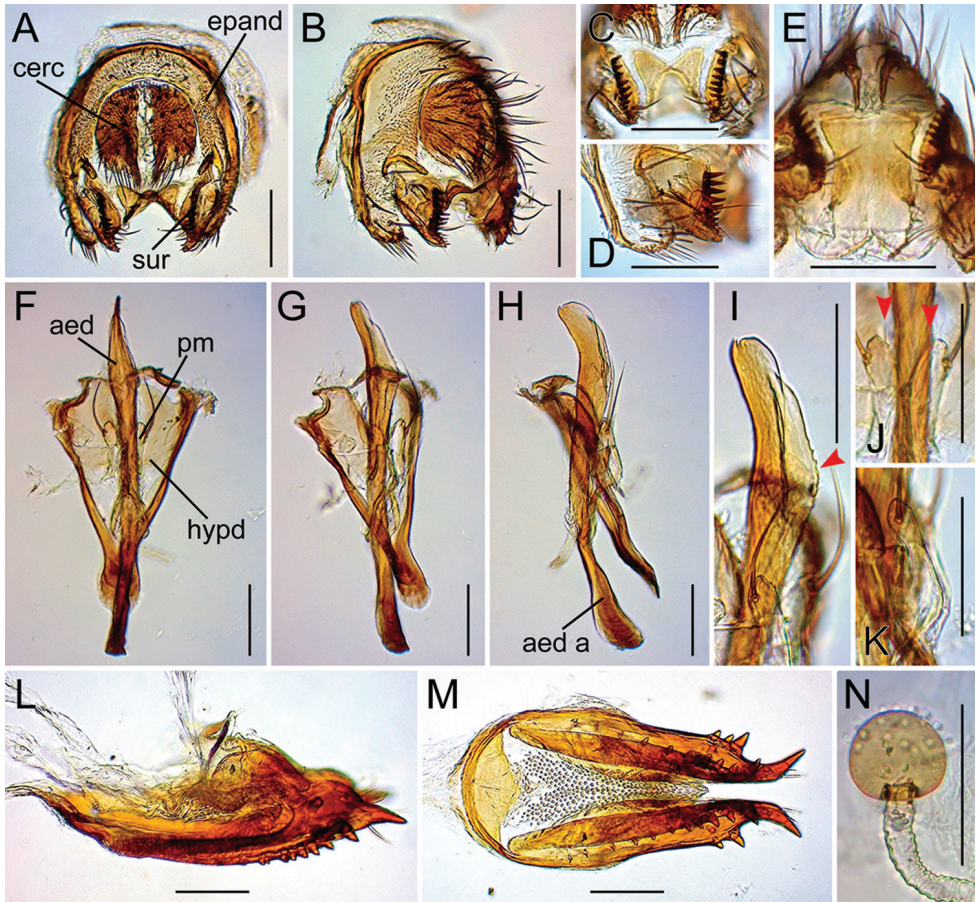


Figure 13. *Drosophila (Dudaica) albipalpis* sp. n. (A–K holotype #03908). **A, B** periphallitic organs (caudal and caudolateral view, respectively) **C** surstyli (caudoventral view) **D** surstylus and epandrial ventral lobe (caudolateral view) **E** tenth sternite and ventral protrusions of cerci (ventral view) **F–H** phallic organs (ventral, ventrolateral, and lateral view, respectively) **I** apical portion of aedeagus with fine serrations (indicated with red arrowhead; ventrolateral view) **J, K** sensilla (indicated with red arrowheads) and apical portion of parameres (ventral and lateral view, respectively). Scale bars: 0.1 mm.

in lateral view (Figure 14K). Nucleotide status in COI sequence = C and C at sites 92 and 226, respectively (Table 3).

Description (characters in common with *D. puberula* sp. n. not repeated). Adult ♂ and ♀. **Head** (Figures 3A, 4E, 5E, 7A, 8E, 9E): Arista with 6–8 dorsal and three ventral branches. Supracervical setae 23–24 per side; postocular setae 15–17 per side. Cibarium with ca. ten medial and ca. nine posterior sensilla per side. Prementum with five (one proximal, two lateral, and two distal) pairs of setae.

Thorax (Figure 3A): Postpronotal lobe with 1–2 prominent and 1–3 short setae.

Legs (Figure 3A): Foreleg first tarsomere shorter than total length of four succeeding tarsomeres. Mid- and hind-leg first tarsomeres slightly shorter than or nearly as long as total length of four succeeding tarsomeres.

Male terminalia (Figure 14A–K): Epandrium caudodorsally with 2–3 and ca. 16 long setae per side on caudodorsal and ventral portions, respectively. Cercus with 31–33 setae. Surstylus with ca. nine prenisetae and ca. ten ventral spines. Hypandrium not pubescent. Paramere apically rounded in ventral view, with one sensillum. Aedeagus apically not darkened, subapically sometimes scarcely serrated along ventrolateral margin.

Female terminalia (Figure 14L–N): Tergite 8 with 4–5 and ca. four setae on ventral and caudodorsal portions, respectively. Oviscapt valve with 3–4 lateral and ca. 14 marginal ovisensilla. Spermathecal introvert ca. 1/6 height of capsule.

Measurements (in mm): BL = 2.72 in holotype (range in 5♂/4♀ paratypes: 1.99–2.36/2.08–3.00), ThL = 1.22 (0.90–0.98/0.82–1.19), WL = 2.30 (1.74–1.82/1.62–2.33), WW = 1.26 (0.88–0.96/0.82–1.24).

Indices. FW/HW = 0.58 (range in 5♂ and 4♀, or less if noted, paratypes: 0.55–0.58), ch/o = 0.09 (0.08–0.13), prorb = 0.68 (5♂, 3♀: 0.50–0.80), rcorb = 0.36 (0.27–0.45), vb = 0.40 (0.32–0.55), orbito = 0.70 (0.50–0.67), dcl = 0.67 (3♂, 4♀: 0.58–0.68), sctl = 0.96 (0.89–1.06), sterno = 0.47 (0.54–0.68), dcp = 0.49 (0.42–0.52), scltp = 0.83 (0.69–1.00), C = 1.66 (1.48–1.87), 4c = 1.46 (1.20–1.61), 4v = 1.88 (1.62–2.00), 5x = 1.36 (1.45–1.90), ac = 2.92 (2.90–3.44), M = 0.73 (0.68–0.83), C3F = 0.61 (0.51–0.62).

Distribution. China (Hainan).

Etymology. Pertaining to the type locality, Hainan (formerly known as “Qiongzhou”).

***Drosophila (Dudaica) orthophallata* Katoh, Toda & Gao, sp. n.**

<http://zoobank.org/BF65BAAF-9A66-4ECD-B4CE-65723DDAB9AE>

Figures 3B, 4F, 5F, 7B, 8F, 9F, 15

Type material. *Holotype* ♂ (#00177): MALAYSIA: Ulu Senagang, Crocker Range, Sabah, 18.x.1999, MJ Toda (ITBC).

Paratypes. MALAYSIA: 2♀ (#03905, #03906), Park Headquarters, Mt. Kinabalu, Sabah, 11.iii.2008, MJ Toda (KPSP, SEHU).

Diagnosis. Palpus broad, flat, with a few moderate setae on outer lateral surface (Figure 9F). Paramere apically somewhat truncated in lateral view (Figure 15G). Aedeagus straight, subapically swollen in lateral view, apically without small, acute claw (Figure 15G).

Description (characters in common with *D. puberula* sp. n. not repeated). Adult ♂ and ♀. *Head* Figures 3B, 4F, 5F, 7B, 8F, 9F): Arista with 6–7 dorsal and 2–3 ventral branches. Supracervical setae 25–26 per side; postocular setae 16–18 per side. Cibarium with ca. nine medial and ca. ten posterior sensilla per side. Prementum with five (one proximal, two lateral, and two distal) pairs of setae.

Thorax (Figure 3B): Postpronotal lobe with 1–2 prominent and 1–3 short setae. Thoracic pleura with four, slightly indistinct stripes.

Legs (Figure 3B): Foreleg first tarsomere shorter than or as long as total length of four succeeding tarsomeres. Mid- and hind-leg first tarsomeres as long as total length of four succeeding tarsomeres.

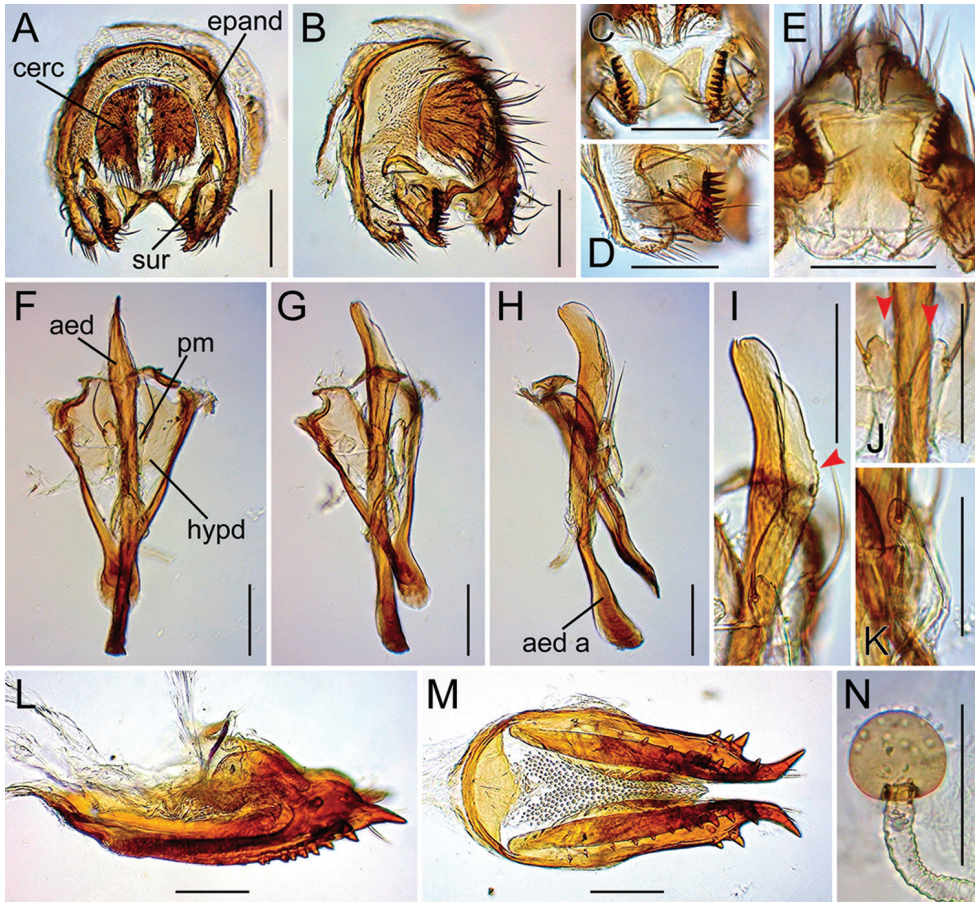


Figure 14. *Drosophila (Dudaica) qiongzhouensis* sp. n. (A–K paratype #03418 L–N paratype #03313). **A, B** periphallallic organs (caudal and caudolateral view, respectively) **C** surstyli (caudoventral view) **D** surstylus and epandrial ventral lobe (caudolateral view) **E** tenth sternite and ventral protrusions of cerci (ventral view) **F–H** phallic organs (ventral, ventrolateral, and lateral view, respectively) **I** apical portion of aedeagus with fine serrations (indicated with red arrowhead; ventrolateral view) **J, K** sensilla (indicated with red arrowheads) and/or apical portion of parameres (ventral and lateral view, respectively) **L, M** oviscapt (lateral and ventral view, respectively) **N** spermatheca. Scale bars: 0.1 mm.

Male terminalia (Figure 15A–H): Epandrium with ca. three and ca. 13 long setae per side on caudodorsal and ventral portions, respectively. Cercus with 26–28 setae. Surstylus with ca. eight prensisetae and 7–8 ventral spines. Tenth sternite damaged. Hypandrium somewhat triangular, anteriorly round, not pubescent. Aedeagus apically not darkened; apodeme ca. $2/5$ length of aedeagus.

Female terminalia (Figure 15I, J): Tergite 8 with 3–4 and ca. three setae on ventral and caudodorsal portions, respectively. Oviscapt valve with three lateral and 17–19 marginal ovisensilla. Data of spermatheca unavailable.

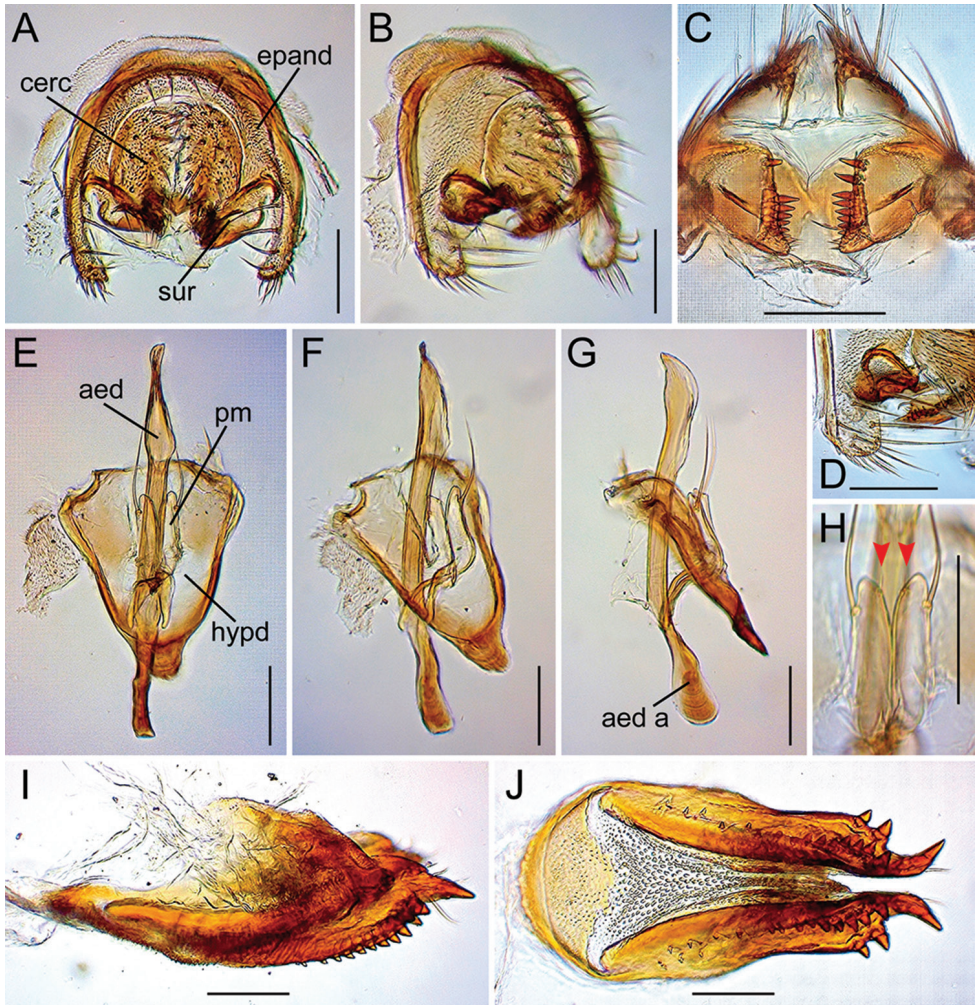


Figure 15. *Drosophila (Dudaica) orthophallata* sp. n. (**A–H** holotype #00177 **I, J** paratype #03906). **A, B** periphallal organs (caudal and caudolateral view, respectively) **C** surstyli, tenth sternite, and ventral protrusions of cerci (ventral view) **D** epandrial ventral lobe (caudolateral view) **E–G** phallic organs (ventral, ventrolateral, and lateral view, respectively) **H** sensilla (indicated with red arrowheads) and apical portion of parameres (ventral view) **I, J** oviscapt (lateral and ventral view, respectively). Scale bars: 0.1 mm.

Measurements (in mm): BL = 2.34 in holotype (range in 2♀ paratypes: 2.20–2.60), ThL = 1.18 (1.18–1.40), WL = 2.00 (2.35–2.63), WW = 1.06 (1.28–1.37).

Indices. FW/HW = 0.56 (range in 2♀, or less if noted, paratypes: 0.56–0.63), ch/o = 0.09 (0.12), pror = 0.68 (1♀: 0.67), rcor = 0.34 (1♀: 0.31), vb = n/a (1♀: 0.50), orbito = 0.65 (0.40–0.55), dcl = 0.65 (0.71–0.75), sclt = 1.00 (1♀: 1.04), sterno = 0.58 (0.63–0.71), dcp = 0.44 (0.43), scltp = 0.72 (0.73–0.85), C = 1.72 (1.76–1.78), 4c = 1.25 (1.27–1.28), 4v = 1.61 (1.59–1.67), 5x = 1.33 (1.33–1.44), ac = 3.56 (2.93–3.04), M = 0.63 (0.67–0.72), C3F = 0.56 (0.54–0.58).

Distribution. Malaysia (Sabah).

Etymology. Referring to the straight aedeagus in the new species.

Remarks. The paratype female specimens #03905 and #03906 were identified as conspecific with the holotype male specimen #00177 (DNA sequence data unavailable), based on close morphological affinity between them. This species can also be distinguished from the other *Dudaica* species by oviscapt valve with 17–19 marginal ovisensilla (Figure 15I, J) in addition to the diagnosis.

***Drosophila (Dudaica) dissimilis* Katoh & Gao, sp. n.**

<http://zoobank.org/BABEAEB4-04FD-43CF-B3BC-60B69F3FE280>

Figures 3C, 4G, 5G, 7C, 8G, 9G, 16

Type material. *Holotype* ♂ (#00430): CHINA: Hesong, Xiding, Menghai, Yunnan, ca. 1,900 m a.s.l., 7.iv.2011, JJ Gao (KIZ).

Diagnosis. Palpus short, club-shaped, medio- to baso-laterally dark grayish brown, with one prominent seta apically and several long setae ventrally (Figure 9G). Cercus without caudoventral process (Figure 16E). Paramere apically somewhat quadrate in lateral view (Figure 16J), ventroapically with three sensilla (Figure 16I, J). Aedeagus distally dilated laterally, somewhat lunate in lateral view (Figure 16F–H).

Description (characters in common with *D. orthophallata* sp. n. not repeated). Adult ♂. *Head* (Figures 3C, 4G, 5G, 7C, 8G, 9G): Longest axis of eye nearly rectangular to body axis. Frontal vitta grayish white. Fronto-orbital plate slightly grayish; anterior reclinate orbital seta situated between proclinate and posterior reclinate orbital setae. Occiput and postgena dark brown, marginally milky white. Arista with six dorsal and three ventral branches. Supracervical setae 16–19 per side; postocular setae 17–19 per side. Cibarium slightly thickened on anterior margin; medial sensilla ca. nine per side and posterior sensilla ca. nine per side; first and second medial sensilla weaker than and anteriorly apart from others. Clypeus not thickened at median portion, laterally dark brown.

Thorax (Figure 3C): Postpronotal lobe pale brownish white in upper half, dark brown in lower half; setae broken. Dorsocentral and scutellar setae broken. Notopleuron pale brownish white. Thoracic pleura nearly entirely dark brown, without stripes.

Wing (Figure 3C) slightly wrinkled at basal portion of R₄₊₅; longitudinal veins pale brown except for basal section of M₁ (brown) and CuA₁ (brown).

Legs (Figure 3C) pale grayish yellow to pale yellow. Foreleg first tarsomere shorter than total length of four succeeding tarsomeres. Mid- and hind-leg first tarsomeres slightly shorter than total length of four succeeding tarsomeres, without subproximal spine.

Abdomen (Figure 3C): Tergites pale brown, each with dark brown caudal band narrower than ca. 1/2 of tergite but laterally extended anteriorly.

Male terminalia (Figure 16): Epandrium with ca. two and ca. 16 long setae per side on caudodorsal and ventral portions, respectively. Cercus with 30–31 setae. Surstylus

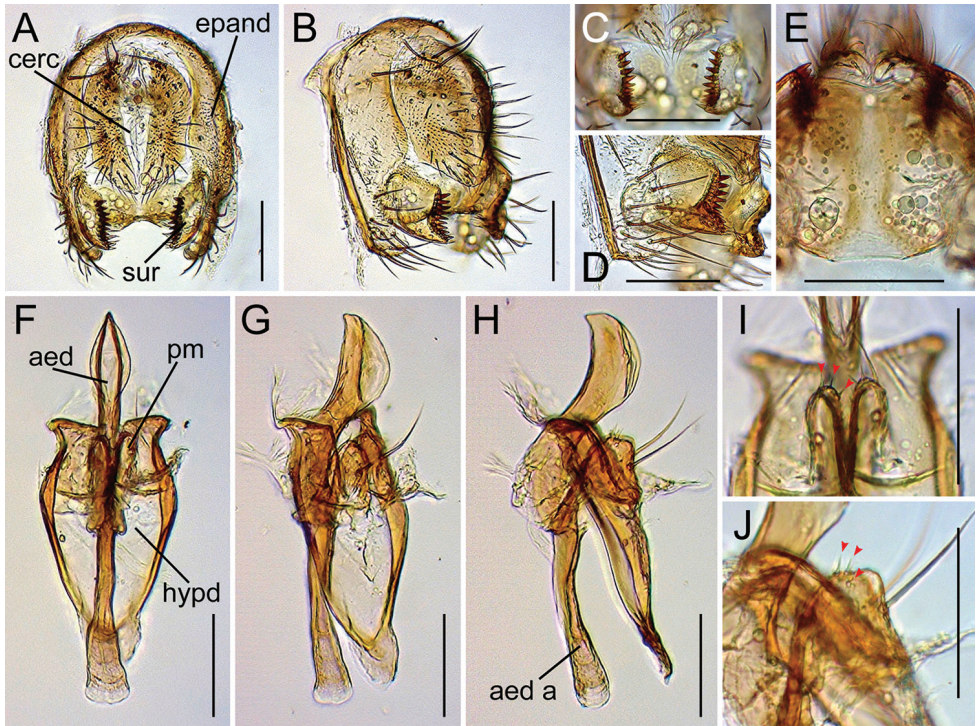


Figure 16. *Drosophila (Dudaica) dissimilis* sp. n. (**A–J** holotype #00430). **A, B** periphallallic organs (caudal and caudolateral view, respectively) **C** surstyli (caudoventral view) **D** surstylus and epandrial ventral lobe (caudolateral view) **E** tenth sternite (ventral view) **F–H** phallic organs (ventral, ventrolateral, and lateral view, respectively) **I, J** sensilla (indicated with red arrowheads) and apical portion of parameres (ventral and lateral view, respectively). Scale bars: 0.1 mm.

with ca. eight prenisetae and ca. ten ventral spines; basal sclerotized ridge indistinct. Tenth sternite flat, not wrinkled. Hypandrium somewhat oval in anterior portion. Aedeagal apodeme apically not flattened, slightly shorter than aedeagus.

Measurements (in mm): BL = 2.33 in holotype, ThL = 1.04, WL = 2.35, WW = 1.16.

Indices. FW/HW = 0.60, ch/o = 0.08, prorb = n/a, rcorb = n/a, vb = n/a, orbito = 0.78, dcl = n/a, sctl = n/a, sterno = 0.62, dcp = 0.65, sctlp = 0.94, C = 2.09, 4c = 1.21, 4v = 1.95, 5x = 1.24, ac = 2.83, M = 0.64, C3F = 0.53.

Distribution. China (Yunnan).

Etymology. Referring to the morphological difference from the other species in the subgenus *Dudaica*.

Remarks. This species is the most different in morphology from the other *Dudaica* species, such as the shape of palpus and parameres, apical prominent seta on palpus, and number of sensilla on parameres. Those characters are also seen in many other species than *Dudaica*, suggesting the plesiomorphic states of these characters.

Acknowledgements

We thank Dr. Shin-ichi Tanabe, Dr. Maklarin B. Lakim and Dr. Maryati Bte Mohamed for their help in field works and Economic Planning Unit of Malaysian Government for research permissions (UPE:40/200/19 SJ. 732 and UPE: 40/200/19 SJ.1194 and 1195) for the study in Sabah, Malaysia, and Prof. E. S. Ratna of Bogor Agricultural University for her help in field works in West Kalimantan, Indonesia. We also thank the Xishuangbanna Tropical Botanical Garden, CAS, the Xishuangbanna National Nature Reserve, and the Jianfengling National Nature Reserve for permitting us to collect flies in the Garden/Reserves. This work was supported by NSFC (Nos 31160429, 31572238), JSPS KAKENHI Grants Numbers 15255006, 21570085, 24370033 and the 21st Century Center of Excellence Program (E-01) of the Ministry of Education, Culture, Sports, Science and Technology, Japan.

References

- Bouckaert R, Heled J, Kühnert D, Vaughan T, Wu CH, Xie D, Suchard MA, Rambaut A, Drummond AJ (2014) BEAST 2: a software platform for Bayesian evolutionary analysis. *PLoS Computational Biology* 10: e1003537. <https://doi.org/10.1371/journal.pcbi.1003537>
- Darriba D, Taboada GL, Doallo R, Posada D (2012) jModelTest 2: more models, new heuristics and parallel computing. *Nature Methods* 9: 772. <https://doi.org/10.1038/nmeth.2109>
- De A, Gupta JP (1996) Records of Drosophilid species from Bhutan. *Drosophila Information Service* 77: 98.
- DeSalle R, Egan MG, Siddall M (2005) The unholy trinity: taxonomy, species delimitation and DNA barcoding. *Philosophical Transactions of the Royal Society B* 360: 1905–1916. <https://doi.org/10.1098/rstb.2005.1722>
- Duda O (1926) Fauna sumatrensis: Drosophilidae (Dipt.). *Supplementa Entomologica* 14: 42–116.
- Folmer O, Black M, Hoeh W, Lutz R, Vrijenhoek R (1994) DNA primers for amplification of mitochondrial cytochrome *c* oxidase subunit I for diverse metazoan invertebrates. *Molecular Marine Biology and Biotechnology* 3: 294–299.
- Grimaldi DA (1990a) Revision of *Zygothrica* (Diptera: Drosophilidae), part II. The first African species, two new Indo-Pacific groups, and the *bilineata* and *samoensis* species groups. *American Museum Novitates* 2964: 1–31.
- Grimaldi DA (1990b) A phylogenetic, revised classification of genera in the Drosophilidae (Diptera). *Bulletin of the American Museum of Natural History* 197: 1–139.
- Guindon S, Gascuel O (2003) A simple, fast, and accurate algorithm to estimate large phylogenies by maximum likelihood. *Systematic Biology* 52: 696–704. <https://doi.org/10.1080/10635150390235520>
- Gupta JP, Sundaran AK (1990) Further record of two new and one known species of *Drosophila* (Diptera: Insecta) from Karnataka, India. *Proceedings of the Zoological Society (Calcutta)* 43: 31–35.

- Hasegawa M, Kishino H, Yano T (1985) Dating of the human-ape splitting by a molecular clock of mitochondrial DNA. *Journal of Molecular Evolution* 22: 160–174. <https://doi.org/10.1007/BF02101694>
- Hebert PDN, Cywinska A, Ball SL, de Waard JR (2003) Biological identifications through DNA barcodes. *Proceedings of the Royal Society of London, Series B* 270: 313–321. <https://doi.org/10.1098/rspb.2002.2218>
- Jukes TH, Cantor CR (1969) Evolution of Protein Molecules. In: Munro HN (Ed.) *Mammalian Protein Metabolism*. Academic Press, New York, 21–132. <https://doi.org/10.1016/B978-1-4832-3211-9.50009-7>
- Kimura M (1980) A simple method for estimating evolutionary rates of base substitutions through comparative studies of nucleotide sequences. *Journal of Molecular Evolution* 16: 111–120. <https://doi.org/10.1007/BF01731581>
- Kumar S, Stecher G, Tamura K (2016) MEGA7: Molecular Evolutionary Genetics Analysis version 7.0 for bigger datasets. *Molecular Biology and Evolution* 33: 1870–1874. <https://doi.org/10.1093/molbev/msw054>
- Li NN, Toda MJ, Fu Z, Li SH, Gao JJ (2014) Taxonomy of the *Colocasiomyia gigantea* species group (Diptera, Drosophilidae), with descriptions of four new species from Yunnan, China. *ZooKeys* 406: 41–64. <https://doi.org/10.3897/zookeys.406.7176>
- McAlpine JF (1981) Morphology and terminology: adults. In: McAlpine JF, Peterson BV, Shewell GE, Teskey HJ, Vockeroth JR, Wood DM (Eds) *Manual of Nearctic Diptera*, Vol. 1. Biosystematics Research Institute, Ottawa, 9–63.
- Pons J, Barraclough T, Gomez-Zurita J, Cardoso A, Duran D, Hazell S, Kamoun S, Sumlin W, Vogler A (2006) Sequence-based species delimitation for the DNA taxonomy of undescribed insects. *Systematic Biology* 55: 595–610. <https://doi.org/10.1080/10635150600852011>
- Puillandre N, Lambert A, Brouillet S, Achaz G (2012) ABGD, Automatic Barcode Gap Discovery for primary species delimitation. *Molecular Ecology* 21: 1864–1877. <https://doi.org/10.1111/j.1365-294X.2011.05239.x>
- Rambaut A, Suchard MA, Xie D, Drummond AJ (2014) Tracer v1.6 <http://tree.bio.ed.ac.uk/software/tracer>
- Ronquist F, Teslenko M, van der Mark P, Ayres DL, Darling A, Höhna S, Larget B, Liu L, Suchard MA, Huelsenbeck JP (2012) MrBayes 3.2: Efficient Bayesian phylogenetic inference and model choice across a large model space. *Systematic Biology* 61: 539–542. <https://doi.org/10.1093/sysbio/sys029>
- Sarkar IN, Thornton JW, Planet PJ, Figurski DH, Schierwater B, DeSalle R (2002) An automated phylogenetic key for classifying homeoboxes. *Molecular Phylogenetics and Evolution* 24: 388–399. [https://doi.org/10.1016/S1055-7903\(02\)00259-2](https://doi.org/10.1016/S1055-7903(02)00259-2)
- Schwarz G (1978) Estimating the dimension of a model. *Annals of Statistics* 6: 461–464. <https://doi.org/10.1214/aos/1176344136>
- Sidorenko VS (1996) Some unrecorded species of Drosophilidae from Viet Nam. *Drosophila Information Service* 77: 97–98.
- Srivathsan A, Meier R (2012) On the inappropriate use of Kimura-2-parameter (K2P) divergences in the DNA-barcoding literature. *Cladistics* 28: 190–194. <https://doi.org/10.1111/j.1096-0031.2011.00370.x>

- Strand E (1943) Verschiedene Insekten Vergleich Crypturus unter “Aves”! Folia Zoologica et Hydrobiologica 12: 212.
- Takada H (1976) Distribution and population constitution of *Drosophila* in southeast Asia and Oceania III. The genus *Zygothrica* with description of three new species. Kontyû 44: 65–72.
- Wheeler MR (1981) The Drosophilidae: A taxonomic overview. In: Ashburner M, Carson HL, Thompson Jr JN (Eds) Genetics and Biology of *Drosophila* Vol. 3a. Academic Press, London, 1–97.
- Yassin A (2013) Phylogenetic classification of the Drosophilidae Rondani (Diptera): the role of morphology in the postgenomic era. Systematic Entomology 38: 349–364. <https://doi.org/10.1111/j.1365-3113.2012.00665.x>
- Zhang WX, Toda MJ (1992) A new species-subgroup of the *Drosophila immigrans* species-group (Diptera, Drosophilidae), with description of two new species from China and revision of taxonomic terminology. Japanese Journal of Entomology 60: 839–850.

A new species of the genus *Euxaldar* Fennah, 1978 from China (Hemiptera, Fulgoroidea, Issidae)

Zheng-Guang Zhang¹, Zhi-Min Chang², Xiang-Sheng Chen²

1 School of Life Sciences, Jinggangshan University, Ji'an, Jiangxi, 343009, PR China **2** Institute of Entomology, Guizhou University, Guiyang, Guizhou Province 550025, PR China

Corresponding author: Xiang-Sheng Chen (chenxs3218@163.com)

Academic editor: M. Wilson | Received 29 May 2018 | Accepted 21 July 2018 | Published 13 August 2018

<http://zoobank.org/92805772-39D9-4CE5-8579-5B478265EE20>

Citation: Zhang Z-G, Chang Z-M, Chen X-S (2018) A new species of the genus *Euxaldar* Fennah, 1978 from China (Hemiptera, Fulgoroidea, Issidae). ZooKeys 781: 51–58. <https://doi.org/10.3897/zookeys.781.27059>

Abstract

A new species *Euxaldar guangxiensis* **sp. n.** is described and illustrated from southeastern China. The generic characteristics are redefined. A checklist and key to the species of the genus *Euxaldar* are provided.

Keywords

Fulgoromorpha, Guangxi Province, Hemisphaeriini, new species

Introduction

The genus *Euxaldar* was erected by Fennah (1978) for a single species *E. jehucal* Fennah, 1978, described from Ninh Binh Province in Northern Vietnam (Fennah 1978). Recently this species was also recorded from Ha Noi, Vinh Phuc, Hoa Binh, and Haiphong Provinces; photos of the holotype of *E. jehucal* were provided (Gnezdilov and Constant 2012). The genus *Euxaldar* was previously placed in the tribe Issini Spinola, 1839 of the subfamily Issinae (Gnezdilov 2013). Recently, Wang et al. (2016) moved it to the tribe Hemisphaeriini Melichar, 1906 according to

molecular phylogeny of Issidae. Gnezdilov et al. (2017) redescribed the type species of the genus, *E. jehucal*, and described one more species, *E. lenis* Gnezdilov, Bourgoïn & Wang, 2017, from southern Vietnam. In this paper, one new species of the genus *Euxaldar* is described and illustrated from southeastern China, the generic characteristics are redefined and a checklist and key to the known species of the genus are provided.

Materials and methods

The morphological terminology of the head and body follows Gnezdilov, Bourgoïn and Wang (2017), and the terminology of male genitalia follows Gnezdilov (2003). The genital segments of the examined specimens were macerated in 10% KOH and drawn from preparations in glycerin jelly using a light microscope. Photographs of the specimens were made using Zeiss stereo Discovery V8. Microscope with Zeiss Axio Cam HRc camera, images were produced using the software Helicon Focus ver.6.7 and Photoshop CS4.0. The holotype of the new species is deposited in School of Life Sciences, Jिंगgangshan University, China.

Taxonomy

Family Issidae Spinola, 1839

Subfamily Hemisphaeriinae Melichar, 1906

Tribe Hemisphaeriini Melichar, 1906

Genus *Euxaldar* Fennah, 1978

Euxaldar Fennah, 1978: 267.

Type species. *Euxaldar jehucal* Fennah, 1978, by monotypy.

Diagnosis. Body hemispherical, head including eyes wider than pronotum. Metope flat and elongate. Coryphe transverse, 2–3 times as wide as long. Fore wings elongate and wide, without hypocoastal plate; venation poorly recognizable. Hind wings one-lobed, rudimentary, much shorter than fore wings. Hind tibia with two lateral spines. First metatarsomere with two latero-apical spines and 6–7 intermediate spines. Gonoplasts rounded. Phallobase asymmetrical, narrow, with basal or subapical processes; ventral phallobase lobe shorter than the dorsal lobe. Aedeagus without ventral hooks. Male anal tube enlarged apically or elongate (in dorsal view).

Distribution. China (Guangxi); Vietnam (Ninh Binh, Ha Noi, Vinh Phuc, Hoa Binh, Haiphong and Lam Dong Provinces) (Figure 21).

List of *Euxaldar* species

E. jebucal Fennah, 1978 (Vietnam: Ninh Binh, Ha Noi, Vinh Phuc, Hoa Binh and Haiphong Provinces)

E. lenis Gnezdilov, Bourgoïn & Wang, 2017 (Vietnam: Lam Dong Provinces)

E. guangxiensis sp. n. (China: Guangxi Province)

Key to species of the genus *Euxaldar* modified from Gnezdilov et al. 2017

- 1 Metope smooth, without any pustules (Gnezdilov et al. 2017: fig. 23).....
*E. lenis* Gnezdilov, Bourgoïn & Wang
- Metope with row of distinct pustules along its lateral margins (Fig. 5; Gnezdilov et al. 2017: fig. 20)..... **2**
- 2 Metopoclypeal suture complete. Male anal tube deeply concave posteromedially (in dorsal view) (Gnezdilov et al. 2017: fig. 6)*E. jebucal* Fennah
- Metopoclypeal suture incomplete medially (Fig. 5). Male anal tube elongate, wide at base, narrow at apical part, laterally with two triangular processes near middle part (Figs 10, 12-13)..... *E. guangxiensis* sp. n.

***Euxaldar guangxiensis* sp. n.**

<http://zoobank.org/D77A38F8-F9C9-423C-9FF3-E30F4E30EABF>

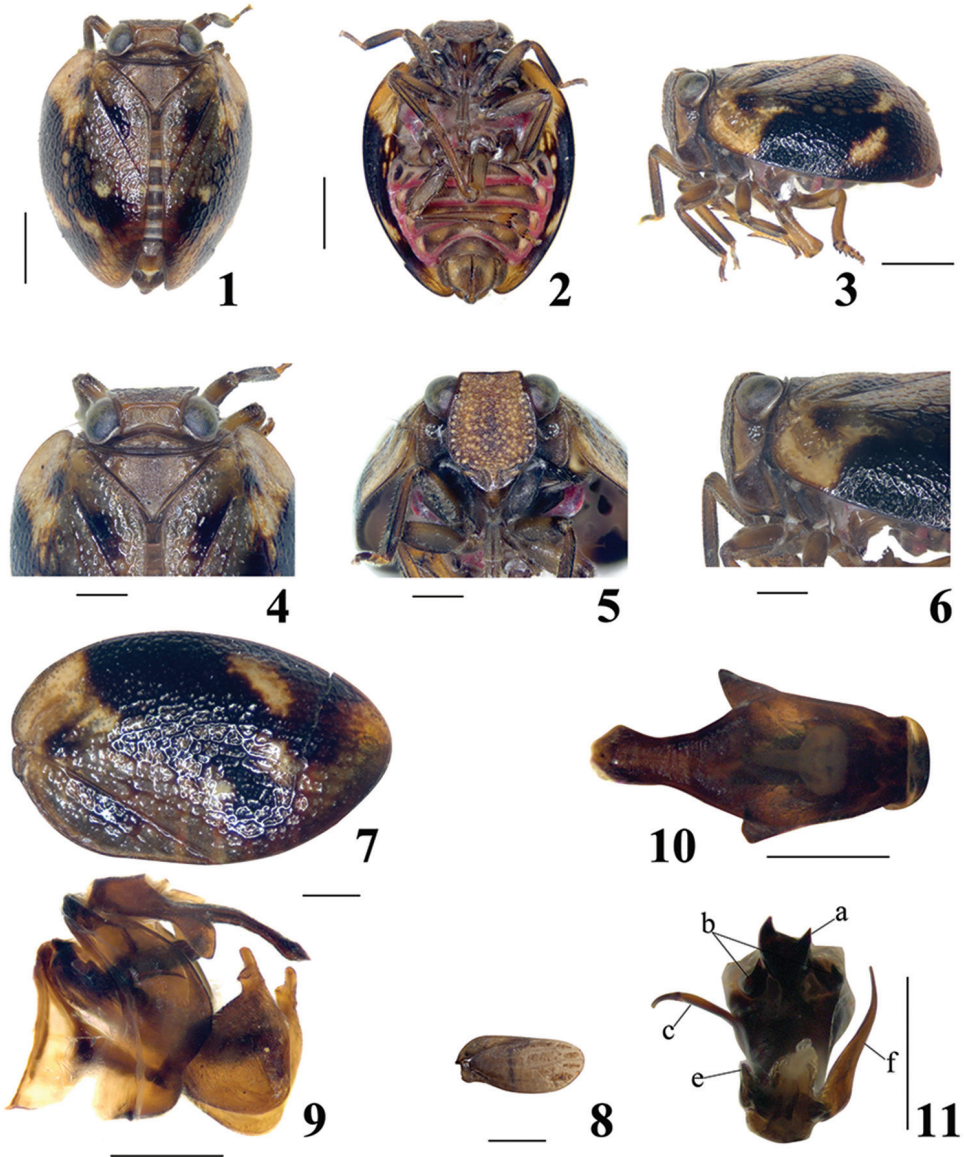
Figs 1–20

Type material. Holotype: 1 ♂, China: Guangxi, Nonggang National Nature Reserve (E106°58'3", N22°28'37"), 163 m, 29 Oct. 2017, K.K. Liu

Description. Body length (from apex of vertex to tip of forewing): male 3.8mm; Forewing: male 3.3mm

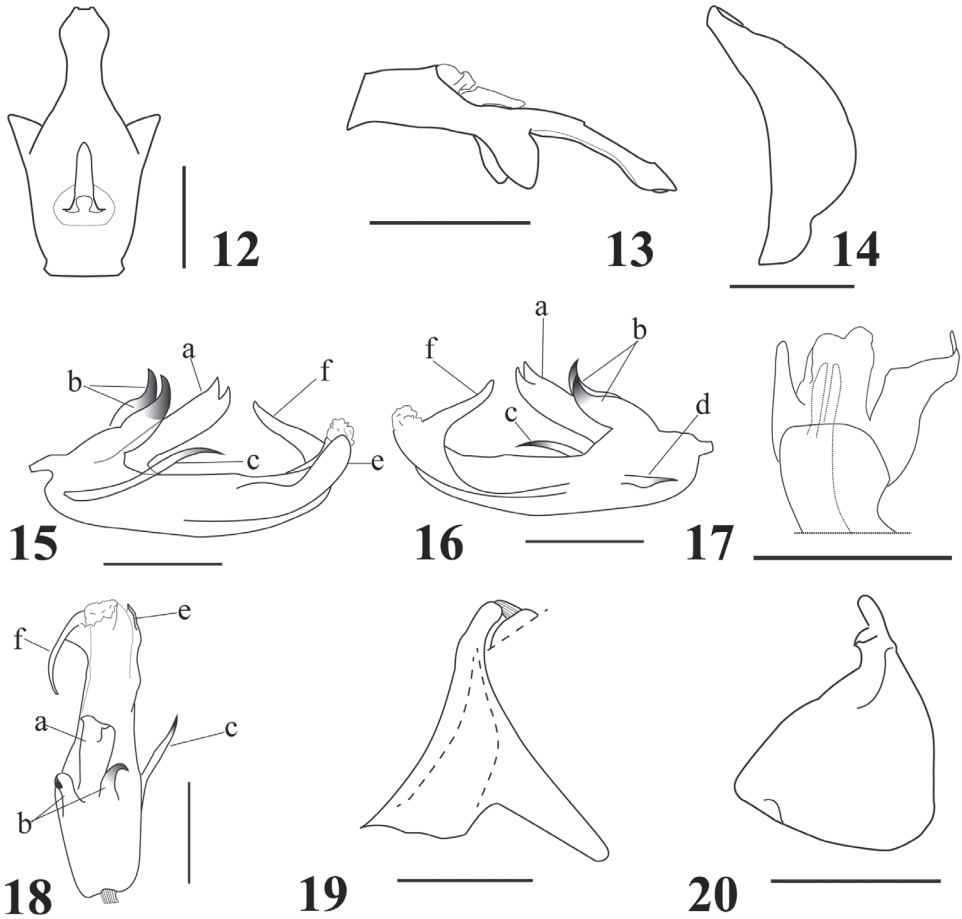
Coloration. Male: Coryphe (Figure 4) dark brown. Metope light brown yellowish, with pale pustules along its lateral margins. Clypeus (Figure 5) pale brown with dark brown band at base, rostrum and antenna dark brown (Figure 5). Pronotum and mesonotum brown (Figure 4). Forewings (Figure 7) dark brown, each with wide black band at midlength from costal margin to almost apex of clavus and with several light yellow patches including large one in basal part of the wing. Hind wing (Figure 8) dark brown. Legs (Figs 2–3) brown with dark brown markings. Abdomen (Figure 2) dark brown, with margins rufous.

Head and thorax. Coryphe (Figure 4) transverse, approximately 3.0 times wider than long, without carinae, anterior margin nearly straight, posterior margin slightly angularly concave. Metope (Figure 5) flat, 1.1 times longer than widest, without a median carina, with a row of distinct pustules along its lateral margins and rather weak pustules inside. Metopoclypeal suture (Figure 5) incomplete medially. Postclypeus



Figures 1–11. *E. guangxiensis* sp. n. **1** Adult (male), dorsal view **2** Adult (male), in ventral view **3** Adult (male), in lateral view **4** Head and thorax (male), in dorsal view **5** Face (male), in frontal view **6** Head (male), in lateral view **7** Fore wing (male) **8** Hind wing (male) **9** Male genitalia, in lateral view **10** Anal tube, in dorsal view **11** Penis, in dorsal view from caudad; Scale bars: 1.0 mm (**1–3**), 0.5 mm (**4–11**).

with wide median carina. Pronotum (Figure 4) short, with keel-shaped margins. Parapical fields very narrow behind the eyes. Mesonotum (Figure 4) 3.3 times longer than pronotum in midline, with lateral carinae. Fore wings (Figure 7) oval, with smoothed, poorly recognizable reticulate venation; CuP distinct. Hind wings (Figure 8) rudimen-



Figures 12–20. *E. guangxiensis* sp. n. **12** Anal tube (male), in dorsal view **13** Anal tube (male), in lateral view **14** Pygofer (male), in lateral view **15** Penis, in lateral view (left) **16** Penis, in lateral view (right) **17** Penis, in ventral view **18** Penis, in dorsal view **19** Connective, in lateral view **20** Gonostylus, in lateral view. Scale bars: 0.5 mm.

tary, 0.3 times as long as fore wings, veins obscure. Hind tibiae with 2 lateral teeth near apex. Spinal formula of the hind leg 7-7-2.

Male genitalia. Anal tube (Figs 10, 12, 13) elongate, wide at base part and narrow at apical part, slightly enlarged near apex, apical margin concave medially, laterally with two triangular processes near its middle. Anal column (Figure 12) located near base, 0.3 times as long as the anal tube in dorsal view. Pygofer (Figs 9, 14) in lateral view, with posterior margin distinctly convex. Phallobase asymmetrical, dorsally with three processes at base (Figure 18a, b), middle process of phallobase (Figs 15–16a, 18a) wide, with two teeth apically, lateral processes of phallobase (Figs 15, 16b, 18b) adjacent to middle process hook-shaped. Phallobase laterally with two processes near base,



Figure 21. Geographic distribution of *Euxaldar* species.

one of them is long and directed caudally (Figure 15c), the other short and directed cephalad (Figure 16d). Lateral phallobase lobes asymmetrical, narrowing apically, one is short directed caudally (Figure 15e), the other is long and curved cephalically (Figs 15f, 16f). Ventral phallobase lobe (Figure 17) not reaching the aedeagal apex, apical margin nearly straight. Connective (Figure 19) in shape of long and narrow cup. Gonostylus (Figure 20) triangular, with moderately convex hind margin, caudo-dorsal angle widely rounded.

Etymology. The specific name refers to the locality, Guangxi province, China.

Host plant. Unknown.

Distribution. China (Guangxi province)

Remarks. This species resembles *E. jehucal* and *E. lenis*, but can be distinguished from the latter in the following characteristics: Anal tube (Figs 10, 12–13) longer than broad, narrowing from half to apex, slightly expanded near apex, apical margin concave medially, laterally with triangular processes; phallobase (Figure 18) with three processes at base in dorsal view, middle process wide (Figs. 15, 16a, 18a), with two teeth apically, lateral processes (Figs 15, 16b, 18b) hook-shaped; phallobase laterally with two processes (Figs 15c, 16d); lateral phallobase lobes asymmetrical, narrowing apically, one is short (Figure 15e), the other is long and curved cephalad (Figs 15f, 16f).

Discussion

The genus *Euxaldar* is similar to *Neohemisphaerius* Chen, Zhang & Chang, 2014, but differs as follows: Posterior margin of coryphe slightly angularly concave (Figure 4); Metope slightly longer in midline than widest, median carinae absent (Figure 5); Metope and clypeus joint at nearly right angle (Figure 6); Clypeus without hump-like processes (Figure 5); Aedeagus without ventral hooks (Figs 15, 16); *Neohemisphaerius*: Posterior margin of coryphe obviously angularly concave (see Chen et al. 2014: figs 2–35C, 2–36C; Zhang et al. 2016: fig. 1); Metope elongate, distinctly longer in midline than widest, median carinae obviously present (see Chen et al. 2014: figs 2–35E, 2–36E; Zhang et al. 2016: figs 3, 6); Metope and clypeus joint at nearly obtuse angle (see Chen et al. 2014: figs 2–35D, 2–36D; Zhang et al. 2016: figs 2, 5); Clypeus with a hump-like process medially (see Chen et al. 2014: figs 2–35E, 2–36E; Zhang et al. 2016: figs 3, 6); Aedeagus with pair of ventral hooks (see Chen et al. 2014: figs 2–35M, 2–36L; Zhang et al. 2016: fig. 9).

Acknowledgments

We are grateful to Mr. KeKe Liu (School of Life Sciences, Jinggangshan University) for collecting valuable specimens. We thank Dr. Wilson and Dr. Gnezdilov for proofreading. This work was supported by the Natural Science Foundation of China (31460157), the Natural Science Foundation of Jiangxi Province, China (20171BAB204010), Science Research Fund of Jiangxi Provincial Education Department (GJJ170639), the Scientific Research Foundation for Doctors of Jinggangshan University (JZ10039) and High Level Discipline of Biology, Jiangxi Province.

References

- Chen XS, Zhang ZG, Chang ZM (2014) Issidae and Caliscelidae (Hemiptera: Fulgoroidea) from China. Guizhou Science and Technology Publishing House, Guiyang, 242 pp.
- Fennah RG (1978) Fulgoroidea (Homoptera) from Vietnam. *Annales Zoologici* 34(9): 207–279.
- Gnezdilov VM, Constant J (2012) Review of the family Issidae (Hemiptera: Fulgoromorpha) in Vietnam with description of a new species. *Annales Zoologici* 62(4): 571–576. <https://doi.org/10.3161/000345412X659632>
- Gnezdilov VM (2013) Modern classification and the distribution of the family Issidae Spinola (Homoptera, Auchenorrhyncha, Fulgoroidea). *Entomologicheskoe obozrenie* 92(4): 724–738. [English translation published in *Entomological Review* (2014) 94(5): 687–697.] <https://doi.org/10.1134/S0013873814050054>
- Gnezdilov VM (2003) Review of the family Issidae (Homoptera, Cicadina) of the European fauna, with notes on the structure of ovipositor in planthoppers. *Chteniya pamyati*

- NA Kholodkovskogo [Meetings in memory of NA Cholodkovsky], St. Petersburg 56(1): 1–145. [In Russian with English summary]
- Gnezdilov VM, Bourgoïn T, Wang ML (2017) Revision of the Genus *Euxaldar* Fennah, 1978 (Hemiptera: Fulgoroidea: Issidae). *Annales Zoologici* 67(1): 13–20. <https://doi.org/10.3161/00034541ANZ2017.67.1.002>
- Wang ML, Zhang Y, Bourgoïn T (2016) Planthopper family Issidae (Insecta: Hemiptera: Fulgoromorpha): linking molecular phylogeny with classification. *Molecular Phylogenetics and Evolution* 105: 224–234. <https://doi.org/10.1016/j.ympev.2016.08.012>
- Zhang ZG, Chang ZM, Chen XS (2016) Review of the planthopper genus *Neohemisphaerius* (Hemiptera, Fulgoroidea, Issidae) with description of one new species from China. *ZooKeys* 568: 13–21. <https://doi.org/10.3897/zookeys.568.6700>

A new species of *Leptopulvinaria* Kanda from China, with a key to species (Hemiptera, Coccoomorpha, Coccidae)

Xiaoying He¹, Yangyang Han², Sanan Wu¹

1 Key Laboratory for Silviculture and Conservation of Ministry of Education, Beijing Forestry University, Beijing 100083, China **2** Shanghai Forestry Station, Shanghai 200072, China

Corresponding author: Sanan Wu (sananwu@bjfu.edu.cn)

Academic editor: R. Blackman | Received 11 April 2018 | Accepted 29 June 2018 | Published 13 August 2018

<http://zoobank.org/48CB967F-8829-4E02-BFE0-CB56F28D7DAC>

Citation: He X, Han Y, Wu S (2018) A new species of *Leptopulvinaria* Kanda from China, with a key to species (Hemiptera, Coccoomorpha, Coccidae). ZooKeys 781: 59–66. <https://doi.org/10.3897/zookeys.781.25713>

Abstract

A new species *Leptopulvinaria sapinda* sp. n. is described and illustrated based on adult females collected on *Sapindus saponaria* (Sapindaceae) from Shanghai and Jiangsu. This is the first report of *Leptopulvinaria* species in China. A key to the species of *Leptopulvinaria* Kanda is provided.

Keywords

China, Pulvinariini, soft scale insect, taxonomy

Introduction

The family Coccidae (Hemiptera: Sternorrhyncha: Coccoomorpha) is the third largest family of the Coccoomorpha after the Diaspididae (armored scales) and Pseudococcidae (mealybugs), consisting of 1185 described species, distributed in 169 genera all over the world (García Morales et al. 2018, Williams and Hodgson 2014). Species belonging to this family are widespread throughout the world and many of them are important pests on agricultural, horticultural, and ornamental plants (Henderson and Hodgson 2005). These include *Pulvinaria salicicola* (Borchsenius), which caused much damage to growth of roadside afforested willows in Lidian County, Heilongjiang Province of

China with an injury rate as high as 90% (Zhang et al. 1993), and *Ceroplastes japonicus* (Green), which can cause deformation or death of poplars and the percentage of damaged trees is more than 65% in some areas of Lianyungang city, Jiangsu Province (Wang et al. 2008).

The genus *Leptopulvinaria* was established by Kanda (1960), based on its type species, *Leptopulvinaria elaeocarpi* Kanda, 1960, and it was diagnosed by absence of tarsal and claw digitules. Tang (1991) placed this genus in the tribe Pulviniini. Hodgson (1994) redescribed the type species based on the type specimen and found that it did in fact have tarsal digitules and claw digitules. He did not affirm the exact taxonomic position of the species, since it is difficult to ascertain the exact distribution of the dorsal and ventral tubular ducts owing to poor condition of type specimens. Recently, Tanaka and Amano (2008) redescribed *L. elaeocarpi* based on newly collected material and described the second species *L. kawaii* Tanaka & Amano from Japan. They also observed the production of ovisacs of both these species at their oviposition periods and clearly and definitely placed this genus in the tribe Pulviniini. Choi and Lee (2017) reported *L. kawaii* from South Korea. Currently, species of this genus are therefore known only from Japan and South Korea and the genus includes only two species, namely *Leptopulvinaria elaeocarpi* Kanda and *Leptopulvinaria kawaii* Tanaka & Amano.

In the course of our taxonomic study of soft scales (Coccidae) in China, we found an undescribed species which clearly belongs to this genus. Here, we describe and illustrate adult female specimens of this new species. This report is the first formal record of the occurrence of *Leptopulvinaria* species in China, and it may be useful for further taxonomic and biogeographic study of the genus and its species. A key to all three species of *Leptopulvinaria* is provided.

Materials and methods

Slide mounting methods for the specimens in this study followed Hodgson and Henderson (2000). Terminology of the morphological features used in the description mainly followed Kondo and Hodgson (2013) and Tanaka and Kondo (2015), who avoided using the term “pregenital disc-pores” or “perivulvar pores”, because in several species of Coccidae, these pores are not restricted to the pregenital or perivulvar area, and can be present throughout the medial area of the venter; so that using the term “pregenital” or “perivulvar” may be misleading. The species described in this study also have the pores not only in the pregenital area but also on the medial area of the venter. The term “multilocular pore” is therefore used herein for the pores with multiple loculi, with the exception of spiracular pores. The mounted specimens were examined under a compound light microscope (Leica DME) fitted with an ocular micrometer. All measurements were given (minimum-maximum range) in micrometers (μm), except for body length and width which are given in millimeters (mm).

All specimens are deposited in the Insect Collection, the Department of Forestry Protection, Beijing Forestry University, Beijing, China (BFUC).

Taxonomy

Genus *Leptopulvinaria* Kanda, 1960

Type species. *Leptopulvinaria elaeocarpi* Kanda, 1960, by monotypy and original designation.

Generic diagnosis. Adult female. Body elongate oval, broadest at thorax or anterior abdomen. *Dorsum*. Derm membranous. Tubular ducts and microducts frequent. Tubercles convex, occasionally absent. *Margin*. Setae spinose, each with a simple pointed apex. Stigmatic clefts not deep but distinct; each with one to four (usually three) stigmatic spines. *Venter*. Antennae with eight or nine (usually eight) segments. Legs each with a well-developed tibio-tarsal articulation and an articulatory sclerosis. Multilocular pores each with nine to eleven loculi, present mainly across most abdominal segments. Spiracular pores each with four to six (usually five) loculi. Two types of tubular ducts present. With one or two pairs of long setae medially on all abdominal and thoracic segments (occasionally lacking on thoracic segments). For further diagnostic characteristics, see Tanaka and Amano (2008).

Key to *Leptopulvinaria* species based on slide-mounted adult females' morphology

- 1 Ventral tubular ducts absent medially on head and thoracic segments, though rarely a few may be present **2**
- Ventral tubular ducts present medially on head and thoracic segments.....
..... *L. kawaii* Tanaka & Amano, 2008
- 2 Dorsal tubular ducts, microducts and setae arranged in a reticulate pattern, multilocular pores absent on head and thorax, though occasionally a few present on metathorax, preopercular pores restricted to anterior anal plates
..... *L. elaeocarpi* Kanda, 1960
- Dorsal tubular ducts, microducts and setae not arranged in a reticulate pattern, multilocular pores numerous on head and thorax, preopercular pores extend from anterior anal plates to prothorax..... *L. sapinda* sp. n.

Leptopulvinaria sapinda sp. n.

<http://zoobank.org/46EDC4B0-9BFD-45DC-82FF-6E3134DC0274>

Material examined. Holotype: Adult female. CHINA, Shanghai City, Qingpu District, 7.vi.2017, on *Sapindus saponaria* L. (Sapindaceae), coll. Yangyang Han, 1♀ (BFUC).

Paratypes: Same data as holotype, 18♀ (BFUC); CHINA, Jiangsu Province, Kunshan City, 11.X.2016, on same host as holotype, coll. Lei Gao, 11♀♀ (BFUC).

Description. Adult female. Unmounted material: (Figure 1A–C). Adult female more or less pointed anteriorly, usually somewhat asymmetrical, the young one whitish

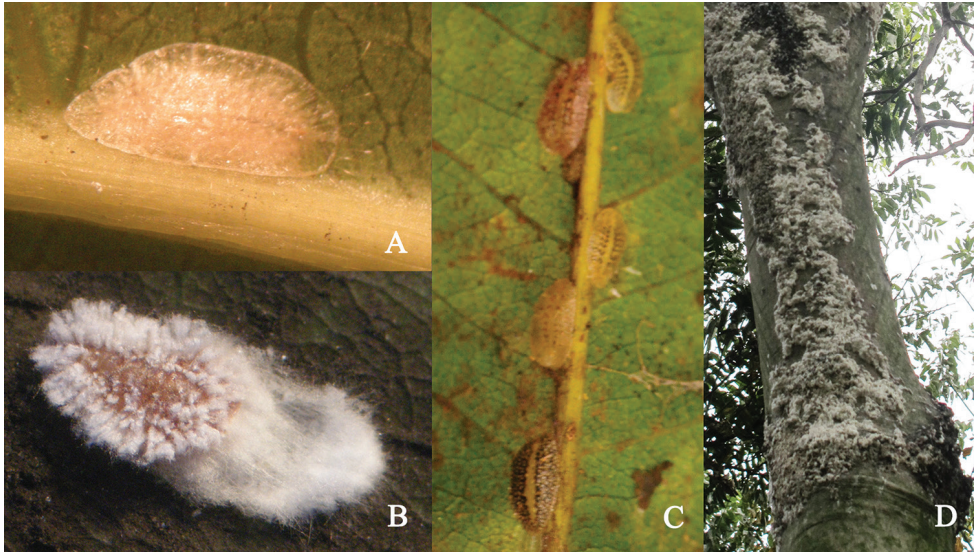


Figure 1. *Leptopulvinaria sapinda* sp. n., **A** young adult female **B** adult female after oviposition **C** adult females from young to mature stages **D** ovisacs on trunk of host tree.

or light yellowish (Figure 1A), changing to with dark brown reticulations on dorsum except midline, the mature one black, with a longitudinal yellowish stripe along middle line of dorsum (Figure 1C). After oviposition (Figure 1B), the dorsum with wax filaments mainly on the marginal and submarginal area; wax secreted forming a short white ovisac.

Mounted material (Figure 2A–R). Body (Figure 2A) elongate oval, 2.2–5.3 mm long, 1.2–3.0 mm wide. Margin with a slight indentation at each stigmatic cleft and sometimes also near each eyespot. Anal cleft 400–770 μm , approximately 1/6–1/7 body length.

Dorsum. Derm membranous. Dermal areolations (Figure 2R) well developed. Dorsal tubercles (Figure 2M) convex, each 11–13 μm in diameter, present on submarginal area, 12–14 between anterior spiracular clefts, 3–5 between each anterior and posterior spiracular clefts, and 10–15 between each posterior spiracular clefts and anal cleft. Preopercular pores (Figure 2L) circular, obvious, each with a diameter of 6–8 μm , present in a small group of 36 to 56 in front of anal plates, extending to prothorax. Tubular ducts (Figure 2P) of one type, outer ductule 8–10 μm long, 2–3 μm wide, inner ductule 12–17 μm long, 1 μm wide, arranged in a reticulate pattern with microducts (Figure 2N). Dorsal setae (Figure 2Q) 6–7 μm long, spiniform, arranged like tubular ducts and microducts. Anal plates (Figure 2K₁) each triangular, 150–158 μm long, 63–75 μm wide, anterolateral margin slightly concave, 78–100 μm long; posterolateral margin slightly convex, 115–138 μm long. Each plate with four apical setae. Ano-genital fold (Figure 2K₂) with two pair of setae along anterior margin and two pairs laterally. Anal ring subcircular, with one or two rows of translucent pores and six or eight anal ring setae. Eyespots present near margin.

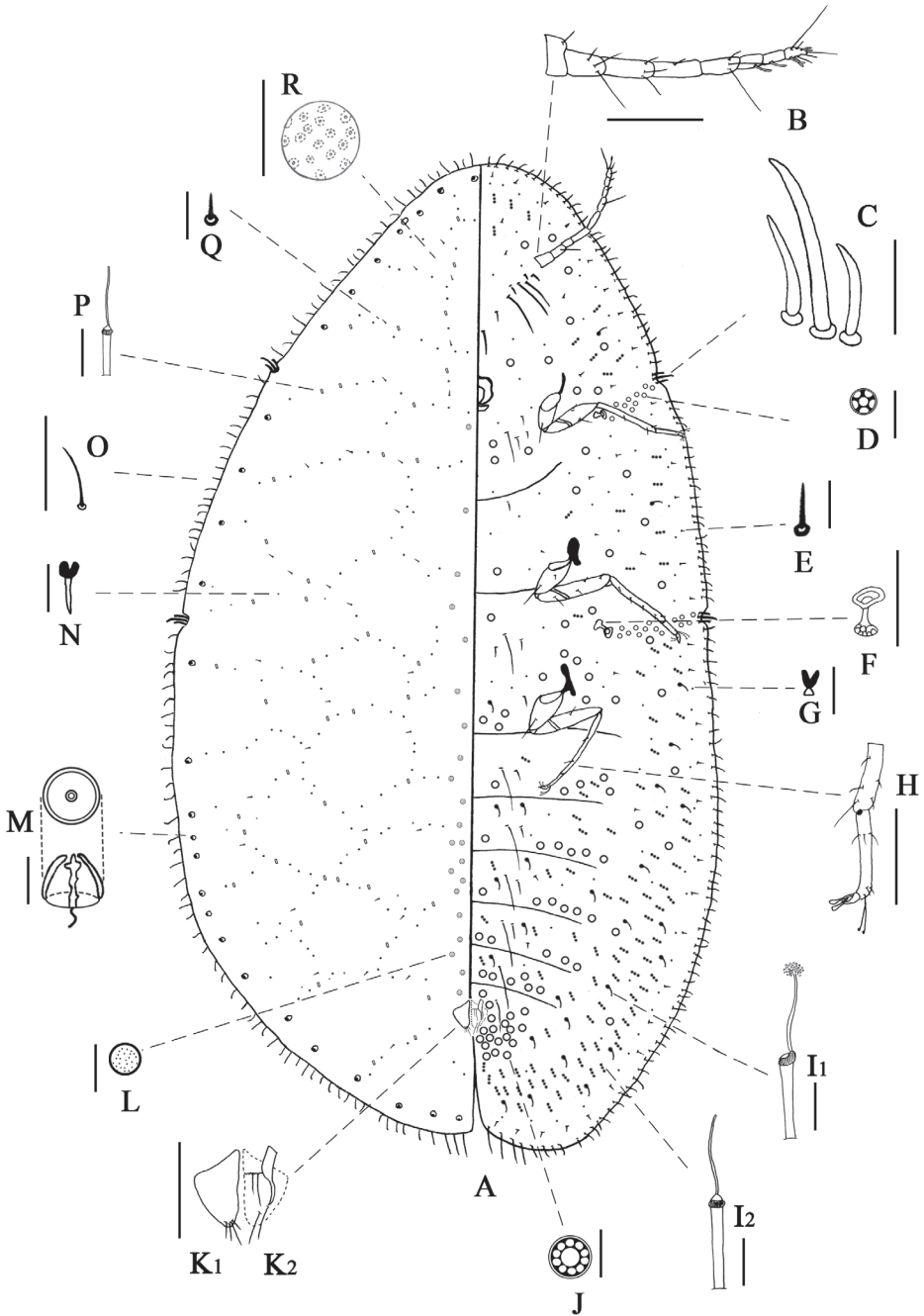


Figure 2. Adult female of *Leptopulvinaria sapinda* sp. n., **A** body derm **B** antennae **C** stigmatic spine **D** spiracular pore **E** submarginal seta **F** spiracle **G** ventral microduct **H** leg **I**₁, **I**₂ ventral tubular duct **J** multilocular pore **K**₁ anal plate **K**₂ ano-genital fold **L** preopercular pore **M** dorsal tubercle **N** dorsal microduct **O** marginal setae **P** dorsal tubular duct **Q** dorsal seta **R** dermal areolation. Scale bars: 200 μm (**B**, **F**, **H**, **K**, **R**); 20 μm (**C**, **O**); 10 μm (**D**, **E**, **G**, **I**, **J**, **L**, **N**, **P**, **Q** except **A**).

Margin. Marginal setae (Figure 2O) 14–29 μm long, straight, or slightly curved, rather bluntly pointed; distributed as follow: 60–69 between anterior stigmatic cleft, 21–27 between each anterior and posterior stigmatic cleft, and 52–64 between each posterior stigmatic cleft and anal cleft. Stigmatic clefts (Figure 2C) not deep but distinct; with three (except one with four) stigmatic spines in each cleft; median spine 32–56 μm long, 1.5–2.3 times as long as lateral spines, slightly curved, bluntly pointed; lateral spines slightly curved, bluntly pointed, 14–34 μm long. Eyespots present on margin.

Venter. Derm membranous. Ventral setae: one or two pairs of long setae, 125–238 μm long, present medially on all abdominal and thoracic segments, and also near each coxa (a few pairs of setae occasionally absent on thoracic segments); three pairs of long setae present between antennae, 225–258 μm long; short setae (Figure 2E) 11–14 μm long, slender, acute, mostly straight, and distributed evenly. Antennae (Figure 2B) well developed, 8-segmented, 493–678 μm long, third segment longest; length of segments I to VIII (μm): 60–75, 75–113, 90–150, 78–125, 65–93, 48–83, 38–68, 43–53, respectively; segment VI; VII; VIII each with 1, 1, 4 fleshy setae. Clypeolabral shield 128–168 μm long, 125–168 μm wide. Labium 68–80 μm long, 80–113 μm wide. Legs (Figure 2H) well developed, with a tibio-tarsal articulation and an articular sclerite; claw without denticle; tarsal digitules slender, knobbed; claw digitules broad, and expanded at apex; hind trochanter + femur 275–370 μm long, hind tibia + tarsus 385–558 μm long; claw 35–45 μm long. Ratio of lengths of hind tibia + tarsus to hind trochanter + femur 1.4–1.8. Ratio of lengths of hind tarsus to tibia 1.9–2.3. Anterior spiracles each 68–88 μm long, 45–60 μm wide; posterior spiracles (Figure 2F) each 75–100 μm long, 55–75 μm wide. Spiracular pores (Figure 2D) present in narrow bands one to three pores wide between margin and each spiracle; each mainly with five loculi, 5 μm in diameter, 22–43 in anterior spiracular pore band, 33–56 in posterior spiracular pore band. Multilocular pores (Figure 2J) 7–8 μm in diameter, mainly ten loculi, frequent around anal area, in transverse bands on abdomen, and also scattered in head and thorax. Ventral microducts (Figure 2G) scattered. Ventral tubular ducts (Figure 2I) of two types present: I) a duct (Figure 2I₁) with a narrow inner ductule and a well-developed terminal gland; outer ductule 10–15 μm long, 3–4 μm wide, inner ductule 16–20 μm long, 1–2 μm wide, 5 μm wide for terminal gland; present submarginally on posterior segments, where they are mixed with type II ducts, a few ducts also present medially on abdominal segments (occasionally present on submarginal head and thorax). II) a duct (Figure 2I₂) with a slender inner filament; outer ductule 14–16 μm long, 2–3 μm wide, inner ductule 13–18 μm long, 1 μm wide; numerous in submarginal area and mixed with ducts of type I, but becoming sparse on thorax and head, a few present medially on abdominal segments.

Distribution. China (Jiangsu and Shanghai)

Host plant. *Sapindus saponaria* L. (Sapindaceae)

Etymology. The specific epithet is taken from the genus name of host plant.

Remarks. The new species is easily distinguished from the two other *Leptopulvinaria* species by having dorsal tubular ducts, microducts, and setae arranged in a re-

ticulate pattern, and numerous multilocular pores on head and thorax. Moreover, *L. sapinda* sp. n. has a group of preopercular pores extending from anterior anal plates to prothorax, and has 10–15 dorsal tubercles between each posterior stigmatic cleft and the anal cleft, whereas *L. elaeocarpi* has a small group of preopercular pores restricted to anterior anal plates, and 1–4 dorsal tubercles between each posterior stigmatic cleft and the anal cleft. In *L. kawaii*, preopercular pores are absent (or if there are any, then they are difficult to see) and there are only 0–7 dorsal tubercles between each posterior stigmatic cleft and the anal cleft.

During the pre-oviposition period, the adult females of this new species suck plant juices mainly along the main and lateral veins of leaves (Figure 1C). When ovipositing, they usually climb to the trunk and branches (although occasionally they stay on the leaves) to lay eggs (Figure 1B, 1D). Similar behavior, namely changing infesting place on the host trees before oviposition is also reported in *L. kawaii* (Kawai 1980). This fact may indicate that *L. sapinda* sp. n. is probably close to *L. kawaii* and supports the placement of the new species in this genus.

Acknowledgements

We are grateful to Dr. Hirota Tanaka (Ehime University, Faculty of Horticulture, Japan) for providing related papers and giving constructive comments on the manuscript. The manuscript also benefited greatly from the comments provided by Dr. Jinyeong Choi (Seoul National University, Department of Agricultural Biotechnology, South Korea) and Dr. Roger Blackman. This study is supported by the National Natural Science Foundation of China (Grant No. 31772488).

References

- Choi J, Lee S (2017) Taxonomic review of the tribe Pulvinariini (Hemiptera: Coccidae) in Korea. *Journal of Asia-Pacific Entomology* 20(1): 89–100. <https://doi.org/10.1016/j.aspen.2016.11.013>
- Deng J, Li HB, Wang XB, WU SA (2014) Introduction to a new invasive pest, *Ceroplastes stellifer* (Westwood) (Hemiptera: Coccoidea: Coccidae). *Chinese Journal of Applied Entomology* 51(1): 278–282
- García Morales M, Denno BD, Miller DR, Miller GL, Ben-Dov Y, Hardy NB (2016) ScaleNet: A literature-based model of scale insect biology and systematics. Database. <https://doi.org/10.1093/database/bav118> [accessed 22 June 2018]
- Henderson RC, Hodgson CJ (2005) Two new species of *Umbonichiton* (Hemiptera: Sternorrhyncha: Coccoidea: Coccidae) from New Zealand. *Zootaxa* 854: 1–11. <https://doi.org/10.11646/zootaxa.854.1.1>
- Hodgson CJ (1994) *The Scale Insect Family Coccidae: An Identification Manual to Genera*. CAB International, Wallingford, Oxon, 639 pp.

- Hodgson CJ, Henderson RC (2000) Coccidae (Insecta: Hemiptera: Coccoidea). Fauna of New Zealand 41: 1–264.
- Kanda S (1960) Descriptions of the Coccidae from Japan (Homoptera). Kontyû 28: 116–123.
- Kawai S (1980) Scale Insects of Japan in Colors. Zenkoku Nôson Kyoiku Kyokai, Tokyo, 455 pp. [In Japanese]
- Kondo T, Hodgson C (2013) A Third Species of *Hemilecanium* Newstead (Hemiptera: Coccoidea: Coccidae) from the New World, with Keys to Species in the Genus. Neotropical Entomology 42(5): 508–520. <https://doi.org/10.1007/s13744-013-0151-3>
- Kosztarab M, Kozár F (1988) Scale Insects of Central Europe. Akadémiai Kiadó, Budapest, 456 pp.
- Tanaka H, Amano H (2008) Taxonomic study of the genus *Leptopulvinaria* Kanda (Hemiptera: Coccidae), with description of a new species. Entomological Science 11: 221–229. <https://doi.org/10.1111/j.1479-8298.2008.00259.x>
- Tanaka H, Kondo T (2015) Description of a new soft scale insect of the genus *Pulvinaria* Targioni Tozzetti (Hemiptera, Coccoidea, Coccidae) from Bogota, Colombia. ZooKeys 484: 111–120. <https://doi.org/10.3897/zookeys.484.9280>
- Tang FT (1991) The Coccidae of China. Shanxi United Universities Press, Taiyuan, 377 pp. [In Chinese]
- Wang YX, Xue CH, Zhang H, Fan JZ, Li L, Wang D (2008) Occurrence regularity and damage of *Ceroplastes japonica* in poplars. Forest Pest and Disease (04): 12–14.
- Williams DJ, Hodgson CJ (2014) The case for using the infraorder Cocomorpha above the superfamily Coccoidea for the scale insects (Hemiptera: Sternorrhyncha). Zootaxa 3869(3): 348–350. <https://doi.org/10.11646/zootaxa.3869.3.9>
- Zhang XK, Li CD, Zhang H, Ma SX, Yuan XC (1993) A preliminary study on the bionomics of *Pulvinaria salicicola* Borchs in Heilongjiang Province. Journal of Northeast Forestry University 22(03): 10–15.

New record of *Microtus mystacinus* in eastern Kazakhstan: phylogeographical considerations

Tereza Holicová¹, František Sedláček¹, Anna Mácová²,
Jakub Vlček¹, Jan Robovský¹

¹ Department of Zoology, Faculty of Science, University of South Bohemia, České Budějovice, Czech Republic

² Department of Parasitology, Faculty of Science, University of South Bohemia, České Budějovice, Czech Republic

Corresponding author: Tereza Holicová (holic.ter@seznam.cz)

Academic editor: R. López-Antoñanzas | Received 29 March 2018 | Accepted 18 June 2018 | Published 13 August 2018

<http://zoobank.org/38FD3EFB-F36E-4E5B-84B4-FA4AD9FF5D80>

Citation: Holicová T, Sedláček F, Mácová A, Vlček J, Robovský J (2018) New record of *Microtus mystacinus* in eastern Kazakhstan: phylogeographical considerations. ZooKeys 781: 67–80. <https://doi.org/10.3897/zookeys.781.25359>

Abstract

The Eastern European vole (*Microtus mystacinus*) is an arvicoline rodent distributed across northern and eastern Europe, the Balkans, Turkey, Armenia, NW and N Iran, Russia as far east as the Tobol River in W Siberia, and W and N Kazakhstan. We present a novel records from eastern Kazakhstan (the village of Dzhambul – 49°14'21.3"N, 86°18'29.9"E and the village of Sekisovka – 50°21'9.18"N, 82°35'46.5"E) based on mtDNA and we discuss implications of this findings on biogeography of eastern Kazakhstan populations. Marine Isotope Stage 11 is considered an important period for the diversification of the *arvalis* species group. In the context of our study, it is important to analyse genetically discontinuous Siberian populations, and the current distribution of *M. mystacinus* in new localities in eastern Kazakhstan.

Keywords

Microtus mystacinus, Kazakhstan

Introduction

The Eastern European vole, *Microtus mystacinus* De Filippi, 1865, is an arvicoline rodent with an unsettled nomenclature. It has been named most commonly as *M. subarvalis* Meyer, Orlov & Skholl, 1972, *M. epiroticus* Ondrias, 1966, *M. rossiaemerdionalis*

Ognev, 1924, and *M. levis* Miller, 1908 (e.g., Musser and Carleton 2005; Kryštufek and Vohralík 2005). We adhere to the name *M. mystacinus*, following the detailed study by Mahmoudi et al. (2017) and the review of Kryštufek (2017). Despite its nomenclature instability, there is a consensus about its phylogenetic affinities: this species has been traditionally attributed to the *arvalis* species group in the subgenus *Microtus* s. str. (Musser and Carleton 2005). This view has been strongly supported by chromosomal and genetic evidence (e.g., Mazurok et al. 2001, Jaarola et al. 2004, Mahmoudi et al. 2017). According to new studies, it is related to the following species: *M. ilaeus* Thomas, 1912 (syn. *M. kirgisorum* Ognev, 1950), *M. transcaspicus* Satunin, 1905, *M. kermanensis* Roguin, 1988, *M. arvalis* (Pallas, 1778), and *M. obscurus* (Eversmann, 1841) (e.g., Golenishchev et al. 2000; Jaarola et al. 2004; Kryštufek and Vohralík 2005; Mahmoudi et al. 2017), but it is the closest relative of *M. arvalis* and *M. obscurus* based on available DNA data (cyt *b*; Mahmoudi et al. 2017).

In general, *M. mystacinus* represents one of the best cases of a cryptic species in arvicolines, because it was primarily recognized by chromosomal number (*M. mystacinus*: $2n = 54$; *M. arvalis*: $2n = 46$) (Meyer et al. 1969; Mazurok et al. 2001; Pavlova and Tchabovsky 2011). It is now generally considered a valid species of the genus *Microtus* based on hybridisation data, and chromosomal and genetic differences (for reviews see Kryštufek and Vohralík 2005 and Musser and Carleton 2005). Several authors have attempted to distinguish *M. mystacinus* from the common vole (*M. arvalis*), the Altai vole (*M. obscurus*), and the Middle Eastern vole (*M. transcaspicus*) based on morphological data (Král et al. 1981; Zagorodnyuk 1991a, b; Masing 1999; Hotzi et al. 2008; Markova et al. 2009, 2012; Markov et al. 2012; Ghorbani et al. 2015). Although some diagnostic characters have been proposed (e.g., qualitative and quantitative cranial and dental morphology) and multivariate morphometric approaches have been applied (e.g., Markov et al. 2012; Markova et al. 2012), these approaches have been lacking in diagnostic power (Kryštufek and Vohralík 2005; Markov et al. 2012), except for characters proposed by Kryštufek and Vohralík (2005).

The distribution and habitat preferences of the Eastern European vole are relatively well known due to the intensive attention devoted to it (see Kryštufek and Vohralík 2005; Musser and Carleton 2005; Shenbrot and Krasnov 2005; Kryštufek 2017, and references therein). It prefers to live in places with high and dense herbaceous or grassy vegetation, hedgerows, and stands of reeds and it avoids short-grass meadows and dry areas (Kryštufek and Vohralík 2005; Aulagnier et al. 2009; Kryštufek 2017). The distribution range of the Eastern European vole, to date, extends from southern Finland, the Baltic eastwards to western Siberia with patches in the southern Urals, the Novosibirsk suburbs to the southwest margin of Lake Baikal and Buryatia, the southern Caucasus, northern Iran to Turkey, connecting to Greece and the majority of the Balkan Peninsula to Ukraine (Baskevich 1996; Gileva et al. 1996; Yakimenko and Kryukov 1997; Musser and Carleton 2005; Shenbrot and Krasnov 2005; Pavlova and Tchabovsky 2011; Ghorbani et al. 2015; Baskevich et al. 2016; Kryštufek 2017; Moroldoev et al. 2017).

Populations occupying the Arctic Svalbard Archipelago (Fredga et al. 1990; recently extinct according to Aulagnier et al. 2009), Jan Mayen Island in the N Atlantic (Kryštufek

2017), Olkhon Island in Lake Baikal (Pavlova and Tchabovsky 2011; Kryštufek 2017) and Far Eastern Russia (Khabarovsk Krai, near Sovetskaya Gavan City, see Kartavtseva et al. 2012; Tiunov et al. 2013) are probably introduced. *M. mystacinus*, *M. arvalis*, and *M. obscurus* broadly overlap in distribution and occur sympatrically in a few regions (e.g., Meyer et al. 1996; Musser and Carleton 2005; Shenbrot and Krasnov 2005 see also Tougard et al. 2013).

When considering the distribution of *M. mystacinus* within Kazakhstan, there are records from the western or north-western parts. The easternmost record is from the Karabalyk district (Kovalskaya 1994; Meyer et al. 1996). Here, we report an additional record of *M. mystacinus* from eastern Kazakhstan and comment on it from a phylogeographic point of view.

Materials and methods

A survey of small mammals conducted in eastern Kazakhstan provided the surprising discovery of three specimens of *M. mystacinus*, that are characterized here based on molecular methods. The first sample (Kazakhstan 1) was collected in July 2006 on pasture land near the village of Dzhabul (GPS coordinates: 49°14'21.3"N, 86°18'29.9"E) by FS and two more specimens (Kazakhstan 2, 3) were collected in September 2017 near a pond not far from the village Sekisovka (GPS coordinates: 50°21'9.18"N, 82°35'46.5"E) by AM and JV.

DNA extraction was carried out using the Genomic DNA Mini Kit – tissue (Geneaid, New Taipei, Taiwan). We amplified the mitochondrial gene cytochrome *b* (cyt *b* hereinafter) using universal primers L14724, L15162, H15149 and H15915 (Irwin et al. 1991). Amplification conditions for cyt *b* consisted of 37 thermal cycles, an initial denaturation step at 94 °C for 3 min, denaturation at 94 °C for 30 seconds, annealing at 50 °C for 1 min, extension at 72 °C for 1.5 min and final extension at 72 °C for 10 min. Sequences were obtained using the Sanger sequencing (Sanger et al. 1977) services at laboratory SEQme s.r.o. (Dobříš, Czech Republic).

We obtained 1137 base pairs long sequences that satisfied the quality of base pairs (GenBank access number LT970847-LT970849). These were compared using available sequences from GenBank, specifically with 250 specimens that comprise all available sequences of *M. mystacinus* (under names *M. levis*, *M. rossiameridionalis* and *M. mystacinus*), and representative sequences of particular clades in *M. arvalis* and *M. obscurus* associated with previous studies (Baker et al. 1996a, b; Haynes et al. 2003; Fink et al. 2004; Jaarola et al. 2004; Triant and DeWoody 2007; Bužan et al. 2010; Thanou et al. 2012; Tougard et al. 2013; Stojak et al. 2016; Mahmoudi et al. 2017). Several more sequences (*M. kirgisorum*, accession number AY513809, AY513810; *M. socialis*, accession number AY513830, AY513831; and *M. transcaspicus*, accession number KX581067-KX581075) were downloaded from GenBank as potentially outgroups. The obtained sequences were aligned using the ClustalW algorithm implemented in GENEIOUS v.10.0.5 (Kearse et al. 2012). We employed a likelihood (ML) and Bayes-

ian inference method (BI) for phylogenetic analyses. Likelihood phylogenetic analyses were conducted using the PhyML plugin for GENEIOUS. Final Bayesian phylogenetic analyses were conducted in BEAST 2.4.5.0 (Drummond et al. 2012), where phylogenetic relationships were reconstructed under the Yule speciation process (Steel and McKenzie 2001) with the GTR model of evolution detected in JModelTest 2.1.7 (Nylander 2004) under the Akaike Information Criterion (AIC). The nucleotide data were run for 30 000 000 generations with a sampling frequency of every 1000th generation; with final burn-in set at 20%. Time estimations were also computed in BEAST2 (Drummond et al. 2012) for the topology detected by the Bayesian phylogenetic analysis. We adopted one fossil calibration point (0.475±0.025 Mya for the origin of *M. arvalis*; Miesenheimer I; Tougaard et al. 2013) to estimate divergence time in studied taxa and to compare estimations with Mahmoudi et al. (2017) (which are based on the following proposed molecular clock rate, 3.27×10^{-7} mutations/site/year for *M. arvalis*; Martínková et al. 2013). The split time with 95% highest posterior density was applied to a relaxed-clock model assuming a constant population size. The convergence and stability of estimated parameters was checked using TRACER 1.6 (Rambaut et al. 2017) and the maximum clade credibility trees were obtained with TREEANNOTATOR 2.4.5.0, and visualized in FIGTREE 1.4.3 (Rambaut 2009).

Some analyses were applied for *M. mystacinus* only. Specifically, haplotype characteristics were identified using DnaSP version 5.0 (Rozas et al. 2003) and the degree of diversification was estimated based on average pairwise distances using the Kimura two-parameters model of substitutions in MEGA5 (Tamura et al. 2011). The detailed haplotype network was conducted in POP ART 1.7 using the median-joining method (Bandelt et al. 1999).

Results and discussion

The obtained sequences of 1137 base pairs from three specimens exhibited close relationships with available *cyt b* sequences of *Microtus mystacinus*, in all comparisons. Specifically, they were nested inside this species, so our study identified this species in eastern Kazakhstan (see also below). All sequences of *M. mystacinus* form a sister group to the *M. obscurus* + *M. arvalis*, in accordance with previous comprehensive studies (e.g., Haynes et al. 2003; Fink et al. 2004; Jaarola et al. 2004; Triant and DeWoody 2007; Tougaard et al. 2013; Stojak et al. 2015, 2016; Mahmoudi et al. 2017).

Considering the intraspecific structure in *Microtus mystacinus*, we can distinguish two deep lineages (Iran, abbreviated as IR) and the rest of populations mostly from Europe, additionally divided into several sub-lineages (TU, EU, GK), concordantly in ML and BI phylogenetic trees and the haplotype network (see Figure 1). This structure, specifically groups IR, TU, and EU, were identified firstly by Mahmoudi et al. (2017). TU lineage consists of Turkish and Armenian samples (without specimen Armenia 1), EU lineage of samples from the majority of Europe, mainly from Ukraine and Romania except for specimens from Greece, which comprise GK lineage, as well as samples

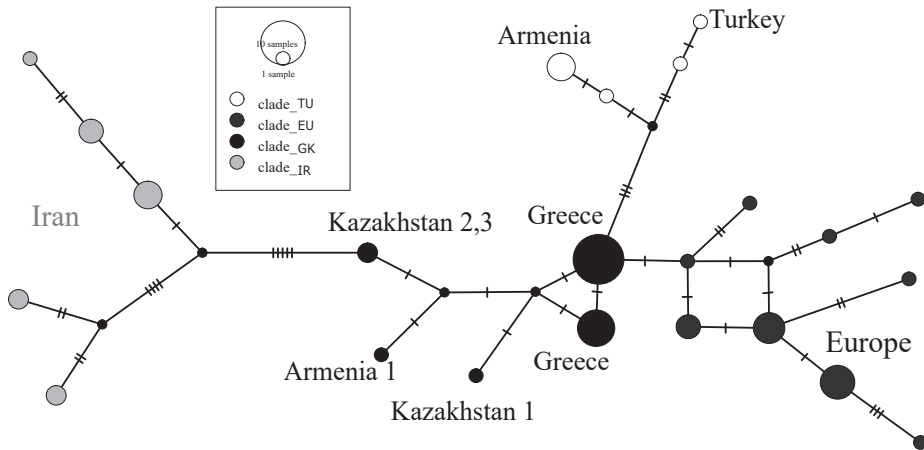


Figure 1. Median Joining Network based on the *cyt b* sequences of *M. mystacinus*.

Table 1. The K2P Inter – and intra-species average estimates of K2 genetic distance for *cyt b* in recognized lineages of *M. mystacinus* (TU – Turkey, Armenia; EU – Europe; GK – Greece, Kazakhstan; IR – Iran).

	1.	2.	3.	4.	5.	6.	7.	8.	9.	10.
1. TU	0.007									
2. EU	0.025	0.007								
3. GR	0.021	0.016	0.006							
4. Armenia_1	0.024	0.019	×	×						
5. Greece	0.016	0.011	×	0.009	0.001					
6. Kazakhstan	0.023	0.018	×	0.007	0.008	0.006				
7. IR	0.035	0.044	0.031	0.031	0.034	0.028	0.013			
8. <i>M. obscurus</i>	0.067	0.066	0.065	0.062	0.066	0.059	0.068	0.028		
9. <i>M. arvalis</i>	0.067	0.057	0.065	0.062	0.066	0.063	0.067	0.059	0.003	
10. <i>M. transaspicus</i>	0.075	0.079	0.071	0.069	0.072	0.065	0.068	0.067	0.084	0.004

from eastern Kazakhstan and the specimen 1 from Armenia. This pattern indicates a complex diversification of *M. mystacinus* across its former and current distribution.

In general, *Microtus mystacinus* exhibited rather low intraspecific *cyt b* distances (except for the Iranian subset) and the obtained interspecific *cyt b* distances (see Table 1) are very similar to the values published in other studies (*M. arvalis* × *mystacinus*: Jaarola et al. (2004): 6–8%; Mahmoudi et al. (2017): 6–7%). As the intraspecific divergence for *Microtus mystacinus* and its cryptic diversity was intensively discussed by Mahmoudi et al. (2017), we would like to note only that the genetic distances cannot be presented as an absolute criterion for deciding whether two operational taxonomic units are distinct species (for detail see Groves et al. 2017), and in the case of species within the *arvalis*-group, some currently recognized species with rather low genetic distances exhibit infertile hybrids or hybrids with a reduced fertility (Meyer et al. 1985; Golenishchev et al. 2000; Jaarola et al. 2004).

The estimated clade divergence times varied substantially according to the calibration used (see Table 2). In summary, our estimations are more similar with other esti-

Table 2. Time to the most recent common ancestor (TMRCA and 95% HPD lower/upper limit – in million years) with BEAST2 for particular *Microtus* species (T – *M. transcaasicus*, M – *M. mystacinus*, O – *M. obscurus*, A – *M. arvalis*) and recognized lineages of *M. levis* (TU – Turkey, Armenia; EU – Europe; GK – Greece, Kazakhstan; IR – Iran).

Nodes	Analysis 1 – fossil calibrations		Mahmoudi et al. 2017	Tougard et al. 2013
	TMRCAs	95% HPD	TMRCAs (95%HPD)	TMRCAs (95%HPD)
a. T+M+O+A	1.102	0.77–1.28	0.238 (0.16–0.35)	–
b. M+O+A	0.797	0.60–1.05	0.217 (0.15–0.31)	0.531 (0.42–0.67)
c. O+A	0.616	0.51–0.78	0.184 (0.12–0.26)	0.478 (0.40–0.56)
d. T	0.537	0.32–0.57	0.040 (0.01–0.08)	–
e. O	0.410	0.27–0.58	0.119 (0.07–0.18)	0.173 (0.10–0.29)
f. A	0.490	0.48–0.54	0.146 (0.10–0.21)	0.446 (0.39–0.49)
g. IR+ EU+GK+TU	0.575	0.04–0.77	0.147 (0.09–0.22)	0.033 (0.00–0.08)
h. EU+GK+TU	0.408	0.28–0.57	0.092 (0.05–0.14)	–
i. EU+GK	0.332	0.23–0.47	–	–
j. TU	0.235	0.10–0.40	0.022 (0.01–0.04)	–
k. EU	0.219	0.14–0.32	0.075 (0.05–0.11)	–
l. GK	0.280	0.19–0.40	–	–
m. IR	0.390	0.24–0.47	0.117 (0.06–0.18)	–

mates based on fossil calibration points (albeit slightly higher) than with estimations based on mutation rates (see Table 2). Focusing on the most studied species, *M. arvalis*, we estimate its time to the most recent common ancestor (TMRCA) as 0.490 Mya, Tougard et al. (2008) 0.472 Mya and Tougard et al. (2013) 0.446 Mya, Stojak et al. (2015, 2016) 0.064–0.067 Myr and Mahmoudi et al. (2017) 0.146. Our estimation is similar to Tougard et al. (2008, 2013) as a logical result of the utilization of the same fossil calibration point, but all other specified estimations are much lower and associated with the same mutation rate (3.27×10^{-7} substitutions/site/year) proposed by Mar-tínková et al. (2013) specifically for *Microtus arvalis* based on a recent geological event. It is not easy to judge which values are realistic, but our estimates seem to be compatible with other phylogenetic studies (e.g., Mazurok et al. 2001; Bannikova et al. 2010) and the fossil record (e.g., Cuenca-Bescós et al. 2001; Markova et al. 2012). Based on this compatibility, we adhere to the values of our estimations. In any case, it would be worth to compare different calibrations methods under different calibrations points and proposed mutations rates in future (e.g., methods of Baker et al. 1996a; Jaarola and Searle 2002), and also to consider the potential biases of the fossil record (e.g., incomplete nature, process of geological dating, reliability of species identification; cf. Ho 2007).

Evolution and diversification of arvicoline rodents, including the *arvalis*-group, has been closely related to Quaternary climatic oscillations and the associated abiotic and biotic environmental factors (e.g., Horáček and Ložek 1988; Horáček 1990; Chaline et al. 1999; Stojak et al. 2016; Tougard 2017 and references therein). For the *arvalis*-group, interglacial periods are considered to be periods of species expansions and glacials as periods of retractions with potential survival of particular species in refu-

gia (e.g., Golenishchev et al. 2000; Tougard et al. 2008; Stojak et al. 2015; Stojak et al. 2016). Golenishchev et al. (2000) considered one of the ancient alpine glaciations as responsible for disrupting the geographic range of *M. arvalis* and *M. obscurus*, whereas Tougard et al. (2008) considered interglacials as the agents of speciation. Based on our time estimations, the diversification of *M. mystacinus* + (*M. arvalis* + *M. obscurus*) group has happened within the last 0.79 Mya, thus comprising several interglacial and glacial periods (Gates 1993; Sirocko et al. 2007; Mahmoudi et al. 2017).

In our data, we observed synchronous, deep intraspecific divergences in all three species around 0.49–0.41 Mya (see Figure 2; in *M. mystacinus* we operated with separate timelines for the Iranian lineage (IR) and the remainder (sub-lineages TU, EU, GK) because the Iranian populations are divergent from the others; pairwise distance shows significant variation, see Table 1). This interval corresponds to the Holstein interglacial period (considering the stratigraphy of Western Europe) that is considered to be equivalent to Marine Isotope Stage (MIS) 11 (Sirocko et al. 2007; see Figure 2). The influence of the Holstein on the *arvalis*-group diversification can be explained by two historical scenarios. First, the preceding period, MIS 12, was characterized by a pronounced cold period (around 0.460 Mya), during which the earliest pan-Eurasian mammoth fauna associated with tundra-steppe habitats (called mammoth steppe, see Guthrie 2001) was formed. Second, the warmest phase of MIS 11 is the phase with the highest temperatures in the last 500 thousand years, persisting, persisting two times longer than the Eemian interglacial and three times longer than the Holocene (Sirocko et al. 2007). Interglacial conditions may have disrupted the mammoth steppe biome due to an increase in precipitation, temperature, and associated forest expansions (for Late Quaternary see Řičánková et al. 2018). Tougard et al. (2008) recognized that the evolutionary history of temperate small mammals is much more complex than previously suggested. Individual species responded to various factors in multiple ways, and at different times during the Pleistocene (Lorenzen et al. 2011). Therefore, we tend to be reserved about whether observed pulses in diversification could be interpreted as expansion alongside some geographical/biotope barriers or fragmentation of some particular populations.

To conclude, our study proved an additional occurrence of *Microtus mystacinus* in Kazakhstan. The studies of Kovalskaya (1994), Meyer et al. (1996) and Okulova et al. (2014) specified the distribution of this species from western or northwestern parts of Kazakhstan, with the easternmost observation from the Karabalyk district (Kovalskaya 1994). Other localities of this species are known around Novosibirsk, several hundred kilometres away from the Kazakhstani border (Pavlova and Tchabovsky 2011). Although our material is not suitable to establish the full distribution range in Kazakhstan, it enables us to extend the range of this species further south.

The distribution of *M. mystacinus* could be partly human-induced, as documented by Tiunov et al. (2013) when regarding the railway across Siberia and the Far East of Russia (e.g., Olkhon Island, Pavlova and Tchabovsky 2011; Buryatia, Moroldoev et al. 2017). If we consider this possibility, the locality near Sekisovka is approx. 30 km distant from the nearest railway from Ust-Kamenogorsk to Ridder, but our second locality (near Dzhambul) is more than 150 km distant from the nearest

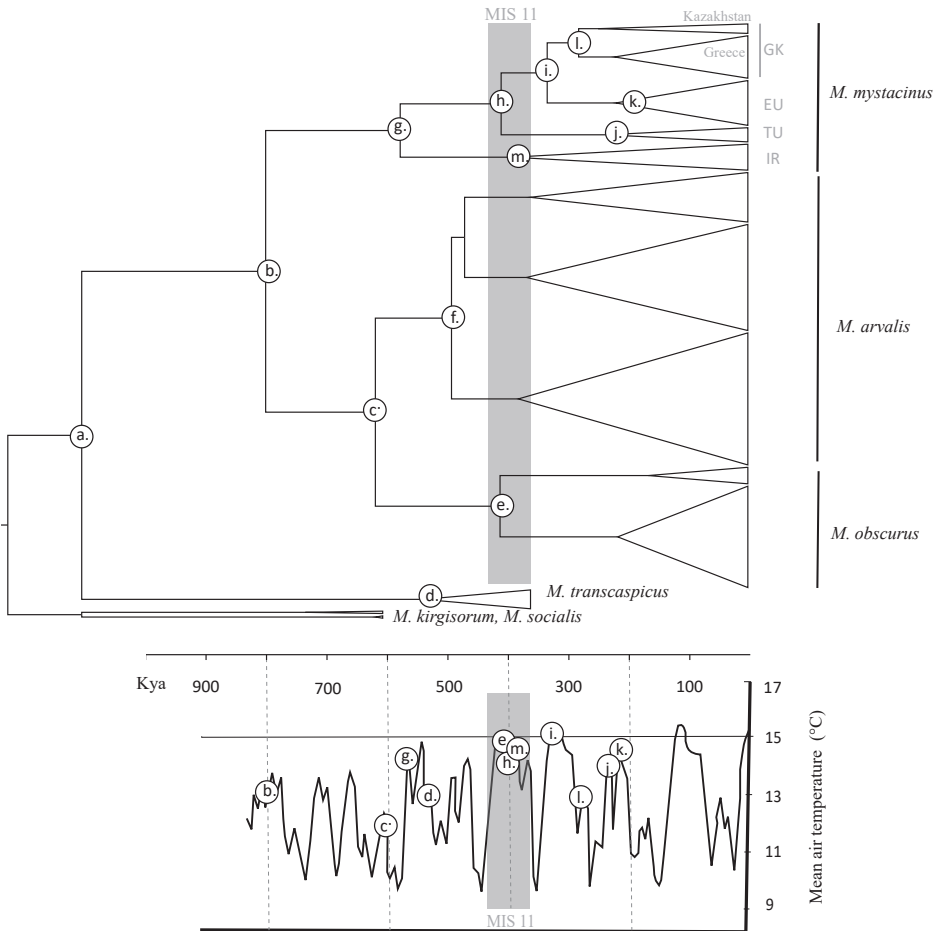


Figure 2. Time of the most recent common ancestor (TMRCA) for *Microtus* species and lineages of *M. mystacinus* using fossil calibrations. Nodes are plotted on a mean air temperature curve in last 800 thousand years (based on Gates 1993). See Table 2 for time estimates.

railway at Zyryanovsk (built after 1930; according to official web page of KTZ – КАЗАКСТАН ТЕМІР ЖОЛЫ). In Russian territory, this species shows pathways of invasion around the Transbaikalia railway and the surrounding agricultural landscape (e.g., Tiunov et al. 2013, Moroldoev et al. 2017). As the Kazakhstani specimens are significantly divergent from other available sequences (approx. 100 kya), we could consider the distribution of *M. mystacinus* in Kazakhstan as natural, but additional evidence is welcomed. Based on the presented network-phylogenetic relationship of samples it seems that a potential route of colonization for Kazakhstan populations could have originated somewhere between the Balkans and sites north of the Black

and Caspian seas, whereas populations in Turkey and parts of Armenia were colonized from a southern route.

Our study is the first genotyping of *M. mystacinus* from the eastern part of its distribution, where its occurrence is more discontinuous. In the context of our study, it is important to analyse genetically these Baikal and Far Eastern populations, and further map out the extent of *M. mystacinus* occurrence in East Kazakhstan.

Acknowledgements

We would like to thank Professor Jan Zrzavý for financial support; AM and JV were supported by grant number 31-17-19831S. We also would like to express our gratitude to Joel James Brown and Nathalie Yonow for professional language editing and to the editor and reviewers for their very valuable comments which helped to improve our manuscript.

References

- Aulagnier S, Haffner P, Mitchell-Jones AJ, Moutou F, Zima J (2009) Mammals of Europe, North Africa and the Middle East. A and C Black Publishers, London, 272 pp.
- Baker RJ, Hamilton MJ, Van Den Bussche RA, Wright AJ, Wiggins LE, Hamilton MJ, Reat EP, Smith MH, Lomakin MD, Chesser RK (1996a) Small mammals from the most radioactive sites near the Chernobyl nuclear power plant. *Journal of Mammalogy* 77(1): 155–170. <https://doi.org/10.2307/1382717>
- Baker RJ, Van Den Bussche RA, Wright AJ, Wiggins LE (1996b) High levels of genetic change in rodents of Chernobyl. *Nature* 380(6576): 707–708. <https://doi.org/10.1038/380707a0>
- Bandelt HJ, Forster P, Röhl A (1999) Median-joining networks for inferring intraspecific phylogenies. *Molecular Biology and Evolution* 16(1): 37–48. <https://doi.org/10.1093/oxfordjournals.molbev.a026036>
- Bannikova AA, Lebedev VS, Lissovsky AA, Matrosova V, Abramson NI, Obolenskaya EV, Tesakov AS (2010) Molecular phylogeny and evolution of the Asian lineage of vole genus *Microtus* (Rodentia: Arvicolinae) inferred from mitochondrial cytochrome *b* sequence. *Biological Journal of the Linnean Society* 99(3): 595–613. <https://doi.org/10.1111/j.1095-8312.2009.01378.x>
- Baskevich MI, Mironova TA, Cherepanova EV, Krivonogov DM (2016) New data on chromosomal variability, distribution of sibling species, and hybridization of 46-chromosomal forms of *Microtus arvalis* sensu lato (Rodentia, Arvicolinae) in the Upper Volga basin. *Biology Bulletin* 43(9): 1281–1291. <https://doi.org/10.1134/S1062359016110042>
- Baskevich MI (1996) On the karyological differentiation in Caucasian population of common vole (Rodentia, Cricetidae, *Microtus*). *Zoologičeskij Žurnal* 75(2): 297–308. [In Russian]
- Bužan EV, Förster DW, Searle JB, Kryštufek B (2010) A new cytochrome *b* phylogroup of the common vole (*Microtus arvalis*) endemic to the Balkans and its implications for the evolu-

- tionary history of the species. *Biological Journal of the Linnean Society* 100(4): 788–796. <https://doi.org/10.1111/j.1095-8312.2010.01451.x>
- Chaline J, Brunet-Lecomte P, Montuire S, Viriot L, Courant F (1999) Anatomy of the arvicoline radiation (Rodentia): palaeogeographical, palaeoecological history and evolutionary data. *Annales Zoologici Fennici* 36(4): 239–267.
- Cuenca-Bescós GC, Canudo JI, Laplana C (2001) La séquence des rongeurs (Mammalia) des sites du Pléistocène inférieur et moyen d'Atapuerca (Burgos, Espagne). *Anthropologie* 105(1): 115–130. [https://doi.org/10.1016/S0003-5521\(01\)80009-1](https://doi.org/10.1016/S0003-5521(01)80009-1)
- Drummond AJ, Suchard MA, Xie D, Rambaut A (2012) Bayesian phylogenetics with BEAUti and the BEAST 1.7. *Molecular Biology and Evolution* 29(8): 1969–73. <https://doi.org/10.1093/molbev/mss075>
- Fink S, Excoffier L, Heckel G (2004) Mitochondrial gene diversity in the common vole *Microtus arvalis* shaped by historical divergence and local adaptations. *Molecular Ecology* 13(11): 3501–14. <https://doi.org/10.1111/j.1365-294X.2004.02351.x>
- Fredga K, Jaarola M, Ims RA, Steen H, Yoccoz NG (1990) The common vole in Svalbard identified as *Microtus epiroticus* by chromosome analysis. *Polar Research* 8: 283–290. <https://doi.org/10.3402/polar.v8i2.6818>
- Gates DM (1993) *Climate change and its biological consequences*. Sinauer Associates, Inc. Sunderland, MA, 280 pp.
- Ghorbani F, Mohammadi Z, Darvish J, Kami HG, Siahsharvie R (2015) Morphological and morphometric characterization of the new records of the East European vole (*Microtus mystacinus* Miller, 1908) from northeast Iran. *Journal of Asia-Pacific Biodiversity* 8(3): 233–237. <https://doi.org/10.1016/j.japb.2015.07.002>
- Gileva EA, Cheprakov MI, Nochrin DY (1996) Voles of the group *Microtus arvalis* (Rodentia, Cricetidae) in Urals. *Zoologičeskij Žurnal* 75(9): 1436–1439 [in Russian].
- Golenishchev FN, Malikov VG, Bulatova NSh, Vaziri ASH, Nazari F (2000) Some new data on morphology and karyology of *Microtus kermanensis* (Rodentia, Arvicolinae) and supposed phylogeographic history of the “arvaloid” voles. In: Agadjanian AK, Orlov VN (Eds) *Systematic and Phylogeny of the Rodents and Lagomorphs*. Teriologicheskoe Obshchestvo, Moscow, 34–36.
- Groves CP, Cotterill FPD, Gippoliti S, Robovský J, Roos C, Taylor PJ, Zinners D (2017) Species definitions and conservation: a review and case studies from African mammals. *Conservation Genetics* 18(6): 1247–1256. <https://doi.org/10.1007/s10592-017-0976-0>
- Guthrie RD (2001) Origin and causes of the mammoth steppe: a story of cloud cover, woolly mammal tooth pits, buckles, and inside-out Beringia. *Quaternary Science Reviews* 20(1): 549–574. [https://doi.org/10.1016/S0277-3791\(00\)00099-8](https://doi.org/10.1016/S0277-3791(00)00099-8)
- Haynes S, Jaarola M, Searle JB (2003) Phylogeography of the common vole (*Microtus arvalis*) with particular emphasis on the colonization of the Orkney archipelago. *Molecular Ecology* 12(4): 951–956. <https://doi.org/10.1046/j.1365-294X.2003.01795.x>
- Ho SYW (2007) Calibrating molecular estimates of substitution rates and divergence times in birds. *Journal of Avian Biology* 38: 409–414. [10.1111/j.0908-8857.2007.04168.x](https://doi.org/10.1111/j.0908-8857.2007.04168.x)
- Horáček I (1990) On the context of Quaternary arvicolid evolution: changes in community development. In: Fejfar O, Heinrich WD (Eds) *International Symposium 'Evolution,*

- Phylogeny and Biostratigraphy of Arvicolids (Rodentia, Mammalia). Geological Survey, Prague, 201–222.
- Horáček I, Ložek V (1988) Palaeozoology and the Mid-European Quaternary past: scope of the approach and selected results. *Rozpravy ČSAV, řada matematických a přírodních věd.* 98: 1–102.
- Hotzi V, Markov G, Csorba G (2008) Taking steps to discover the East-European vole (*Microtus levis*) in Hungary. *Állattani Kozlemenyek* 93: 47–57. [In Bulgarian]
- Irwin DM, Kocher TD, Wilson AC (1991) Evolution of the cytochrome *b* gene of mammals. *Journal of Molecular Evolution* 32(2): 128–144. <https://doi.org/10.1007/BF02515385>
- Jaarola M, Martínková N, Gündüz I, Brunhoff C, Zima J, Nadachowski A, Amorif G, Bula-tovag NS, Chondropoulou B, Fraguadakis-Tsolish S, Gonzalez-Estebani J, Lopez-Fuster MJ, Kandaurov AS, Kefelioğlu H, da Luz Mathias M, Villatei I, Searle JB (2004) Molecular phylogeny of the speciose vole genus *Microtus* (Arvicolinae, Rodentia) inferred from mitochondrial DNA sequences. *Molecular Phylogenetics and Evolution* 33(3): 647–63. <https://doi.org/10.1016/j.ympev.2004.07.015>
- Jaarola M, Searle JB (2002) Phylogeography of field voles (*Microtus agrestis*) in Eurasia inferred from mitochondrial DNA sequences. *Molecular Ecology* 11(12): 2613–2621. <https://doi.org/10.1046/j.1365-294X.2002.01639.x>
- Kartavtseva IV, Tiunov MP, Lapin AS, Visotchina NP, Ryabkova AV (2012) Invasion of *Microtus rossiaemeridionalis* into the territory of the Russian Far East. *Russian Journal of Biological Invasions* 3(1): 11–15. <https://doi.org/10.1134/S2075111712010031>
- Kearse M, Moir R, Wilson A, Stones-Havas S, Cheung M, Sturrock S, Buxton S, Cooper A, Markowitz S, Duran C, Thierer T, Ashton B, Mentjies P, Drummond A (2012) Geneious Basic: an integrated and extendable desktop software platform for the organization and analysis of sequence data. *Bioinformatics* 28(12): 1647–1649. <https://doi.org/10.1093/bioinformatics/bts199>
- Kovalskaya YM (1994) On the distribution of voles of the group *arvalis* (Rodentia) in Kazakhstan. *Zoologičeskij Žurnal* 73(3): 120–125. [In Russian]
- Král B, Zima J, Hrabě V, Libosvářský J, Šebela M, Červený J (1981) On the morphology of *Microtus epiroticus*. *Folia Zoologica Brno* 30(4): 317–330.
- Kryštufek B, Vohralik V (2005) Mammals of Turkey and Cyprus. Rodentia I: Sciuridae, Dipodidae, Gliridae, Arvicolinae. University of Primorska, Science and Research Centre Koper, Koper, 292 pp.
- Kryštufek B (2017) The East European Vole. In: Wilson DE, Lacher Jr TE, Mittermeier RA (Eds) *Handbook of the mammals of the World, Volume 7*. Lynx Edicions, Barcelona, 352.
- Lorenzen ED, Nogués-Bravo D, Orlando L, Weinstock J, Binladen J, Marske KA, Ugan A, Borregaard MK, Gilbert TP, Nielsen R, Ho SYW, Goebel T, Graf KE, Byers D, Stenderup JT, Rasmussen M, Campos PF, Leonard JA, Koepfli KP, Froese D, Zazula G, Stafford TV, Aaris-Sørensen K, Batra P, Haywood AM, Singarayer JS, Valdes PJ, Boeskorov G, Burns JA, Davydov SP, Haile J, Jenkins DL, Kosintsev P, Kuznetsova T, Lai X, Martin LD, McDonald HG, Mol D, Meldgaard M, Munch K, Stephan E, Sablin M, Sommer RS, Sipko T, Scott E, Suchard MA, Tikhonov A, Willerslev R, Wayne RK, Cooper A, Hofreiter M., Sher A., Shapiro B, Rahbek C, Willerslev E (2011) Species-specific responses of Late

- Quaternary megafauna to climate and humans. *Nature* 479(7373): 359–364. <https://doi.org/10.1038/nature10574>
- Mahmoudi A, Darvish J, Aliabadian M, Moghaddam FY, Kryštufek B (2017) New insight into the cradle of the grey voles (subgenus *Microtus*) inferred from mitochondrial cytochrome *b* sequences. *Mammalia* 81(6): 583–593. <https://doi.org/10.1515/mammalia-2016-0001>
- Markov G, Csorba G, Kocheva M, Gospodinova M (2012) Skull features of the common vole (*Microtus arvalis* sensu lato) from Hungary: craniometrical evidence for its taxonomic detachment. *Turkish Journal of Zoology* 36(3): 283–290. <https://doi.org/10.3906/zoo-1002-49>
- Markova E, Malygin V, Montuire S, Nadachowski A, Quéré JP, Ochman K (2009) Dental variation in sibling species *Microtus arvalis* and *M. rossiaemeridionalis* (Arvicolinae, Rodentia): between species comparisons and geography of morphotype dental patterns. *Journal of Mammalian Evolution* 17: 121–139. <https://doi.org/10.1007/s10914-009-9128-8>
- Markova E, Beeren Z, van Kolschoten T, Strukova T, Vrieling K (2012) Differentiating sibling species in the Quaternary fossil record: a comparison of morphological and molecular methods to identify *Microtus arvalis* and *M. rossiaemeridionalis* (Arvicolinae, Rodentia). *Journal of Systematic Palaeontology* 10(3): 585–597. <https://doi.org/10.1080/14772019.2011.618146>
- Martínková N, Barnett R, Cucchi T, Struchen R, Pascal M, Fischer MC, Higham T, Brace S, Ho SYW, Quéré JP, O’ Higgins P, Excoffier L, Heckel G, Hoelzel RA, Dobney KM, Searle JB (2013) Divergent evolutionary processes associated with colonization of offshore islands. *Ecology* 22(20): 5205–5220. <https://doi.org/10.1111/mec.12462>
- Masing M (1999) The skull of *Microtus levis* (Arvicolidae, Rodentia). *Folia Theriologica Estonica* 4: 76–90.
- Mazurok NA, Rubtsova NV, Isaenko AA, Pavlova ME, Slobodyanyuk SY, Nesterova TB, Zakian SM (2001) Comparative chromosome and mitochondrial DNA Analyses and phylogenetic relationships within common voles (*Microtus*, Arvicolidae). *Chromosome Research* 9(2): 107–120. <https://doi.org/10.1023/A:1009226918924>
- Meyer MN, Golenishchev FN, Radjabli SI, Sablina OV (1996) Voles (subgenus *Microtus* Schrank) of Russia and adjacent territories. *Proceedings of the Zoological Institute of the Russian Academy of Sciences* (232): 1–320. [in Russian]
- Meyer MN, Orlov VN, Scholl ED (1969) Utilization of karyological, physiological and cytological analysis for the separation of new species of rodents (Rodentia, Mammalia). *Doklady Akademii Nauk USSR* 188: 1411–1414 [in Russian].
- Meyer MN, Radjabli SI, Bulatova NS, Golenishchev FN (1985) Karyological peculiarities and probable relations of common voles of the group “arvalis” (Rodentia, Cricetidae, *Microtus*). *Zoologičeskij Žurnal* 64(3): 417–428.
- Moroldoev IV, Sheremetyeva IN, Kartavtseva IV (2017) The first finding of East European vole (*Microtus rossiaemeridionalis*) in Buryatia. *Russian Journal of Biological Invasions* 8(3): 266–271. <https://doi.org/10.1134/S2075111717030109>
- Musser GG, Carleton MD (2005) Subfamily Arvicolinae. In: Wilson DE, Reeder DM (Eds) *Mammal species of the world: a taxonomic and geographic reference*. The Johns Hopkins University Press, Baltimore, 956–1039.
- Nylander JAA (2004) MrModeltest v2. Program distributed by the Author. Evolutionary Biology Centre, Uppsala University.

- Okulova NM, Khlyap LA, Bidashko FG, Warshavskiy AA, Grazhdanov AK, Neronov VV (2014) Rodent communities of the Western Kazakhstan oblast of the Republic of Kazakhstan 1: Maps of rodent communities and zoogeographic regionalization. *Arid Ecosystems* 4(2): 75–84. <https://doi.org/10.1134/S2079096114020073>
- Pavlova SV, Tchabovskiy AV (2011) Presence of the 54-chromosome common vole (Mammalia) on Olkhon Island (Lake Baikal, East Siberia, Russia), and the occurrence of an unusual X-chromosome variant. *Comparative Cytogenetics* 5(5): 433–40. <https://doi.org/10.3897/CompCytogen.v5i5.1720>
- Rambaut A (2009) Computer program and documentation distributed by the author. <http://beast.bio.ed.ac.uk>
- Rambaut A, Drummond AJ, Xie D, Baele G, Suchard MA (2017) Tracer v1.7, Available from <https://github.com/beast-dev/tracer>
- Rozas J, Sánchez-DelBarrio JC, Messeguer X, Rozas R (2003) DnaSP DNA polymorphism analyses by the coalescent and other methods. *Bioinformatics* 19(18): 2496. <https://doi.org/10.1093/bioinformatics/btg359>
- Řičánková VP, Horsák M, Hais M, Robovský J, Chytrý M (2018) Environmental correlates of the Late Quaternary regional extinctions of large and small Palaearctic mammals. *Ecography* 41(3): 516–527. <https://doi.org/10.1111/ecog.02851>
- Sanger FS, Nicklen S, Coulson AE (1977) DNA sequencing with chain termination inhibitors. *Proceedings of the National Academy of Sciences of the USA* 74(12): 5463–5467. <https://doi.org/10.1073/pnas.74.12.5463>
- Shenbrot GI, Krasnov BR (2005) Atlas of the geographic distribution of the arvicoline rodents of the world (Rodentia, Muridae: Arvicolinae). Pensoft, Sofia-Moscow, 336 pp.
- Sirocko F, Claussen M, Litt T, Sanchez-Goni MF (2007) The climate of past interglacials (Vol. 7). Elsevier, Amsterdam, 622 pp.
- Steel M, McKenzie A (2001) Properties of phylogenetic trees generated by Yule-type speciation models. *Mathematical Biosciences* 170(1): 91–112. [https://doi.org/10.1016/S0025-5564\(00\)00061-4](https://doi.org/10.1016/S0025-5564(00)00061-4)
- Stojak J, McDevitt AD, Herman JS, Searle JB, Wójcik JM (2015) Post-glacial colonization of eastern Europe from the Carpathian refugium: evidence from mitochondrial DNA of the common vole *Microtus arvalis*. *Biological Journal of the Linnean Society* 115(4): 927–939. <https://doi.org/10.1111/bij.12535>
- Stojak J, McDevitt AD, Herman JS, Kryštufek B, Uhlíková J, Purger JJ, Lavrenchenko LA, Searle JB, Wójcik JM (2016) Between the Balkans and the Baltic: Phylogeography of a Common Vole mitochondrial DNA lineage limited to Central Europe. *PLoS ONE* 11(12): e0168621. <https://doi.org/10.1371/journal.pone.0168621>
- Tamura K, Peterson D, Peterson N, Stecher G, Nei M, Kumar S (2011) MEGA5: molecular evolutionary genetics analysis using maximum likelihood, evolutionary distance, and maximum parsimony methods. *Molecular Biology and Evolution* 28(10): 2731–9. <https://doi.org/10.1093/molbev/msr121>
- Thanou E, Tryfonopoulos G, Chondropoulos B, Fraguadakis-Tsolis S (2012) Comparative phylogeography of the five Greek vole species infers the existence of multiple South Balkan subrefugia. *Hystrix Italian Journal of Mammalogy* 79(3): 363–376. <https://doi.org/10.1080/11250003.2011.651163>

- Tiunov MP, Kartavtseva IV, Lapin AS (2013) Morphotype analysis of the sibling vole (*Microtus rossiaemeridionalis*) casually introduced to the Russian Far East. *Acta Theriologica* 58(1): 79–82. <https://doi.org/10.1007/s13364-012-0092-y>
- Tougaard C, Renvoise E, Petitjean A, Quéré JP (2008) New insight into the colonization processes of Common Voles: Inferences from molecular and fossil evidence. *PLoS ONE* 3(10): e3532. <https://doi.org/10.1371/journal.pone.0003532>
- Tougaard C (2017) Did the Quaternary climatic fluctuations really influence the tempo and mode of diversification in European rodents? *Journal of Zoological Systematics and Evolutionary Research* 55(1): 46–56. <https://doi.org/10.1111/jzs.12152>
- Tougaard C, Montuire S, Volobouev V, Markova E, Contet J, Aniskin V, Quere JP (2013) Exploring phylogeography and species limits in the Altai vole (Rodentia: Cricetidae). *Biological Journal of the Linnean Society* 108(2): 434–452. <https://doi.org/10.1111/j.1095-8312.2012.02034.x>
- Triant DA, DeWoody JA (2007) Extensive mitochondrial DNA transfer in a rapidly evolving rodent has been mediated by independent insertion events and by duplications. *Gene* 401(1): 61–70. <https://doi.org/10.1016/j.gene.2007.07.003>
- Yakimenko LV, Kryukov AP (1997) On karyotype variation in common vole *Microtus rossiaemeridionalis* (Rodentia, Cricetidae). *Zoologičeskij Žurnal* 76(3): 375–378. [In Russian]
- Zagorodnyuk IV (1991a) Polytypical Arvicolidae in Eastern Europe: taxonomy, distribution and diagnostics. Institute of Zoology, Kiev, 63 pp.
- Zagorodnyuk IV (1991b) Systematic position of *Microtus brevisrostris* (Rodentiformes): materials toward the taxonomy and diagnostics of the "arvalis" group. *Vestnik Zoologii* 25(3): 26–35.

Taxonomic review of genus *Microrhagus* Dejean, 1833 from Korea, with description of a new species (Coleoptera, Eucnemidae, Melasinae, Dirhagini)

Jinbae Seung^{1,2}, Seunghwan Lee^{1,2}

1 *Insect Biosystematics Laboratory, Department of Agricultural Biotechnology, Seoul National University, Seoul 151-921, Republic of Korea* **2** *Research Institute for Agricultural and Life Sciences, Seoul National University, Seoul 151-921, Republic of Korea*

Corresponding author: *Seunghwan Lee* (seung@snu.ac.kr)

Academic editor: *H. Douglas* | Received 20 September 2016 | Accepted 19 July 2018 | Published 13 August 2018

<http://zoobank.org/50D89B9A-A54F-4FF1-BDEF-E847458EF03D>

Citation: Seung J, Lee S (2018) Taxonomic review of genus *Microrhagus* Dejean, 1833 from Korea, with description of a new species (Coleoptera, Eucnemidae, Melasinae, Dirhagini). *ZooKeys* 781: 81–95. <https://doi.org/10.3897/zookeys.781.21106>

Abstract

The genus *Microrhagus* Dejean, 1833 is reviewed with four species from Korea: *Microrhagus foveolatus* (Fleutiaux, 1923), *Microrhagus jejuensis* **sp. n.**, *Microrhagus mystagogus* (Fleutiaux, 1923), and *Microrhagus ramosus* (Fleutiaux, 1902). Herein, all Korean *Microrhagus* species are redescribed. A key to species of Korean *Microrhagus* and photographs of the diagnostic characters are also provided.

Keywords

Eucnemidae, Korea, *Microrhagus*, new species, taxonomy

Introduction

The tribe Dirhagini Reitter, 1911 is a large group of the subfamily Melasinae with a worldwide distribution. Dirhagini is characterized by crenulate or incomplete pronotal lateral carina, most also with well-developed notosternal antennal grooves, an apical sex-comb on male protarsomere I, and without basal struts of the aedeagal median lobe (Muona 1993, 2011).

The genus *Microrhagus* Dejean, 1833 is the largest genus in its tribe, with more than 130 species worldwide and 17 species in the Palearctic Region, including seven species from Japan (Muona 2007, 2011; Kovalev 2013, 2016). Only *Microrhagus ramosus* was known from Korea (Suzuki 2014).

The genus *Microrhagus* is distinguished from other genera by strongly approximate antennal sockets, hypomeron with pits close to procoxae, well-developed notosternal antennal grooves, simple elytral apices, laterally narrowed metacoxal plates, and apically notched median lobe and long ventral lobe of aedeagus (Fleutiaux 1935; Hisamatsu 1960; Muona 2000).

We review genus *Microrhagus* with four species, including an undescribed species, *Microrhagus jejuensis* sp. n., and two previously unreported species, *Microrhagus foveolatus* (Fleutiaux, 1923) and *M. mystagogus* (Fleutiaux, 1923) from Korea. A key to species of Korean *Microrhagus*, diagnoses, redescriptions, and photographs for the diagnostic characters are provided.

Materials and methods

Most samples examined were collected using flight intercept traps between 2015 and 2016. Samples were preserved in 95% ethanol and made into dried specimens by double mounted method (pinned with a micropin to a block of cork, which is mounted on a standard insect pin) for exact identification. To examine the antennae, legs, and aedeagus, specimens were softened in boiling water for 30–60 minutes and dissected using forceps and micro-pin probes. Dried specimens were examined under a microscope (S8APO, Leica, Germany) and separate organs were observed under a microscope (DM4000B, Leica, Germany). Photographs were taken using EOS-600D, CANON camera, through MP-E 65mm lens.

All specimens (including types) are deposited in the insect collection of the College for Agriculture and Life Sciences, Seoul National University (CALS, SNU, Seoul, Korea).

The concept of genus *Microrhagus* follows Muona (1993) and morphological terminology follows Muona (1993) and Otto (2016). Lateral lobes and secondary lateral lobes of aedeagus refer to the lateral and mesal apices of the parameres, respectively.

Identification of species was done using Fleutiaux (1902, 1923, 1935) and Hisamatsu (1960, 1985). Identifications were rechecked by J. Muona who has examined the relevant type specimens of Palearctic species of *Microrhagus*, including *Microrhagus pectinicornis*, closely similar to new species. Also, W. Suzuki confirmed identifications in process.

Results

Family Eucnemidae Eschscholtz, 1829

Subfamily Melasinae Fleming, 1821

Tribe Dirhagini Reitter, 1911

Genus *Microrhagus* Dejean, 1833

Microrhagus Dejean, 1833: 85. Type species: *Elater pygmaeus* Fabricius, 1792.

Diagnosis. Head: pits present between eyes and antennal sockets; frontoclypeal region strongly narrowed at base; antennae serrate or pectinate; antennomere III not longer than antennomeres IV–V combined. Prothorax: pronotal lateral carina divided into anterolateral carina and posterolateral carina; notosternal antennal grooves well developed. Pterothorax: mesepimeron fused with mesepisternum; metepisternum subparallel-sided or widened posteriorly; metacoxal plate expanded inward. Leg: male protarsomere I with apical sex-comb; metatarsomere I not shorter than metatarsomeres II–III combined, metatarsomere IV slightly dilated. Abdomen: abdominal ventrites connate; abdominal ventrite V obtusely produced or simply rounded at apex in ventral view; median lobe of aedeagus bifurcate at apex and secondary lateral lobes small (de Bonvouloir 1872; Reitter 1921; Fleutiaux 1923, 1935; Hisamatsu 1960, 1985; Muona 2000).

Key to species of Korean *Microrhagus*

- 1 Frons with carina or groove at midline; pronotum narrowed anteriorly, with paired dimples near middle; male antennae pectinate from antennomere III...2
- Frons without carina or groove (Fig. 3G); pronotum nearly parallel-sided, without dimples; male antennae pectinate from antennomere IV (Fig. 3E)...
..... ***M. mystagogus* (Fleutiaux)**
- 2 Pronotum without groove at midline; elytra less than 2.5 × longer than combined width; male antennomere III with process at base, antennomere IV with process at mid-length, antennomeres V–X with processes at apex; lateral lobes of aedeagus narrowly produced apically..... **3**
- Pronotum with a longitudinal groove at midline (Fig. 2A, B); elytra 2.7 × longer than combined width; male antennomeres III–X with process near apex (Fig. 2E); lateral lobes of aedeagus truncate (Fig. 2M) ***M. jejuensis* sp. n.**
- 3 Pronotum less densely punctate, average distance between punctures greater than puncture diameter; antennal process III as long as length of antennomere III (Fig. 1E); ventral lobe of aedeagus broadened toward apex (Fig. 1M) ***M. foveolatus* (Fleutiaux)**
- Pronotum very densely punctate, average distance between punctures smaller than puncture diameter; antennal process III 1.4 × longer than length of antennomere III (Fig. 4E); ventral lobe of aedeagus subparallel-sided (Fig. 4M).....
..... ***M. ramosus* Fleutiaux**

***Microrhagus foveolatus* (Fleutiaux, 1923)**

Fig. 1

Dirhagus foveolatus Fleutiaux, 1923: 308.

Diagnosis. Body: mostly shiny black. Head: frons with a weak carina at midline; antennae pectinate from antennomere III in male. Prothorax: pronotum with sparse punctures, average distance between punctures greater than puncture diameter, disc with paired dimples near middle; notosternal antennal grooves slightly widened posteriorly. Pterothorax: elytra 2.5 × longer than combined width; metepisternum gradually widened posteriorly, its greatest width narrower than outer edge of metacoxal plate; metacoxal plate expanded inward; abdominal ventrite V narrowly rounded at apex.

Redescription. Male (Fig. 1A, C–D) 5.1–6.0 mm long and 1.6–1.9 mm wide. **Body** mostly black; tarsi yellow-brown; surface glossy, with yellow pubescence. **Head** with circular and regularly sized punctures, denser at frontoclypeal region; frons with a weak carina at midline; frontoclypeal region slightly depressed at base, broadly rounded, with anterior edge slightly sinuate, anterior edge 3.7 × wider than distance between antennal sockets (Fig. 1G). **Antennae** (Fig. 1E) almost reaching metacoxal plate, with yellow-brown pubescence, and pectinate from antennomere III; processes of antennomeres III, IV, and V 1.1, 2.1 and 2.1 × as long as corresponding antennomeres; antennomere I robust; antennomere II shortest; antennomere III with process near base, 1.7 × longer than II, and 1.3 × longer than IV; antennomere IV with process at mid-length; antennomeres V–X with processes near apex; apical antennomere strongly elongate, curved, 9.5 × longer than wide, and 2.5 × longer than previous one. **Pronotum** 1.2 × wider than long, subparallel-sided near base, gradually narrowed anteriorly; surface with punctures, average distance between punctures greater than puncture diameter; disc with paired dimples near middle and a short carina at base of midline; anterolateral carina exceeding half as long as pronotum; posterolateral carina almost reaching pronotal mid-length, fused with anterolateral carina in some; antescutellar area almost straight in dorsal view; pronotal posterior angles sharply projecting, exceeding posterior edge of antescutellar area. **Scutellum** slightly raised, 1.1 × longer than wide, gradually narrowed posteriorly, and rounded at apex; surface coarse, densely punctate, pubescent with dense setae, especially at apex. **Elytra** 2.5 × longer than combined width, gradually narrowing posteriorly; disc striate, with irregularly sized and spaced punctures; interstriae moderately convex, with several large, deep punctures near apices; apices simply rounded. **Prosternum** with curved sides, anterior margin shallowly bisinuate; punctures slightly denser anteriorly and posteriorly; prosternal process stout, tapered and curved dorsally at posterior end; hypomeron with punctures less than on prosternum; notosternal antennal grooves (Fig. 1I) slightly expanded posteriorly, sparsely punctate, glabrous, and with pits. **Mesoventrite** with irregularly sized punctures; mesopleuron with rough surface, especially anteriorly. **Metaventrte** with finer and denser punctures than on prosternum, especially at middle; disc with a weak median groove, not reaching anterior edge; metepisternum (Fig. 1J) gradually

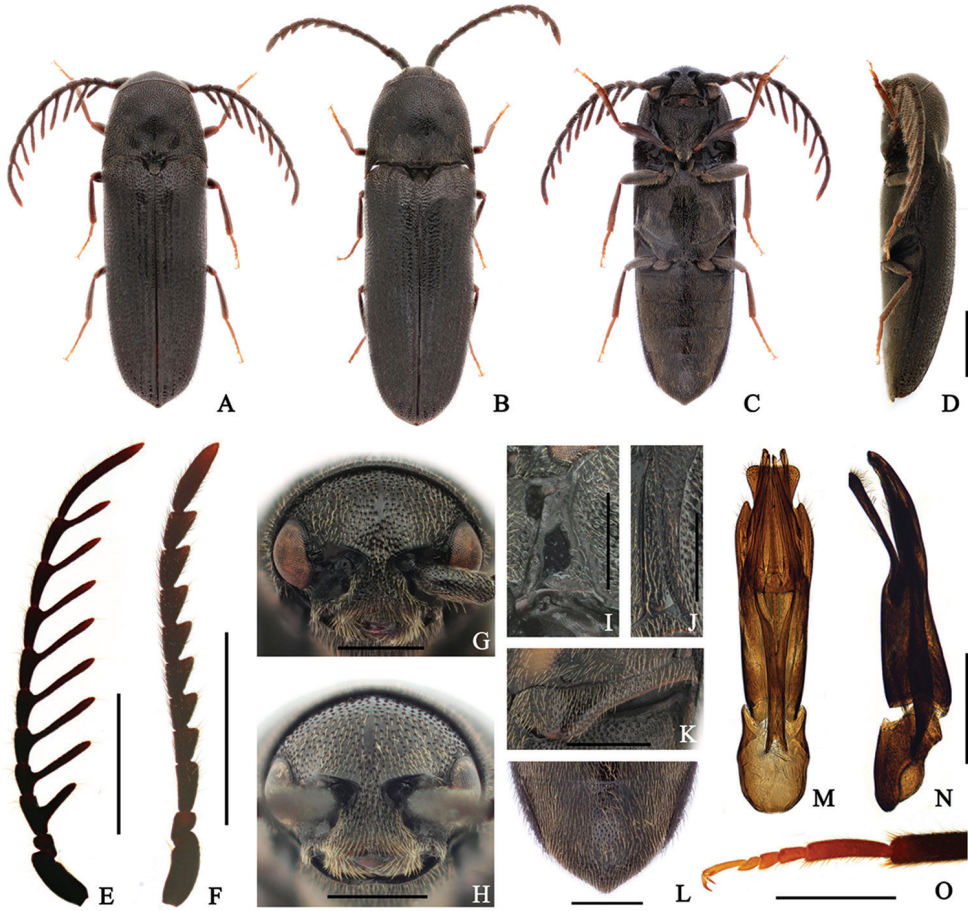


Figure 1. *Microrhagus foveolatus* (Fleurtiaux, 1923). **A, C-E, G, I-O** male **B, F, H** female. **A, B** dorsal habitus **C** ventral habitus **D** lateral habitus **E-F** antenna **G-H** frons **I** antennal groove **J** metepisternum **K** metacoxal plate **L** abdominal ventrite **V** **M-N** aedeagus **O** metatarsus. Scale bar: 1 mm (**A-F**); 0.5 mm (**G-O**).

widened posteriorly, its greatest width four-fifths of outer edge of metacoxal plate; metacoxal plate (Fig. 1K) expanded inward, medially $2.3 \times$ wider than laterally. **Legs** (Fig. 1O) slender; metatarsomere I $1.2 \times$ longer than II–IV combined; metatarsomere II $1.3 \times$ longer than III; metatarsomere V $1.7 \times$ longer than II; claws simple. **Abdomen** with finer punctures than metaventrite; ventrite V narrowly rounded at apex (Fig. 1L). **Aedeagus** (Fig. 1M–N) $4.3 \times$ longer than wide; median lobe slightly curved ventrally, bifurcate at apex; lateral lobes as long as median lobe, feebly curved ventrally, blunt at apex, and with basally attached secondary lateral lobes; secondary lateral lobes shorter than lateral lobes, bent ventrally, parallel-sided, blunt at apex, and with long setae; ventral lobe as long as median lobe, gradually expanded apically, broadly truncate at apex, and densely pubescent; phallobase rectangular, $1.8 \times$ longer than wide, one-third as long as entire aedeagus. **Female** (Fig. 1B) is distinguished from male by follow-

ing characters: body stouter, 5.3–6.4 mm long and 1.7–2.1 mm wide; frontoclypeal region with anterior edge, $3.5 \times$ wider than distance between antennal sockets (Fig. 1H); antennae (Fig. 1F) serrate, not reaching metacoxal plate; antennomere II short, as long as IV; antennomere III $1.9 \times$ longer than wide, $1.7 \times$ longer than each length of II and IV; antennomeres IV–X gradually increasing in length, narrowing, and more strongly toothed toward antennal apex; apical antennomere $3.5 \times$ longer than wide, $2.2 \times$ longer than X.

Specimens examined. <Seoul> 1♀, Gil-dong Natural Ecology Park, Gildong, Gangdong-gu, Seoul-si, N37°32'31.56", E127°9'18.58", 56m alt., 16 May, 2016, B. H. Jung leg. (SNU). <Gyeonggi-do> 1♀, Deoksu-ri, Danwol-myeon, Yangpyeong-gun, N37°33'22.97", E127°41'13.65", 166m alt., Flight intercept trap, 08–22 May, 2016, Seung and Jung leg. (SNU). <Gangwon-do> 1♀, Suha-ri, Daegwanryeong-myeon, Pyeongchang-gun, N37°36'36.29", E128°43'11.47", 803m alt., flight intercept trap, 05–29 June, 2016, Seung and Jung leg. (SNU); 1♀, Hoenggye-ri, Daegwanryeong-myeon, Pyeongchang-gun, N37°40'58.95", E128°45'21.80", 830m alt., flight intercept trap, 05–29 June, 2016, Seung and Jung leg. (SNU). <Jeju Is.> 1♂1♀, Gyorae gotjawal, Gyorae-ri, Jocheon-eup, Jeju-si, N33°26'21.88", E126°40'12.16", 422m alt. 10 June, 2016, J. B. Seung leg. (SNU); 2♂, Gyorae gotjawal, Gyorae-ri, Jocheon-eup, Jeju-si, N33°26'21.15", E126°40'12.75", 428m alt., flight intercept trap, 13 May–10 June, 2016, Seung and Jung leg. (SNU); 1♂, Seongpanak, Gyorae-ri, Jocheon-eup, Jeju-si, N33°23'10.82", E126°37'13.77", 752m alt., flight intercept trap, 13 May–10 June, 2016, Seung and Jung leg. (SNU).

Distribution. Korea (New record), Japan, Russia (Far East).

Remarks. *Microrhagus foveolatus* is differentiated from *M. ramosus* by following characters: with relatively shorter antennal processes; pronotum with sparser punctures, distance between punctures greater than its diameter; elytra relatively more elongate; ventral lobe of aedeagus gradually broadened toward apex. Adults were observed on a standing dead tree with peeling loose bark and covered with hyphae.

***Microrhagus jejuensis* sp. n.**

<http://zoobank.org/FDACE8CB-A261-4A41-B19F-15233F45707F>

Fig. 2

Diagnosis. Body: shiny black. Head: frons with a groove at midline; antennae pectinate from antennomere III in male. Prothorax: pronotum with paired dimples at middle and a groove at midline; notosternal antennal grooves slightly widened posteriorly, with outer marginal carina. Pterothorax: scutellum slightly elevated; elytra $2.7 \times$ longer than combined width; metepisternum narrow, slightly widened posteriorly, its greatest width as wide as outer edge of metacoxal plate; metacoxal plate expanded inward. Abdomen: abdominal ventrite V narrowly rounded at apex.

Description. **Holotype male** (Fig. 2A, C, D) 5.2 mm long and 1.5 mm wide. **Body** mostly black; antennomere II, antennal processes, mandible, and tibiae red-

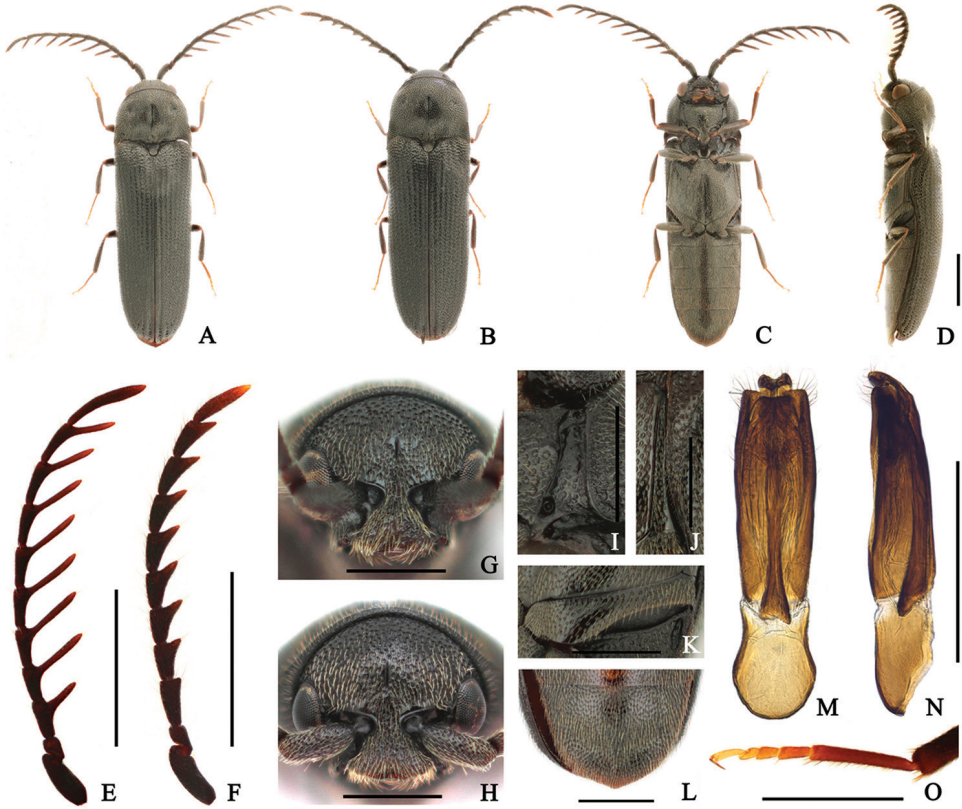


Figure 2. *Microrhagus jejuensis* sp. n. **A, C-E, G, I-O** male **B, F, H** female. **A, B**, dorsal habitus **C** ventral habitus **D** lateral habitus **E-F** antenna **G-H** frons **I** antennal groove **J** metepisternum **K** metacoxal plate **L** abdominal ventrite **M-N** aedeagus **O** metatarsus. Scale bar: 1 mm (**A-F**); 0.5 mm (**G-O**).

brown; maxillary palpi and tarsi yellow-brown; surface glossy, with yellow pubescence. **Head** with circular, irregularly sized punctures, especially at frontoclypeal region; frons with a short median groove; frontoclypeal region slightly depressed at base, broadly bifurcate and feebly concave at anterior edge, anterior edge $3.9 \times$ wider than distance between antennal sockets (Fig. 2G). **Antennae** (Fig. 2E) almost exceeding abdominal ventrite I, with yellow-brown setae, and pectinate from antennomere III; processes of antennomeres III, IV, and V 1.1 , 1.7 , and $1.8 \times$ as long as corresponding antennomeres; antennomere I robust; antennomere II shortest; antennomere III $1.7 \times$ longer than II, as long as IV; antennomeres III–X with processes near apex, gradually lengthened apically; apical antennomere elongate, curved, $7.3 \times$ longer than wide, and $1.9 \times$ longer than previous one. **Pronotum** $1.3 \times$ wider than long, subparallel-sided near base, gradually narrowed anteriorly from basal two-thirds; surface mostly with finer, sparser, and more regularly sized and spaced punctures than on head, larger and denser at sides; disc with a paired dimples near middle and a groove at midline, weakly swollen posteriorly; anterolateral carina short, almost one-third as long as pronotum; posterolateral carina

almost reaching three-fifths length of pronotum; antescutellar area almost straight, weakly sinuate in dorsal view; pronotal posterior angles sharply projecting, slightly extended outward, and exceeding posterior edge of antescutellar area. **Scutellum** slightly raised; 1.2 × longer than wide, gradually narrowed posteriorly, and rounded at apex; surface coarse, densely pubescent. **Elytra** 2.7 × longer than combined width, parallel-sided, gradually narrowing near apices; disc striate, with irregularly sized and spaced punctures; interstriae weakly convex, with several large and deep punctures near apices; apices simply rounded. **Prosternum** with curved sides, slightly widened anteriorly, and anterior margin shallowly bisinuate; surface mostly with larger, sparser, and more regularly sized and spaced punctures than on head, especially at center; prosternal process robust, gradually tapered and curved dorsally at posterior end; hypomerion with rough surface, with larger, denser punctures than on prosternum; surface rugose at coxal cavities; notosternal antennal grooves (Fig. 2I) slightly widened posteriorly, with outer marginal carina, with several irregularly sized and spaced punctures posteriorly, glossy, and with pits. **Mesoventrite** with coarse surface, with shallow punctures; mesopleuron with rough surface, especially anteriorly. **Metaventrite** mostly with finer and denser punctures than on prosternum; disc with a groove at midline, not reaching anterior edge; metepisternum (Fig. 2J) narrow, gradually widened posteriorly, its greatest width as wide as outer edge of metacoxal plate; metacoxal plate (Fig. 2K) expanded inward, medially 1.6 × wider than laterally. **Legs** (Fig. 2O) slender; metatarsomere I 1.5 × longer than II–IV combined; metatarsomere II 1.3 × longer than III; metatarsomere V 1.2 × longer than II; claws simple. **Abdomen** with finer and denser punctures than on metaventrite; ventrite V narrowly rounded at posterior edge (Fig. 2L). **Aedeagus** (Fig. 2M–N) 4.3 × longer than wide; median lobe curved ventrally near apex, broadly bifurcate at apex with setae; lateral lobes slender with apical tooth inward, truncate and with long setae at apex; ventral lobe shorter and broader than median lobe, almost truncate at apical edge; phallobase globose basally with concave sides near apex, 1.5 × longer than wide, one-third as long as entire aedeagus. **Allotype female** (Fig. 2B) like male, except for following characters: 6.1 mm long and 1.8 mm wide; frontoclypeal region with anterior edge, 3.7 × wider than distance between antennal sockets (Fig. 2H); antennae (Fig. 2F) serrate, not exceeding metacoxal plate; antennomere III subrectangular, approximately twice longer than wide, 1.7 × longer than II, and 1.3 × longer than IV; apical antennomere 5.3 × longer than wide, and 1.8 × longer than X.

Type material. **Holotype:** Korea: 1♂, Jeju Is., Hwasun gotjawal, Hwasun-ri, Andeok-myeon, Seogwipo-si, N33°15'52.88", E126°19'53.59", 120m alt., 12 May, 2016, J. B. Seung leg. (SNU). **Allotype:** Korea: 1♀, Jeju Is., Gyorae gotjawal, Gyorae-ri, Jocheon-eup, Jeju-si, N33°26'21.15", E126°40'12.75", 428m alt., flight intercept trap, 12 May–10 June, 2016, Seung and Jung leg. (SNU). **Paratypes:** Korea: 1♀, Jeju Is., Donnaeko, Sanghyo-dong, Seogwipo-si, N33°18'1.34", E126°34'49.02", 280m alt., 12 May, 2016, J. B. Seung leg. (SNU); 1♀, Jeju Is., Gyorae gotjawal, Gyorae-ri, Jocheon-eup, Jeju-si, N33°26'21.15", E126°40'12.75", 428m alt., flight intercept trap, 12 May–10 June, 2016, Seung and Jung leg. (SNU); 2♂1♀, Jeju Is. Hwasun gotjawal, Hwasun-ri, Andeok-myeon, Seogwipo-si, N33°15'52.62", E126°19'52.43", 128m

alt., flight intercept trap, 12 May–10 June, 2016, Seung and Jung leg. (SNU); 1♂2♀, Seongpanak, Gyorae-ri, Jocheon-eup, Jeju-si, N33°23'10.82", E126°37'13.77", 752m alt., flight intercept trap, 12 May–10 June, 2016, Seung and Jung leg. (SNU).

Distribution. Korea (Jeju Island).

Remarks. *Microhagus jejuensis* sp. n. similar to *M. foveolatus*, but is distinguished from *M. foveolatus* by following characters: frons with a groove at midline; pronotum with a short groove at midline; elytra elongate, width $2.7 \times$ longer than combined width; lateral lobes of aedeagus short and truncate at apex. The structure of aedeagus resembles that of *M. pectinicornis*, but the latter species differs from the new species in longer processes of antennomeres (processes of antennomeres III, IV, and V 2.2 , 3.6 , and $4 \times$ as long as corresponding antennomeres). Additionally, each process of male antennomeres III and IV is near base in *M. pectinicornis*, and not in *M. jejuensis*.

Etymology. The species is named refers to its occurrence locality, Jeju Island.

Microhagus mystagogus (Fleutiaux, 1923)

Fig. 3

Dirhagus mystagogus Fleutiaux, 1923: 309.

Diagnosis. Body: mostly dull black. Head: antennae pectinate from antennomere IV in male. Prothorax: pronotum convex, as long as wide; notosternal antennal grooves subparallel-sided. Pterothorax: elytra $2.3 \times$ longer than combined width; metepisternum narrow, slightly widened posteriorly, its greatest width narrower than outer edge of metacoxal plate; metacoxal plate expanded inward; abdominal ventrite V simply rounded at apex.

Redescription. Male (Fig. 3A, C–D) 3.2–3.9 mm long and 1.0–1.2 mm wide. **Body** mostly black; antennae and femur dark red-brown; tibiae and tarsi yellow-brown; surface weakly glossy, with yellow pubescence. **Head** with circular punctures, becoming denser and irregularly sized near frontoclypeal region; frons without carina or groove at midline; frontoclypeal region slightly depressed at base, rounded and weakly sinuate at anterior edge, anterior edge $3.9 \times$ wider than distance between antennal sockets (Fig. 3G). **Antennae** (Fig. 3E) almost exceeding metacoxal plate, with yellow-brown pubescence, and pectinate from antennomere IV; processes of antennomeres IV, V, and VI 1.4 , 2.3 and $2.6 \times$ as long as corresponding antennomeres; antennomere I stout; antennomere II shortest; antennomere III gradually expanded toward apex, $1.9 \times$ longer than wide, three \times longer than II, and $1.8 \times$ longer than IV; antennomeres IV–X with processes near apex, gradually lengthened toward apex; apical antennomere strongly elongate, curved, $11.5 \times$ longer than wide, and $2.9 \times$ longer than previous one. **Pronotum** as long as wide, parallel-sided; surface with more regularly sized and spaced punctures than on head, slightly larger and sparser posteriorly; disc with a short carina at base of midline; anterolateral carina short, almost reaching one-third length of pronotum; posterolateral carina exceeding two-thirds length of pronotum; antes-

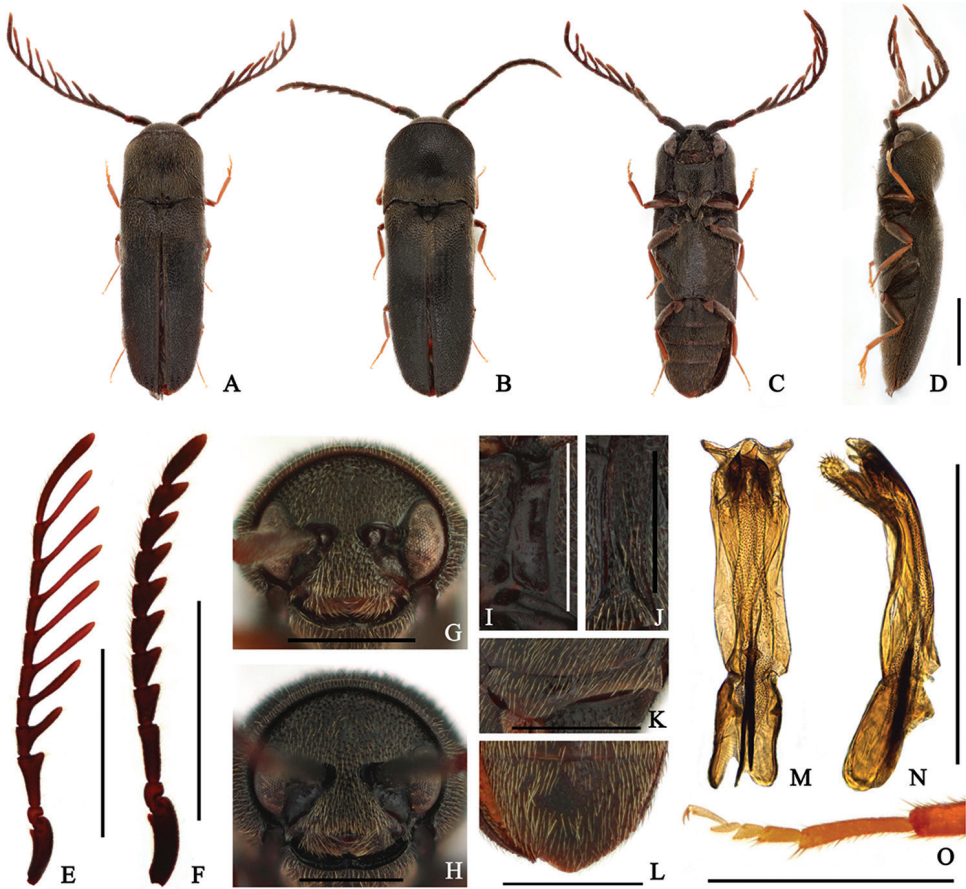


Figure 3. *Microrhagus mystagogus* (Fleutiaux, 1923). **A, C–E, G, I–O** male **B, F, H**, female **A, B** dorsal habitus **C** ventral habitus **D** lateral habitus **E–F** antenna **G–H** frons **I** antennal groove **J** metepisternum **K** metacoxal plate **L** abdominal ventrite **V** **M–N** aedeagus **O** metatarsus. Scale bar: 1 mm (**A–F**); 0.5 mm (**G–O**).

cutellar area almost straight; pronotal posterior angles sharply projecting, exceeding posterior edge of antescutellar area. **Scutellum** subtriangular, 1.1 × wider than long, gradually narrowed posteriorly, and rounded at apex; surface rough, barely pubescent. **Elytra** 2.3 × longer than combined width, parallel-sided, gradually narrowing near apices; disc barely striate, with shallow and irregularly sized and spaced punctures; several large and deep punctures present near apices; apices simply rounded. **Prosternum** subparallel-sided, anterior margin shallowly bisinuate; surface mostly with punctures as on pronotum, slightly larger laterally; prosternal process robust basally, abruptly tapered and curved dorsally at posterior end; hypomeron mostly punctate as prosternum; surface wrinkled at coxal cavities; notosternal antennal grooves (Fig. 3I) subparallel-sided, with outer marginal carina, rarely punctate, glabrous, and with pits. **Mesoventrite** with coarse surface; mesopleuron with irregularly sized and spaced

punctures, especially anteriorly. **Metaventricle** mostly with finer punctures than on prosternum, slightly larger laterally; disc with a groove at midline, not reaching anterior margin; metepisternum (Fig. 3J) widened posteriorly, its greatest width four-fifths of outer edge of metacoxal plate; metacoxal plate (Fig. 3K) expanded inward, medially $1.8 \times$ wider than laterally. **Legs** (Fig. 3O) slender; metatarsomere I $1.3 \times$ longer than II–IV combined; metatarsomere II $1.3 \times$ longer than III; metatarsomere V $1.2 \times$ longer than II; claws simple. **Abdomen** with finer and denser punctures than on metaventricle; ventrite V simply rounded at apex (Fig. 3L). **Aedeagus** (Fig. 3M–N) $3.9 \times$ longer than wide, compressed dorsoventrally; median lobe slightly bent ventrally, fused with lateral lobes; lateral lobes strongly curved ventrally, enlarged near apex, densely setose; ventral lobe bifurcate apically, with dense short pubescence; phallobase strongly emarginate basally, $1.6 \times$ longer than wide, approximately one-fifth as long as aedeagus. **Female** (Fig. 3B) is distinguished from male by following characters: body stouter, 3.4–3.9 mm long and 1.1–1.3 mm wide; frontoclypeal region (Fig. 3H) with anterior edge, $3.7 \times$ wider than distance between antennal sockets; antennae (Fig. 3F) serrate, almost reaching metacoxal plate; antennomere III subrectangular, $3.1 \times$ longer than wide, $2.3 \times$ longer than II, and $1.6 \times$ longer than IV; antennomeres IV–X gradually more strongly serrate; apical antennomere $3.5 \times$ longer than wide, and approximately twice longer than X.

Specimens examined. <Gyeonggi-do> 1♀, Deoksu-ri, Danwol-myeon, Yangpyeong-gun, N37°33'22.97", E127°41'13.65", 166m alt., flight intercept trap, 29 June–16 July, 2016, Seung and Jung leg. (SNU). <Gangwon-do> 1♀, Yeongheung-ri, Yeongwol-eup, Yeongwol-gun, N37°12'19.84", E128°27'17.77", 308m alt., flight intercept trap, 19 June–02 July, 2015, Seung and Lee leg. (SNU); 1♂, Beopheung-ri, Suju-myeon, Yeongwol-gun, N37°22'41.19", E128°15'15.50", 550m alt., flight intercept trap, 03–16 July, 2015, Seung and Lee leg. (SNU); 1♂2♀, Beopheung-ri, Suju-myeon, Yeongwol-gun, N37°22'41.19", E128°15'15.50", 550m alt., flight intercept trap, 05–29 June, 2016, Seung and Jung leg. (SNU).

Distribution. Korea (New record), Japan, Russia (Far East).

Remarks. *Microrhagus mystagogus* is easily distinguished from other Korean *Microrhagus* species by its antennae: male antennae pectinate from antennomere IV. Also, convex pronotum and structure of aedeagus are characteristic. Its aedeagal structure is well-illustrated in Kovalev's (2013) work.

Microrhagus ramosus Fleutiaux, 1902

Fig. 4

Microrhagus ramosus Fleutiaux, 1902: 24.

Diagnosis. Body: mostly weakly shiny black. Head: frons with a weak carina at midline; antennae pectinate from antennomere III in male. Prothorax: pronotum with dense punctures, average distance between punctures smaller than puncture diameter,

disc with paired dimples at middle; notosternal antennal grooves slightly expanded posteriorly. Pterothorax: elytra $2.2 \times$ longer than combined width; metepisternum gradually widened posteriorly, its greatest width wider than outer edge of metacoxal plate; metacoxal plate expanded inward. Abdomen: abdominal ventrite V weakly narrowly rounded at apex.

Redescription. Male (Fig. 4A, C, D) 3.3–4.8 mm long and 1.0–1.5 mm wide. **Body** mostly black; antennal branches and tibiae orange-brown; tarsi yellow-brown; surface weakly glossy, with yellow pubescence. **Head** regularly sized, circular punctures, becoming finer and denser near frontoclypeal region; frons with a weak carina at midline; frontoclypeal region slightly depressed at base, weakly sinuate at anterior edge, anterior edge $4.2 \times$ wider than distance between antennal sockets (Fig. 4G). **Antennae** (Fig. 4E) almost exceeding metacoxal plate, with yellow-brown pubescence, pectinate from antennomere III; processes of antennomeres III, IV, and V 1.4 , 2.5 , and $2.4 \times$ as long as corresponding antennomeres; antennomere I robust; antennomere II shortest; antennomere III with process near base, $1.7 \times$ longer than II, and $1.3 \times$ longer than IV; antennomere IV with process at mid-length; antennomeres V–X with processes near apex, gradually lengthened and narrowing toward apex; apical antennomere strongly elongate, curved, $9.4 \times$ longer than wide, and $2.2 \times$ longer than X. **Pronotum** $1.1 \times$ wider than long, subparallel-sided near base, gradually narrowed anteriorly from basal two-thirds; surface mostly with denser punctures than on head, average distance between punctures smaller than puncture diameter; disc with paired dimples at middle and a short carina at base of midline, and symmetrically depressed near base; anterolateral carina almost reaching pronotal mid-length; posterolateral carina almost exceeding pronotal mid-length, fused with anterolateral carina in some; antescutellar area weakly notched in dorsal view; pronotal posterior angles sharply projecting, exceeding posterior edge of antescutellar area. **Scutellum** raised; triangular, $1.3 \times$ longer than wide, gradually narrowed posteriorly, and rounded at apex; surface rough, densely pubescent, especially near apex. **Elytra** $2.2 \times$ longer than combined width, subparallel-sided, gradually narrowed posteriorly; disc weakly striate, with irregularly sized and spaced punctures; interstriae slightly convex, with several large and deep punctures near apices; apices simply rounded. **Prosternum** with curved sides, anterior margin slightly bisinuate; surface with more scattered and regularly sized punctures than on pronotum; prosternal process stout, gradually tapered and curved dorsally at posterior end; hypomerion with denser, and larger punctures than on prosternum; notosternal antennal grooves (Fig. 4I) slightly widened posteriorly, barely punctate, glabrous, and with pits. **Mesoventrite** with coarse surface, with irregularly sized and spaced punctures; mesopleuron with rough surface, especially anteriorly. **Metaventrite** with finer and sparser punctures than on prosternum, especially at middle; disc with a weak groove at midline, not reaching anterior margin; metepisternum (Fig. 4J) gradually widened posteriorly, its greatest width $1.2 \times$ wider than outer edge of metacoxal plate; metacoxal plate (Fig. 4K) expanded inward, medially $2.3 \times$ wider than laterally. **Legs** (Fig. 4O) slender; metatarsomere I $1.3 \times$ longer than II–IV combined; metatarsomere II $1.3 \times$ longer than III; metatarsomere V $1.5 \times$ longer than II; claws simple. **Abdomen** punctate as metaventrite; ventrite V narrowly

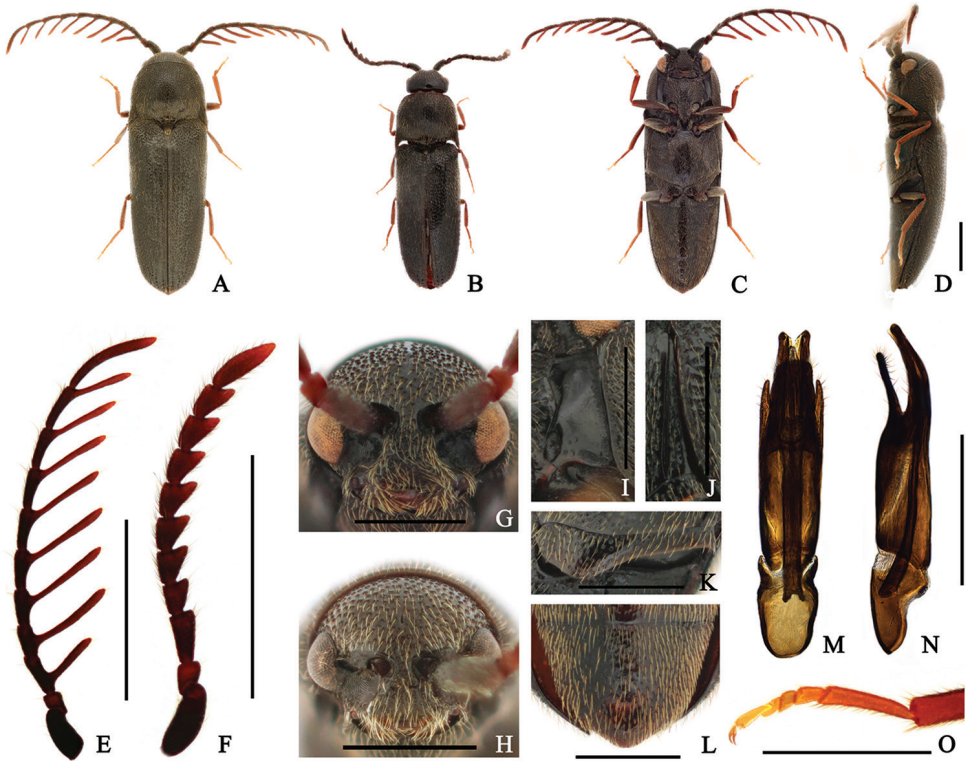


Figure 4. *Microrhagus ramosus* (Fleutiaux, 1902). **A, C-E, G, I-O** male **B, F, H** female **A, B** dorsal habitus **C** ventral habitus **D** lateral habitus **E-F** antenna **G-H** frons **I** antennal groove **J** metepisternum **K** metacoxal plate **L** abdominal ventrite **M-N** aedeagus **O** metatarsus. Scale bar: 1 mm (**A-F**); 0.5 mm (**G-O**).

rounded at apex (Fig. 4L). **Aedeagus** (Fig. 4M–N) five \times longer than wide; median lobe slightly curved ventrally, deeply bifurcate at apex; lateral lobes as long as median lobe, subparallel-sided, curved ventrally, with basally attached secondary lateral lobes; secondary lateral lobes parallel-sided, curved ventrally, pointed at apex; ventral lobe shorter than median lobe, parallel-sided, truncate at apex, and densely pubescent; phallobase rectangular, 1.6 \times longer than wide, almost one-third of entire length of aedeagus. **Female** (Fig. 4B) is distinguished from male by following characters: frontoclypeal region with anterior edge, four \times longer than distance between antennal sockets (Fig. 4H); antennae (Fig. 4F) serrate, not reaching metacoxal plate; antennomere I stout; antennomere II short, as long as IV; antennomere III 1.9 \times longer than wide, 1.7 \times longer than IV; antennomere IV–X gradually lengthened, narrowing and more strongly toothed toward antennal apex; apical antennomere elongate, 3.5 \times longer than wide, 2.2 \times longer than previous one.

Specimens examined. <Gangwon-do> 3♂1♀, Beopheung-ri, Suju-myeon, Yeongwol-gun, N37°22'41.19", E128°15'15.50", 550m alt., flight intercept trap, 19 June–02 July, 2015, Seung and Lee leg. (SNU); 2♂1♀, Deokgu-ri, Sangdong-eup, Yeong-

wol-gun, N37°5'34.46", E128°48'59.53", 648m alt., flight intercept trap, 19 June–02 July 2015, Seung and Lee leg. (SNU); 3♂, Deokgu-ri, Sangdong-eup, Yeongwol-gun, N37°5'34.46", E128°48'59.53", 648m alt., flight intercept trap, 02–16 July, 2015, Seung and Lee leg. (SNU); 5♂, Hoenggye-ri, Daegwanryeong-myeon, Pyeongchang-gun, N37°40'58.95", E128°45'21.80", 830m alt., flight intercept trap, 05–29 June, 2016, Seung and Jung leg. (SNU); 1♂, Jindong-ri, Girin-myeon, Inje-gun, N37°58'11.10", E128°24'23.97", 619m alt., 13 July, 2016, M. S. Oh leg. (SNU). <Jeollanam-do> 1♂, Donggok-ri, Ongnyong-myeon, Gwangyang-si, N35°5'13.37", E127°36'48.93", 577m alt., flight intercept trap, 04–15 July, 2016, Seung and Lee leg. (SNU). <Jeju Is.> 1♂, Gyorae gotjawal, Gyorae-ri, Jocheon-eup, Jeju-si, N33°26'21.15", E126°40'12.75", 428m alt., flight intercept trap, 13 May–10 June, 2016, Seung and Jung leg. (SNU); 1♂, Seongpanak, Gyorae-ri, Jocheon-eup, Jeju-si, N33°23'10.82", E126°37'13.77", 752m alt., flight intercept trap, 13 May–10 June, 2016, Seung and Jung leg. (SNU).

Distribution. Korea, Japan.

Remarks. *Microrhagus ramosus* shows morphological variation as below: pronotal anterolateral carina and posterolateral carina obscure in some, appearing fused in some; ventral lobe of aedeagus sub-parallel sided in some, slightly widened near apex.

Acknowledgments

We are thankful to J Muona (Finnish Museum of Natural History, Zoological Museum) for confirmation of identifications. We are also grateful to RL Otto (Department of Entomology, University of Wisconsin – Madison, USA), AV Kovalev (Zoological Institute of the Russian Academy of Sciences), and H Douglas (Agriculture and Agri–Food Canada) for valuable comments of the paper. We acknowledge to BH Jung (Korean Entomological Institute, Korea University, Korea), SJ Lee (Seoul National University Forest), SH Lee, and MS Oh for assistance to collect samples for this study. The research on the species newly recorded in Korea was supported by a grant from the National Institute of Biological Resources (NIBR), funded by the Ministry of Environment (MOE) of the Republic of Korea (NIBR201601203).

References

- de Bonvouloir HA (1872) Monographie de la Famille des Eucnémides (2nd part). Annales de la Société entomologique de France 4 (Partie Supplémentaire): 289–560.
- Flautiaux E (1902) Deuxième liste des Cicindelidae, Elateridae et Melasidae (Eucnemidae) recueillis au Japon par M. J. Harmand. Bulletin du Museum National d'Histoire Naturelle (Paris) 8: 18–25.
- Flautiaux E (1923) Les Melasidae du Japon. Annales de la Société Entomologique de France 91: 291–328.

- Fleutiaux E (1935) Essai d'un genera des Eucnemididae paléarctiques. *Revue Française d'Entomologie* 2: 1–18.
- Hisamatsu S (1960) A revision of the genus *Dirrhagus* Latreille of Japan (Coleoptera: Eucnemidae). *Transactions of the Shikoku Entomological Society* 6: 92–103.
- Hisamatsu S (1985) Eucnemidae. Colored illustrations of the Coleoptera of Japan, vol. III. Osaka, 40–51.
- Kovalev AV (2013) Two new species of the tribe Dirhagini (Coleoptera: Eucnemidae) from Palaearctic region. *Proceedings of the Zoological Institute RAS* 317: 268–274.
- Kovalev AV (2016) Two new species of *Microrhagus* from the Russian Far East with notes on some Palaearctic Dirhagini (Coleoptera: Eucnemidae). *Zoosystematica Rossica* 25: 277–290.
- Muona J (1993) Review of the phylogeny, classification and biology of the family Eucnemidae (Coleoptera). *Entomologica Scandinavica Supplement* 44: 1–133.
- Muona J (2000) A revision of the Nearctic Eucnemidae. *Acta Zoologica Fennica* 212: 1–106.
- Muona J (2007) Family Eucnemidae. *Catalogue of Palaearctic Coleoptera*. Vol. 4. Apollo Books, 81–86.
- Muona J (2011) Eucnemidae.info. Finnish Museum of Natural History. <http://dol.luomus.fi:8080/> [Accessed: 03 May 2017]
- Otto R (2016) The false click beetles (Coleoptera: Eucnemidae) of Laos. *Entomologica Basiliensia et Collectionis Frey* 35: 181–427.
- Reitter E (1921) Bestimmungs-Tabellen des europaischen Coleopteren 90. Trixagidae, Eucnemidae, Cerophytidae und Phylloceridae. *Wiener Entomologische Zeitung* 38: 65–90.
- Suzuki W (2014) Three eucnemid species newly recorded from Korea. *Sayabane Newseries* 13: 44–45.

Taxonomic review of the genus *Dirrhagofarsus* in Korea (Coleoptera, Eucnemidae)

Jinbae Seung^{1,2}, Jyrki Muona³, Seunghwan Lee^{1,2}

1 Insect Biosystematics Laboratory, Department of Agricultural Biotechnology, Seoul National University, Seoul 151-921, Republic of Korea **2** Research Institute for Agricultural and Life Sciences, Seoul National University, Seoul 151-921, Republic of Korea **3** Finnish Museum of Natural History, Zoological Museum, FIN-00014 University of Helsinki, Finland

Corresponding author: Seunghwan Lee (seung@snu.ac.kr)

Academic editor: H. Douglas | Received 17 November 2018 | Accepted 19 July 2018 | Published 13 August 2018

<http://zoobank.org/503D2C20-D06F-41DF-B29A-3098569ECE2B>

Citation: Seung J, Muona J, Lee S (2018) Taxonomic review of the genus *Dirrhagofarsus* in Korea (Coleoptera, Eucnemidae). ZooKeys 781: 97–108. <https://doi.org/10.3897/zookeys.781.22335>

Abstract

The genus *Dirrhagofarsus* is firstly recorded from Korea with three species: *Dirrhagofarsus lewisi* (Fleutiaux, 1900), *Dirrhagofarsus modestus* (Fleutiaux, 1923), and *Dirrhagofarsus unicolor* (Hisamatsu, 1960). A key to Korean species of *Dirrhagofarsus*, with diagnoses, redescriptions, and photographs of important structures is provided. In this work, *Dirrhagus modestus* f. *unicolor* Hisamatsu, 1960 is regarded as a valid species, *Dirrhagofarsus unicolor* (Hisamatsu, 1960), **comb. n.**

Keywords

Dirrhagofarsus, Eucnemidae, Korea, new combination, taxonomy

Introduction

The genus *Dirrhagofarsus* was originally characterized by strongly convex elytral apices, dilate tarsomere IV and shiny notosternal antennal grooves (Fleutiaux 1935). Ford and Spilman (1979) described the biology and larval features of the type species, *Dirrhagofarsus lewisi* (Fleutiaux) adding a new diagnostic feature, the lateral frontal carinae. Muona (1993) transferred two species to *Dirrhagofarsus*: *Hypocaelus attenuatus* Mäklin, 1845 and *Dirrhagus modestus* Fleutiaux, 1923. Subsequently, Otto et al. (2014)

described *Dirrhagofarsus ernae* from North America. Also, Otto (2016) described *Dirrhagofarsus foveicollis* from Laos. Finally, Kovalev (2016) transferred *Dirrhagus ferrugineus* Reitter, 1889 to *Dirrhagofarsus*. Thus, genus *Dirrhagofarsus* included six species worldwide (Muona 2007; Otto et al. 2014; Otto 2016; Kovalev 2016).

Hisamatsu (1960) described what he considered a light-coloured form of *Dirrhagus modestus* as *Dirrhagus modestus* f. *unicolor*. After that, Muona and Alaruikka (2007) commented that f. *unicolor* was proposed as infrasubspecific name and omitted it from their catalogue. However, JM studied four such specimens collected in Japan (Fukushima Pref., Fukushima City, Moniwa, 1976-06-19, male and two females; Fukushima Pref., Mt. Asahi, 1974-07-29; S. Ohmomo leg.) and observed that they were a distinct species. Although the holotype has not been studied, Hisamatsu (1960) provided excellent images of the characteristic aedeagus, and illustrations of all other features are also as he described. Close to that time, JS and SL discovered an apparently new *Dirrhagofarsus* species from Korea. After discussion, the authors concluded that the Korean and Japanese forms were identical. Species names given to infrasubspecific forms are usually unavailable; however, there are exceptions to this. If such names are proposed before 1 January 1961 (ICZN, article 10.2), they are available with the original authority unless the description includes information showing that the author intended it an infrasubspecific grouping. This is not the case with Hisamatsu (1960) and thus the name of this previously ignored species becomes *Dirrhagofarsus unicolor* (Hisamatsu, 1960), comb. n., stat. n.

Herein, we firstly report and review Korean species of genus *Dirrhagofarsus*, including three species: *Dirrhagofarsus lewisi* (Fleutiaux, 1900), *D. modestus* (Fleutiaux, 1923), *D. unicolor* (Hisamatsu, 1960). A key to Korean species of *Dirrhagofarsus*, with diagnosis, redescriptions, and photographs is provided.

Materials and methods

Most samples were collected using flight intercept traps, light trapping, or by hand during 2015 and 2016. Samples were preserved in 95% ethanol and made into dried specimens by the double mounted method (pinned with a micropin to a block of cork, which is mounted on a standard insect pin). In order to examine detailed structures, some specimens were softened in distilled water for an hour and dissected using a micro-pin and forceps. Photographs for each species were taken using a digital camera (Canon EOS-600D) through MP-E 65mm lens. Samples for this study are deposited in the insect collection of the College for Agriculture and Life Sciences, Seoul National University (CALS, SNU, Seoul, Korea).

Morphological terminology follows Muona (1993) and Otto (2016). We measured the length of the pronotum, from the anterior edge of the pronotum to the apex of pronotal posterior angle.

We identified the species by literature comparison (Fleutiaux 1900, 1923, 1935; Hisamatsu 1960, 1985; Otto et al. 2014).

Results

Family Eucnemidae Eschscholtz, 1829

Subfamily Melasinae Fleming, 1821

Tribe Dirrhagini Reitter, 1911

Genus *Dirrhagofarsus* Fleutiaux, 1935

Dirrhagofarsus Fleutiaux, 1935: 15. Type species: *Microrhagus lewisi* Fleutiaux, 1900.

Diagnosis. Head: vertex with transverse row of dense vestiture; frons with a pair of longitudinal carinae near compound eyes; antennae subfiliform to serrate; antennomere II shorter than IV. Prothorax: pronotum parallel-sided, about as long as wide; lateral carina divided into anterior and posterior parts; antennal grooves notosternal, parallel-sided, with lateral marginal carina. Pterothorax: elytra with strongly convex apices in lateral view; mesepimeron fused with mesepisternum; metepisternum narrow, subparallel-sided, 7–9 × longer than wide; metacoxal plate strongly expanded medially. Leg: tibiae and tarsi slender; metatarsomere I 1.5 × longer than II–IV combined; tarsal claws simple. Abdomen: ventrites connate, ventrite V sinuate and acute in ventral profile. Aedeagus: dorsoventrally compressed; median lobe bifurcate at apex; lateral lobes not fused with ventral plate, slender, narrowing apically (Fleutiaux 1935; Muona 2000, 2011; Otto et al. 2014).

Key to species of Korean *Dirrhagofarsus*

- 1 Antennomere III of male less than 1.5 × longer than IV; elytra 2.65–2.70 × longer than combined width..... **2**
- Antennomere III of male more than 1.5 × longer than IV (Fig. 3E); elytra 2.5 × longer than combined width (Fig. 3A)..... ***D. unicolor* (Hisamatsu), comb. n.**
- 2 Frons without medio-longitudinal carina (Fig. 1E); elytra with strongly convex apices in lateral view, apices pointed and raised above ventrite V (Fig. 1C)..... ***D. lewisi* (Fleutiaux)**
- Frons with weak medio-longitudinal carina (Fig. 2G); elytra with simply convex apices in lateral view, apices blunt and contact with ventrite V (Fig. 2D)..... ***D. modestus* (Fleutiaux)**

Dirrhagofarsus lewisi (Fleutiaux, 1900)

Fig. 1

Microrhagus lewisi Fleutiaux, 1900: 358.

Dirrhagus lewisi Fleutiaux, 1923: 308.

Dirrhagofarsus lewisi Fleutiaux, 1935: 16.

Diagnosis. Body: mostly coloured dark brown. Head: frons simple, without medio-longitudinal carina; anterior edge of frontoclypeal region $2.7 \times$ wider than distance between antennal sockets in female; antennomere III $1.3 \times$ longer than IV in female. Pronotum: anterolateral carina one-fifth as long as pronotum; posterolateral carina four-fifths as long as pronotum. Pterothorax: elytra $2.65 \times$ longer than combined width, apices with strongly convex apices in lateral view. Leg: metatarsomere II $1.6 \times$ longer than III, as long as V.

Redescription. Female (Fig. 1A–C) 6.1–7.7 mm long and 1.7–2.2 mm wide. **Body** brown to dark brown; antennae and legs red-brown; surface weakly glossy, covered with yellow-brown pubescence. **Head** deeply inserted into prothorax, barely visible in dorsal view; surface coarse, with circular, irregularly sized and spaced punctures, more rugose near occiput and frontoclypeal region; frons simple, without medio-longitudinal carina; frontoclypeal region (Fig. 1E) slightly depressed at base, obtusely trilobate at anterior edge, anterior edge $2.7 \times$ wider than distance between antennal sockets. **Antennae** (Fig. 1D) weakly serrate, almost reaching abdominal ventrite II, with yellow-grey pubescence; antennomere II conical and shortest; antennomere III $2.5 \times$ longer than II, and $1.3 \times$ longer than IV; antennomeres IV–X subequal, slightly shortened apically; antennomere XI $2.9 \times$ longer than wide, and $1.5 \times$ longer than X. **Pronotum** as long as wide and obtusely arcuate anteriorly; surface with finer, more regularly sized and regularly spaced punctures than on head, especially anteriorly; disc with a medio-longitudinal carina at basal half; anterolateral carina one-fifth as long as pronotum; posterolateral carina four-fifths as long as pronotum; antescutellar lobe obtusely notched; pronotal posterior angles acute, exceeding posterior edge of antescutellar lobe. **Scutellum** straight anteriorly and evenly arcuate behind anterolateral angles, $1.1 \times$ wider than long; surface rough, sparsely pubescent. **Elytra** $2.65 \times$ longer than combined width, parallel-sided in dorsal view, and attenuate near apices; disc weakly striate, with shallow, irregularly sized and spaced punctures; several large, deep punctures present near apices; apices strongly convex in lateral view, apices pointed and raised above ventrite V (Fig. 1F). **Prosternum** wider than long, slightly widened anteriorly; punctures finer and more regularly spaced than on head; prosternal process gradually tapered, and curved dorsally posteriorly; hypomeron with coarse surface, with larger punctures than on prosternum; antennal grooves (Fig. 1H) well-developed, notosternal, parallel-sided, with lateral marginal carina, non-punctate. **Mesoventrite** with coarse surface. **Metaventrte** with punctures denser than on prosternum; with a weak median groove along length of metaventrte; metepisternum (Fig. 1I) slightly widened posteriorly, widest part $1.7 \times$ wider than outer edge of metacoxal plate; metacoxal plate (Fig. 1J) medially four \times longer than laterally. **Legs** (Fig. 1G) with metatarsomere II $1.6 \times$ longer than III, as long as V. **Abdomen** with denser punctures than on metaventrte (Fig. 1K). **Male.** Not examined.

Specimens examined. Gyeonggi-Do 1♀, Mt. Bara, Hagui-dong, Uiwang-si, N37°22.34', E127°1.37', 189m alt., light trap, 22 June 2015, J. B. Seung leg. (SNU); **Gangwon-Do** 1♀, Beopheung-ri, Suju-myeon, Yeongwol-gun, N37°22.69', E128°15.26', 550m alt., flight intercept trap, 03–16 July 2015, leg. Seung and Lee leg.

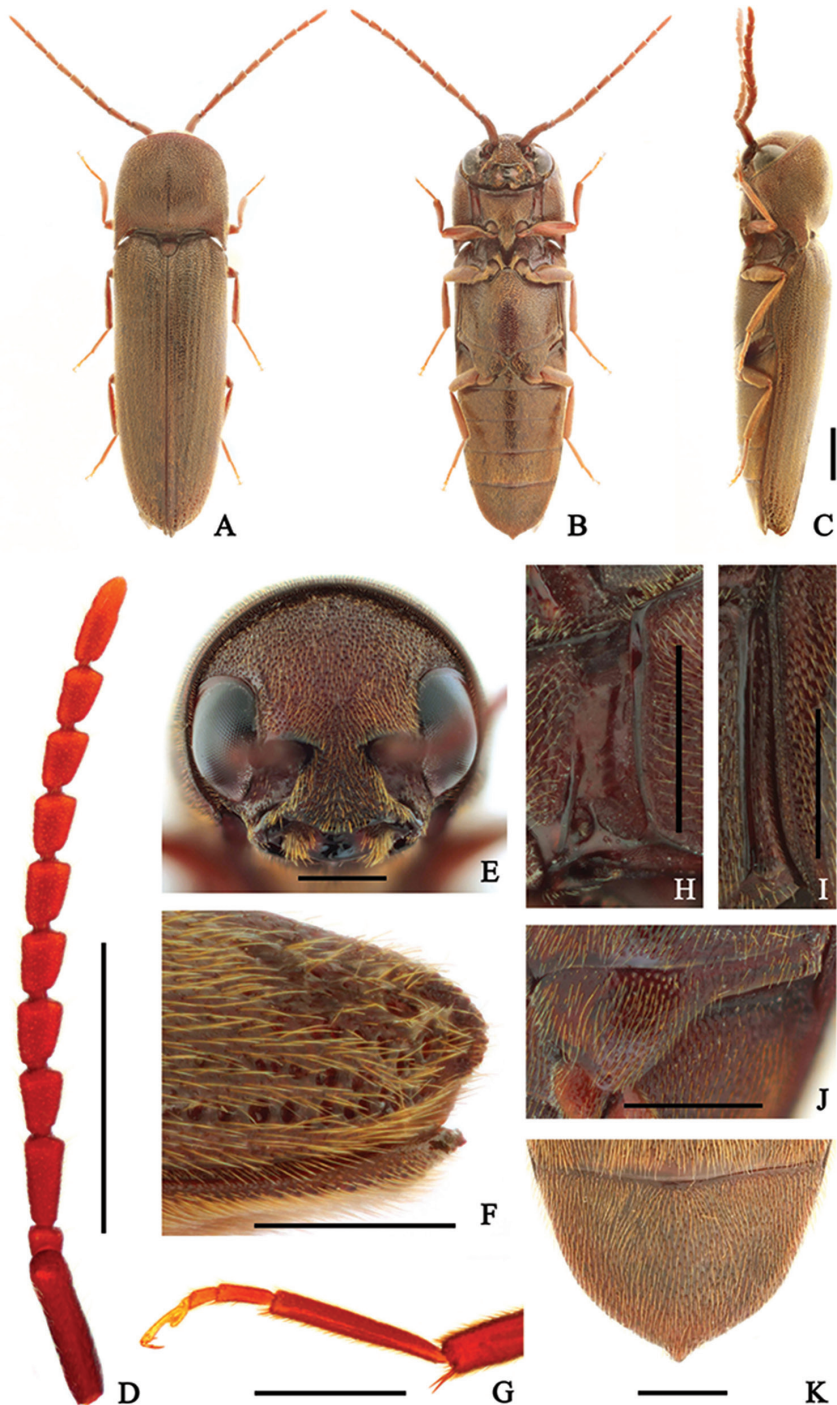


Figure 1. *Dirrhagofarsus lewisi* (Fleutiaux, 1900). female. **A** dorsal habitus; **B** ventral habitus **C** lateral habitus **D** antenna **E** frons **F** elytral apex in lateral view **G** metatarsus **H** hypomeron **I** metepisternum **J** metacoxal plate **K** abdominal ventrite V. Scale bar: 1 mm (**A–D**); 0.5 mm (**E–K**).

(SNU); 1♀, Seorim-ri, Seo-myeon, Yangyang-gun, N37°56.66', E128°31.17', 292m alt., 09 July 2016, S. H. Lee leg. (SNU); **Jeollanam-Do** 1♀, Jungdae-ri, Ganjeon-myeon, Gurye-gun, N35°6.44', E127°35.90', 668m alt., flight intercept trap, 04–15 July 2016, Seung and Lee leg. (SNU).

Distribution. Korea (New record), Japan, Nearctic Region (USA).

Remarks. A female individual of *Dirrhagofarsus lewisi* is observed under bark of rotten fallen tree. Additionally, they were rarely collected at light traps. They were observed clicking as well as flying and running.

Dirrhagofarsus modestus (Fleutiaux, 1923)

Fig. 2

Dirrhagus modestus Fleutiaux, 1923: 308.

Rhacopus modestus Hisamatsu, 1985: 50.

Dirrhagofarsus modestus Muona, 1993: 46.

Diagnosis. Body: mostly coloured black. Head: frons with a weak medio-longitudinal carina; anterior edge of frontoclypeal region $2.9 \times$ wider than distance between antennal sockets in male, $2.7 \times$ wider in female; antennomere III $1.35 \times$ longer than IV in male, $1.7 \times$ longer in female. Pronotum: anterolateral carina one-sixth as long as pronotum; posterolateral carina four-fifths as long as pronotum. Pterothorax: elytra $2.7 \times$ longer than combined width, apices with fairly convex apices in lateral view. Leg: metatarsomere II $1.6 \times$ longer than III, as long as V. Aedeagus: $5.3 \times$ longer than wide; lateral lobes as long as median lobe, phallobase trapezoidal, one-sixth as long as aedeagus.

Redescription. Male (Fig. 2A, C–D) 4.5–5.9 mm long and 1.2–1.5 mm wide. **Body** black; antennae, mouthparts, anterior and posterior edge of pronotum red-brown; tibiae and tarsi brown to red-brown; surface shiny, covered with yellow-brown pubescence. **Head** deeply inserted into prothorax; surface coarse, with circular, irregularly sized and spaced punctures, rugose and more irregular near frontoclypeal region; frons with a weak medio-longitudinal carina; frontoclypeal region (Fig. 2G) weakly depressed at base, obtusely rounded at anterior edge, anterior edge $2.9 \times$ wider than distance between antennal sockets. **Antennae** (Fig. 2E) weakly serrate, almost reaching abdominal ventrite II, with yellow-brown pubescence; antennomere II conical and shortest; antennomere III rectangular, $2.5 \times$ longer than wide, two \times wider than II, and $1.35 \times$ longer than IV; antennomeres IV–X gradually lengthened and narrowed apically; antennomere XI $5.5 \times$ longer than wide, and $1.7 \times$ longer than X. **Pronotum** as long as wide and rounded anteriorly; surface with finer and denser punctures than on head, gradually more rugose laterally; disc with a medio-longitudinal carina at basal half; anterolateral carina one-sixth as long as pronotum; posterolateral carina approximately four-fifths as long as pronotum. **Scutellum** with straight anterior edge, gradually narrowed posteriorly with rounded apex; surface rough, sparsely pubescent. **Elytra** $2.7 \times$ longer than combined width; disc weakly striate, with shallow, scattered

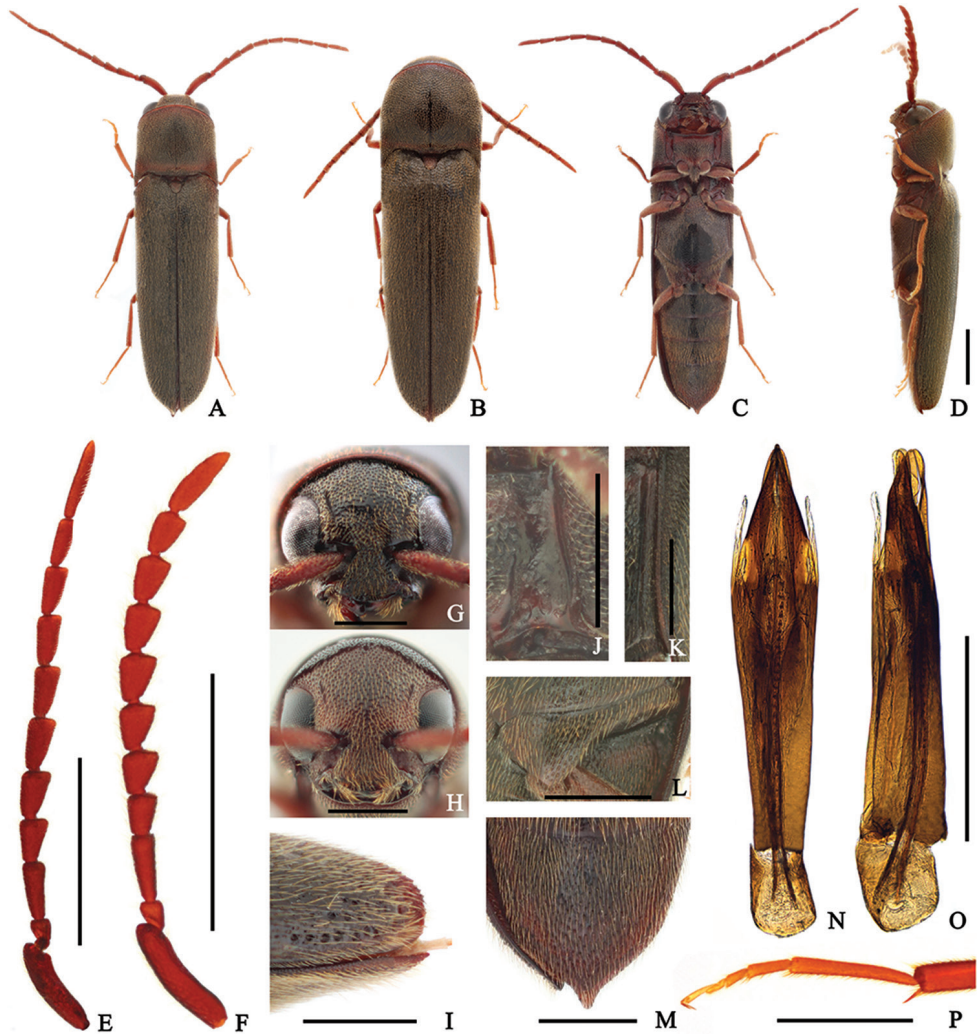


Figure 2. *Dirrhagofarsus modestus* (Fleutiaux, 1923). **A, C-E, G, J-P** male **B, F, H, I** female **A-B** dorsal habitus **C** ventral habitus **D** lateral habitus **E-F** antenna **G-H** frons **I** elytral apex in lateral view **J** hypomeron **K** metepisternum **L** metacoxal plate **M** abdominal ventrite **N-O** aedeagus **P** metatarsus. Scale bar: 1 mm (**A-F**); 0.5 mm (**G-P**).

punctures on intervals; several large, deep punctures present near apices; apices simply convex in lateral view in both sexes, apices blunt and contact with ventrite V (Fig. 2I). **Prosternum** slightly wider than long, parallel-sided; punctures more regularly spaced than on head, finer and denser at anterior and posterior regions; prosternal process gradually tapered and curved dorsally posteriorly; hypomeron with coarse surface, more irregularly sized than on prosternum; antennal grooves well-developed, notosternal, parallel-sided, with lateral marginal carina, barely punctate, and glabrous (Fig. 2J). **Mesoventrite** with rough surface. **Metaventrite** with finer, sparser, punctures

than on prosternum, especially at middle; metepisternum (Fig. 2K) parallel-sided, width of posterior edge as wide as outer edge of metacoxal plate; metacoxal plate (Fig. 2L) medially four \times longer than laterally. **Legs** (Fig. 2P) with metatarsomere II 1.6 \times longer than III, as long as V. **Abdomen** with finer punctures than on metaventricle (Fig. 2M). **Aedeagus** (Fig. 2N–O) 5.3 \times longer than wide; median lobe almost straight, gradually narrowed distally, deeply bifurcate at apex; endophallus reaching basal piece; lateral lobes as long as median lobe, with basally attached secondary lateral lobes; secondary lateral lobes slender, subparallel-sided, weakly pointed apically; phallobase trapezoidal, 1.25 \times longer than wide and one-sixth as long as aedeagus.

Sexual dimorphism. Female (Fig. 2B) can be distinguished from male by following characters: body larger and stouter, 5.2–6.8 mm long, 1.4–1.9 mm wide; base of frontoclypeal region wider, anterior edge 2.7 \times wider than distance between antennal sockets (Fig. 2H); antennae (Fig. 2F) relatively shorter, almost reaching metacoxal plate; antennomere III 1.7 \times longer than IV; antennomeres IV–X stouter; antennomere XI 3.3 \times longer than wide.

Specimens examined. Seoul-Si 7♂9♀, Mt. Gwanak, Daehak-dong, Gwanak-gu, Seoul-si, N37°27.06', E126°56.82', 184m alt., 18 January 2016, J. B. Seung leg. (collected in overwintering larval stage, 03. iv. 2016, adult emergence) (SNU); **Gyeonggi-Do** 1♀, Mt. Bara, Hagui-dong, Uiwang-si, N37°22.34', E127°1.37', 189m alt., light trap, 22 June 2015, J. B. Seung leg. (SNU); 2♂1♀, Mt. Bara, Hagui-dong, Uiwang-si, N37°22.38', E127°1.34', 174m alt., light trap, 01 June 2016, J. B. Seung leg. (SNU); **Gangwond-Do** 1♂, Beopheung-ri, Suju-myeon, Yeongwol-gun, N37°22.69', E128°15.26', 550m alt., flight intercept trap, 19 June–02 July 2015, Seung and Lee leg. (SNU); 1♀, Deokgu-ri, Sangdong-eup, Yeongwol-gun, N37°5.57', E128°48.99', 648m alt., flight intercept trap, 19 June–02 July 2015, Seung and Lee leg. (SNU); 1♀, Beopheung-ri, Suju-myeon, Yeongwol-gun, N37°22.69', E128°15.26', 550m alt., flight intercept trap, 03–16 July 2015, leg. Seung and Lee leg. (SNU); 1♀, Hoenggye-ri, Daegwanryeong-myeon, Pyeongchang-gun, N37°40.84', E128°45.78', 902m alt., flight intercept trap, 05–29 June 2016, Seung and Jung leg. (SNU); 3♀, Suha-ri, Daegwanryeong-myeon, Pyeongchang-gun, N37°36.60', E128°43.19', 803m alt., flight intercept trap, 05–29 June, 2016, Seung and Jung leg. (SNU); **Jeollanam-Do** 2♀, Jungdae-ri, Ganjeon-myeon, Gurye-gun, N35°6.44', E127°35.90', 668m alt., flight intercept trap, 04–15 July 2016, Seung and Lee leg. (SNU); **Jeju-Do (Is.)** 2♂, Gyoraegotjawal, Gyoraeri, Jocheon-eup, Jeju-si, N33°26.35', E126°40.21', 428m alt., flight intercept trap, 10 June–21 July 2016, Seung and Jung leg. (SNU).

Distribution. Korea (New record), Japan, Russia (Far East).

Remarks. Mature larvae of *Dirrhagofarsus modestus* were observed in U-form in oval larval cells in standing dead *Alnus japonica* (Thunb.) Steudel (Fagales, Betulaceae) in January. Adults emerged at the same time as eucnemid species, *Dirrhagofarsus unicolor* and *Hylis* sp. 70 days later following rearing at room temperature. They were commonly collected at light traps. They were observed clicking as well as flying and running.

***Dirrhagofarsus unicolor* (Hisamatsu, 1960), comb. n., stat. n.**

Fig. 3

Dirrhagus modestus f. *unicolor* Hisamatsu, 1960: 102.

Diagnosis. Body: mostly coloured brown. Head: frons simple, without medio-longitudinal carina; anterior edge of frontoclypeal region $3 \times$ wider than distance between antennal sockets in male, $2.8 \times$ wider in female; antennomere III $1.5 \times$ longer than IV in male, $1.75 \times$ longer in female. Pronotum: anterolateral carina one-sixth as long as pronotum; posterolateral carina four-fifths as long as pronotum. Pterothorax: elytra $2.5 \times$ longer than combined width, apices with weakly convex apices in lateral view. Leg: metatarsomere II $1.3 \times$ longer than III, metatarsomere V $1.2 \times$ longer than II. Aedeagus: $4.5 \times$ longer than wide; lateral lobes slightly longer than median lobe; phallobase rectangular, almost one-fifth as long as aedeagus.

Redescription. Male (Fig. 3A, C–D) 4.3–5.3 mm long and 1.2–1.5 mm wide. **Body** brown with yellow-brown tarsi; surface moderately glossy, covered with golden pubescence. **Head** moderately inserted into prothorax; surface with circular and regularly sized punctures, denser near frontoclypeal region; frons simple, without medio-longitudinal carina; frontoclypeal region (Fig. 3G) weakly depressed at base, feebly trilobate at anterior edge, anterior edge $3 \times$ wider than distance between antennal sockets. **Antennae** (Fig. 3E) serrate, almost reaching metacoxal plate, with yellow-brown pubescence; antennomere II conical and shortest; antennomere III rectangular, $2.3 \times$ longer than wide, $2 \times$ longer than II, and $1.5 \times$ longer than IV; antennomeres IV–X subequal, gradually narrowed apically; antennomere XI $3.8 \times$ longer than wide, and $1.7 \times$ longer than X. **Pronotum** as long as wide and arcuate anteriorly; surface rougher than head; disc weakly depressed at middle; with a short median carina at base; anterolateral carina one-sixth as long as pronotum; posterolateral carina four-fifths as long as pronotum. **Scutellum** triangular, $1.3 \times$ wider than long, gradually narrowed posteriorly to slightly rounded posterior edge; surface coarse, densely pubescent. **Elytra** $2.5 \times$ longer than combined width; disc barely striate, with irregularly sized and spaced punctures; several large, deep punctures present near apices; apices weakly compressed and simply rounded near sutural region in lateral view (Fig. 3I). **Prosternum** wider than long, parallel-sided; surface with punctures like as on head, slightly larger laterally; prosternal process gradually tapered and curved dorsally posteriorly; hypomerion with coarse surface, with punctures more irregularly sized than on prosternum; with deep pore at posterior fossae; antennal grooves (Fig. 3J) well-developed, notosternal, parallel-sided, with lateral marginal carina, barely punctate, and glabrous. **Mesoventrite** with coarse surface, with irregularly sized and spaced punctures. **Metasventrite** with punctures like as on prosternum, slightly larger and denser laterally; median groove present, not reaching anterior edge; metepisternum (Fig. 3K) slightly widened posteriorly, and widest part $1.5 \times$ wider than outer edge of metacoxal plate; metacoxal plate (Fig. 3L) medially four \times longer than laterally. **Legs** (Fig. 3P) with metatarsomere II $1.3 \times$ longer than

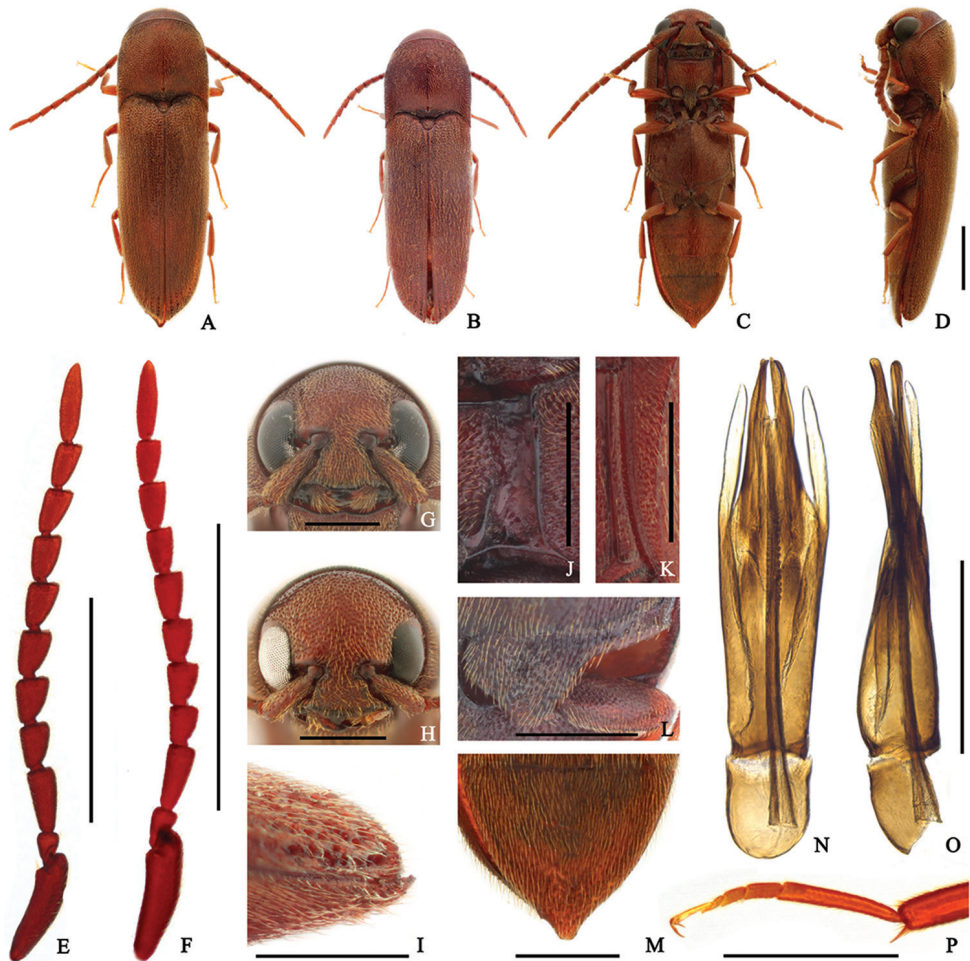


Figure 3. *Dirrhagofarsus unicolor* (Hisamatsu, 1960). **A, C–E, G, I–P** male **B, F, H** female. **A–B** dorsal habitus **C** ventral habitus **D** lateral habitus **E–F** antenna **G–H** frons **I** elytral apex in lateral view **J** hypomeron **K** metepisternum **L** metacoxal plate **M** abdominal ventrite **N–O** aedeagus **P** metatarsus. Scale bar: 1 mm (**A–F**); 0.5 mm (**G–P**).

III; metatarsomere V $1.2 \times$ longer than II; claws simple. **Abdomen** with denser punctures than on metaventrite (Fig. 3M). **Aedeagus** (Fig. 3N–O) $4.5 \times$ longer than wide; median lobe almost straight, gradually narrowed distally, deeply and narrowly bifurcate apically; endophallus reaching basal piece; lateral lobes slightly longer than median lobe, slightly curved ventrally, with basally attached secondary lateral lobes; secondary lateral lobes subparallel-sided, weakly pointed apically; phallobase rectangular, almost one-fifth as long as aedeagus.

Sexual dimorphism. **Female** (Fig. 3B) can be distinguished from male by following characters: body slightly stouter, 4.5–5.7 mm long and 1.3–1.7 mm wide; base of frontoclypeal region slightly wider, anterior edge $2.8 \times$ wider than distance between

antennal sockets (Fig. 3H); antennomere III 1.75 × longer than IV; antennomeres IV–X stouter (Fig. 3F).

Specimens examined. **Seoul-Si** 4♂, Mt. Gwanak, Daehak-dong, Gwanak-gu, Seoul-si, N37°27.06', E126°56.82', 184m alt., 18 January 2016, J. B. Seung leg. (collected in overwintering larval stage, 03. iv. 2016, adult emergence) (SNU); **Gyeonggi-Do** 2♂, Mt. Bara, Hagui-dong, Uiwang-si, N37°22.34', E127°1.37', 189m alt., light trap, 22 June 2015, J. B. Seung leg. (SNU); 1♂, Mt. Bara, Hagui-dong, Uiwang-si, N37°22.38', E127°1.34', 174m alt., light trap, 01 June 2016, J. B. Seung leg. (SNU); 1♂, Mt. Bara, Hagui-dong, Uiwang-si, N37°22.38', E127°1.34', 174m alt., light trap, 04 June 2016, M. S. Oh leg. (SNU); 2♀, Baekgok-ri, Mado-myeon, Hwaseong-si, N37°10.65', E126°43.64', 115m alt., flight intercept trap, 06–28 June 2016, Seung and Yeom leg. (SNU).

Distribution. Korea (New record), Japan.

Remarks. Last instar larvae of *Dirrhagofarsus unicolor* were collected in standing dead *A. japonica* trees in January. They remained in U-form in oval larval cells. Adults emerged together with other eucnemid species, *Dirrhagofarsus modestus* and *Hylis* sp., 70 days later following rearing at room temperature. Most of specimens were collected by light trap, occasionally by flight intercept traps. They were observed clicking as well as flying and running.

Acknowledgments

We are very grateful to Dr. R.L. Otto (Department of Entomology, University of Wisconsin–Madison, USA) for the helpful comments and advice to this study. We also appreciate to Dr. Boohee Jung (Korean Entomological Institute, Korea University, Korea), Mr. Seunghyun Lee, Mr. Minsuk Oh, and Ms. Moonok Yeom for collecting samples for this study. The research on the species newly recorded in Korea was supported by a grant from the National Institute of Biological Resources (NIBR), funded by the Ministry of Environment (MOE) of the Republic of Korea (NIBR201601203).

References

- Fleutiaux E (1900) Liste des Cicindelidae, Elateridae et Eucnemidae recueillis dans le Japon Central par M. le Dr. J. Harmand de 1894 à 1897. Bulletin du Museum national d'Histoire naturelle (Paris) 6: 356–361.
- Fleutiaux E (1923) Les Melasidae du Japon. Annales de la Société Entomologique de France 91: 291–328.
- Fleutiaux E (1935) Essai d'un genera des Eucnemididae Paléarctiques. Revue Française d'Entomologie 2: 1–18.
- Ford EJ, Spilman TJ (1979) Biology and immature stages of *Dirrhagofarsus lewisi*, a species new to the United States (Coleoptera, Eucnemidae). The Coleopterists Bulletin 33: 75–84.

- Hisamatsu S (1960) A revision of the genus *Dirrhagus* Latreille of Japan (Coleoptera: Eucnemidae). Transactions of the Shikoku Entomological Society 6: 92–103.
- Hisamatsu S (1985) Eucnemidae. Colored Illustrations of the Coleoptera of Japan, vol. III, Osaka, Japan, 40–51.
- ICZN (1999) International Code of Zoological Nomenclature, Fourth Edition. The International Trust for Zoological Nomenclature, London, UK. <http://www.iczn.org/iczn/index.jsp>
- Kovalev A (2016) Two new species of *Microrhagus* from the Russian Far East with notes on some Palaeartic Dirhagini (Coleoptera: Eucnemidae). Zoosystematica Rossica 25: 277–290.
- Muona J (1993) Review of the phylogeny, classification and biology of the family Eucnemidae (Coleoptera). Entomologica Scandinavica Supplement 44: 1–133.
- Muona J (2000) A revision of the Nearctic Eucnemidae. Acta Zoologica Fennica 212: 1–106.
- Muona J (2007) Family Eucnemidae, In: Löbl I, Smetana A (Eds) Catalogue of Palaeartic Coleoptera, Vol. 4, Elateroidea–Derodontoidea–Bostrichoidea–Lymexyloidea–Cleroidea–Cucujoidea. Apollo Books, Stenstrup, Denmark, 81–86.
- Muona J (2011) Eucnemidae.info. Finnish Museum of Natural History. <http://dol.luomus.fi:8080/> [Accessed: 30 December 2016]
- Muona J, Alaruiikka D (2007) Eucnemidae. New nomenclatorial and taxonomic acts, and comments. In: Löbl I, Smetana A (Eds) Catalogue of Palaeartic Coleoptera, Vol. 4, Elateroidea–Derodontoidea–Bostrichoidea–Lymexyloidea–Cleroidea–Cucujoidea. Apollo Books, Stenstrup, Denmark, 32.
- Otto RL, Muona J, McClarin J (2014) Description of *Dirrhagofarsus ernae* n. sp. with a key to the known *Dirrhagofarsus* species (Coleoptera: Eucnemidae). Zootaxa 3878: 179–184. <https://doi.org/10.11646/zootaxa.3878.2.4>
- Otto RL (2016) The false click beetles (Coleoptera: Eucnemidae) of Laos. Entomologica Basiliensia et Collectionis Frey 35: 181–427.

Two new species of the family Nippobodidae (Acari, Oribatida), including a description of the leg-folding process

Nestor Fernandez^{1,2}, Pieter Theron², Sergio Leiva³

1 National Council of Scientific and Technological Research (CONICET), Evolutive Genetic Laboratory FCEQyN, Misiones National University, Felix de Azara 1552, 6º, 3300 Posadas Misiones, Argentina **2** Research Unit for Environmental Sciences and Management, North-West University, Potchefstroom, 2520, South Africa **3** National Institute Agricultural Technology (INTA), Experimental Rural Agency, Aimogasta, Argentina

Corresponding author: Nestor Fernandez (nestorfernand51@yahoo.fr)

Academic editor: V. Pesic | Received 15 June 2018 | Accepted 14 July 2018 | Published 14 August 2018

<http://zoobank.org/C7FA94CF-666A-438A-8AA7-EEF1C1E0CE4F>

Citation: Fernandez N, Theron P, Leiva S (2018) Two new species of the family Nippobodidae (Acari, Oribatida), including a description of the leg-folding process. ZooKeys 781: 109–139. <https://doi.org/10.3897/zookeys.781.27389>

Abstract

Nippobodes panemorfs **sp. n.** and *Leobodes trypasis* **sp. n.** are described by means of optical and Scanning Electron Microscopy (SEM) and compared to other congeners. The leg-folding process is described and illustrated.

Nippobodes panemorfs **sp. n.** is characterised by interlocking, double hook-shaped, posterior prodorsal condyle and anterior zone humeral apophysis; posterior prodorsal depression present. Tutorium a large lamina defining a pocket-shaped structure; bothridial opening ovoid, situated at the bottom of a U-shaped structure; deep, rounded-ovoid anterior notogastral depression present; ten pairs of notogastral setae; *c* setae looped, dentate, sharply tipped. Marginal setae *h*₃, *p*₃ on large promontories, followed by deep V-shaped incision; notogaster completely surrounded by circumgastric depression; lateral genital zone with locking structure constituted by longitudinal cuticular elevation, with promontories and a parallel furrow involved in the leg-folding process; genital plate smaller than anal plate.

Leobodes trypasis **sp. n.** is characterised by: the presence of posterior prodorsal depression and anterior notogastral depression; bridge-shaped anterior prodorsal condyles; heart-shaped frontal prodorsal orifice; ten pairs of notogastral setae; posterior prodorsal condyle and humeral condyle interlocked, forming double hook-like structure; circumgastric furrow surrounding entire notogaster; setae *lp*, *h*₂, *h*₁ situated on shallow medial furrow; notogastral setae *lm*, *lp*, *h*₁, *h*₂ medially aligned; *p*₁, *p*₂, *p*₃, *h*₃ marginally situated. Legs I-IV, tutorium, pedotectum I, and pedotectum II involved in leg folding which is inferred to be a protection mechanism.

Keywords

Leg-folding process; new cuticular structures; Nippobodidae; systematics

Introduction

In 1959 Aoki described the new genus *Nippobodes* from material collected by Mr. K. Kaneko in Hiketa-Machi Kagama, south Japan. Aoki compared the genus to *Tetracondyla*, but in the same paper, without further explanation, included the new genus in the family Carabodidae. *Nippobodes insolitus* Aoki, 1959 was the first species to be described, and in 1961 Aoki gave a diagnosis for a new family, Nippobodidae, incorporating the genus *Nippobodes*. Other species were later added, such as: *Nippobodes latus* Aoki, 1970; *N. brevisetiger* Aoki, 1981; *N. yuwanensis* Aoki, 1984; *N. monstruosus* Jeleva & Vű, 1987; *N. tokaraensis* Aoki, 1989; *N. chejuensis* Choi, 1996; and *N. tamlaensis* Choi, 1996.

Leobodes Aoki, 1965 was the second genus to be added to the family Nippobodidae, with *Leobodes mirabilis*, collected in Mae Ngon Luang, Thailand, as type species. Other species were subsequently described: *L. mirabilis* Aoki, 1965; *L. anulatus* Aoki, 1965; *L. lijiangensis* Aoki, 2000; and *L. yinae* Aoki, 2000.

Three species were collected in China and described as new species of *Nippobodes*: *N. flagellifer* Chen & Wang, 2007; *N. peniculatus* Chen & Wang, 2007 and *N. pseudo-brevisetiger* Chen & Wang, 2007. In the same paper the authors added two new species of *Leobodes*: *L. carinatus* Chen & Wang, 2007 and *L. praeconcauus* Chen & Wang, 2007, transferring *Nippobodes monstruosus* Jeleva & Vű, 1987 to the genus *Leobodes* as: *L. monstruosus* (Jeleva & Vű, 1987).

Chen and Wang 2007 proposed a revised diagnosis of the family and provided a key of species described worldwide. That study was based on adult stages, making use of optical microscopy and including some digital images. Legs were discussed in a fragmentary fashion but detailed elements were not included in previous studies and the leg-folding process was not mentioned.

More than five years ago, the current authors embarked on a revision of the Carabodidae family. During these studies, we observed a series of similar characters in Carabodidae and Nippobodidae not discussed in previous studies of Nippobodidae. Aspects such as the leg-folding process, discussed by Fernandez et al. with reference to the Carabodidae family (Fernandez et al. 2013a), are also present in Nippobodidae, with some similarities and significant differences.

Difficulties were encountered in our efforts to provide detailed comparisons with previous papers, mainly due to simplified drawings and descriptions. Frontal and lateral views are often lacking, making it difficult to determine if some structures are absent in previously described species, or if they were not mentioned by authors. We explain the leg-folding process by use of illustrations, complementing the study with SEM micrographs, and include a comparison of the two families.

Materials and methods

Specimens studied by means of light microscopy followed the techniques described by Grandjean 1949 and Krantz and Walter 2009. Specimens studied under SEM, followed the techniques of Alberti and Fernandez 1990a, 1990b; Alberti et al. 1991, 1997, 2007; Fernandez et al. 1991. Equipment used was the same as for previous studies (see Fernandez et al. 2016).

Optical drawings should be considered semi-schematic with regard to cuticular microsculpture and setal shape. The shape of these specimens made it difficult to orientate the material and obtain the same position consecutively. Studies with SEM provided high levels of precision and detailed Figures; another very important aspect was the positioning system, permitting orientation of material with a much higher level of precision, as well as being able to return to an initial position.

Body measurements taken: total length (from tip of rostrum to posterior edge of notogaster); width (widest part of notogaster). Setal measurements taken on three specimens under SEM. Leg chaetotaxy studies used optical microscopy (standard, polarised, and phase contrast) and SEM.

Setal formulae of legs include the number of solenidia (in parentheses); tarsal setal formulae include the famulus (ϵ). All measurements are given in micrometres (μm).

Morphological terms and abbreviations used are those developed by Grandjean (1928–1974) (cf. Travé and Vachon 1975; Norton and Behan-Pelletier 2009; Aoki 1959; 1961; 1965a; 1965b; 1989; Fernandez et al. 2013; 2013 a, b, c; 2014; Chen and Wang 2007. For setal types Evans (1992: 73) and for ornamentation of cuticular surfaces Murley (1951) were used. Additional terms and abbreviations are given below.

Abbreviations:

MNHG Museum of Natural History, Geneva, Switzerland.

a.o frontal prodorsal orifice

a.pr.b bridge-shaped anterior prodorsal condyles

la.le lateral ledge

m.f medial shallow furrow

p.pr.co posterior prodorsal condyle

New taxon descriptions

Nippobodes panemorfis sp. n.

<http://zoobank.org/9A5846B8-B060-4F6C-9314-1F75B751C374>

Figures 1–53

Etymology. The specific epithet “panemorfis” is derived from “panemorfi” (πανεμορφη in Greek) meaning beautiful, due to the aesthetic features of the cuticle and setae.

Diagnosis (adult female). *Prodorsum*. Complex shape; triangular in dorsal view with rounded central posterior zone; double hook-shaped, interlocking posterior prodorsal condyle and anterior zone humeral apophysis; rounded rostrum, with groove and large hump; deep, easily discernible round-ovoid prodorsal posterior depression; tutorium strongly curved, large lamina, connected to prodorsal wall, determining a pocket structure. Reticulate-foveate microsculpture on tutorium, pedotectum I, pedotectum II. Polyhedral bothridium situated under zone where humeral part, overlaps with anterior prodorsal zone; bothridial opening ovoid, located at bottom of U-shaped structure. Notogaster: deep, round-ovoid anterior notogastral depression present; ten pairs of setae *c*, *la*, *lm*, *lp*, *h₁*, *h₂*, *h₃*, *p₁*, *p₂*, *p₃*; setae *c* looped, dentate, sharply tipped; marginal setae *h₃*, *p₃* on conspicuous promontories, followed by deep v-shaped incision; circumgastric depression completely surrounding notogaster, originating before setae *la*, running between setae *la*, *h₁*, *h₂* and *h₃*, *p₃*, *p₂*, *p₁*; setae *1c*, *3c*, *4b* situated marginally; setae *1b* largest; genital opening on elevated zone; lateral genital zone locking structure with, longitudinal cuticular elevation, promontories with parallel furrow; genital plate smaller than anal plate; adanal setae *ad₁*, *ad₂* inserted on elevated zone; *ad₃* setae smallest.

Material examined. Holotype: ♀♀ Female. Label details: “Thailande. Khao Yai National Park (nord-est de Bangkok) Khao Khieo au-dessous d’Air Force check point; 1150 m; versant nord, forêt assez sèche; tamisage débris. 28/XI/1985. Leg: D.H. Burckhardt et L. Löbl”. **Paratypes:** Two adult females, same locality and date as Holotype; deposited in Collection of NHMG; preserved in 70 % ethanol. **Additional material** studied using SEM: six specimens, not deposited. “Thailande. Khao Yai National Park (nord-est de Bangkok) Khao Khieo au-dessous d’Air Force check point; 1150 m; versant nord, forêt assez sèche; tamisage débris. 28/XI/1985. Leg: D.H. Burckhardt et L. Löbl”

Description. Measurements. SEM: 597 (542–720) × 368 (332–401) (n = 6). Light microscopy: 610 × 360 (n = 1); all specimens female. *Shape.* Rounded-ovoid (dorsal view) (Figure 1). Elongate oval (lateral view) (Figures 11, 23).

Colour. Black, slightly shiny when observed in reflected light; rarely dark brown.

Cerotegument. Not observed; small particles, similar to rest of cerotegumental layer on circumgastric depression (*s.c*) lateral zone (Figure 16); the layer may have existed.

Integument. Microsculpture complex, varying according to body region. *Smooth:* prodorsum (on Figure 4 indicated by ✱); notogaster (on Figures 1, 7 indicated by ✱); on most epimeral surface (on Figures 28, 41 indicated by ✱); genital, anal, aggenital zones. *Tuberculate:* rostrum (Figure 14, indicated by ✱); infracapitulum near setae *h* (Figure 42, indicated by ✱); epimeral zone between setae *1a*, *1b* (Figure 28, indicated by ✱).

Reticulate-foveate: Tutorium (*Tu*) (on Figure 26 indicated by ✧); Pedotectum I (*Pd I*) (on Figures 26, 27 indicated by ✧), Pedotectum II (*Pd II*) (Figure 20, indicated by ✧). *Rugose:* external zone of humeral apophyse (*h.ap*). (Figures 1, 4, 7, 8, 9, 23, indicated by ⊙). *Favulariate:* bothridial zone (Figure 24a, indicated by *). *Sulcate:* zone of bothridial opening (Figure 24a, b indicated by ◀). *Punctate:* Discidium (*dis*) (Figure 30 indicated by ▶); epimeral zone surrounding setal insertion (Figures 30, 43, indicated by ▶).

Prodorsum. Complex shape: in dorsal view, more or less triangular with central posterior zone rounded (Figures 1, 4); lateral posterior zone with interlocking double hook-shaped posterior prodorsal condyle (*p.pr.co*) (indicated by ◼) and anterior zone humeral apophysis (*h.ap*) (Figures 8, 9); lateral view: triangular; with complex lateral posterior zone, with double hook and sigmoid lamellae (Figure 23).

Rostrum round, with a conspicuous groove parallel to margin (Figure 23 indicated by ➤) large hump visible in front of groove (Figures 14).

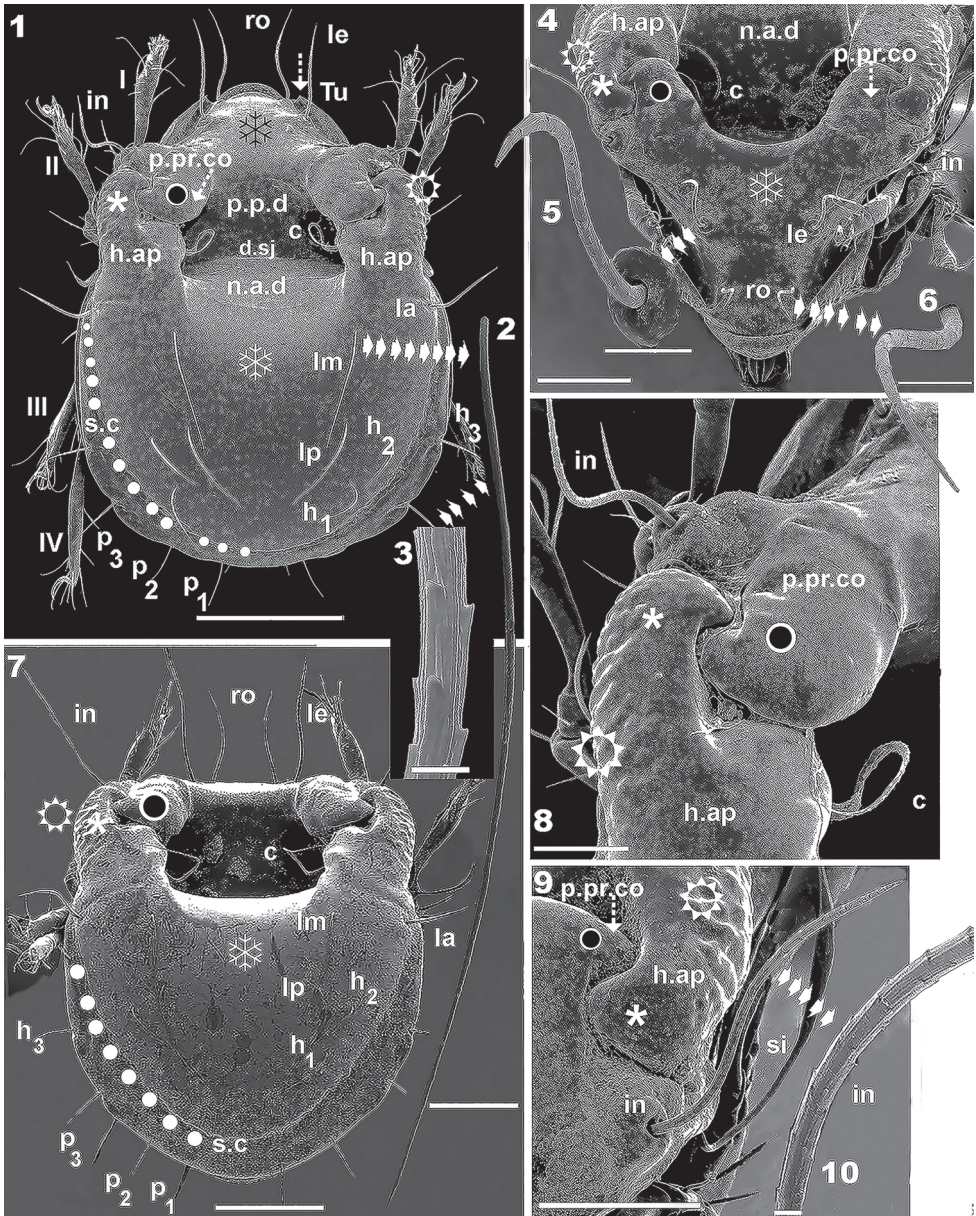
Setae: sigmoid, with small dentitions and thin parallel longitudinal ridges: Rostral (*ro*), interlamellar (*in*), lamellar (*le*) setae (Figures 1, 4, 5, 6, 9, 10, 21, 22): length: 123 (106–141) (n = 12); setae *le*, *in*, inserted each on large tubercle, setae *ro* inserted on small tubercle (Figures 1, 4, 9, 26); setae *ro* situated behind region of tuberculate microsculpture, marginally to depression created by *Tu* and lateral prodorsal wall (Figures 4, 26); *le* setae inserted on anterior end of lamellar zone (Figure 26), situated posteriorly and to the exterior of *ro* setal insertion alignment (Figures 1, 4, 7); setae *in* situated behind and externally to *le* setal insertion level (Figures 1, 4, 7), inserted near the double hook (Figures 8, 9); deep, rounded-ovoid prodorsal posterior depression (*p.p.d*) clearly discernible between dorsosejugal furrow (*d.sj*) and notogastral anterior depression (*n.a.d*) (Figure 1).

Lamellae (*Lam*) clearly visible in lateral view (Figures 11, 23) (see Lateral Region). Bothridium (*bo*) (Figures 23, 24) situated under double hook zone (See: Lateral view). Sensillus (*si*) (Figures 17, 18) sickle-shaped, strongly curved, directing upward with long stalk followed by a swollen zone, plentifully scattered with small asperities and with small barbs (Figure 18 indicated by ◀); long sharp apical tip; length 152 (149–160) (n = 6). *Tu* well developed, sharply tipped; lacking free extremity, welded to lateral prodorsal wall, determining pocket-like structure (Figures 4, 26). Pocket structure conceals leg I when leg-folding process is activated (See: Leg-Folding Process).

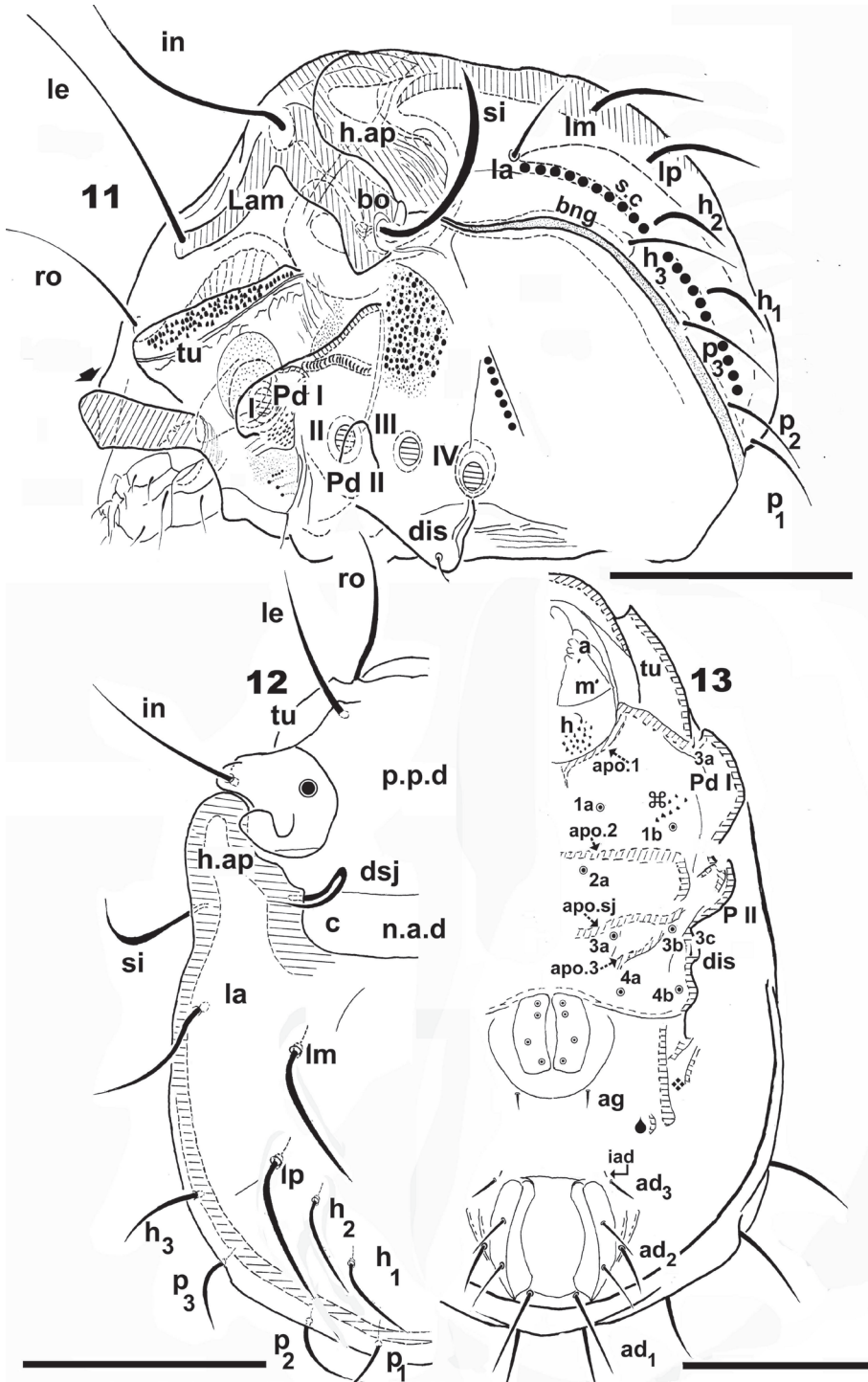
Interlocking double hook. The interlocking double-hook zone is complex, formed by *p.pr.co* and anterior zone *h.ap* (Figures 1, 4, 7, 8, 9, 23); where *h.ap* situated externally (indicated by *), grips on to *p.pr.co* (indicated by ◼) on the interior. Cuticular surface of *p.pr.co* smooth with some irregular depressions (Figure 8); cuticular surface of *h.ap* rugose externally (Figures 1, 4, 7, 8, 9 indicated by ✪), internally smooth.

Notogaster. Dorsal view, notogaster polyhedral-rectangular shape (Figure 9); *d.sj* convex, clearly delimited (Figure 1). Deep, round-ovoid *n.a.d* present, extending posteriorly from *d.sj*.

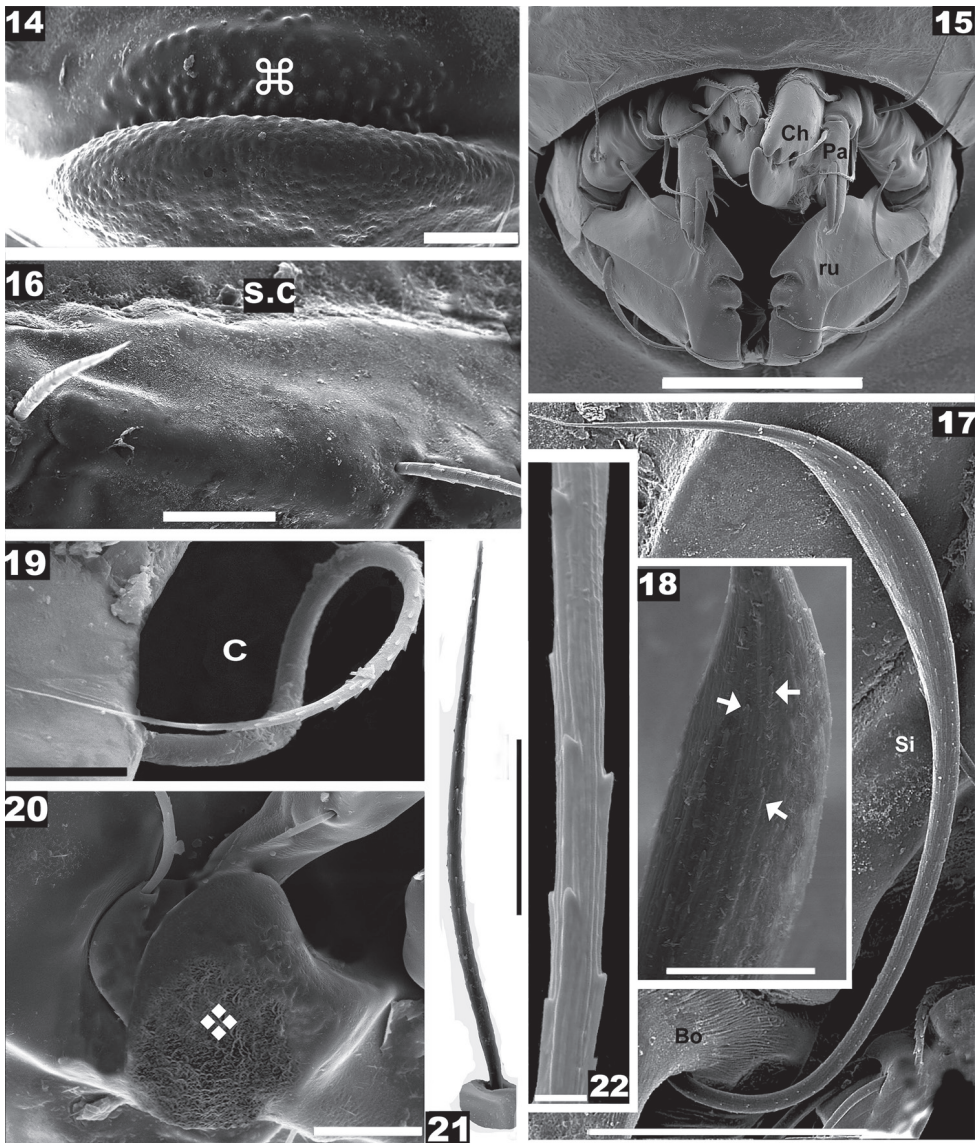
Ten pairs of setae *c*, *la*, *lm*, *lp*, *h₁*, *h₂*, *h₃*, *p₁*, *p₂*, *p₃*; setae *c* situated on lateral margin of *n.a.d* (Figures 1, 4, 7); setae *c*: *looped*, *dentate*, *sharply tipped* (Figure 19). Length: 150 (144–175); *la*, *lm*, *lp*, *h₁*, *h₂*, *h₃*, *p₁*, *p₂*, *p₃* (Figures 1, 2, 16, 23, 25); *simple*, *small dentitions*, *with parallel longitudinal ridges*, *sharply tipped* (Figure 3); four pairs situated laterally: *h₃*, *p₁*, *p₂*, *p₃*; three pairs (*la*, *h₂*, *h₁*) situated internally to *s.c*; two pairs (*lm*, *lp*) situated internally to *la*, *h₂* (Figures 1, 7, 23). Setae *h₃*, *p₃* inserted on conspicuous promontories (Figure 1, 23, 25, 42); deep v shaped incision observed behind each seta (Figure 25, indicated by ➤), determining a scalloped notogastral margin in this region (Figure 1). Setal lengths: *la* 102 (97–112); *lm* 134 (127–142); *lp* 125 (118–132); *h₁*, *h₂*



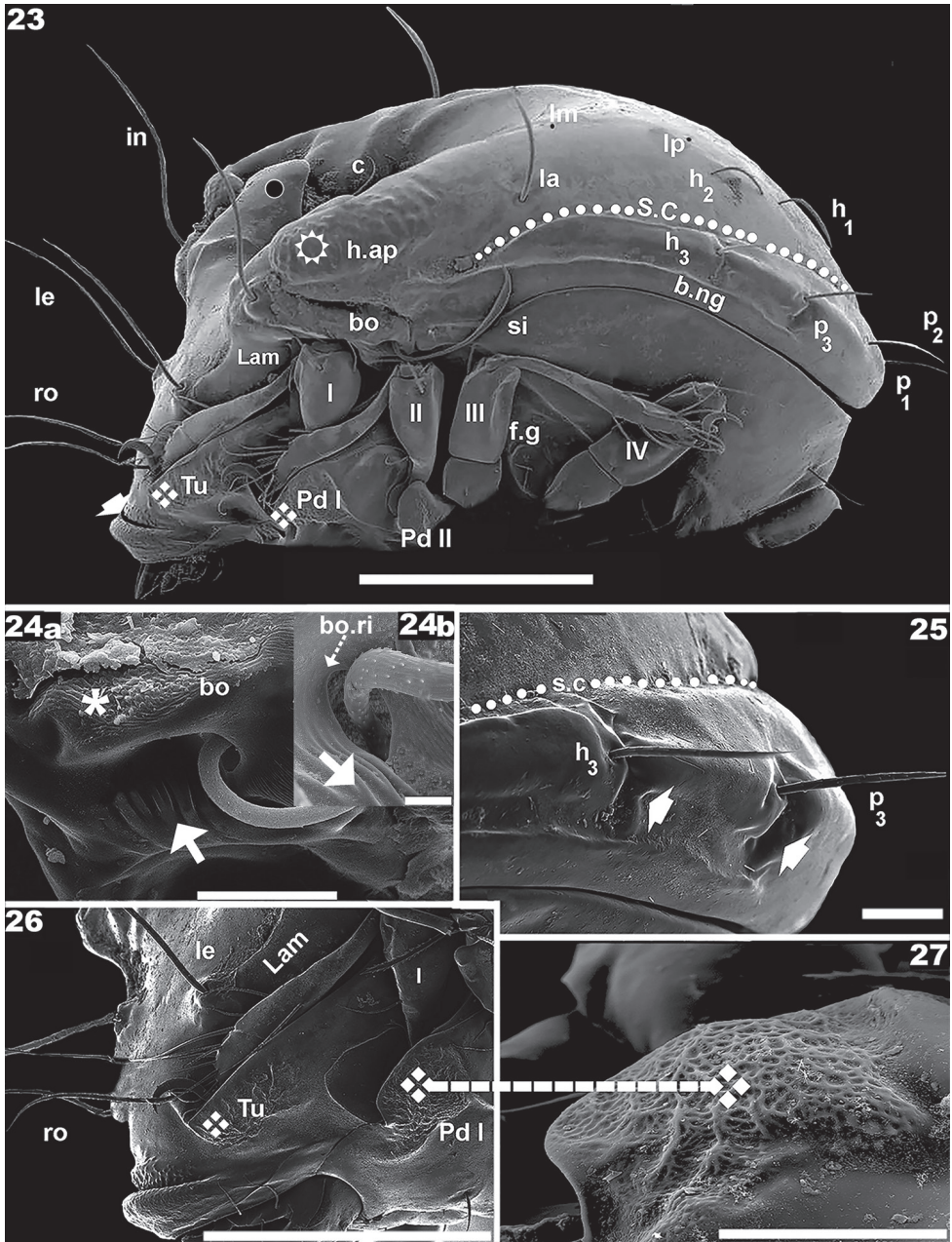
Figures 1–10. *Nippobodes panemorfis* sp. n. Adult female, SEM. **1** dorsal view **2** detail of notogastral *lm* setae **3** detail of notogastral *lm* setae microsculpture, high magnification **4** frontal view **5** prodorsal lamellar (*le*) setae, detail **6** rostral (*ro*) setae, detail **7** dorsal anteroposterior view **8** prodorsal posterior condyle interlocked with humeral apophysis anterior zone **9** anterior view, humeral apophysis and interlamellar seta **10** interlamellar seta, detail. For abbreviations: see “Material and methods”. Scale bars: 200 μm (**1**); 100 μm (**4**, **7**); 50 μm (**5**, **6**, **8**); 25 μm (**9**); 17 μm (**2**); 3 μm (**10**); 2 μm (**3**).



Figures 11–13. *Nippobodes panemorphis* sp. n. Adult female, Optical observations. 11 lateral view 12 dorsal view 13 ventral view. Scale bars: 200 μm (11); 270 μm (12); 180 μm (13).



Figures 14–22. *Nippobodes panemorfis* sp. n. Adult female, SEM observations. **14** rostrum, frontal view **15** subcapitulum, frontal view **16** notogaster, partial lateral view **17** sensillus, lateral view **18** apical zone, sensillus **19** seta *c*, dorsal view **20** pedotectum II, lateral view **21** lamellar seta **22** lamellar seta, detail. Scale bars: 50 μ m (**15**, **17**, **20**); 20 μ m (**14**, **16**); 10 μ m (**18**, **19**); 5 μ m (**21**); 2 μ m (**22**).



Figures 23–27. *Nippobodes panemorfnis* sp. n. Adult female, SEM observations. **23** lateral view **24a** bothridial zone **24b** bothridial opening **25** lateral view, zone of h_3 , p_3 setae **26** prodorsum, lateral view **27** pedotectum I, lateral view. Scale bars: 200 μm (**23**, **26**); 30 μm (**24**, **27**); 20 μm (**25**); 5 μm (**24**).

70 (68–76); h_3 91 (86–98); p_3 59 (56–64); p_2, p_1 43 (41–47); *s.c* completely surrounding notogaster, originating slightly in front of setae *la*, running between setae *la*, h_1 , h_2 and h_3 , p_3 , p_2 , p_1 (Figures 1, 7 trajectory indicated by ●).

Posterior notogastral view (Figure 7). Deep ovoid *p.p.d* as well as *n.a.d* clearly visible; setae *c* situated on paraxial zone of *h.ap*.

Trajectory of *s.c* indicated by ●; externally to *s.c*, flat surface of notogaster extending from *s.c* to notogastral margin; scalloped zone (behind setae h_3 , p_3), some distance from *s.c*, not interrupting its trajectory.

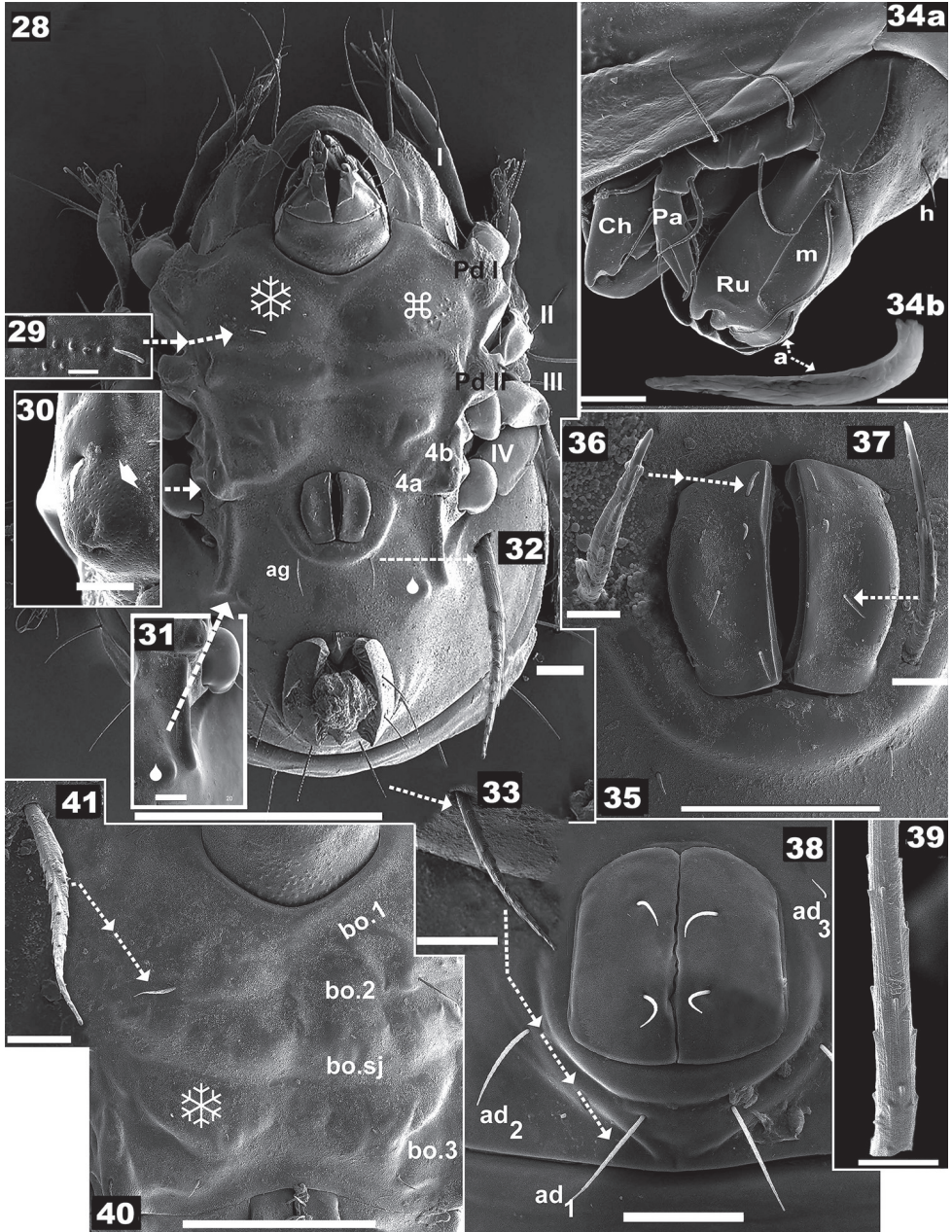
Lateral region. *Tu* strong, large lamina, together with prodorsal wall and lamellae determining a pocket structure; anterior *Tu* ending in sharp angle, with interior part welded to prodorsal wall (Figure 1 indicated by †); behind *le* setal insertion level, pocket structure internally delimited by the *Lam* (Figures 23, 26) (See Leg-folding process). *Pd I*, prominent extended lamina; (Figures 26, 27). *Pd II*, small lamina, rounded apex (Figures 20, 23); *Tu*, *Pd I*, *Pd II* with reticulate-foveate cuticular microsculpture (Figures 20, 26, 27 indicated by ❖).

Complex, polyhedral *bo* situated under the zone where *h.ap* overlaps the anterior prodorsal zone (Figure 23). Bothridial opening observed at the bottom of a long U-shaped structure (Figures 24a, 24b), with sulcate microsculpture on inferior zone (Figure 24a, 24b indicated by ◀); smooth bothridial ring (*bo.ri*) surrounding ovoid bothridial opening; *Lam* sigmoid, lacking sharp cuspis (Figures 23, 26); setae *le* inserted on promontories at *Lam* apical zone; *s.c* clearly visible, originating in zone anterior to *la* setal insertion level (Figure 23, trajectory indicated by ●); v-shaped incision observed behind h_3 , p_3 setae (Figure 25, indicated by ▶); *b.ng* convex (Figure 23).

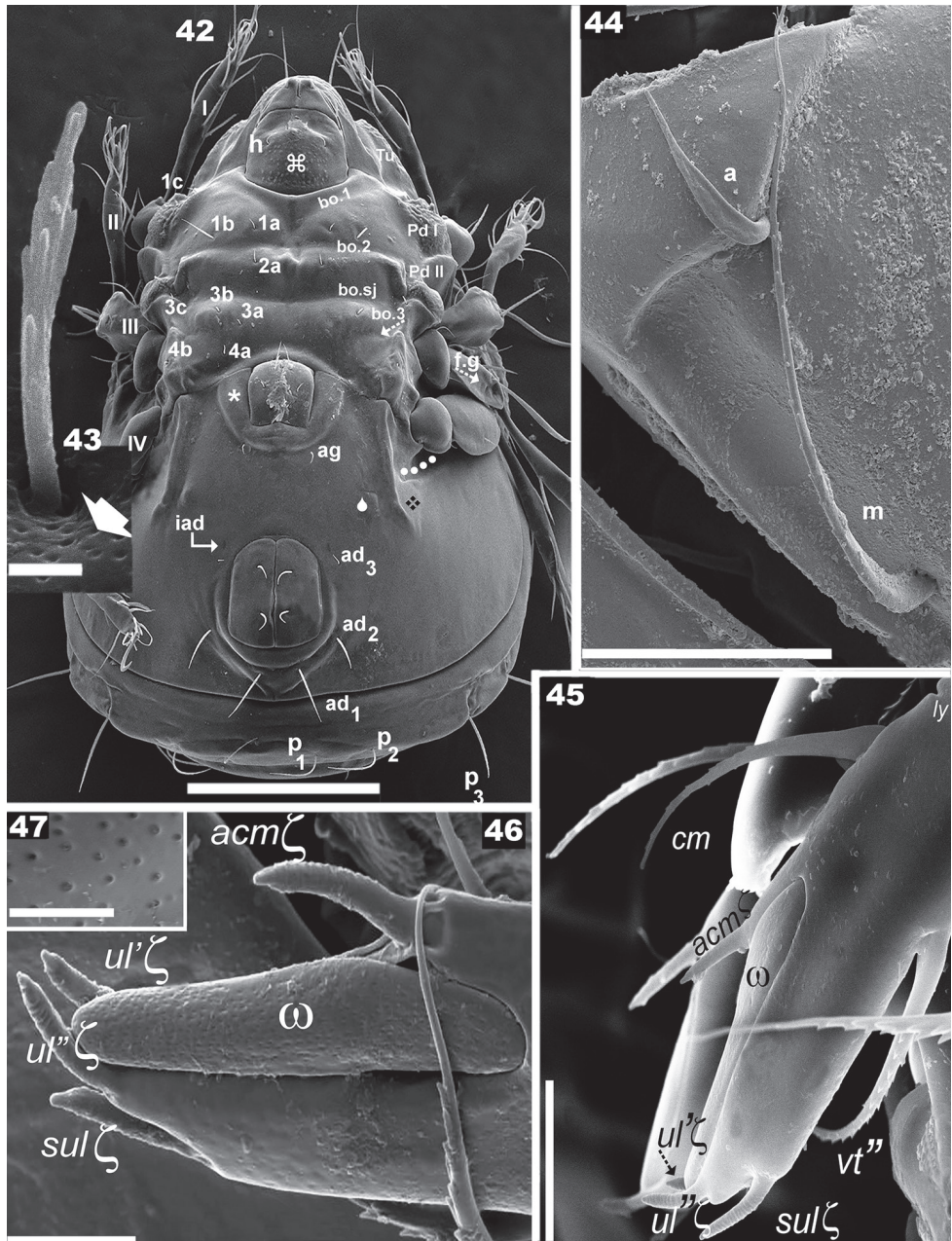
Ventral region. Epimeral chaetotaxy 3–1–3–2 (Figures 13, 42); setae *1c*, *3c*, *4b* situated marginally (Figure 30); setae *1b* largest (Figure 41); epimeral borders easily observed; *bo.2*, *b.sj* traversing medial plane; *bo.3* small; apodemes *apo.1*, *apo.2*, *apo.dj*, *apo.3* clearly visible (Figure 13); small setae, many small barbs (Figure 30); length: 9 (5–18).

Genital plate ovoid, with four pairs of setae (Figure 35, 36, 37); genital setae: with small barbs, variable in shape (Figures 36, 37); length: 5 (4–7); genital opening on elevated zone (Figures 28, 35); setae *ag* in margin of elevated zone (Figures 28, 32, 42); medium sized setae *ag* with small dentitions, sharp tip (Figures 32) *ag*: 20 (8–21). Complex structure involved in leg-folding process (see Locking structure), situated laterally to setae *ag* (Figures 28, 31, 42); constituted by longitudinal cuticular elevation, with parallel furrow and lateral to it a cuticular promontory and opposite, a polyhedral plate (in Figures 28, 42 indicated by ●) (see Leg-folding process); genital plate smaller than anal plate (Figures 28, 42). Anal opening with elevated zone posterior to h_3 insertion level (well visible in ventral posterior view) (Figure 42); anal plate more or less rectangular with rounded anterior and posterior zones; two pairs of anal setae (Figures 28, 32, 38, 42).

Setae: *an* small dentitions, parallel ridges (Figure 39), length 14 (15–20); three pairs of adanal setae (Figures 28, 33, 38, 42); setae ad_1 , ad_2 inserted on elevated zone; ad_3 setae smallest (Figures 38, 42); adanal setae: medium sized, small dentitions, sharply tipped (Figures 32, 33), length 32 (30–36). Three pairs of subcapitular setae, *h*, *m* and *a*: *h*, *m* simple, finely barbate (Figures 34a, 44), *a* elongated leaf-shaped, with some narrow, shallow



Figures 28–41. *Nippobodes panemorfs* sp. n. Adult female, SEM observations. **28** ventral view **29** tuberculate zone **30** discidium with epimeral seta *3c* **31** ridge associated with leg folding **32** aggenital setae **33** adanal setae **34a** subcapitulum **34b** subcapitular setae *a* **35** genital zone **36** genital seta type 1 **37** genital seta type 2 **38** anal zone **39** ornamentation of anal setae **40** epimeral zone **41** epimeral seta *1a*. Scale bars: 200 μ m (**28**); 50 μ m (**35**, **38**, **40**); 20 μ m (**31**, **34**); 10 μ m (**29**, **30**, **33**); 5 μ m (**41**); 3 μ m (**34**); 2 μ m (**32**, **36**, **37**, **39**).



Figures 42–47. *Nippobodes panemorfis* sp. n. Adult female, SEM. **42** ventral view **43** epimeral seta 2a **44** subcapitulum anterior zone **45** palp, lateral view **46** palp, anterior zone **47** porose area, detail w sole-nidium. Scale bars: **42** 200 μm ; **44** 20 μm ; **45** 10 μm ; 5 μm (**46**); 2 μm (**43**); 0.1 μm (**47**).

Table 1. *Nippobodes panemorfis* sp. n. setae and solenidia.

	Femur	Genu	Tibia	Tarsus	Claw
Leg I					
setae	<i>dp, da, l'', v</i>	<i>d, v</i>	<i>d, (l), v</i>	<i>(ft), ε, (tc), (it), (p), (u), (a), s, (pv)</i>	1
solenidia		σ	φ ₁ , φ ₂	ω ₁ , ω ₂	
Leg II					
setae	<i>dp, da, l'', v</i>	<i>d, v, l''</i>	<i>lv</i>	<i>(pv)(ft), (tc), (it), (p), (a), (u), s,</i>	1
solenidia		σ	φ	ω ₁ , ω ₂	
Leg III					
setae	<i>d, l', v</i>	<i>d</i>	<i>l', v</i>	<i>(pv), s, (a), (u), (p), (it), (tc), (ft)</i>	1
solenidia			φ	-	
Leg IV					
setae	<i>d, v</i>	<i>l'</i>	<i>l'', v</i>	<i>fī'', (tc), (it), (p)(u), (a), s, (pv)</i>	1
solenidia		-	φ	-	

longitudinal furrows (Figure 34b); setae *h* situated in margin of tuberculate zone (Figure 42 indicated by ⌘); setae *m* curving, lengths: *h* 10 (9–12); *m* 30 (28–32); *a* 11 (10–12).

Palp (Figure 34): the first four segments display normal setation (0–2–1–3); tarsus particular, presenting only: *cm* barbate, (*vt*) barbate, w solenidion and eupathid *acmx*, *sulx*, *ul'x*, *ul''x*. Solenidion unusually shaped (Figures 45, 46), with porous surface (Figure 47); eupathid *sulx*, *ul'x*, *ul''x* with an obvious apical perforation (Figure 46).

Legs. See Figures 48–53, Table 1. All legs with very small genu and long tibia. Femur leg IV with large round porose area (Figure 53). Femur III with large femoral groove (*f.g*) (Figures 51, 52) (see Leg-folding process). Setal formulae I (1–4–2–4–16–1) (1–2–2); II (1–4–3–2–15–1) (1–1–2); III (2–3–1–2–15–1) (0–1–0); IV (1–2–1–2–14–1) (0–1–0).

Remarks. Future ontogenetic studies are necessary in order to confirm nomination of notogastral setae. As only the adult stase was available for study, we used standard, previously used notation (see Morphological terminology). We were unable to locate information on the palp in previous studies. Setae *l'* of genu II were indicated by Chen and Wang (2007) as bifurcate; however, in our studies only one instance of bifurcate setae *l'* was observed. Another particularity is the presence of (*it*) on tarsus IV. The femoral groove was observed, though not indicated in any previous study.

Leobodes trypasis sp. n.

<http://zoobank.org/09F0BA2C-4623-46E3-8275-DFFA740A3966>

Figures 54–76

Etymology. The specific epithet “trypasis” is derived from τρύπα in Greek meaning a hole, due to the characteristics of the anterior prodorsum.

Diagnosis. Rostrum ovoid; smooth cuticula with isolated verrucous tubercles; setae *ro* sigmoid; setae *le* curved, directing forward and upward; setae *in* slightly sigmoid, direct-

ing forward; deep round-ovoid posterior prodorsal depression; massive posterior prodorsal condyles, posterolaterally located, extending anteromedially to form a curved bridge, interlocking medially in undulate zone. Lateral lamellae, curved ribbon; frontal orifice, heart shaped; translamella curved; tatorium welded to lateral prodorsal wall, determining pocket structure, sharply tipped, but welded to lateral prodorsal wall; sensillus sickle-shaped, strongly curved, upwards; long stalk, swollen middle zone, apically long sharp end. Anterior notogastral depression deep, ovoid-elongate shape; humeral apophysis overlapping posterior prodorsal condyle, extending to the proximity of interlamellar setae; circumgastric depression, surrounding whole entire notogaster; setae *c* hook-shaped; flat smooth surface surrounding laterally whole notogaster; flat, smooth lateral ledge, surrounding entire notogaster; anterior zone, ribbon shaped; genital plate smaller than anal plate.

Material examined. Holotype: ♀ Female “VN 12/03c Vietnam. Vinh Phuc Prov. evergreen Forest 1 km SE Tam Dao city. 21°26'49"N, 105° 39'06"E. 13/14/V/2012. Leg. P. Schwendinger & A. Schulz”.

Description. Measurements. SEM: 680 (610–750) × 336 (302–400) (n = 5). Light microscopy: 701 × 341 (n = 1); all specimens female.

Shape. Oval (Figure 54).

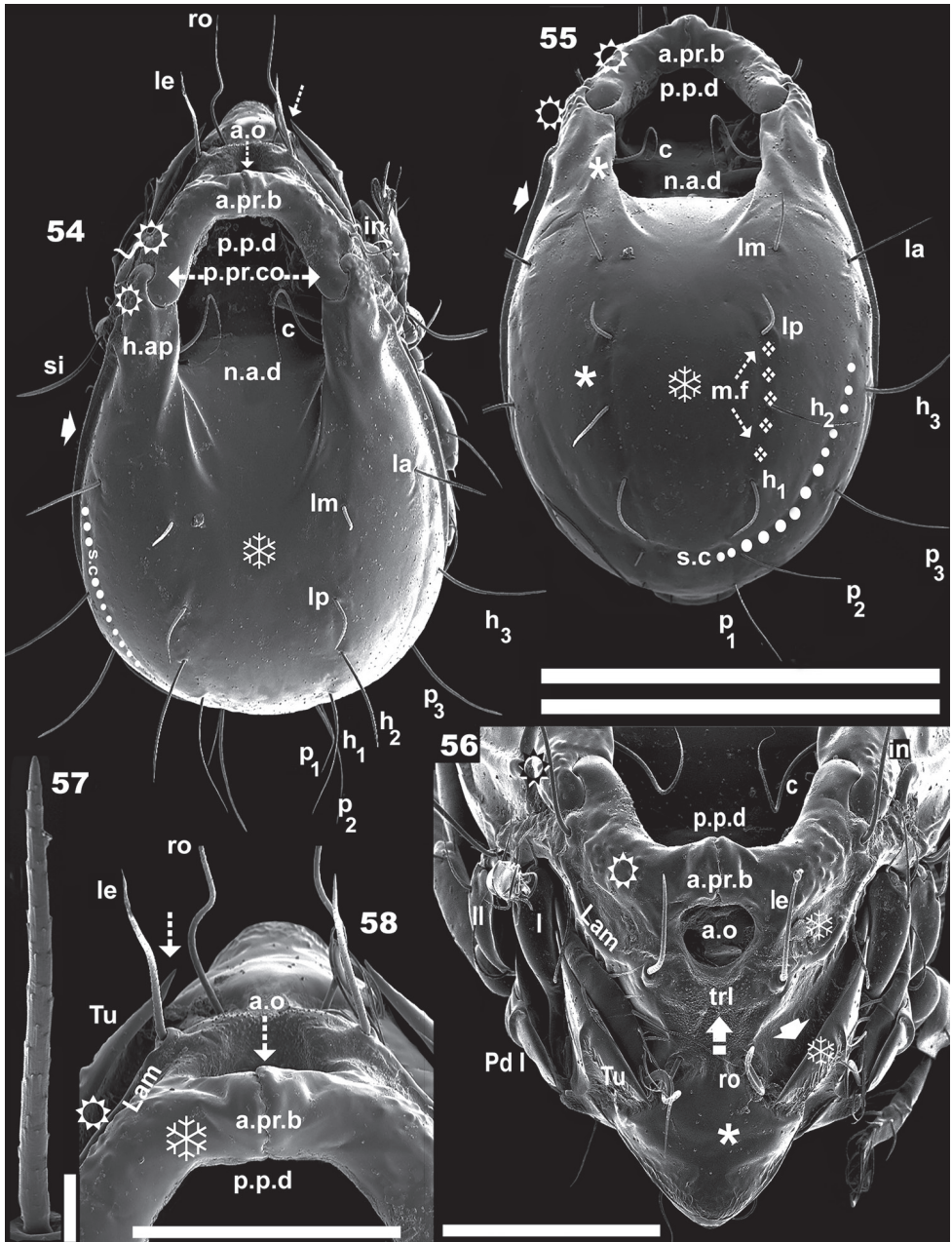
Colour. Dark brown to black; slightly shiny when observed in reflected light.

Cerotegument. Not present.

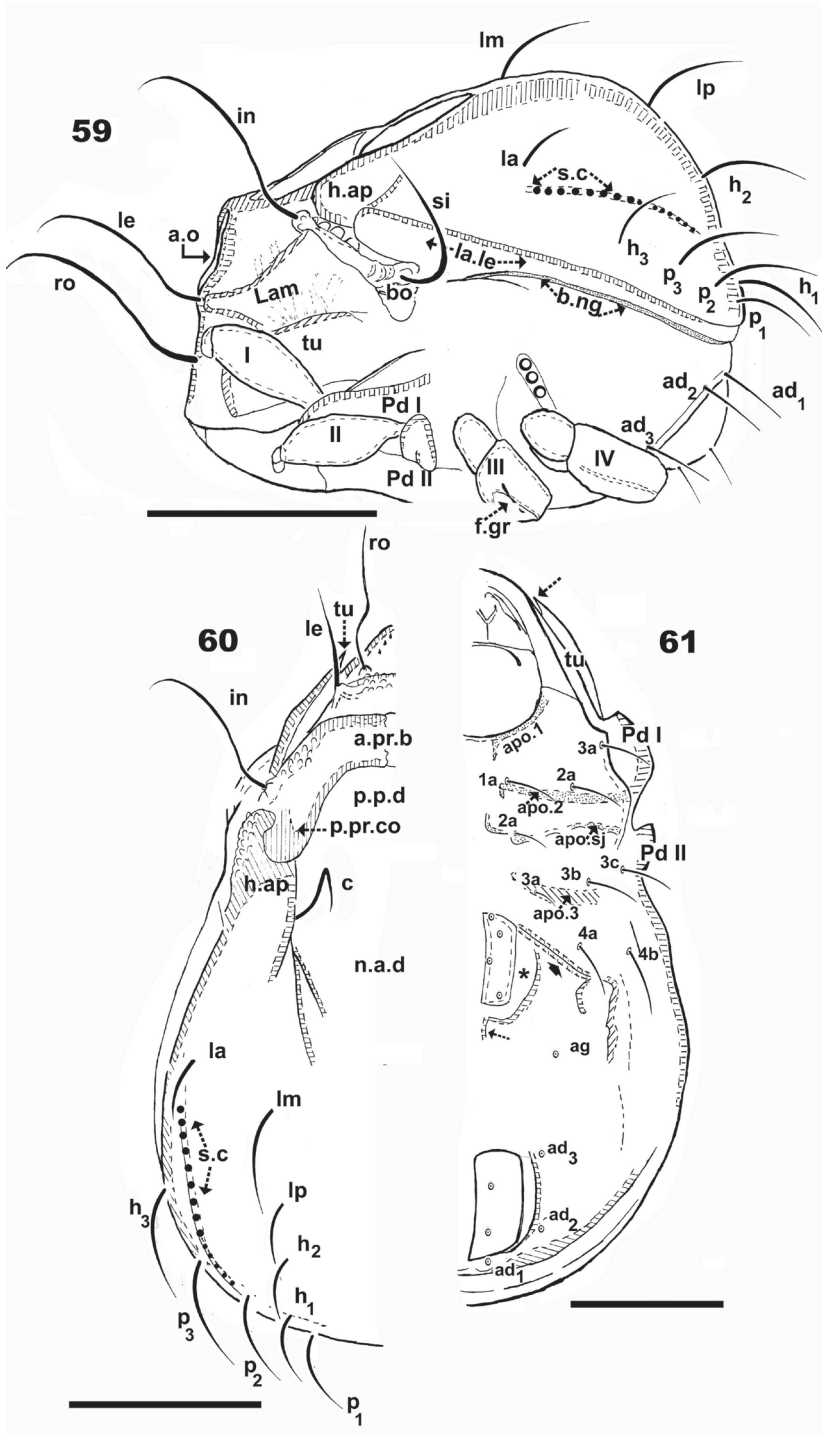
Integument. Microsculpture varying according to body region: *Smooth*: *p.pr.co* anterior zone; transversal bridge-shaped structure (*a.pr.b*) (Figures 54, 55, 58); superior *Lam* zone; superior and apical region *Tu* (on Figures 56, 65 indicated by *). Notogaster: central zone; marginal zone between *s.c* and *b.ng* (on Figure 62 indicated by *); flat lateral ledge (*la.le*) situated immediately above *b.ng* (see below) (on Figures 62, 63 indicated by *); epimeral zone (on Figures 71, 72 indicated by *); infracapitulum (on Figure 71 indicated by *). *Tuberculate* (two types). *Small tubercles*: prodorsal zone below frontal orifice (*a.o*) and between setae *le* (on Figure 56 indicated by ♁); *large verrucous tubercles* (Figure 70): isolated tubercles, dispersed on prodorsum (Figures 56 indicated by *), notogaster (Figure 55, indicated by *), and ventral zone (Figure 62, indicated by *). *Rugose*: external zone *h.ap*, external zone of *pr.co* (Figures 54, 55, 56, 58 indicated by ☼). *Reticulate-foveate*: basal zone of *Lam*, (Figure 62, indicated by ♦); *Tu* (Figure 62, indicated by ♦); *Pd I* anterior zone. *Sulcate*: area of bothridial opening (Figure 64, indicated by ◀).

Setation (legs not included). *Simple, smooth*: subcapitular setae *a*. *Simple, small, dentate, parallel longitudinal ridges* (Figure 66): prodorsal (Figures 67, 68), notogastral (Figure 57, 69), epimeral, subcapitular *m*, *h*; genital, aggenital, adanal, and anal setae.

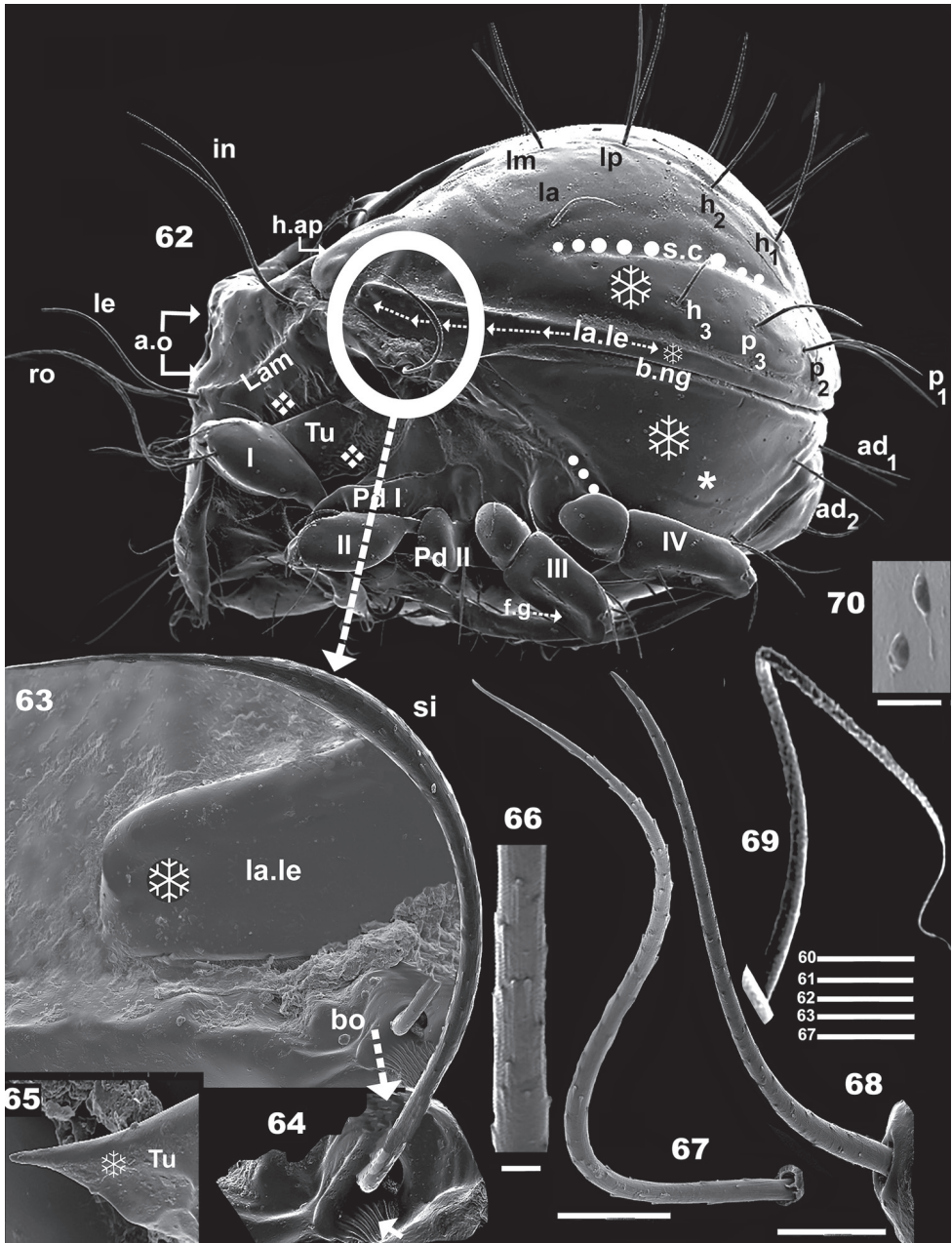
Prodorsum. More or less triangular in dorsal view, central posterior concave; lateral view: polyhedral (Figure 62); lateral posterior zone with double hook, interlocking posterior prodorsal condyle (*p.pr.co*) and *h.ap* anterior zone (Figures 54, 55). Rostrum ovoid. Smooth cuticula with some isolate verrucous tubercles (Figures 56, 58) on zone delimited by rostrum and *ro* setal insertion level. Setae *ro*, *le*, *in* inserted each on large tubercle; *ro* sigmoid, directing forward (Figure 67), length 150 (142–161) (n = 10); *le* setae curved, directing forward and upward, length: 106 (102–112) (n = 10), situ-



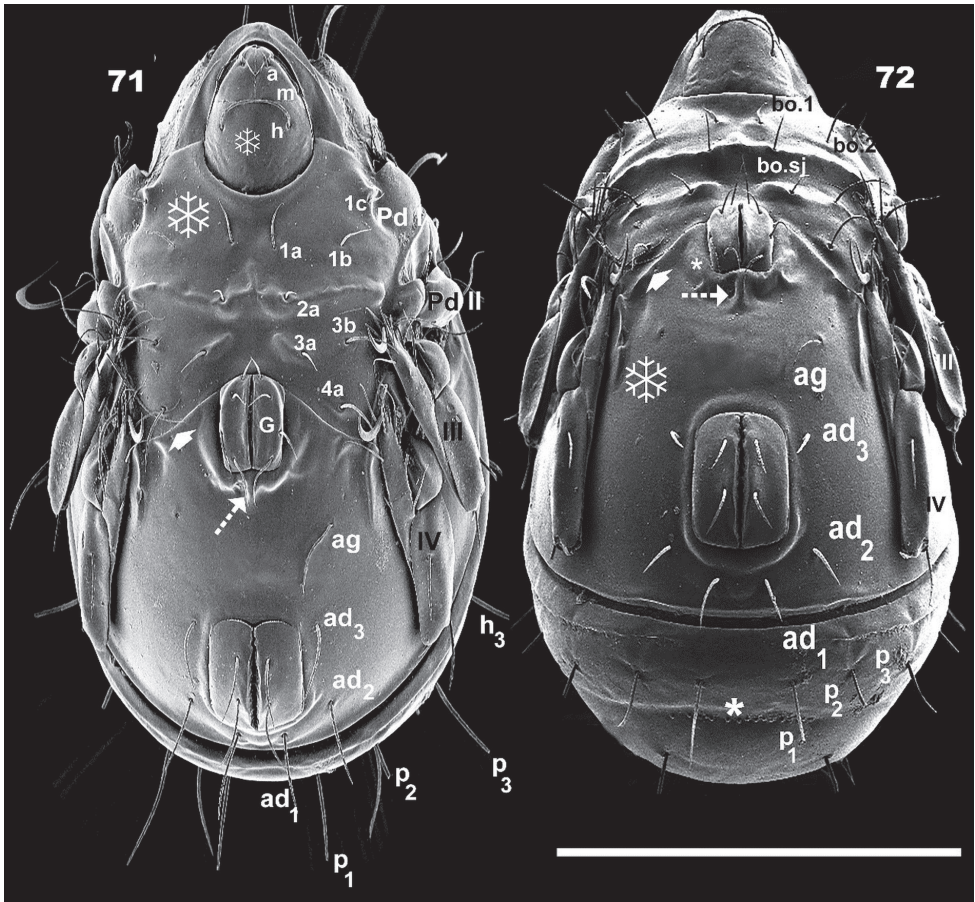
Figures 54–58. *Leobodes trypasis* sp. n. Adult female, SEM. **54** dorsal view **55** posterior dorsal view **56** prodorsum anterior view **57** notogastral seta *la* **58** anterior prodorsal zone. Scale bars: 500 μ m (**54**); 300 μ m (**55**); 150 μ m (**56**); 16 μ m (**57**).



Figures 59–61. *Leobodes tryptasis* sp. n. Adult female, optical observations. **59** lateral view **60** dorsal view **61** ventral view. Scale bars: 280 μ m (**59**); 250 μ m (**60**); 200 μ m (**61**).



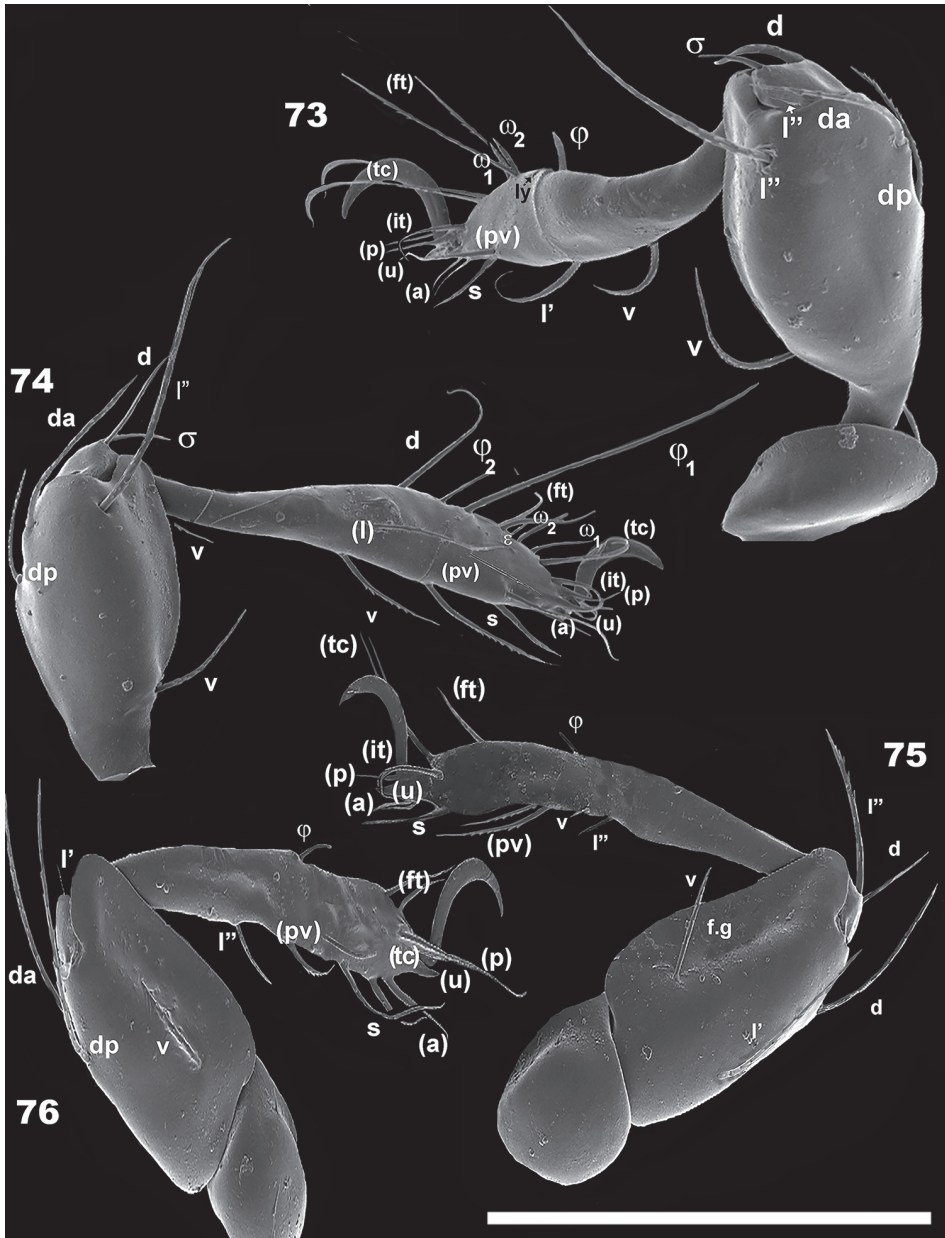
Figures 62–70. *Leobodes trypasis* sp. n. Adult female, SEM observations. **62** lateral view, (circle indicating the area where *bo*, *si*, *la.le* are situated (see Figures 63, 64) **63** detail, humeral apophysis **64** bothridium, sensillus detail **65** apical zone *Tu* **66** detailed microculture, notogastral setae **67** setae *ro* **68** setae *le* **69** setae *c* **70** large verrucous tubercles. Scale bars: 100 μm (**62**); 32 μm (**69**); 25 μm (**68**); 20 μm (**63**, **64**, **65**, **67**); 2 μm (**66**); 0,7 μm (**70**).



Figures 71–72. *Leobodes trypasis* sp. n. Adult female, SEM observations. **71** ventral view **72** posterior anterior view. Scale bars: 450 μ m (**71**, **72**).

ated on apical lamellar zone (Figures 56, 68); setae *in* length: 178 (172–190) ($n = 10$); slightly sigmoid, directing forward, situated externally, anterior to *h.ap* (which overlaps with posterior prodorsal zone) and posterior to rugose lateral zone of *p.pr.co* (Figures 56); *p.p.d* clearly discernible, deep, round-ovoid in shape (Figure 54, 55, 56, 58). Massive *p.pr.co*, hook-shaped, located posterolaterally; anteromedially curved bridge (*a.pr.b*), interlocking medially in an undulate zone (Figures 54, 55, 56, 58).

Lamellae (*Lam*) clearly visible; lateral longitudinal rib, dorsally concave (Figure 56, 57). Conspicuous heart-shaped *a.o* (Figures 56, 58), located below the *a.pr.b*, and between setae *le*, limited inferiorly by Translamella (*trl*); *trl* a curved structure, running parallel to and below *a.o* (Figure 56). *Tu* well developed; welded to lateral prodorsal wall, determining a pocket (Figures 56 indicated by \blacktriangleright); large sharp tip (Figures 54, 58 indicated by \blacktriangleright). *Bo* complex (Figures 62, 64), situated under *la.le* (see: Lateral region). *Si* (Figure 64) sickle-shaped, strongly curved, directing upward with long stalk, fol-



Figures 73–76. *Leobodes trypasis* sp. n. Adult female, SEM observations. **73.** leg II, antiaxial **74** leg I, antiaxial **75** leg III, antiaxial **76** leg IV, antiaxial. Scale bar: 130 μ m (**73–76**).

lowed by swollen zone, long sharp apical tip; plentiful small asperities and small barbs on swollen zone (Figure 64); length: 150 (146–161) (n = 12).

Notogaster. Deep, elongate ovoid *n.a.d* present, extending from posterior to more or less half of total notogastral length; medial posterior *n.a.d* zone, open without clear-

ly defined margin; *n.a.d* lateral marginal zone with three lines; more externally: a short, concave line on interior of *h.ap* margin; rectilinear central line; third line lateral to posterior margin (Figure 54). Anterior *h.ap* zone overlapping *p.pr.co* (double hook), extending to the proximity of setae *in* (Figures 54, 56); *s.c* completely surrounding the notogaster; originating at level of *la* setal insertion, running internally to setae h_3, p_3, p_2, p_1 (Figures 54, 55, 62 trajectory indicated by ●).

Ten pairs of setae: *c, la, lm, lp, h₁, h₂, h₃, p₁, p₂, p₃* (Figures 60, 62); setae *c* hook-shaped (Figure 69), situated on lateral margin of *n.a.d* (Figures 54, 55, 56); four pairs situated marginally: p_1, p_2, p_3, h_3 ; four, more or less aligned pairs lm, lp, h_2, h_1 , situated internally (Figure 55); lp, h_2, h_1 on medial shallow furrow (*m.f*); only clearly discernible in dorsoposterior view (on Figure 55 indicated by ❖); setae *la* situated between h_3, p_1, p_2, p_3 and lm, lp, h_2, h_1 (Figures 54, 55). Setal lengths. *c*: 167 (156–172); *la*: 100 (83–102); *lm*: 75 (72–81); *lp*: 83 (81–89); h_3 : 125 (123–131); h_2 : 145 (93–147); h_1 : 154 (101–162); p_3 : 125 (100–132); p_2 : 145 (116–137); p_1 : 73 (71–78).

Lateral region. The tutorium (*Tu*) strong, large lamina, attached to prodorsal wall, determining a pocket structure; terminating anteriorly in long sharp tip (Figure 65); the welded zone of *Tu* is U-shaped, and the claw of leg I is extended outwards during the leg-folding process (Figure 56) (see Leg-folding process).

Lamella (*Lam*) forming conspicuous curved ribbon (Figure 56, 59); running more or less parallel to *Tu* margin; setae *le* situated on promontories on apical zone. *Pd I*: prominent lamina, directing forward, slightly tilted down. *Pd II* a small lamina, rounded apex; on basal zone a small hump directing outwards (Figure 62). The area immediately above *b.ng* is flat, smooth, surrounding the entire notogaster (Figure 62, trajectory indicated by †); this flat surface, forms a prominent *la.le*, parallel to *h.ap* (Figure 62); *la.le* anterior zone, ribbon shaped, (Figure 59, 62, 63); *b.ng* slightly convex (Figure 62).

Bo complex: polyhedral, situated below *la.le* (Figure 64); bothridial opening situated at the bottom of a long U-shaped structure; inferior zone with sulcate microsculpture (Figure 64), indicated by ◀); bothridial opening ovoid, surrounded by smooth *bo.ri*; *s.c* clearly visible, originating at level of *la* insertion setal level (Figure 62 indicated by ●).

Ventral zone. Epimeral chaetotaxy 3-1-3-2 (Figures 61, 71, 72); setae *1c, 3c, 4b* situated marginally; setal lengths: *1a*: 35 (32–38); *1b*: 35 (30–37); *1c*: 29 (25–31); *2a*: 12 (10–15); *3a*: 22.5 (20–25); *3b*: 38 (35–42); *3c*: 18 (16–19); *4a*: 50 (45–52); *4b*: 38 (41–45); epimeral borders clearly visible; *bo.sj* crossing transverse medial plane (Figure 72); *bo.3* small; apodemes *apo.1, apo.2, apo.dj, apo.3* clearly visible (Figure 61). *Pd I, Pd II* clearly discernible (Figures 71, 72).

Genital aperture rectangular, anterior margin rounded, four pairs of setae: $g_1, 71$ (68–73); $g_2, 49$ (44–52); $g_3, 37$ (34–43); $g_4, 35$ (31–38); Elevated ridge surrounding genital opening medially and towards posterior zone (Figure 72, indicated by *), in posterior zone a small vertical column present (Figure 71, 72 indicated by †); setae *ag* distanced from genital opening (Figures 71, 72); length: 73 (71–83). Posterior limit epimere IV, oblique lineal ridge laterally directed (Figure 71, 72 indicated by ▶); originating in anterior zone of genital plate (Figures 71, 72 indicated by ▶). Complex structure lateral to

Table 2. *Leobodes trypasis* sp. n. setae and solenidia.

	Femur	Genu	Tibia	Tarsus	Claw
Leg I					
setae	<i>da,dp,l'',v</i>	<i>d,v</i>	<i>d,(l),v</i>	<i>(pv),(it),(tc),(ft),e,(p),s,(a)(u)</i>	1
solenidia		s	<i>j₁, j₂</i>	<i>w₁, w₂</i>	
Leg II					
setae	<i>da,dp,v,l''</i>	<i>d,l''</i>	<i>l',v</i>	<i>(ft)(tc)(it)(p)(u)(a),s(pv)</i>	1
solenidia		s	j	<i>w₁, w₂</i>	
Leg III					
setae	<i>l',v</i>	<i>l',v,d</i>	<i>d,l''</i>	<i>(ft)(it)(tc)(p)(u)(a),s,(pv)</i>	1
solenidia			j		
Leg IV					
setae	<i>da,dp,v</i>	<i>l'</i>	<i>(l),v</i>	<i>(p)(u)(a)s,(pv)ft''(it)(tc)</i>	1
solenidia		-	j	-	

setae *ag*, with a longitudinal cuticular elevation, parallel furrow and promontories (see leg folding “locking structure”); genital plate smaller than anal plate (Figures 71, 72).

Anal aperture more or less rectangular with rounded anterior and posterior zones; two pairs of anal setae (Figures 61, 71, 72), length: 37 (35–39); three pairs of adanal setae: *ad₁*: 73 (71–75); *ad₂*: 75 (73–78); *ad₃*: 80 (77–83). Three pairs of subcapitular setae: *h*, *m* simple, barbate; *a* simple, smooth: lengths: *a*: 12 (9–15); *m*: 29 (28–33); *h*: 42 (39–45).

Legs (Figures 73–76, Table 2). Very small genua and long tibia in all legs. Femur III with *f.g* (Figure 75) (see Leg-folding process). Setal formulae: I (1-4-2-4-16-1) (1-2-2); II (1-4-3-2-15-1) (1-1-2); III (2-3-1-2-15-1) (0-1-0); IV (1-2-1-2-14-1) (0-1-0).

Discussion

Aoki, when establishing the new genus *Nippobodes* in 1959, initially included it in the family Carabodidae. Almost sixty years later, we propose that the family Nippobodidae presents a series of characters linking these families, as knowledge of the families Nippobodidae and Carabodidae has grown significantly in the intervening years. We consider here only some elements that indicate important similarities: 1) prodorsal posterior depression and notogastral anterior depression situated either side of *d.sj*; 2) the projection of *h.ap* overlapping the posterior area of prodorsum; 3) the structures involved in leg folding such as turtorium, pedotectum I, genu (functioning as a hinge), femoral groove in femur III, shapes of femurs. These three elements are insufficient for a comparison, but highlight some aspects indicating a possible relationship between the families. More detailed analysis is required, but hampered by the lack of immature specimens of Nippobodidae and for the greater part of Carabodidae.

Unfortunately descriptions of genera in the family Nippobodidae are often superficial, and in many instances the frontal and posterior views were neglected although

they could potentially provide important information. Leg chaetotaxy is problematic and we endeavour to obtain new material in order to study legs in a larger number of specimens. Much of our study material was collected many years ago, and does not permit detailed study, resulting in leg chaetotaxy necessarily being considered provisional.

It has been difficult to find a species related to *Nippobodes panemorfis* sp. n. due to its particular characteristics. *Nippobodes flagellifer* Chen & Wang, 2007 displays the most characters in common, as both species present similar disposition of: setae *ro* on tubercle near lateral margin of prodorsum; setae *le* inserted on tubercle on anterior on lamella; sensillus curved, sickle-shaped, swollen medially; posterior prodorsal condyles interlocking with notogastral humeral apophyse (but dissimilar in shape). Notogastral surface smooth; ten pairs of notogastral setae.

The taxonomy of *Leobodes trypasis* sp. n. is complex. The species is difficult to compare to other congeners due to their dissimilarity, and the often simplified original descriptions impede adequate comparison. However, there are similarities to *L. anulatus* Aoki, 1965, such as the presence of a heart-shaped prodorsal orifice, but occurring in a dorsal and not frontal position as in *L. trypasis*.

Leg-folding process (Figures 77–88)

Fernandez et al. (2013a) have studied the folding of legs as a part of the protection mechanism in various genera of the family Carabodidae. We were fortunate to have the opportunity to examine this process in vivo on adults of *Carabodes* sp. under light microscopy and document the different steps. Additionally, material was available for SEM-studies, facilitating comparison with other SEM images. For this paper we were unable to conduct in vivo studies of the leg-folding process, but based on a series of observed morphological characteristics and a large number of SEM observations, we do not doubt the presence of similar functions and processes as observed in genera of the family Carabodidae.

Some morphological characteristics, however, suggest some variation in aspects of this mechanism.

To understand this process one needs, first of all, to embark on detailed studies of leg structures in *Nippobodes* (Figures 48–53) and *Leobodes* (Figures 73–76), as well as other body structures related to leg positioning. Due to the high number of images obtained from more than fifty specimens, selected from a total of more than three hundred animals, only the most representative images of this mechanism have been included for the sake of clarity.

Structures involved

The legs

The following is generally observed: tibia-tarsal articulation by means of a small section of synarthrodial membrane, allowing limited movement. Tibia and tarsus are long

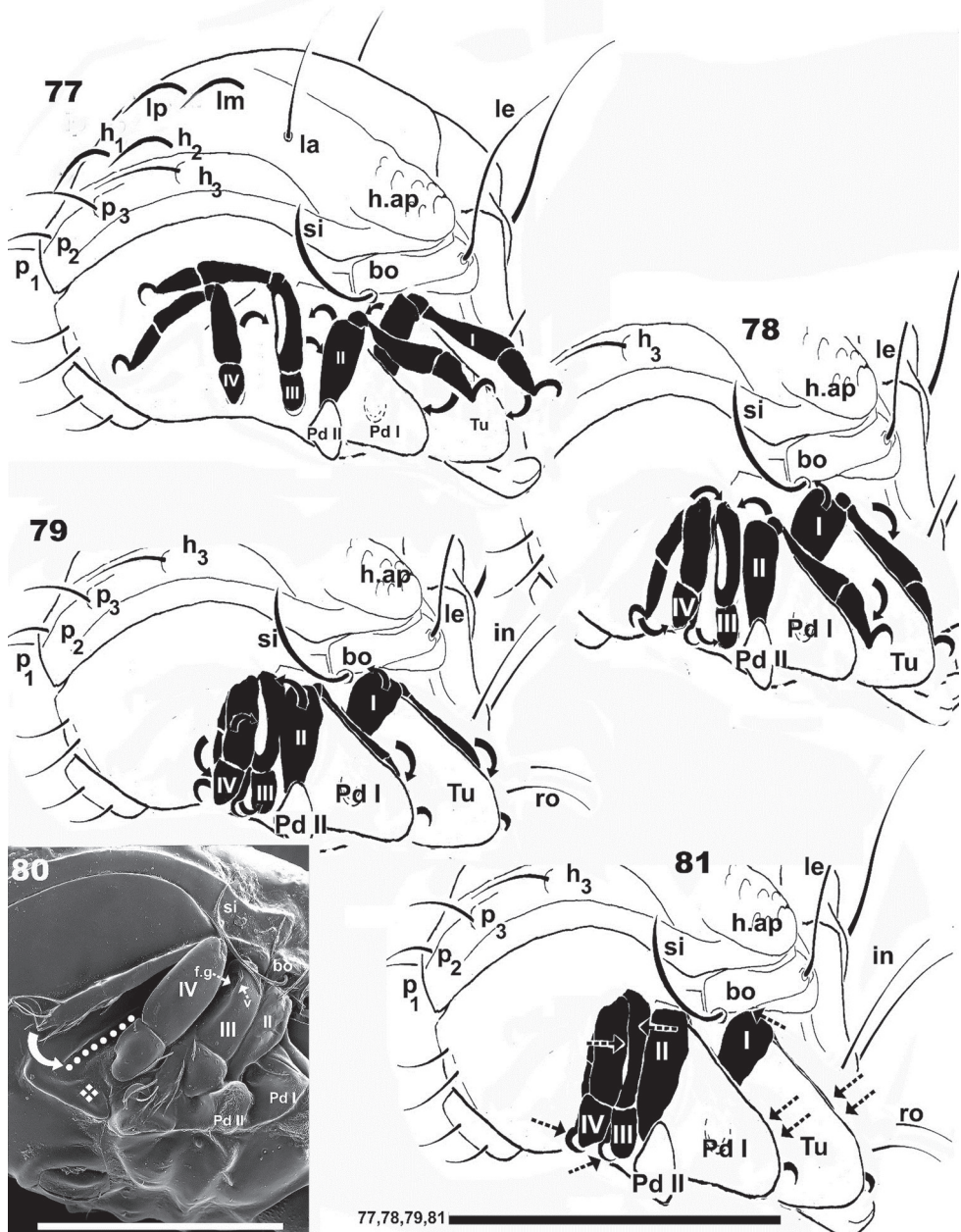
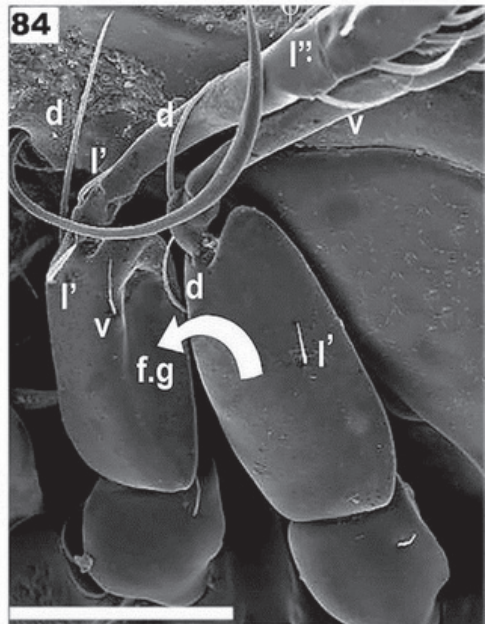
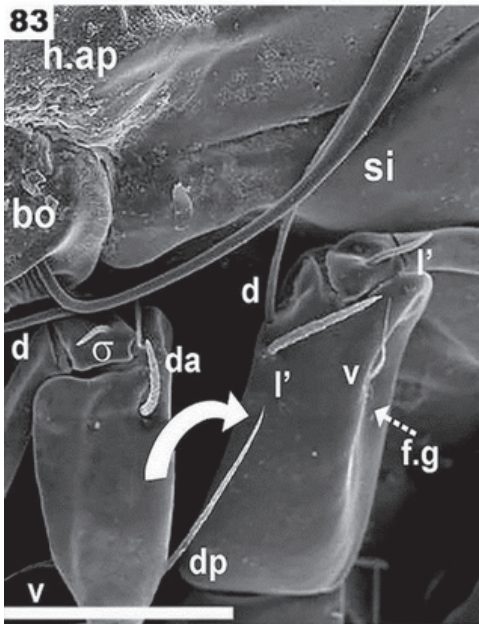
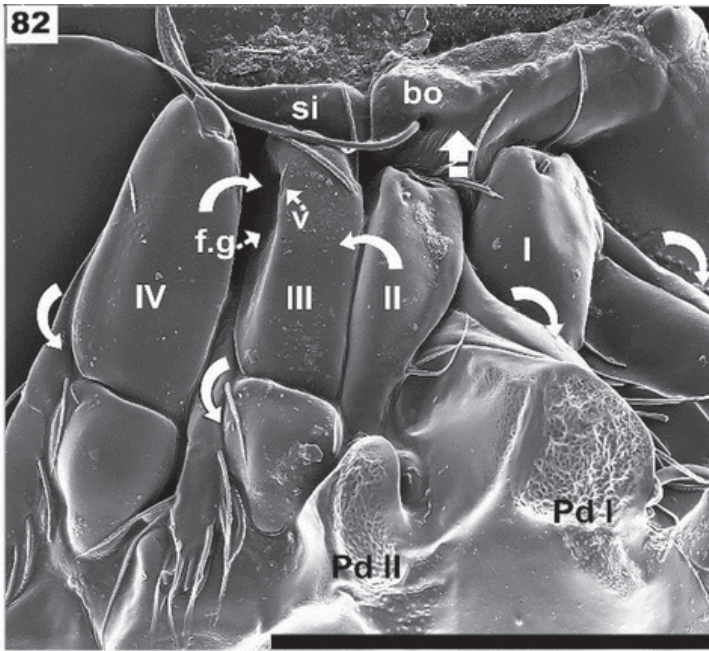
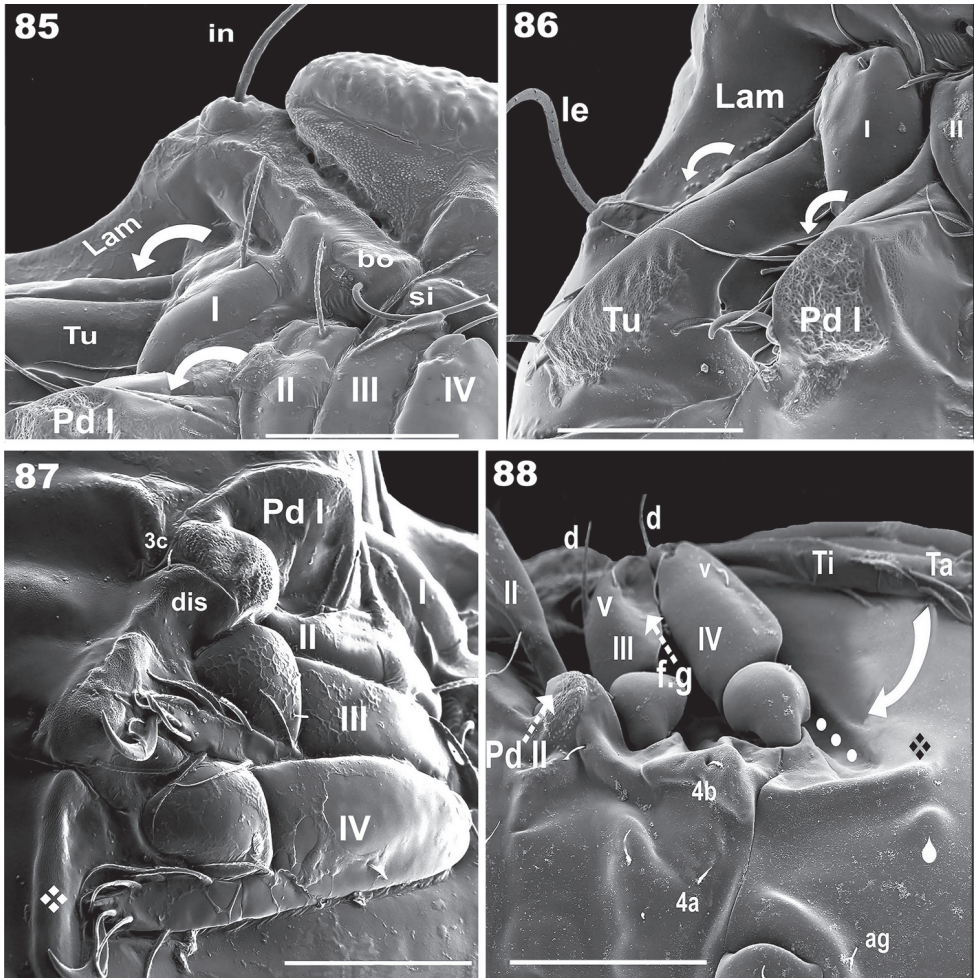


Figure 77–81. Schematic figures of leg-folding process based and SEM observations of *Nippobodes panemorfis* sp. n. **77** phase I **78** phase II **79** phase III **81** final phase **80** complementary explanation for insertion of tarsus and tibia IV into longitudinal depression. Scale bars: 390 μ m (**77–81**); 300 μ m (**80**).



Figures 82–84. Complementary figures of leg-folding process. SEM observations of *Nippobodes panemorfis* sp. n. **82.** position close to the final stage of the leg-folding process **83** moment when the femur II approaches the back of the femur III **84** femur III and IV, femur III moving towards femoral groove. Scale bars: 200 μm (**82**); 100 μm (**83**, **84**).



Figures 85–88. Complementary figures of leg-folding process. SEM observations of *Nippobodes panemorfs* sp. n. **85** lateral posterior–anterior view, final position of legs I and II **86** final position legs I and II **87** posterior–anterior view, final position of tarsus III and IV **88** legs III, IV and cuticular structures involved in leg folding, legs III and IV lateral view. Scale bars: 100 μm (**85**, **87**, **88**); 150 μm (**86**).

and narrow, facilitating positioning either in a pocket-shaped structure delimited by the tutorium (See below), or behind pedotectum I, femur III, and IV (Figures 77–88). Particular characteristics present in superior part of femur I, allows for partial concealment under the lateral prodorsal zone, in front of the bothridial zone (Figure 82). Femur II presents a slightly curved, smooth posterior surface (Figure 83), coapting with the posterior area of femur III. These structures and surfaces of femurs III and IV permit perfect coaptation, to allow tibia and tarsus to slip in behind and be concealed by them (Figures 82, 87).

Leg III plays a vital role. The femoral groove on femur III is a rather deep, triangular to ovoid groove, with a small seta near the depression. The groove and seta permit an-

Table 3. Comparison of *N. panemorfis* sp. n. and *N. flagellifer* Chen & Wang, 2007.

	<i>Nippobodes panemorfis</i> sp. n.	<i>Nippobodes flagellifer</i> Chen & Wang, 2007
Rostrum	rounded, conspicuous parallel groove to margin; large hump in front of groove.	rostrum protruding dorsally
<i>p.p.d.</i>	deep, rounded-ovoid	polyhedral
Interlocking double hook	<i>h.ap</i> situated externally, grips on to <i>p.pr.co</i> on the interior	large rectangular <i>h.ap</i> interlocking with posterior part of <i>p.pr.co</i> , triangular to polyedral in shape (Fig. 18 Chen and Wang 2007)
<i>Tu</i>	strong, large lamina, anterior zone ending in sharp angle, with interior part welded to prodorsal wall	well developed, large lamina, blunt tip (Fig. 20 Chen and Wang 2007)
<i>n.a.d</i>	deep, rounded-ovoid	polyhedral
<i>c</i> setae	looped, dentate, sharply tipped	proximal half directing anteromedially, distal half curving posterolaterally
<i>h_y p₃</i>	inserted on conspicuous promontories; v-shaped incision behind setal insertion	Neither promontories nor incision observed (Chen and Wang 2007: Fig.18)
<i>s.c</i>	completely surrounding notogaster; originating slightly in front of <i>la</i> setae, running between <i>la</i> , <i>h_p</i> , <i>h₂</i> , and <i>h₃ p₃ p₂ p₁</i>	starts behind <i>h₃</i> insertion, running between <i>h₁</i> , <i>h₂</i> and <i>p₁</i> , <i>p₂</i> , <i>p₃</i> (Chen and Wang 2007: Fig.18)

choring of femur IV into the groove. Femora III and IV each presents a ventral carina, permitting the tibia and tarsus to be concealed under them (Figures 75, 76, 82, 84).

The tiny genu plays a fundamental role as hinge, and generally presents a reduced number of setae (Figures 48–53; 73–76). The particular shape of the anterior zone of the femur improves the genu-hinge function and assists in the tibia-tarsus in the required position.

Related structures

Tutorium

The tutorium plays a very particular role, forming a pocket-shaped structure with the lateral prodorsal zone, permitting concealment of tibia-tarsus I. The pocket shaped structure ends in a sharp point, which protects the leg, and houses the claw (Figures 56, 57). Pedotectum I conceals the tibia and tarsus of leg II.

Lateral zone of body

The lateral area of body is adapted to receive the legs, with depressions and smooth areas to facilitate their positioning, along with tutorium, pedotectum I, and between legs II, III, and IV.

The “locking structure”

Ventrally, behind leg IV, a locking structure is observed. It consists of a longitudinal furrow (on Figures 42, 62, 80, 88, trajectory indicated by ●), ending in a bean-shaped structure (on Figures 42, 80, 87, 88 indicated by ❖), with a lateral promontory (Figures 42, 88, in-

licated by ♣). Tibia-tarsus IV is inserted into the longitudinal furrow (Figure 80) and the claw positioned in the depression of the bean-shaped structure (Figures 80, 87, 88). The femur resembles a lid closing a box, preventing the tibia-tarsus from moving and anchoring the entire leg in one position (Figure 81, 82, 88).

The process

Phase 1 (Figure 77): Initial position prior to leg folding, arrows indicating the directions in which legs will move.

Phase 2 (Figure 78): Leg I: femur moves backwards and approaches bothridial zone; this movement is facilitated by the genu functioning as a hinge. By rotating, it permits the tibia and tarsus to approach the margin of tutorium. Then, the tibia and tarsus are positioned ready to initiate installation into the tutorium pocket. Leg II: the femur moves upward and backward, approaching the posterior zone of femur III; the tibia and tarsus approach the margin of pedotectum I and move downwards, to conceal those two segments behind pedotectum I. Leg III: rotates towards the posterior and femur III moves closer to femur II. The tibia and tarsus slide in under ventral trochanteric-femoral carinas for concealment. Leg IV: the femur is directed backwards in order to locate the femoral groove and settle into it. The tibia and tarsus move back to settle into the longitudinal depression indicated by ● (Figure 80).

Phase 3 (Figure 79): Leg I. Femur I approaches the final position on the bothridial zone; the tarsus and tibia are almost completely concealed behind the tutorium and embedded in the pocket tutorial depression. Leg II. Femur is coapted to the posterior zone of femur III. The tibia and tarsus are almost completely hidden behind pedotectum I. Legs III and IV are very close to each other; femur IV is almost entirely within the femoral groove of femur III. Tibia and tarsus IV are installed in the longitudinal depression of the locking structure and tibia and tarsus III slide in and are concealed under femoral and trochanteral carinae; the claw is visible between trochanters III and IV.

Phase 4, the final position (Figure 81). Leg I: apical dorsal area of femur positioned under the anterior part of bothridium (indicated by ◀). The genu rotates inwards and its dorsal part, as well as the tibia and the tarsus are concealed deep in the tutorial pocket depression. Leg II. The genu turns inwards to position the tibia and tarsus in the optimal position; the tibia is slightly curved. With slight rotation of the genu, the tibia is similar in shape to pedotectum I; the tibio-tarsus articulation gives important rigidity. The tibia and tarsus descend and are perfectly concealed behind pedotectum I. Leg III. The posterior zone of femur II glides underneath the anterior part of femur III. Tibia and tarsus III slide in under the carina of trochanter–femur III for concealment, and the tarsal claw is visible between trochanters III and IV. Leg IV: the posterior part of femur IV is placed inside the femoral groove of femur III. Femur IV is inclined upwards to enable the tibia and tarsus to glide in underneath the femur, and tibia and

tarsus IV are placed into the longitudinal furrow of the locking structure. To conclude the mechanism, femur IV acts as a lid, blocking this segment and concealing the leg segments in the longitudinal depression, with the claw placed in a horizontal position resting on the bean-shaped structure of the locking structure (Figure 80).

During the final stages of the coaptation process, the relationship between the legs and body depressions can be described as follows: tibia and tarsus IV are located in the longitudinal furrow (of the locking structure), concealed by the femur; the posterior part of femur IV anchors in the groove of femur III; the apical distal expansion of femora III and IV partially conceal the genu; apical zone of tarsus III is situated between trochanter III and trochanter IV (Figures 79, 81). The *f.g* allows the posterior part of femur IV to fold into femur III.

Supplementary SEM images

In Figure 82 the final position has almost been reached, with an indication of structures involved, and arrows indicating the final movement to conclude the process. Figure 83 indicates the step where femur II is directed to the anterior part of femur III. The surfaces of the femurs about to come into contact can clearly be seen to fit together perfectly, and other structures such as the setae are located in such a way that they do not impede this process. On the posterior zone of Femur III, the femoral groove shows the seta *v*, which will assist in anchoring femur IV inside the depression. Figure 84 shows the displacement of femur IV towards the femoral groove (femur III). The carina of the trochanter and femur is clearly visible, which will permit the tarsus and tibia of leg III and leg IV to be partially concealed. Figure 85 posterior view, indicates the final position of legs I, II. The arrows indicate the position of tibia and tarsus I and II, concealed behind the pedotectum I and tutorium. Figure 86 Shows the lateral view of final position of legs I and II. Figure 87, posterior view. Tarsus III and tarsus IV are clearly visible, as well as the claw of tarsus IV and the bean-shaped structure of the locking structure supporting claw IV. Figure 88 shows the set of fundamental elements of legs III and IV, as well as cuticular surfaces necessary for the leg-folding process.

Similarities and differences in leg folding between Carabodidae and Nippobodidae

The system is very similar in the two families, and importantly, the following are common to both: all legs are involved in the process; the presence of the femoral groove on femur III; a tiny genu, which plays the role of a hinge; the involvement of pedotectum I and tutorium to conceal legs I and II.

Differences: 1) In Nippobodidae leg I is concealed in a pocket structure formed by the attachment of the tutorium to the lateral wall of the prodorsum. This connection to the prodorsal body wall resulting in the formation of the pocket structure is very different to Carabodidae (see Fernandez et al. 2013a). 2) The complexity of the locking structure in Nippobodidae, specifically the longitudinal depression where tibia and tarsus IV are inserted, femur IV which functions as a lid, and the bean-shaped structure where the claw rests, are dissimilar to what is observed in Carabodidae.

Acknowledgements

This work is based on research supported in part by the National Research Foundation of South Africa (UID) 85288. Any opinion, findings, and conclusions or recommendations expressed in the manuscript are those of the authors and therefore the NRF does not accept any liability in regard thereto.

References

- Alberti G, Fernandez N (1990a) Aspects concerning the structure and function of the lenticulus and clear spot of certain oribatids (Acari: Oribatida). *Acarologia* 31: 65–72.
- Alberti G, Fernandez N (1990b) Fine structure and function of the lenticulus and clear spot of Oribatids (Acari: Oribatida). In: Andre HM, Lions J-CI (Eds) *L'ontogénese et le concept de stase chez les arthropodes*. Agar, Wavere, 343–354.
- Alberti G, Fernandez N, Coineau Y (2007) Fine structure of spermiogenesis, spermatozoa and spermatophore of *Saxidromus delamarei* (Saxidromidae, Actinotrichida, Acari). *Arthropod Structure Development* 36: 221–231. <https://doi.org/10.1016/j.asd.2006.11.002>
- Alberti G, Fernandez N, Kummel G (1991) Spermatophores and spermatozoa of oribatid mites (Acari: Oribatida). Part II. Functional and systematical considerations. *Acarologia* 32: 435–449.
- Alberti G, Norton R, Adis J, Fernandez N, Franklin E, Kratzmann M, Moreno A, Ribeiro E, Weigmann G, Woas S (1997) Porose integumental organs of oribatid mites (Acari: Oribatida). *Zoologica* 48: 33–114.
- Aoki J (1959) Die Moosmilben (Oribatei) aus SüdJapan. *Bulletin of the Biogeographical Society of Japan* 21(1):1–22.
- Aoki J (1961) Notes on the oribatid mites (I). *Bulletin of the Biogeographical Society of Japan* 22(6):75–79.
- Aoki J (1965a) Oribatiden (Acarina) Thailand. I. Nature and life in Southeast Asia 4: 129–193.
- Aoki J (1965b) Oribatid mites (Acarina: Oribatei) from Himalaya with descriptions of several new species. *Journal of the College of Arts and Sciences, Chiba University* 4(3): 289–302.
- Aoki J (1970) The oribatid mites of the Islands of Tsushima. *Bulletin of the National Science Museum* 13(3): 395–442.
- Aoki J (1981) Discovery of the second species of the genus *Nippobodes* from Ohsumi Islands (Acari: Oribatei). *Bulletin of the Biogeographical Society of Japan* 36(4): 29–33.
- Aoki J (1984) New and unrecorded oribatid mites from Amami-Oshima Island, Southwest Japan. *Zoological Science* 1(1): 132–147.
- Aoki J (1989) A revision of the family Nippobodidae (Acari: Oribatida). *Acta Arachnologica* 38 (1): 15–20. <https://doi.org/10.2476/asjaa.38.15>
- Aoki J (2000) Two new species of the family Nippobodidae (Acari: Oribatida) from Yunnan, Southwest China, with a key to the species. In: Aoki J, Yin WY, Imadaté G (Eds) *Taxonomical Studies on the Soil Fauna of Yunnan Province in Southwest China*. Tokai University Press, Tokyo, 1–6.

- Chen J, Wang H (2007) Taxonomic study on the family Nippobodidae (Acari: Oribatida) from China. *Zootaxa* 1464: 45–63.
- Choi S (1996) Study of soil microarthropods Mt.Hanla in Cheju-do 1. Four new species of oribatid mites at Sangumburi. *Korean Journal Applied Entomology* 35(4): 280–286.
- Fernandez NA, Alberti G, Kummel G (1991) Spermatophores and spermatozoa of some Oribatid mites (Acari: Oribatida) Part I. Fine structure and histochemistry. *Acarologia* 32: 261–286.
- Fernandez N, Theron P, Rollard C (2013a) The family Carabodidae (Acari: Oribatida) I. Description of a new genus, *Bovicarabodes* with three new species, and the redescription of *Hardybodes mirabilis* Balogh, 1970. *International Journal of Acarology* 39(1): 26–57. <http://dx.doi.org/10.1080/01647954.2012.741144>
- Fernandez N, Theron P, Rollard C (2013b) Revision of the family Carabodidae (Acari: Oribatida) IV. *Aftibodes anjavidilavai* n.gen., n.sp., *Rugocephus joffrevillei* sp.n, and redescription of the genus *Rugocephus* Mahunka, 2009. *International Journal of Acarology* 39(6): 462–480. <https://doi.org/10.1080/01647954.2013.822928>
- Fernandez N, Theron P, Rollard C (2013c) The family Carabodidae (Acari: Oribatida) V. The genus *Congocephus* (second part), with a redescription of *Congocephus involutus* Mahunka 1997, and descriptions of *Congocephus gabonensis* and *Congocephus extactastesi* sp. nov. *Zoosystema* 35(4): 551–579. <https://doi.org/10.5252/z2013n4a8>
- Fernandez N, Theron P, Leiva S (2016) Revision of the family Carabodidae (Acari: Oribatida) XI. *Congocephus kardiae* sp. nov. and *Zimbabweae plusioiae* gen. nov., sp. nov. from the Republic of Zimbabwe. *International Journal of Acarology* 42(7): 341–357. <http://dx.doi.org/10.1080/01647954.2016.1199138>
- Grandjean F (1949) Formules anales, gastronomiques, génitales, aggénitales du développement numérique des poils chez les Oribates. *Bulletin Société Zoologique France* 74: 201–225.
- Krantz G, Walter D (2009) A manual of acarology. Third edition. Texas Tech University Press, Lubbock, Texas, 807 pp.
- Norton R, Behan-Pelletier V (2009) Suborder Oribatida. In: Krantz GW, Walter DE (Eds) A manual of acarology. Third edition. Texas Tech University Press, Lubbock, Texas, 430–564.
- Jeleva M, Vŭ M (1987) New Oribatids (Oribatei, Acari), from the Northern Part of Vietnam. *Acta Zoologica Bulgarica* 33: 10–18.
- Travé J, Vachon M (1975) François Grandjean 1882–1975 (Notice biographique et bibliographique). *Acarologia* 17(1): 1–19.

Five new species of *Drosophila guarani* group from the Andes of southern Ecuador (Diptera, Drosophilidae)

Ana Danitza Peñafiel-Vinueza¹, Violeta Rafael¹

¹ *Laboratorio de Genética Evolutiva, Facultad de Ciencias Exactas y Naturales, Pontificia Universidad Católica del Ecuador, Av. 12 de Octubre y Roca, Aptdo. 17-01-2184, Quito, Ecuador*

Corresponding author: Ana Danitza Peñafiel-Vinueza (adpenafiel@puce.edu.ec)

Academic editor: O. Lonsdale | Received 8 December 2017 | Accepted 12 July 2018 | Published 15 August 2018

<http://zoobank.org/88AFA04F-CA5B-464E-82E4-9A1DA6F50C41>

Citation: Peñafiel-Vinueza AD, Rafael V (2018) Five new species of *Drosophila guarani* group from the Andes of southern Ecuador (Diptera, Drosophilidae). ZooKeys 781: 141–163. <https://doi.org/10.3897/zookeys.781.22841>

Abstract

Five species of the genus *Drosophila* are described and illustrated: *D. zamorana* **sp. n.**, *D. quinarensis* **sp. n.**, *D. sachapuyu* **sp. n.**, *D. casarumi* **sp. n.**, and *D. misi* **sp. n.** from the cloud forests of the Podocarpus National Park, in the southern Ecuadorian Andes. Flies were captured using plastic bottles containing pieces of fermented banana with yeast. All the species were found to belong to the *Drosophila guarani* species-group.

Keywords

Drosophila, *guarani* group, new species, southern Ecuador, terminalia

Introduction

The *guarani* group of *Drosophila* was proposed by Dobzhansky & Pavan (1943) and included 12 species until 1993: *D. alexandrei* Cordeiro, 1951; *D. araucana* Brncic, 1957; *D. griseolineata* Duda, 1927; *D. guaraja* King, 1947; *D. guaru* Dobzhansky & Pavan, 1943; *D. huilliche* Brncic, 1957; *D. limbinervis* Duda, 1925; *D. maculifrons* Duda, 1927; *D. ornatifrons* Duda, 1927; *D. peruensis* Wheeler, 1959; *D. subbadia* Patterson & Mainland, 1943, and *D. tucumana* Vilela & Pereira, 1985 (Vilela and Pereira 1993). There was a misidentification of *D. peruensis* which would have been the thirteen

member of the *guarani* group, *Drosophila urubamba* (Vilela & Pereira, 1993). Ratcov and Vilela 2007 proposed transferring *D. peruensis* from the *guarani* group to a new one named *peruensis*. Vela and Rafael (2004) described three new species from the Pasochoa forest in Pichincha, Ecuador: *Drosophila ecuatoriana*, *D. pichinchana*, and *D. quitensis*. Later Vela and Rafael (2005) described *D. cuscungu*, which also became part of the *guarani* group. In a recent study Ratcov et al. (2017) described *D. butantan* and assigned *D. nigrifemur* Duda, 1927 to this group. An anthophilic species *D. peixotoi* was found breeding in the inflorescences of *Goepfertia monophylla* by Vaz et al. (2018). This group is restricted to Central and South America (Kastritsis 1969).

Studies of the polytene chromosomes of some species of the *guarani* group (Kastritsis 1969) split of the *guarani* group into two subgroups, the *guarani* Dobzhansky & Pavan, 1943 subgroup with *D. ornatifrons*, *D. subbadia*, *D. guaru*, and the *guaramunu* King, 1947 subgroup with *D. maculifrons*, *D. griseolineata*, and *D. guaraja*. The *guarani* species group is probably not monophyletic which would invalidate this traditional subgroup division (Robe et al. 2002).

Most of these species are of medium size, have a brown coloration, but differ in shade and intensity. They have two prominent oral bristles of approximately equal length, pollinose mesonota and pleurae, and divergent anterior scutellar bristles. All species have strongly clouded cross veins in the wings except *D. guaraja* that has slightly clouded cross veins (King 1947a).

Our recent collections in southern Ecuador discovered five new species of *Drosophila* from the *guarani* group, which are described below: *Drosophila zamorana* sp. n., *Drosophila quinarensis* sp. n., *Drosophila caxarumi* sp. n., *Drosophila sachapuyu* sp. n. and *Drosophila misi* sp. n. We discuss the similarities between these new species and the others in the *guarani* group.

Materials and methods

The flies were collected in Loja and Zamora Chinchipe Provinces of Ecuador, in the cloud forests of the Podocarpus National Park and the surrounding areas. Collections were made at three localities, San Francisco Scientific Station at 2190m (3°59'16.7"S; 79°5'35"W) and Cajanuma 1 at 2675m (4°6'53.7"S; 79°10'54.6"W) and Cajanuma 2 at 2800m (4°6'58.9"S; 79°10'11.9"W). Fifteen fermented banana traps were placed in each location ten meters apart from each other and one meter above the base of the trees. Traps were made using recycled 500 ml plastic bottles and baited with banana pieces fermented with yeast 24 hours before placement.

Living flies were captured with an entomological aspirator and transferred to vials with gelatin-banana media (Rafael et al. 2000). Females were individually isolated to produce isofemale lines. Adult specimens were preserved in microcentrifuge tubes with ethanol (70–80%) and glycerin (100%) solution (Márquez Luna 2005). The fermented banana baits were put inside glass jars sealed with cotton plugs for transport to the laboratory where the baits were retained until the emergence of adults.

External morphology of each fly was examined under a stereomicroscope (Zeiss; Discovery V8). Male and female terminalia were dissected and placed in KOH (10%) and boiled for ten minutes; they were then placed in 60% glycerin for females and 100% glycerin for males. Terminalia were compared with literature descriptions to determine the new species. The new species were illustrated using a microscope (Zeiss-46 70 86) with a camera lucida (Zeiss-47 46 20 9900). Structure measurements were made using the software AXIO VISION V4. Descriptive terms and indices follow the system of Bächli et al. (2004).

The holotypes and paratypes of the new species have been deposited in the Museo de Zoología – Invertebrados, Pontificia Universidad Católica del Ecuador, Quito (QCAZ-I).

Taxonomy

Drosophila zamorana sp. n.

<http://zoobank.org/BFFCB2CF-365E-42D0-80CD-F4D98E26A595>

Figs 1A–D, 2A–F, 3A–C

Type material. Holotype. ♂ (dissected, terminalia in microvial), Ecuador, Zamora Chinchipe, San Francisco, 2190 m, 3°59'16.7"S; 79°5'35"W, IV.2015, Apr. 2015, A. Peñafiel col., A. Peñafiel & V. Rafael det. (QCAZ-I 3266). Allotype ♀ (dissected, terminalia in microvial), Ecuador, Zamora Chinchipe, San Francisco, 2190 m, 3°59'16.7"S; 79°5'35"W, Apr.2015, A. Peñafiel col., A. Peñafiel & V. Rafael det. (QCAZ-I 3267).

Paratypes. 9 ♂♂ and 9 ♀♀ (dissected, terminalia in microvial, descendants of isofemale line), Ecuador, Zamora Chinchipe, San Francisco, 2190 m, same data as holotype, A. Peñafiel col., A. Peñafiel & V. Rafael det. (QCAZ-I 3268-3285).

Diagnosis. Aristae generally with five dorsal and three ventral branches, plus terminal fork. Two prominent equally long oral bristles. Thorax brown, with bristles arising from dark brown spots, scutellum brown with some irregular light spots. Wings beige, veins bM-Cu and dM-Cu strongly clouded tips of R2 + 3, R4 + 5 radial and M veins darkened. Abdomen dark brown, 1st tergite beige, 2nd–4th tergites of males with dorsal midline and white butterfly-shaped areas, followed by a white rounded area at the edge of each tergite; 5th and 6th tergites dark brown. Cerci not fused to epandrium. Hypandrium shield-shaped. Gonopod elongated, bearing one long bristle. Aedeagus voluminous with two ventral sheets covered in spines, dorsally with two membranous sheets covered with tiny spines studs. Paraphyses triangular, bearing two small bristles.

Description. Male. Holotype external morphology: total length (body + wings) 3.08 mm, body length 2.50 mm. Body color dark brown (Figure 1A).

Head. Aristae with five dorsal and three ventral branches, plus terminal fork. Frons dark brown, frontal length 0.20 mm; frontal index = 0.73; top to bottom width ratio = 1.44. Medial vertical seta was closer to lateral vertical seta and slightly towards the

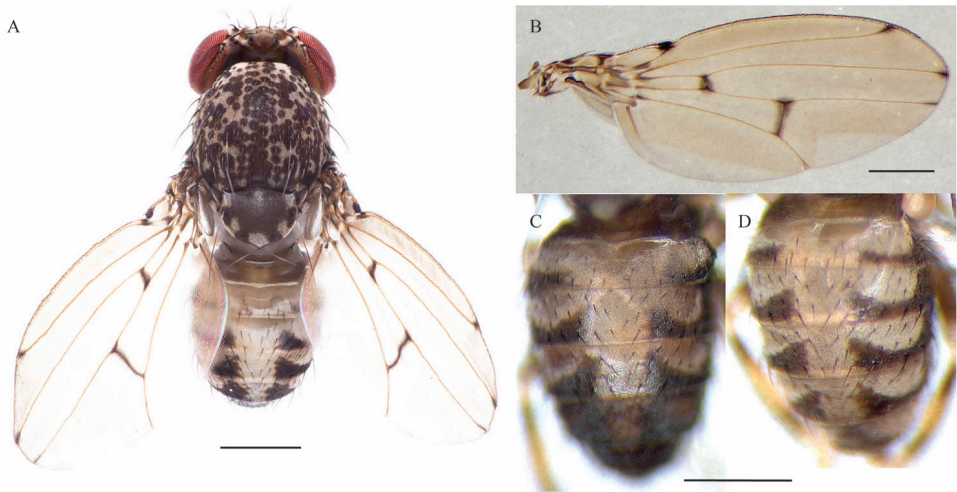


Figure 1. *Drosophila zamorana* sp. n., male holotype and female allotype external morphology. **A** Adult male, dorsal view **B** Male wing pigmentation **C, D** Abdomen, dorsal view, male and female respectively. Scale bars: 0.5 mm.

outer edge of the orbital plate; distance of or3 to or1 = 0.08, distance of or3 to vtm = 0.09; or1-or3 ratio = 1.7, or2-or1 ratio = 0.23, distance of ocellar setae = 1 of frontal length, distance of postocellar setae = 0.64 of frontal length. vt index = 0.66. Ocellar triangle dark brown, 48% of frontal length, ocellus yellow; frontal triangle brown. Frontal vitta yellowish brown. Gena and postgena dark brown. Carina not sulcate. Cheek index = 7.5. Eyes wine red; eye index = 1.4. Two prominent equally long oral bristles; vibrissa index = 1.1.

Thorax. Brown, with bristles arising from dark brown spots, thorax length 0.80 mm, acrostichal hairs in six rows between the two anterior dorsocentral setae, h index = 0.81. Transverse distance of dorsocentral setae = 2.28, dc index = 0.87. Scutellum brown with some irregular white spots (Figure 1A), distance between apical scutellar seta = 1, scut index = 1.13; medial katepisternal seta one third of the previous, sterno index = 2.16. Legs light brown, coxae and femora dark brown, tibiae with two brown rings. **Wings** beige, alar length 2.10 mm, width 0.90 mm, veins bM-Cu and dM-Cu strongly clouded tips of R2+3, R4+5 radial and M veins darkened. First costal section apex black (Figure 1B). Indices: alar = 2.25; C = 3.61; ac = 2.29; hb = 0.53; 4c = 0.86; 4v = 2.08; 5x = 1.65; M = 0.73 and prox. x = 0.77.

Abdomen. Dark brown, 1st tergite beige, 2nd – 5th tergites of males with dorsal mid-line and white butterfly-shaped areas with posterior dark pigmentation which reaches the exterior margin, leaving a white rounded laterally area; 6th tergite dark brown (Figure 1C).

Male terminalia. Epandrium dorsally microtrichose with two lower and no upper bristles, four bristles on the ventral lobe. Cerci sclerotized and not fused to epandrium, with some microtrichose areas in the middle (Figure 2A). Surstylus triangular with a

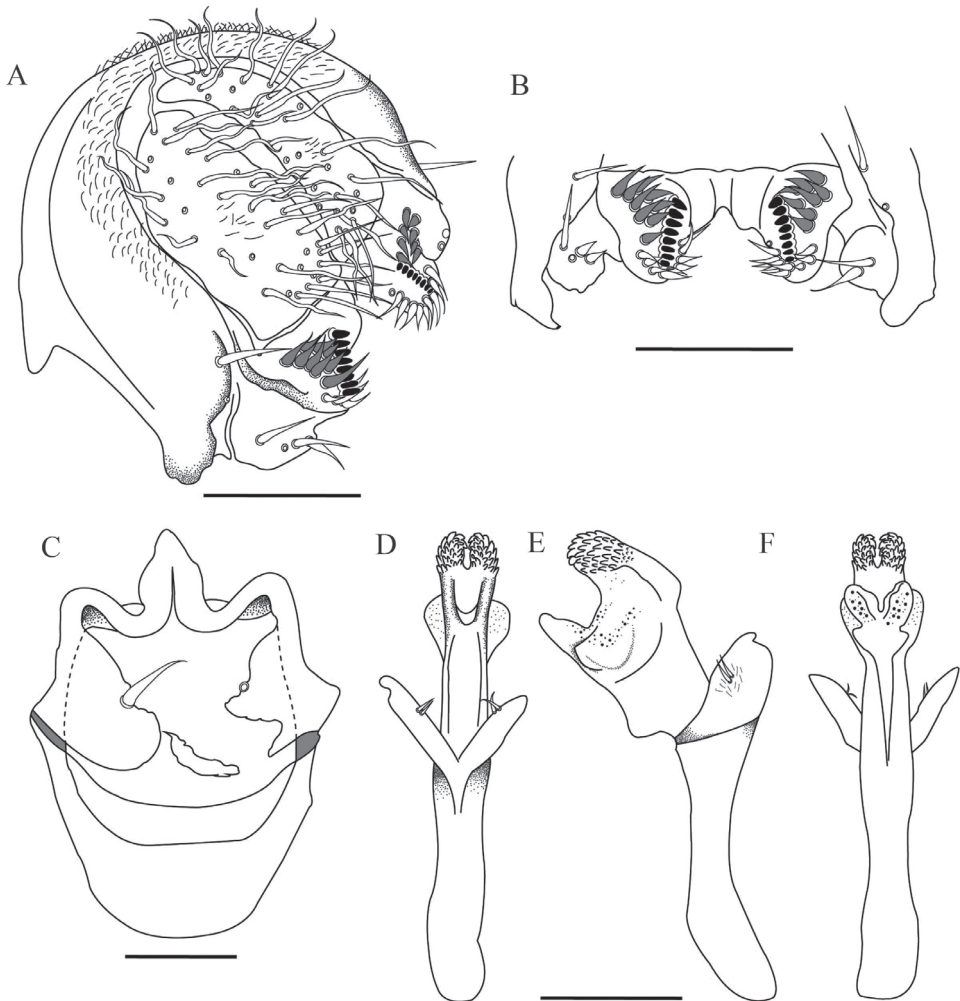


Figure 2. *Drosophila zamorana* sp. n., male terminalia of holotype. **A** Epandrium, cerci, surstylus **B** Decasternum **C** Hypandrium and gonopods in ventral view **D, E, F** Aedeagus and paraphyses in ventral, lateral and dorsal view, respectively. Scale bars: 100 μ m.

row of eight primary teeth, nine secondary pointed teeth on the right and eight on the left; nine marginal bristles on the right and ten on the left (Figure 2B). Hypandrium sclerotized in shield-shape. Gonopod elongated bearing one long bristle (Figure 2C).

Aedeagus. Sclerotized, voluminous with two ventral sheets covered in short spines, dorsally with two membranous sheets covered with tiny spines. Paraphyses triangular and slightly microtrichose, bearing two small bristles (Figure 2D-F).

Variation in paratypes (dry mounted specimens). Total length (body + wings) 2.95–3.12 mm, body length 2.35–2.6 mm. Head. Frontal length 0.24–0.34 mm, frontal index = 0.73–1.12, top to bottom width ratio = 1.5–2.04; distance of or3 to or1 = 0.07–0.1, dis-

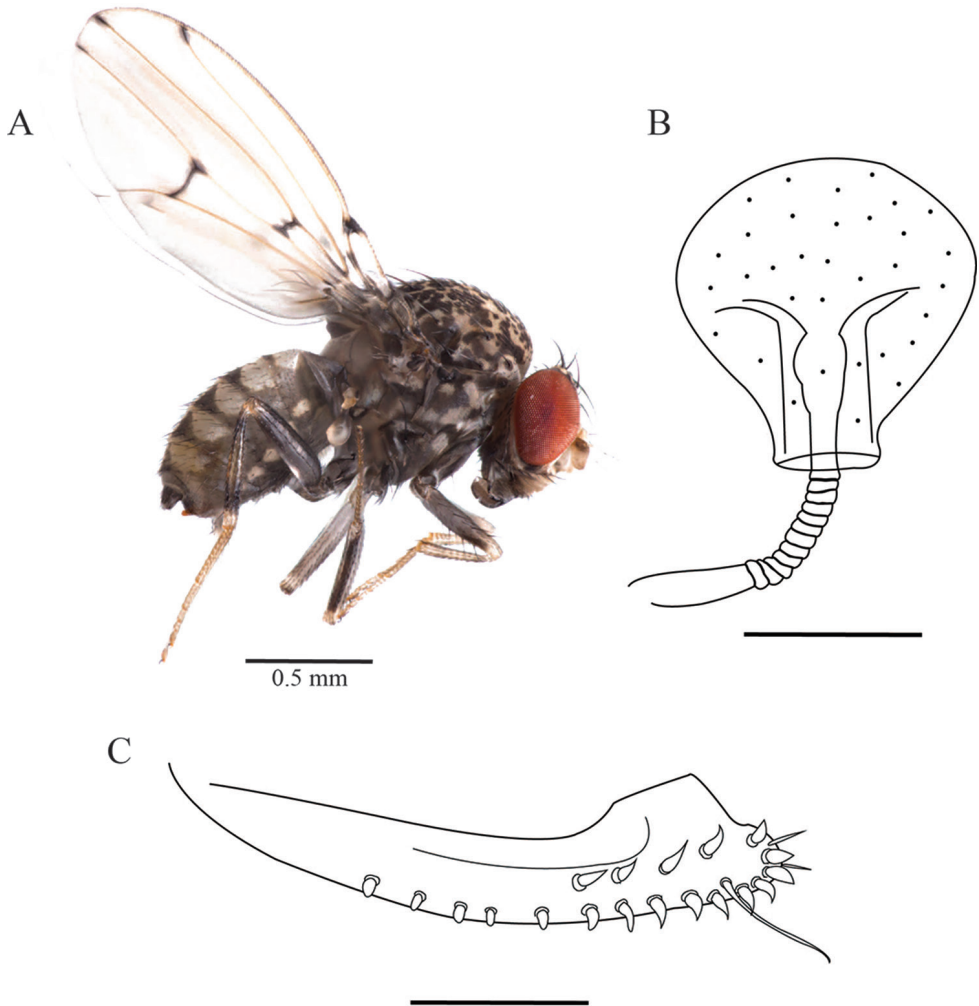


Figure 3. *Drosophila zamorana* sp. n., female external morphology and terminalia of allotype. **A** Adult female, lateral view **B** Spermatheca **C** Ovipositor. Terminalia scale bars: 100 μ m.

tance of or3 to vtm = 0.9–0.11, or1-or3 ratio = 0.52–0.94, or2-or1 ratio = 0.18–0.42, distance of ocellar setae = 0.5–1.04 of frontal length, distance of postocellar setae = 0.46–0.7 of frontal length, vt index = 0.96–1.21; cheek index = 7.0–9.8; vibrissa index = 0.92–1.12; eye index = 1.15–1.68. Thorax. Length 0.64–0.77 mm, h index = 0.85–1.04. Transverse distance of dorsocentral setae = 1.68–2.46, dc index = 0.69–0.70. Distance between apical scutellar seta = 0.94–1.05. scut index = 0.87–1.13; sterno index = 0.94–2.87.

Female. Allotype and paratypes (isofemale descendants). Allotype: total length (body + wings) 3.24 mm, body length 2.43 mm. Body color dark brown (Figure 3A).

External morphology. Same as the male except abdomen. Abdomen 1st tergite beige, 2nd – 6th tergites with dorsal midline and white butterfly-shaped areas with posterior

dark pigmentation which reaches the exterior margin, leaving a white rounded lateral area (Figure 1D). Wings beige, alar length 2.54 mm, width 1.07 mm, veins bM-Cu and dM-Cu strongly clouded tips of R2+3, R4+5 radial and M veins darkened. First costal section apex black. Indices: alar = 2.37; C = 4.04; ac = 2; hb = 0.42; 4c = 0.73; 4v = 1.98; 5x = 1.88; M = 0.56 and prox. x = 0.82.

Terminalia. Spermatheca lightly pigmented, bulb-shaped, covered with tiny spines, duct partially invaginated (Figure 3B). Ovipositor elongated, sclerotized, with 13 marginal and six discal teeth, one long bristle, and two fine hairs (Figure 3C).

Variation in paratypes (dry mounted specimen). Head. Frontal length 0.23–0.27 mm, frontal index = 0.6–0.71, top to bottom width ratio = 1.31–1.36; distance of or3 to or1 = 0.07–0.09, distance of or3 to vtm = 0.09–0.12, or1-or3 ratio = 0.8–1.0, or2-or1 ratio = 0.22–0.57, distance of ocellar setae = 1.0–1.3 of frontal length, distance of postocellar setae = 0.60–0.68 of frontal length, vt index = 0.77–1.0; cheek index = 5.62–7.83; vibrissa index = 0.85–0.94; eye index = 1.20–1.27. Thorax length 0.81–0.89 mm, h index = 0.86–1.0. Transverse distance of dorsocentral setae = 2.17–3.0, dc index = 0.70–0.83. Distance between apical scutellar seta = 1. scut index = 1.08–1.25; sterno index = 0.92–0.95.

Etymology. Named in recognition of the collection site, Zamora Chinchipe province of Ecuador.

Distribution. Known only from the type locality.

Ecology. Unknown. The type specimen was found in the banana-bait traps placed at the locality, which suggests that this species feeds on fermented fruits as do many other *Drosophila* species. This species has been reared with gelatin banana media devised by Rafael et al. (2000). The habitat is a relatively well-preserved montane forest.

Relationship to other species. This species belongs to the *guarani* species-group. The most similar species are *Drosophila urubamba* Vilela & Pereira, 1993 and *Drosophila tucumana* Vilela & Pereira, 1985. *Drosophila zamorana* sp. n. is similar to *D. urubamba* but the most important difference is in the aedeagus. First, the distal end of the aedeagus in *D. zamorana* is narrower than in *D. urubamba*. Second, the form of the aedeagus in *D. urubamba* is bulkier than in *D. zamorana*. There is a little difference in the paraphyses; *D. zamorana* has some microtrichose areas surrounding the two small bristles that *D. urubamba* does not have. These differences distinguish these two species, mainly because of the cryptic external morphology.

***Drosophila quinarensis* sp. n.**

<http://zoobank.org/CAA65626-0E02-4464-A97B-187887EE1F08>

Figs 4A–F, 5A–B

Type material. Holotype ♂ (dissected, terminalia in microvial), Ecuador, Loja, Cajanuma, 2800 m, 4°6'58.9"S; 79°10'11.9"W, 19 Nov. 2015, A. Peñafiel col., A. Peñafiel & V. Rafael det. (QCAZ-I 3286). Allotype ♀ (dissected, terminalia in microvial), Ecuador, Loja, Cajanuma, 2800 m, 4°6'58.9"S; 79°10'11.9"W, 19 Nov. 2015, A. Peñafiel col., A. Peñafiel & V. Rafael det. (QCAZ-I 3287).

Paratypes. 6 ♂♂ and 1 ♀♀ (dissected, terminalia in microvial, descendants of isofemale line), Ecuador, Loja, Cajanuma, 2800 m, 4°6'58.9"S; 79°10'11.9"W, 19 Nov. 2015, A. Peñafiel col., A. Peñafiel & V. Rafael det. (QCAZ-I 3288–3293, 3297). 3 ♀♀ (dissected, terminalia in microvial, descendants of isofemale line), Ecuador, Loja, Cajanuma, 2675 m, 4°6'53.7"S; 79°10'54.6"W, 19 Nov. 2015, A. Peñafiel col., A. Peñafiel & V. Rafael det. (QCAZ-I 3298–3300).

Diagnosis. Aristae with four dorsal and two ventral branches. Two prominent oral bristles, the second slightly shorter than the first. Thorax brown. Abdomen yellow, 2nd – 5th tergites with dorsal midline, with posterior dark pigmentation which reaches and covers the exterior margin. Cerci not fused to epandrium. Aedeagus voluminous, with two ventral asymmetrical projections covered in short spines and two dorsal projections with tiny spines. Hypandrium is shield-shaped with a sclerotized edge. Gonopod bearing one bristle. Paraphyses strongly sclerotized and joined to gonopod, bearing two small bristles.

Description. Male. Holotype external morphology: total length (body + wings) 3.38 mm, body length 2.36 mm. Body color dark brown.

Head. Aristae with four dorsal and two ventral branches, plus terminal fork and fine hairs. Orbital plate yellowish brown, frontal length 0.29 mm; frontal index = 0.96; top to bottom width ratio = 1.7. Medial vertical seta was closer to lateral vertical seta and slightly towards the outer edge of the orbital plate, distance of or3 to or1 = 0.11, distance of or3 to vtm = 0.12, or1-or3 ratio = 1.30, or2-or1 ratio = 0.35, distance of postocellar setae = 0.68 of frontal length. vt index = 0.85. Ocellar triangle brown, 48.27% of frontal length, ocellus yellow, frontal vitta yellowish brown. Two prominent oral bristles, second slightly shorter than the first. Carina not sulcate.

Thorax. Brown, acrostichal hairs in six rows between the two anterior dorsocentral setae that decrease in number towards the rear. Medial katapisternal seta smaller than the previous seta. **Wings** yellow. Alar length 2.62 mm, alar width 1.29 mm. Vein dM-Cu clouded. Alar indices: alar = 1.07; C = 5.62; ac = 1.37; 4c = 0.43; 4v = 1.25; 5x = 1.20; M = 0.40 and prox. x = 0.37. Legs yellow, femora and tibiae dark brown, metatarsi and tarsi light brown.

Abdomen. Yellow, 1st tergite brown, 2nd – 5th tergites with dorsal midline and posterior dark pigmentation which reaches and covers the exterior margin, 6th tergite dark (Figure 4A).

Male terminalia. Epandrium strongly sclerotized, microtrichose, with seven lower and no upper bristles, four bristles on the ventral lobe. Cerci microtrichose not fused to epandrium. Surstylus oval with nine primary teeth on the right and ten on the left; sharp secondary teeth strongly sclerotized, in two groups, five upper and nine lower on the right, six upper and seven lower on the left; with eleven marginal bristles (Figure 4B). Hypandrium in shield-shape, with edge strongly sclerotized. Gonopod elongated bearing one bristle (Figure 4C).

Aedeagus. Aedeagus voluminous, with two ventral asymmetrical projections covered in short spines and two dorsal projections with bright tiny spines. Primitive ventral rod.

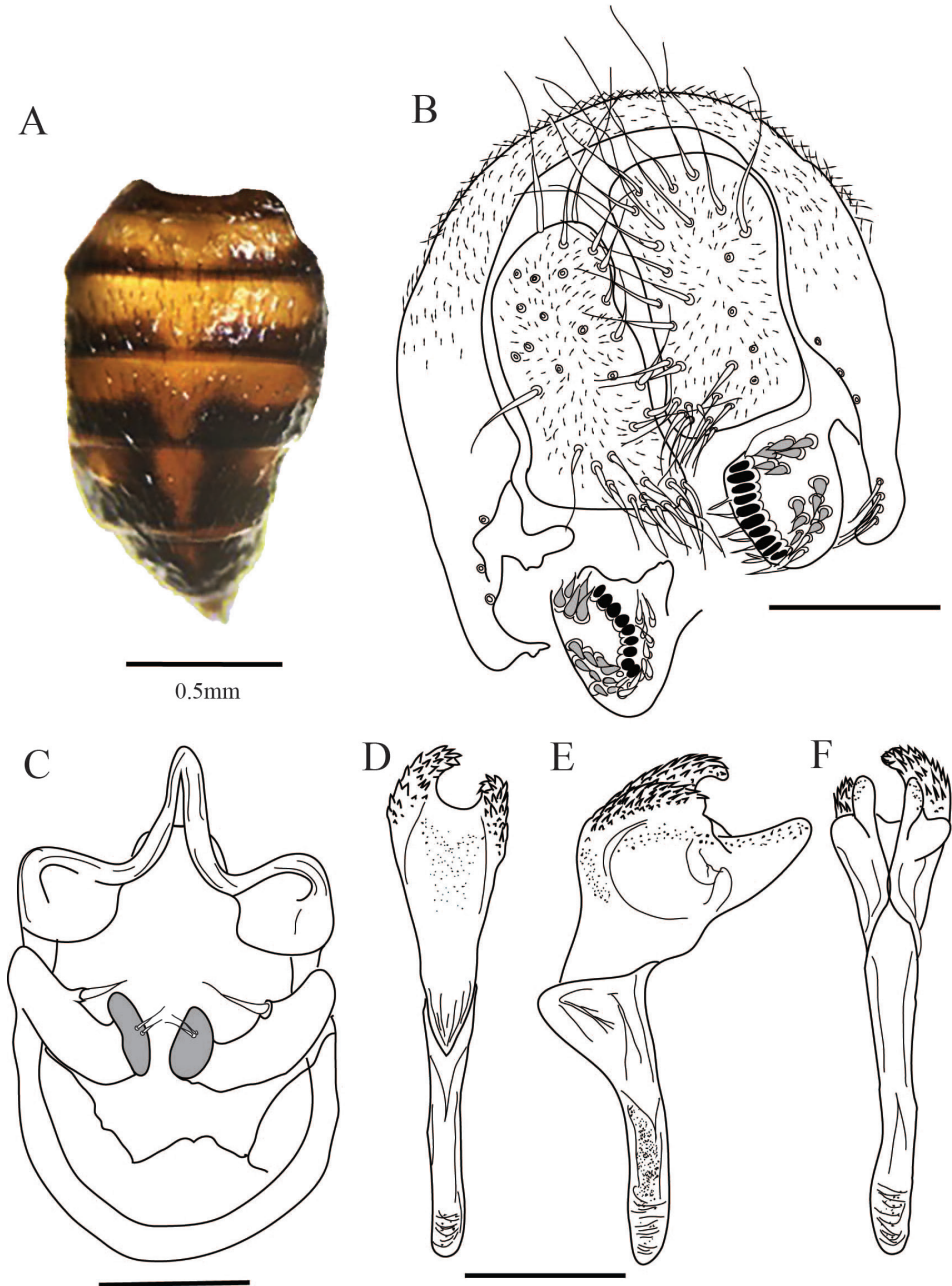


Figure 4. *Drosophila quinarensis* sp. n., abdomen and male terminalia of holotype. **A** Male abdomen, dorsal view **B** Epandrium, cerci, surstylus and decasternum **C** Hypandrium, gonopods and paraphyses, ventral view **D, E, F** Aedeagus in ventral, lateral and dorsal view, respectively. Terminalia scale bars: 100 μ m.

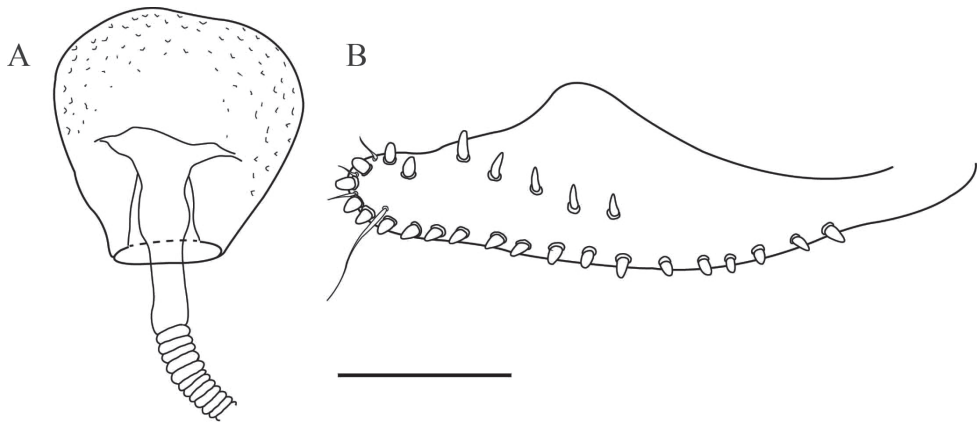


Figure 5. *Drosophila quinarensis* sp. n., female terminalia of allotype. **A** Spermatheca **B** Ovipositor. Scale bar: 100 μ m.

Aedeagal apodeme slightly sclerotized (Figure 4D–F). Paraphyses joined to gonopod strongly sclerotized bearing two small bristles (Figure 4C).

Variation in paratypes (dry mounted specimens). Total length (body + wings) 4.19–4.73 mm, body length 1.96–3.01 mm. Head. Frontal length 0.27–0.42 mm, frontal index = 0.66–0.85, top to bottom width ratio = 1.20–1.38; distance of or3 to or1 = 0.11–0.14, distance of or3 to vtm = 0.12–0.13, or1-or3 ratio = 0.85–1.05, or2-or1 ratio = 0.19–0.34, distance of ocellar setae = 0.69–1.03 of frontal length, distance of postocellar setae = 0.84–0.85 of frontal length, vt index = 0.87–1.12; cheek index = 6.77–8.42; vibrissa index = 0.86–1.05; eye index = 1.17–1.51. Thorax length 0.89–1.07 mm, h index = 0.84–1.21. Transverse distance of dorsocentral setae = 1.91–2.55, dc index = 0.84–0.87. Distance between apical scutellar seta = 0.95–1.09. scut index = 1.11–1.39; sterno index = 1–1.04.

Female. Allotype and paratypes (isofemale descendants). Allotype: total length (body + wings) 5.11 mm, body length 3.08 mm. Body color dark brown.

External morphology. Same as the male.

Wings yellow. Alar length 3.7 mm, alar width 1.65 mm. Vein dM-Cu clouded. Alar indices: alar = 2.24; C = 4.27; ac = 1.87; hb = 0.32; 4c = 0.56; 4v = 1.54; 5x = 1.22; M = 0.42 and prox. x = 0.39.

Like male except yellow abdomen, 1st tergite brown, 2nd – 6th tergites with dorsal midline and white butterfly-shaped areas with posterior dark pigmentation which reaches the exterior margin, leaving a white rounded lateral area.

Terminalia. Spermatheca lightly pigmented, bulb-shaped, with small indents, duct partway invaginated (Figure 4A). Ovipositor elongated, sclerotized, with 19 marginal and seven discal teeth, one long bristle, and three fine hairs (Figure 4B).

Variation in paratypes (dry mounted specimens). Total length (body + wings) 3.13–5.11 mm, body length 2.3–3.08 mm. Head. Frontal length 0.4 mm, frontal index = 0.81–0.85, top to bottom width ratio = 1.18–1.40; distance of or3 to or1 = 0.13–0.15, distance of or3 to vtm = 0.07–0.15, or1-or3 ratio = 0.54–0.62, or2-or1 ratio = 0.35–0.54, distance of ocellar setae = 0.85–0.87 of frontal length, distance of postocellar setae = 0.72–0.73 of

frontal length, vt index = 0.85–1.08; cheek index = 7.35–10.16; vibrissa index = 0.84–1.11; eye index = 1–1.27. Thorax. Length 1.05–1.08 mm, h index = 0.94–1.06. Transverse distance of dorsocentral setae = 1.77–2.18, dc index = 0.68–0.70. Distance between apical scutellar setae = 0.77–0.96. scut index = 0.96–1.33; sterno index = 0.92–1.24.

Etymology. Name refers to the Quinara district in Loja Province of Ecuador. In this district there is a legend that the treasure demanded by the Spaniards to release Arahualpa from captivity is still hidden among the old farms in the region.

Distribution. Known only from the type locality.

Ecology unknown. The type specimen was found in the banana-bait traps placed at the locality, which suggests that this species feeds on or breeds in fermented fruits as do many other *Drosophila* species. The habitat is a well-preserved montane forest.

Relationship to other species. The general shape of the male terminalia, especially the asymmetrical projections of the aedeagus, suggests a close relationship to *Drosophila quitensis* Vela & Rafael, 2004. The main difference is in the aedeagus. The eedeagus of *D. quinarensis* is more elongate than in *D. quitensis*.

***Drosophila caxarumi* sp. n.**

<http://zoobank.org/F1912DEF-831A-4BB0-86EA-992F73AE57C8>

Figs 6A–B, 7A–E, 8A–F

Type material. Holotype ♂ (dissected, terminalia in microvial), Ecuador, Loja, Cajanuma, 2675 m, 4°6'53.7"S; 79°10'54.6"W, 19 Nov. 2015, A. Peñafiel col., A. Peñafiel & V. Rafael det. (QCAZ-I 3306).

Paratypes. 2 ♂♂ (dissected, terminalia in microvial), Ecuador, Napo, Río Guango, 2548 m, 00°32'14.0"S; 77°57'13.4"W, 19 Sep. 2015, A. B. Manzano col., A. Peñafiel & V. Rafael det. (QCAZ-I 3307–3308).

Diagnosis. Body color yellow. Aristae with four dorsal and two ventral branches. Two prominent oral bristles. Thorax brown. Clear wings. Aedeagus with two dorsal membranes covered in microprojections which continue to a sclerotized triangular projection and another distally serrated sheet joined ventrally by a membrane. Hypandrium in shield-shape. Gonopod fused to paraphyses, bearing a long bristle and short bristle.

Description. Male. Holotype external morphology: total length (body + wings) 2.90 mm, body length 2.30 mm. Body color brown.

Head. Aristae with four dorsal and two ventral branches plus terminal fork and small hairs. Orbital plate yellowish brown; frontal length 0.25 mm, frontal index = 1.0; top to bottom width ratio = 1.68. Medial vertical seta closer to lateral vertical seta and slightly towards the outer edge of the orbital plate. Distance of or3 to or1 = 0.06, distance of or3 to vtm = 0.09, or1-or3 ratio = 0.59; or2-or1 ratio = 0.30. Ocellar triangle yellow, distance of postocellar setae = 0.52 of frontal length, ocellus yellow; frontal vitta yellow. Two prominent oral bristles, vibrissa index = 0.85. Cheek index = 3.33. Carina not sulcate. Eyes wine red, eye index = 1.30.

Thorax. Brown (Figure 6A), thorax length 0.66 mm. h index = 1.18. Transverse distance of dorsocentral setae = 1.53, dc index = 0.81. Distance between apical scutel-

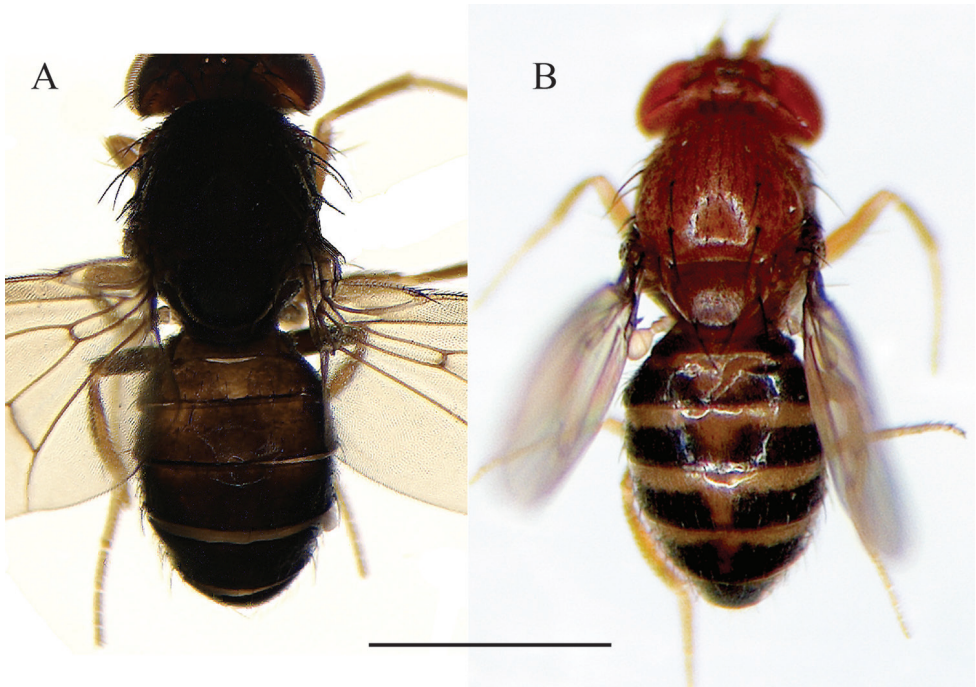


Figure 6. **A** *Drosophila caxarumi* sp. n., male holotype external morphology, dorsal view. **B** *Drosophila guaraja* King, from Zamora Chinchipe, Ecuador, male external morphology, dorsal view. Scale bar: 1 mm.

lar seta = 1.38, scut index = 0.93, sterno index could not be calculated (broken bristles in holotype). Clear wings. Alar length 1.65 mm, alar width 0.86 mm. Alar indices: alar index = 1.91; C = 3.37; ac = 1.94; hb = 0.25; 4c = 0.89; 4v = 2.25; 5x = 1.44; M = 0.66 and prox. x = 0.46.

Abdomen. Yellow, 1st – 6th tergites with dark brown pigmentation that covers entirely each tergite (Figure 6A).

Male terminalia. Epandrium microtrichose with four lower and no upper bristles, one bristle on the ventral lobe. Cerci not fused to epandrium, microtrichose, tip bearing four cotton swab-shaped bristles. Surstylus rectangular with seven primary teeth, six secondary sharp teeth on the right and five on the left, six marginal bristles (Figs 7A, 8A). Hypandrium in shield-shape and sclerotized. Gonopod elongated, fused to the paraphyses, bearing a long bristle and other short one (Figs 7B, 8B).

Aedeagus. Sclerotized, with two dorsal membranes covered in microprojections which continue to a sclerotized triangular projection and another distally serrated sheet joined ventrally by a slightly sclerotized membrane (Figs 7C–E, 8C).

Variation in paratypes (dry mounted specimen). Cannot be calculated, broken bristles in paratypes.

Etymology. Name refers to the *Caxarumi* district in Loja Province of Ecuador. In Kichwa, *caxa* refers to *Chakka* (possum) and *rumi* (stone, rock).

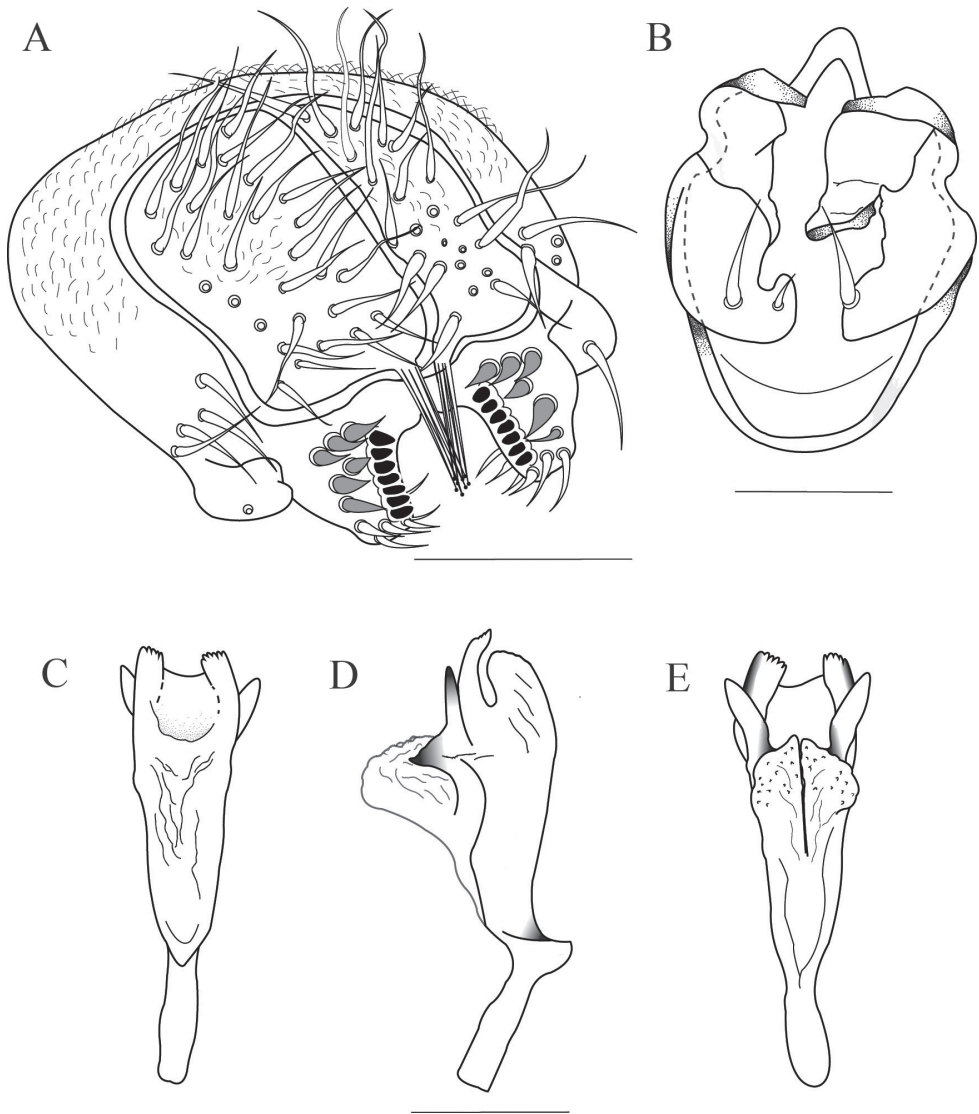


Figure 7. *Drosophila caxarumi* sp. n., male terminalia of holotype. **A** Epandrium, cerci, surstylus, and decasternum **B** Hypandrium, gonopods and paraphyses, ventral view **C, D, E** Aedeagus in ventral, lateral and dorsal view, respectively. Scale bars: 100 μ m.

Distribution. *Drosophila caxarumi* is known from two localities (elevation range is 2548–2675 m) from Loja Province, Podocarpus National Park and Napo Province, Río Guango.

Ecology. Unknown. The type specimen was found in the fermented banana-bait traps placed at the locality, which suggests that this species feeds or breeds on fermented fruit as many other *Drosophila* species. The habitat is a well-preserved intermediate montane forest.

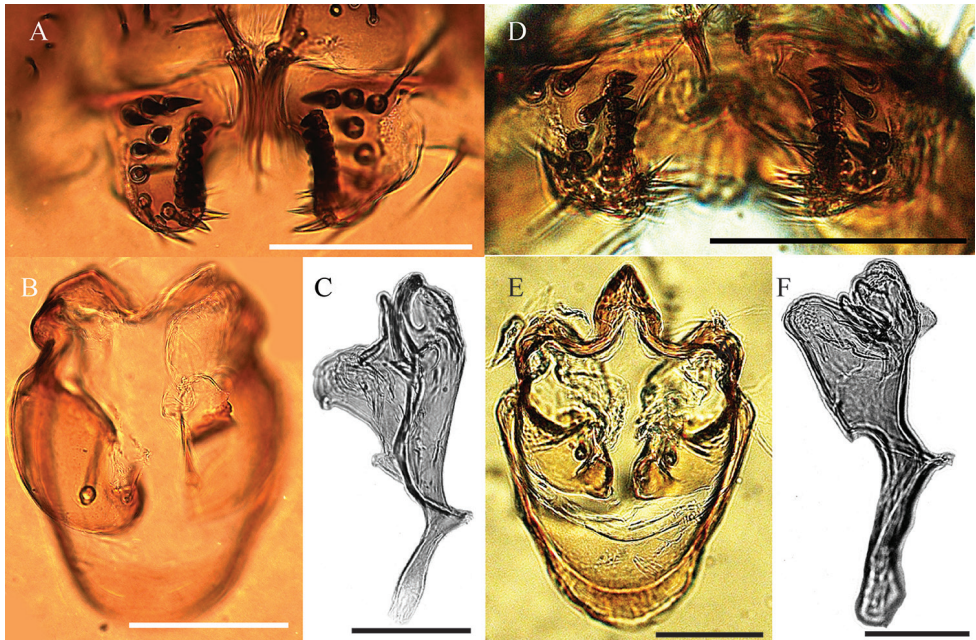


Figure 8. *Drosophila caxarumi* sp. n., male terminalia of holotype. **A** Surstylus, and decasternum **B** Hypandrium, gonopods and paraphyses, ventral view **C** Aedeagus in lateral view. *Drosophila guaraja* King, from Zamora Chinchipe, Ecuador. **D** Surstylus, and decasternum **E** Hypandrium, gonopods and paraphyses, ventral view **F** Aedeagus in lateral view. Scale bars: 100 μ m.

Relationship to other species. The most similar species to *Drosophila caxarumi* sp. n. is *D. guaraja* King, 1947b. We compared *D. caxarumi* with descendants of *D. guaraja* reared from an isofemale line named ZBCI036 from Podocarpus National Park, Bombuscaro, 1000 msnm. These two species share the same cotton swab-shaped bristles on the ventral side of the cerci (Figure 8A, D). *Drosophila caxarumi* and *D. guaraja* differ in the general shape of the aedeagus (Figure 8C, F). In *D. caxarumi* the aedeagus is bent towards the dorsal side. In *D. guaraja* the paraphyses are microtrichose while in *D. caxarumi* they are smooth and hairless. Both species differ markedly in external morphology (Figure 6A, B), body color of *D. caxarumi* is mainly brown while in *D. guaraja* is yellow. *D. guaraja* abdomen is yellow with broad, dark brown bands different from the brown abdomen in *D. caxarumi* (Figure 6A, B).

***Drosophila sachapuyu* sp. n.**

<http://zoobank.org/C4F4A33E-ED73-44E3-A87A-6BE026A2DD93>

Figs 9A–F, 10A–C

Type material. Holotype ♂ (dissected, terminalia in microvial), Ecuador, Loja, Cajanuma, 2675 m, 4°6'53.7"S; 79°10'54.6"W, 23 Apr. 2015, A. Peñafiel col., A. Peñafiel

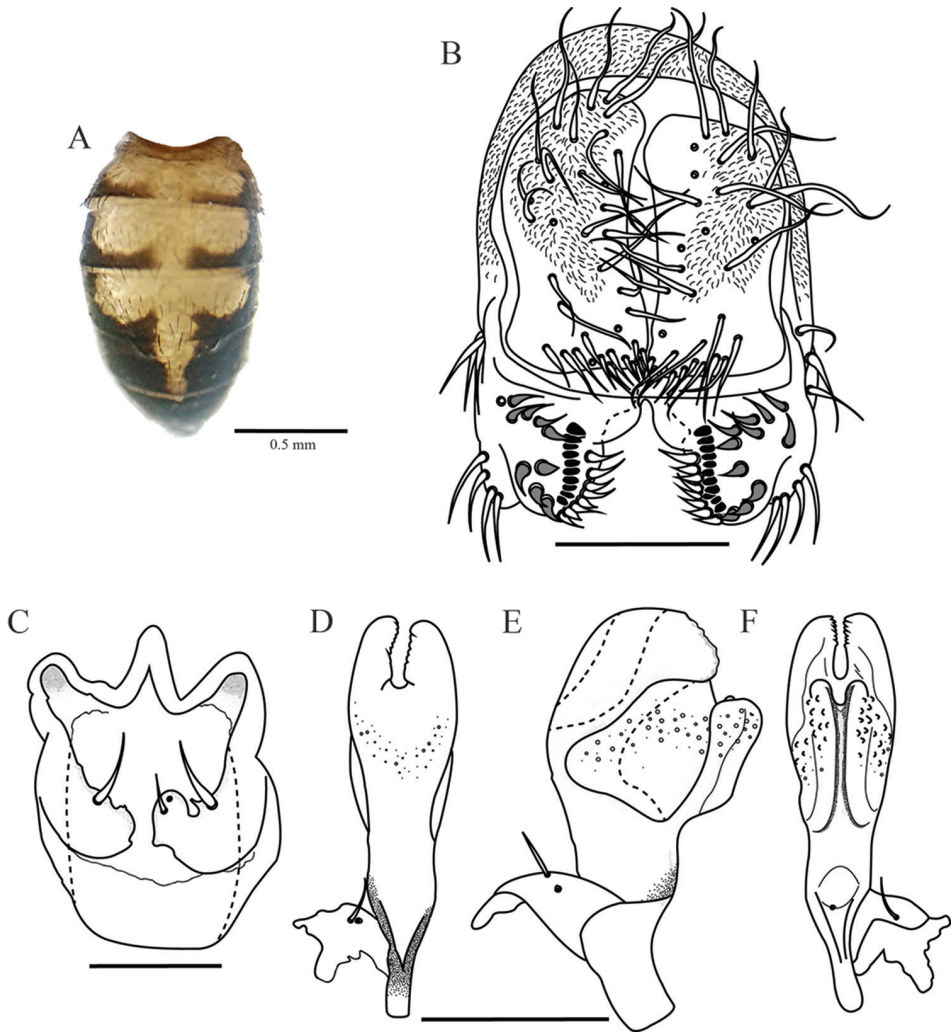


Figure 9. *Drosophila sachapuyu* sp. n., abdomen and male terminalia of holotype. **A** Male abdomen, dorsal view **B** Epandrium, cerci, surstylus and decasternum **C** Hypandrium, gonopods and paraphyses, ventral view **D, E, F** Aedeagus and paraphyses in ventral, lateral and dorsal view, respectively. Terminalia scale bars: 100 μ m.

& V. Rafael det. (QCAZ-I 3309). Allotype ♀ (dissected, terminalia in microvial), Ecuador, Loja, Cajanuma, 2675 m, 4°6'53.7"S; 79°10'54.6"W, 23 Apr. 2015, A. Peñafiel col., A. Peñafiel & V. Rafael det. (QCAZ-I 3310).

Paratypes. 9 ♂♂ and 9 ♀♀ (dissected, terminalia in microvial, descendants of isofemale line), Ecuador, Loja, Cajanuma, 2675 m, 4°6'53.7"S; 79°10'54.6"W, 23 Apr. 2015, A. Peñafiel col., A. Peñafiel & V. Rafael det. (QCAZ-I 3311–3328).

Diagnosis. Body color yellow. Aristae with six dorsal and two ventral branches. Two prominent oral bristles. Thorax yellow. Wings clear. Cerci not fused to epan-

drium. Aedeagus with two sheets fused by a membrane with tiny spines, with a ventral blade with wavy edge. Hypandrium in shield-shape. Gonopod bearing one long bristle. Paraphyses fused to gonopod bearing two small bristles.

Description. Male. Young specimen. Holotype external morphology: total length (body + wings) 3 mm, body length 2.40 mm. Body color yellow.

Head. Aristae with six dorsal and two ventral branches plus terminal fork and fine hairs. Orbital plate yellowish brown, frontal length 0.29 mm; frontal index = 0.82; top to bottom ratio = 0.14; Medial vertical seta closer to lateral vertical seta. Distance of or3 to or1 = 0.11, distance of or3 to vtm = 0.09, or1-or3 ratio = 0.62; or2-or1 ratio = 0.47, vt index = 0.84. Ocellar triangle yellowish brown, ocellus yellow, distance of ocellar setae = 0.51 of frontal length, distance of postocellar setae = 0.75 of frontal length; frontal vitta yellow. Two prominent oral bristles of the same size, vibrissa index = 0.84. Cheek index = 4.58. Carina not sulcate. Eyes wine red, eye index = 1.28.

Thorax. Yellow, thorax length 0.60 mm, acrostichal hairs in eight rows between the two anterior dorsocentral setae that decrease in number toward the rear. h index = 1.2. Transverse distance of dorsocentral setae = 2.17, dc index = 0.65. Distance between apical scutellar seta = 1.16, scutellum yellow, scut index = 1.34. Medial katepisternal seta three quarters of the length of the anterior seta, sterno index = 2.2. Clear wings. Alar length 2.29 mm, alar width 1.09 mm. Alar indices: alar = 2.10; C = 2.76; ac = 2.04; hb = 0.30; 4c = 0.47; 4v = 1.25; 5x = 1.5; M = 0.4 and prox. x = 0.31.

Abdomen. Yellow with dorsal midline that reaches the 5th tergite, 1st tergite yellowish brown, 2nd–4th tergites with posterior dark pigmentation which reaches and covers the exterior margin leaving a round clear area, 5th tergite with dark pigmentation which covers the entire tergite, 6th tergite totally dark (Figure 9A).

Male terminalia. Epandrium microtrichose with three lower and no upper bristles, four bristles on the ventral lobe. Cerci not fused to epandrium. Surstylus triangular, with ten primary teeth on the right and eleven on the left side, ten sharp secondary teeth on the right and eleven on the left side, eight marginal bristles on each side (Figure 9B). Hypandrium in shield-shape and membranous. Gonopod elongated bearing one long bristle (Figure 9C).

Aedeagus. Young specimen slightly sclerotized, ends in two sheets fused by a membrane with small bright tiny spines, with a wider blade with wavy edge. Aedeagus apodeme broken. Paraphyses fused to gonopod bearing two small bristles (Figure 9 D-F).

Variation in paratypes (dry mounted specimen). Total length (body + wings) 3.82–4.43 mm, body length 2.49–3.08 mm. Head. Frontal length 0.28–0.32 mm, frontal index = 0.7–0.85, top to bottom width ratio = 1.08–1.59; distance of or3 to or1 = 0.07–0.12, distance of or3 to vtm = 0.11–0.14, or1-or3 ratio = 0.86–1.40, or2-or1 ratio = 0.20–0.38, distance of ocellar setae = 0.83–1.17 of frontal length, distance of postocellar setae = 0.68–0.96 of frontal length, vt index = 0.77–0.93; cheek index = 5.36–10.66; vibrissa index = 0.86–1.07; eye index = 1.08–1.40. Thorax length 0.76–0.98 mm, h index = 0.69–1.27. Transverse distance of dorsocentral setae = 1.0–2.47, dc index = 0.61–1.06. Distance between apical scutellar seta = 0.76–1.0, scut index = 1.10–1.51; sterno index = 1.28–2.60.

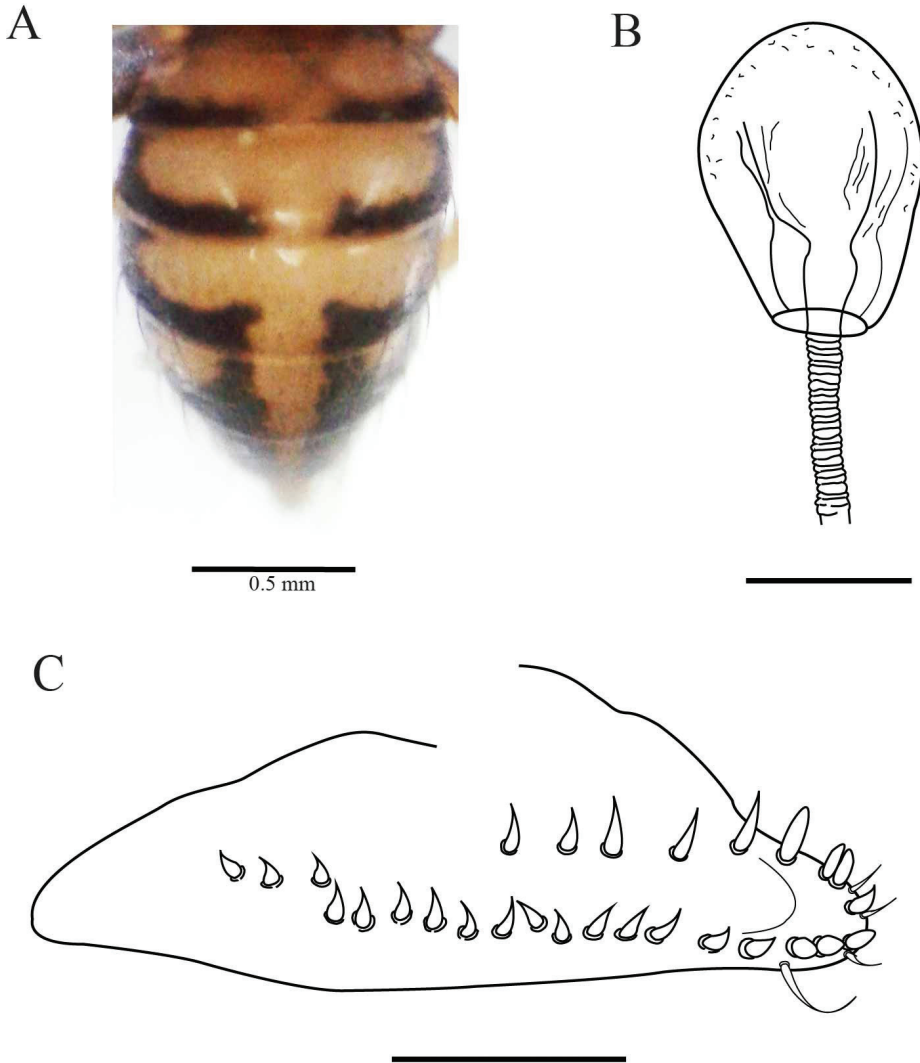


Figure 10. *Drosophila sachapuyu* sp. n., abdomen and female terminalia of allotype. **A** Female abdomen, dorsal view **B** Spermatheca **C** Ovipositor. Terminalia scale bars: 100 μ m.

Female. Allotype and paratypes (isofemale descendants). Allotype: total length (body + wings) 4.41 mm, body length 2.94 mm. Body color dark brown.

External morphology. Same as the male except abdomen, which is yellow with dorsal midline that reaches the 6th tergite, 1st tergite yellowish brown, 2nd – 5th tergites with posterior dark pigmentation which reaches and covers the exterior margin leaving a round clear area, 6th tergite totally dark (Figure 10A). Wings yellow. Alar length 3.6 mm, alar width 1.38 mm. Alar indices: alar = 2.21; C = 4.32; ac = 1.78; hb = 0.44; 4c = 0.51; 4v = 1.40; 5x = 1.20; M = 0.36 and prox. x = 0.42.

Terminalia. Spermatheca lightly pigmented, balloon-shaped, with small indentations, deeply invaginated to three-quarters (Figure 10B). Ovipositor elongated, sclerotized, with 20 marginal and eight discal teeth, one long bristle and three fine hairs (Figure 10C).

Variation in paratypes (dry mounted specimen). Total length (body + wings) 4.12–5.05 mm, body length 2.49–3.27 mm. Head. Frontal length 0.31–0.39 mm, frontal index = 0.72–0.84, top to bottom width ratio = 1.16–1.55; distance of or3 to or1 = 0.08–0.15, distance of or3 to vtm = 0.11–0.16, or1-or3 ratio = 0.5–2, or2-or1 ratio = 0.10–0.46, distance of ocellar setae = 0.70–1.11 of frontal length, distance of postocellar setae = 0.64–0.88 of frontal length, vt index = 0.74–1.34; cheek index = 5.40–9.83; vibrissa index = 0.88–1.0; eye index = 1.07–1.35. Thorax. Length 0.86–1.04 mm, h index = 0.65–1.26. Transverse distance of dorsocentral setae = 1.76–2.50, dc index = 0.64–0.82. Distance between apical scutellar seta = 0.69–1.12. scut index = 1.05–1.72; sterno index = 1.20–2.23.

Etymology. In Kichwa, *sachapuyu* refers to *sacha* (forest) and *puyu* (cloud). This species was found on a cloud forest habitat.

Distribution. Known only from the type locality.

Ecology. Unknown. The type specimen was found in the fermented banana-bait traps placed at the locality, which suggests that this species feeds and breeds in fermented fruit as do many other *Drosophila* species. This species has been reared with gelatin banana media devised by Rafael et al. 2000. The habitat is a well-preserved intermediate montane forest.

Relationship to other species. The general shape of the terminalia of *Drosophila sachapuyu* sp. n. has similarities with the terminalia of *D. pichinchana* Vela & Rafael, 2004. The two smaller ventral sheets and two heavier dorsal sheets are fused by a membranous medial region. Both species have four bristles on the ventral lobe. *Drosophila sachapuyu* and *Drosophila pichinchana* differ in the general shape of the aedeagus. The aedeagus of *D. sachapuyu* is dorsally flattened.

***Drosophila misi* sp. n.**

<http://zoobank.org/F892199E-0A33-40A1-AE63-F0A70C124EC1>

Fig 11A–F

Type material. Holotype ♂ (dissected, terminalia in microvial), Ecuador, Loja, Cajanuma, 2800 m, 4°6'58.9"S; 79°10'11.9"W, 19 Nov. 2015, A. Peñafiel col., A. Peñafiel & V. Rafael det. (QCAZ-I 3329).

Paratypes. 6 ♂♂ (dissected, terminalia in microvial), same data as holotype, 19 Nov. 2015, A. Peñafiel col., A. Peñafiel & V. Rafael det. (QCAZ-I 3330–3335). 1 ♂♂ (dissected, terminalia in microvial) Ecuador, Loja, Cajanuma, 2675 m, 4°6'53.7"S; 79°10'54.6"W, 19 Nov. 2015, A. Peñafiel col., A. Peñafiel & V. Rafael det. (QCAZ-I 3294).

Diagnosis. Aristaes with five dorsal and two ventral branches. Two prominent oral bristles. Thorax yellowish brown. Wings yellow, dM-Cu slightly clouded. Abdomen

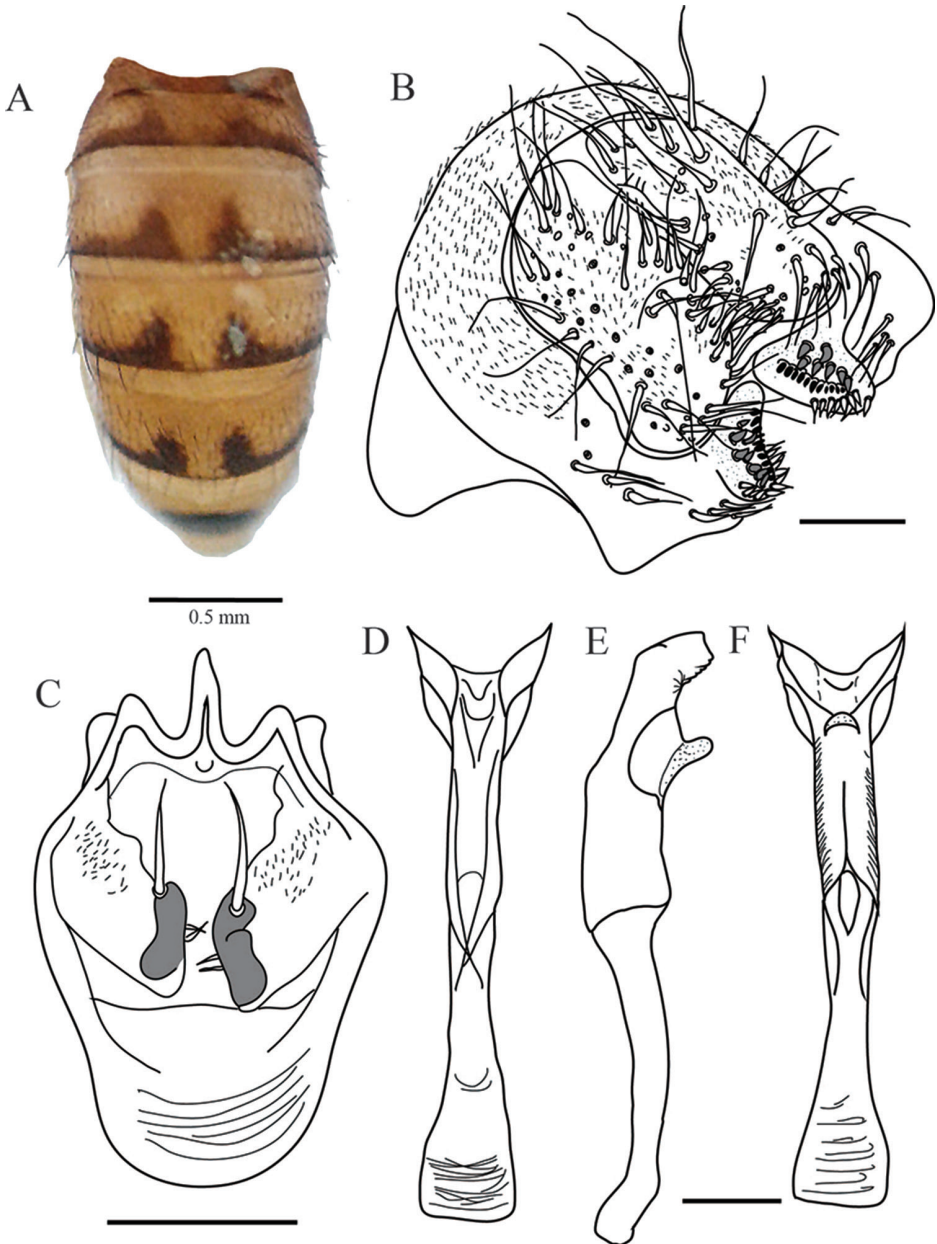


Figure 11. *Drosophila misi* sp. n., abdomen and male terminalia of holotype. **A** Male abdomen, dorsal view **B** Epandrium, cerci, surstylus and decasternum **C** Hypandrium, gonopods and paraphyses, ventral view **D, E, F** Aedeagus in ventral, lateral and dorsal view, respectively. Terminalia scale bars: 100 μ m.

yellow with dorsal midline, 1st tergite yellowish brown, 2nd – 5th tergites with triangular pigmentation that thins laterally, 6th tergite with pigmented circle in the middle. Cerci not fused to epandrium. Aedeagus sclerotized, tube-like, apex with two dorsal

sclerotized projections, dorsally with a finger-like projection covered with tiny projections. Hypandrium in shield-shape. Gonopod microtrichose bearing one long bristle. Paraphyses fused to gonopod bearing two small bristles on each side.

Description. Male. Holotype external morphology: total length (body + wings) 5 mm, body length 3.40 mm. Body color yellowish brown.

Head. Aristae with five dorsal and two ventral branches plus terminal fork and fine hairs, pedicel and flagellomere brown. Orbital plate brown, frontal length 0.27 mm; frontal index = 0.61; top to bottom width ratio = 1.59. Distance of or3 to or1 = 0.10, distance of or3 to vtm = 0.12, or1-or3 ratio = 0.76; or2-or1 ratio = 0.39. Medial vertical seta closer to lateral vertical seta, vt index = 1.33. Ocellar triangle brown, distance of postocellar setae = 0.77 of frontal length, ocellus yellow. Frontal vitta yellowish brown. Carina prominent brown, not sulcate. Cheek index = 4.66. Two prominent oral bristles the second almost the same size as the first, vibrissa index = 1. Eyes red, eye index = 1.16.

Thorax. Yellowish brown, thorax length 0.85 mm, acrostichal hairs in six rows between the two anterior dorsocentral setae that decrease in number toward the rear. h index = 1.07. Transverse distance of dorsocentral setae = 2.15, dc index = 0.95. Basal scutellar setae parallel, distance between apical scutellar seta = 0.68, scut index = 1.27. Medial katepisternal seta slightly smaller than the previous seta, sterno index = 1.66. Legs yellow. Clear wings, dM-Cu slightly clouded. Alar length 3.28 mm, alar width 1.41 mm. Alar indices: alar = 2.17; C = 4.55; ac = 1.87; hb = 0.20; 4c = 0.43; 4v = 1.07; 5x = 1.12; M = 0.26 and prox. x = 0.31.

Abdomen. Yellow, with dorsal midline, 1st tergite yellowish brown, 2nd – 5th tergites with triangular pigmentation that thins laterally, 6th tergite with pigmented circle in the middle (Figure 11A).

Male terminalia. Epandrium microtrichose, ventral lobe membranous with nine bristles. Cerci not fused to epandrium. Surstylus triangular, granular, with ten primary teeth on the right and eleven on the left, eight secondary teeth on the right and seven on the left, nine marginal bristles on the right and 12 on the left (Figure 11B). Hypandrium sclerotized, in shield-shape. Gonopod microtrichose bearing one long bristle (Figure 11C).

Aedeagus. Sclerotized tube-like, apex with two dorsal sclerotized projections with serrated edge. Dorsally with a finger-like projection covered in tiny projections. Ventral rod absent. Aedeagus apodeme sclerotized straight and wide (Figure 11D-F). Paraphyses strongly sclerotized fused to gonopod bearing two small bristles on each side (Figure 11C).

Variation in paratypes (dry mounted specimen). Head. Frontal length 0.26–0.31 mm, frontal index = 0.73–0.88, top to bottom width ratio = 1.51–1.68; distance of or3 to or1 = 0.07–0.09, distance of or3 to vtm = 0.10–0.14, or1-or3 ratio = 0.50–1.03, or2-or1 ratio = 0.22–0.41, distance of ocellar setae = 0.67–1.07 of frontal length, distance of postocellar setae = 0.61–0.80 of frontal length, vt index = 0.81–1.36; cheek index = 4.36–8.66; vibrissa index = 0.78–1.0; eye index = 0.95–1.36. Thorax. Length 0.84–1.03 mm, h index = 0.83–1.33. Transverse distance of dorsocentral setae = 1.30–2.31, dc index = 0.95–1.16. Distance between apical scutellar seta = 0.73–0.90. scut index = 1.23–1.27.

Etymology. In Kichwa, *misi* means cat; the apex of the aedeagus resembles the ears of a cat.

Distribution. *Drosophila misi* is known from two localities (elevation range is 2675–2800 m) from Loja Province, Podocarpus National Park.

Ecology. Unknown. The type specimen was found in the fermented banana-bait traps placed at the locality, which suggests that this species feeds and breeds in fermented fruit as do many other *Drosophila* species. The habitat is a well-preserved montane forest.

Relationship to other species. The general shape of the male terminalia suggests that this species belongs to the *Drosophila guarani* group

Discussion

Nineteen species have been previously placed in the *guarani* group (Vilela and Bächli 1990; Vilela and Pereira 1993; Vela and Rafael 2004; Vela and Rafael 2005; Ratcov et al. 2017; Vaz et al. 2018). Their distribution is restricted to Central and South America (Kastritsis 1969). Collections in Loja Province of Ecuador revealed two species, *D. griseolineata* and *D. urubamba* (Rafael & Vela, 2003). *Drosophila guarani* group has the second highest species richness after the *Drosophila tripunctata* group in Podocarpus National Park, with eleven species (Peñañiel 2016). With the five new species described in this paper, the southern Andes of Ecuador are home to almost the same number of *guarani* group species previously described.

Characteristics such as the alar pigmentation, spotted thorax and abdominal pigmentation are similar between *D. zamorana*, *D. urubamba* and *D. tucumana*. We propose the cluster formed by these three spotted-thorax species. These species clearly belong to *guarani* group because they share two prominent oral bristles of approximately equal length, divergent anterior scutellars, cerci not fused to epandrium and shield-shaped hypandrium. Previously the *guarani* group did not include spotted-thorax species (Vilela and Val 2004).

Drosophila misi sp. n. is not similar to other species in the *guarani* group. It shares the important key characters of *guarani* group. This species has a brownish body color; two prominent vibrissal setae of nearly equal size, divergent basal scutellar setae, clouded crossveins and tergites usually with interrupted, dark marginal bands (Vilela and Bächli 1990). The genitalia characteristics of *D. misi* including the cerci not being fused to the epandrium, the shield-shaped hypandrium and the general shape of the aedeagus are characteristic of species in the *guarani* group.

Acknowledgements

This work was supported by the Pontificia Universidad Católica del Ecuador, and is part of the projects L13240 and M1347. The Ecuadorian Ministerio de Ambiente provided research and collection permits N°003-15IC-FAU-DNB/MA and MAE-DNB-

CM-2016-0030. We thank to Ana Belén Manzano for providing the paratypes, Fernanda Salazar for her assistance in archiving the specimens in the museum. Dr Carlos Vilela and Dr Clifford Keil provided helpful comments to the manuscript. Dr David Donoso, Luz Marina Llangarí, María Isabel Tamayo, and Jonathan Rondal are thanked for their assistance in the field.

References

- Bächli G, Vilela CR, Andersson S, Saura A (2004) The Drosophilidae (Diptera) of Fennoscandia and Denmark. Brill, Leiden, New York 39, 7–15.
- Dobzhansky T, Pavan C (1943) Studies on Brazilian species of *Drosophila*. Separata do Bol. Faculdade de Filosofia Ciência e Letras Universidad Sao Paulo 36: 7–72. <http://www.drosophila.jp/jdd/class/030703/03070372.pdf>
- Duda O (1927) Die südamerikanischen Drosophiliden (Dipteren) unter Berücksichtigung auch der anderen neotropischen sowie der nearktischen Arten. Archiv für Naturgeschichte 91A(11/12): 1–228.
- Kastritsis CD (1969) The chromosomes of some species of the *guarani* group of *Drosophila*. Journal of Heredity 60: 51–57. <https://doi.org/10.1093/oxfordjournals.jhered.a107930>
- King JC (1947a) Interspecific relationships within the *guarani* group of *Drosophila*. Evolution 1: 143–153. <https://doi.org/10.2307/2405490>
- King JC (1947b) A comparative analysis of the chromosomes of the *guarani* group of *Drosophila*. Evolution 1: 48–62. <https://doi.org/10.2307/2405403>
- Márquez Luna J (2005) Técnicas de colecta y preservación de insectos. Boletín Sociedad Entomológica Aragonesa 37: 385–408.
- Peñafiel A (2016) Estudio taxonómico del género *Drosophila* (Diptera, Drosophilidae) en el Parque Nacional Podocarpus, Loja y Zamora Chinchipe, Ecuador. Bachelor thesis. Pontificia Universidad Católica del Ecuador. http://repositorio.puce.edu.ec/bitstream/handle/22000/13497/Ana_Danitza_Pe%C3%B1afiel_Vinueza_Disertacion.pdf?sequence=1&isAllowed=y
- Rafael V, Arcos G, Arcos L (2000) Ecología y distribución del género *Drosophila* en Guayllabamba y el Quinche, provincia de Pichincha-Ecuador. Revista de la Pontificia Universidad Católica del Ecuador 65: 130–155.
- Rafael V, Vela D (2003) *Drosophila yangana* sp. nov. un nuevo miembro del grupo *repleta* subgrupo inca (Diptera: Drosophilidae). Revista de la Pontificia Universidad Católica del Ecuador 71: 129–139.
- Ratcov V, Vilela CR (2007) A new Neotropical species of spot-thoraxed *Drosophila* (Diptera, Drosophilidae). Revista Brasileira de Entomologia 51(3): 305–311. <http://dx.doi.org/10.1590/S0085-56262007000300009>
- Ratcov V, Vilela CR, Goñi B (2017) A new species of Neotropical *Drosophila* (Diptera, Drosophilidae) belonging to the *guarani* group. Revista Brasileira de Entomologia 61: 232–238. doi: <https://doi.org/10.1016/j.rbe.2017.06.002>
- Robe LJ, da Silva LB, da Silva EL (2002) Phylogenetic relationships among four species of the *guarani* group of *Drosophila* (Diptera, Drosophilidae) as inferred by molecular and mor-

- phological analyses. *Revista Brasileira de Entomologia* 46(4): 515–519. doi: <http://dx.doi.org/10.1590/S0085-56262002000400004>
- Vaz SC, Vilela CR, Carvalho AB (2018) Two new species of *Drosophila* (Diptera, Drosophilidae) associated with inflorescences of *Goepertia monophylla* (Marantaceae) in the city of São Paulo, state of São Paulo, Brazil. *Revista Brasileira de Entomologia* 62(2): 159–168. <https://doi.org/10.1016/j.rbe.2018.03.003>
- Vela D, Rafael V (2004) Tres nuevas especies del grupo *guarani* género *Drosophila* (Diptera, Drosophilidae) en el Bosque Pasochoa, Provincia de Pichincha. *Revista Ecuatoriana de Medicina y Ciencias Biológicas* 26: 14–21. <http://remcb-puce.edu.ec/index.php/remcb/article/view/185>
- Vela D, Rafael V (2005) Catorce nuevas especies del género *Drosophila* (Diptera, Drosophilidae) en el bosque húmedo montano del Volcán Pasochoa, Pichincha, Ecuador. *Revista Ecuatoriana de Medicina y Ciencias Biológicas* 27: 27–41. <http://remcb-puce.edu.ec/index.php/remcb/article/view/191>
- Vilela CR, Pereira MA (1985) Notes on two species of spot-thoraxed *Drosophila* belonging to the *guarani* group (Diptera, Drosophilidae). *Revista Brasileira de Entomologia* 29(3/4): 435–442.
- Vilela CR, Bächli G (1990) Taxonomic studies on Neotropical species of seven genera of Drosophilidae (Diptera). *Mitteilungen der Schweizerischen Entomologischen Gesellschaft* 63: 1–332. <http://www.drosophila.jp/jdd/class/030704/03070404.pdf>
- Vilela CR, Pereira MA (1993) A case of misidentification of neotropical species of *Drosophila* (Diptera, Drosophilidae) Belonging to the *guarani* group. *Revista Brasileira de Entomologia* 37(4): 819–820.
- Vilela CR, Val FC (2004) A new spot-thoraxed species of *Drosophila* from the Atlantic Forest of southeastern Brazil (Diptera, Drosophilidae) *Revista Brasileira de Entomologia* 48(1): 4. <http://dx.doi.org/10.1590/S0085-56262004000100008>

